Civil Engineering Study

Structural Series 85-20

OPTIMAL DESIGN OF 3-D REINFORCED CONCRETE AND STEEL BUILDINGS SUBJECTED TO STATIC AND SEISMIC LOADS INCLUDING CODE PROVISIONS

by

Franklin Y. Cheng
Professor

Kevin Z. Truman
Graduate Assistant

Department of Civil Engineering

University of Missouri-Rolla

Rolla, Missouri

Report Series

Prepared for the National Science Foundation under grants

NSF PFR 8019625 and NSF CEE 8213477

BIBLIOGRAPHIC DATA SHEET	1. Report No. Structural Series 85-20	2.	3. Recipient's Accession No. PB86 168564/AS
4. Title and Subtitle Optimal Design of 3-D Reinforced Concrete and Steel Buildings Subjected to Static and Seismic Loads Including Code Provisions			5. Report Date June, 1985 6.
7. Author(s) Franklin Y. Cheng and Kevin Z. Truman			8. Performing Organization Rept. No. Structural Series
9. Performing Organization Name and Address Civil Engineering Department University of Missouri-Rolla Rolla, MO 65401			10. Project/Task/Work Unit No. 11. Contract/Grant No. NSF PFR 8019625 NSF CEE 8213477
12. Sponsoring Organization Name and Address National Science Foundation Washington, DC			13. Type of Report & Period Covered 14.

15. Supplementary Notes

16. Abstracts

An optimization algorithm and a computer program are developed for both analysis and design of 3-D building systems. About 75 design cases are provided in this report to illustrate the usefulness of the research results. Several significant design results indicate that the optimal solutions resulting from multi- and single seismic components can be quite different and are affected by the relative location of mass and stiffness centers at each floor; the ATC-3 modal and equivalent lateral force procedures produce similar stiffness distribution but different magnitudes for both regular and irregular building configurations; the actual values of ATC-3 stability function, θ, are much less than the maximum value of 0.1; and the fundamental natural periods resulting from optimal designs are always greater than the approximate building period, T_a, as well as $1.2T_a$, which is the upper bound supposed to be used in determining the lateral forces in ATC-3. A verification of the ATC-3 requirements is recommended.

17. Key Words and Document Analysis. 17a. Descriptors

ATC-3
Building systems
Code Provisions
Computer Methods
Multicomponent Earthquakes
Reinforced Concrete
Steel
Structural Optimization

17b. Identifiers/Open-Ended Terms

17c. COSATI Field/Group

18. Availability Statement	19. Security Class (This Report) UNCLASSIFIED	21. No. of Pages 414
	20. Security Class (This Page UNCLASSIFIED	22. Price $34.95

INSTRUCTIONS FOR COMPLETING FORM NTIS-35 (Bibliographic Data Sheet based on COSATI Guidelines to Format Standards for Scientific and Technical Reports Prepared by or for the Federal Government, PB-180 600).

1. **Report Number.** Each individually bound report shall carry a unique alphanumeric designation selected by the performing organization or provided by the sponsoring organization. Use uppercase letters and Arabic numerals only. Examples FASEB-NS-73-87 and FAA-RD-73-09.

2. Leave blank.

3. **Recipient's Accession Number.** Reserved for use by each report recipient.

4. **Title and Subtitle.** Title should indicate clearly and briefly the subject coverage of the report, subordinate subtitle to the main title. When a report is prepared in more than one volume, repeat the primary title, add volume number and include subtitle for the specific volume.

5. **Report Date.** Each report shall carry a date indicating at least month and year. Indicate the basis on which it was selected (e.g., date of issue, date of approval, date of preparation, date published).

6. **Performing Organization Code.** Leave blank.

7. **Author(s).** Give name(s) in conventional order (e.g., John R. Doe, or J.Robert Doe). List author's affiliation if it differs from the performing organization.

8. **Performing Organization Report Number.** Insert if performing organization wishes to assign this number.

9. **Performing Organization Name and Mailing Address.** Give name, street, city, state, and zip code. List no more than two levels of an organizational hierarchy. Display the name of the organization exactly as it should appear in Government indexes such as Government Reports Index (GRI).

10. **Project/Task/Work Unit Number.** Use the project, task and work unit numbers under which the report was prepared.

11. **Contract/Grant Number.** Insert contract or grant number under which report was prepared.

12. **Sponsoring Agency Name and Mailing Address.** Include zip code. Cite main sponsors.

13. **Type of Report and Period Covered.** State interim, final, etc., and, if applicable, inclusive dates.

14. **Sponsoring Agency Code.** Leave blank.

15. **Supplementary Notes.** Enter information not included elsewhere but useful, such as: Prepared in cooperation with . . . Translation of . . . Presented at conference of . . . To be published in . . . Supersedes . . . Supplements . . . Cite availability of related parts, volumes, phases, etc. with report number.

16. **Abstract.** Include a brief (200 words or less) factual summary of the most significant information contained in the report. If the report contains a significant bibliography or literature survey, mention it here.

17. **Key Words and Document Analysis. (a). Descriptors.** Select from the Thesaurus of Engineering and Scientific Terms the proper authorized terms that identify the major concept of the research and are sufficiently specific and precise to be used as index entries for cataloging.
(b). Identifiers and Open-Ended Terms. Use identifiers for project names, code names, equipment designators, etc. Use open-ended terms written in descriptor form for those subjects for which no descriptor exists.
(c). COSATI Field/Group. Field and Group assignments are to be taken from the 1964 COSATI Subject Category List. Since the majority of documents are multidisciplinary in nature, the primary Field/Group assignment(s) will be the specific discipline, area of human endeavor, or type of physical object. The application(s) will be cross-referenced with secondary Field/Group assignments that will follow the primary posting(s).

18. **Distribution Statement.** Denote public releasability, for example "Release unlimited", or limitation for reasons other than security. Cite any availability to the public, other than NTIS, with address, order number and price, if known.

19 & 20. **Security Classification.** Do not submit classified reports to the National Technical Information Service.

21. **Number of Pages.** Insert the total number of pages, including introductory pages, but excluding distribution list, if any.

22. **NTIS Price.** Leave blank.

ABSTRACT

A structural optimization algorithm based upon an optimality criteria approach is presented for three-dimensional statically and dynamically loaded steel and/or reinforced concrete structures. The theoretical work is presented in terms of scaling, sensitivity analyses, optimality criteria, and Lagrange multiplier determination. The structures can be subjected to a combination of static and/or dynamic displacement and stress, and natural frequency constraints. The dynamic analyses are based upon the ATC-03 provisions or multi-component response spectra modal analyses. Using the algorithm presented, a computer program called ODRESB-3D was developed for both analysis and design of building systems. About 75 design examples are provided in this report to illustrate the rapid convergence and the practicality of the presented method as well as the effects of ATC-03 provisions and multicomponent seismic input on the optimal structural parameters. Several interesting results are: 1) the optimal solutions resulting from multi- and single component excitation can be quite different and are affected by the relative location of the mass and stiffness centers at each floor of a system, 2) ATC-03 modal and equivalent lateral force procedures produce similar stiffness distributions but different

magnitudes for both regular and irregular structural configurations, 3) ATC-03 stability function values are much less than the upper bound value of 0.1 in the provisions, and 4) the fundamental natural periods obtained at the optimum are always greater than the approximate building period, T_a, as well as $1.2T_a$, which is the upper bound that is recommended to be used in determining the lateral seismic forces as indicated in ATC-3. A verification of the requirements in ATC-3 is recommended.

ACKNOWLEDGMENTS

This is one of a series of reports on optimum design of structural systems with parametric multicomponent earthquake motion and code provisions supported by the National Science Foundation under the grant PFR 8019625 and partially under the grant CEE 8213477. Supports for this study are gratefully acknowledged. Dr. K. Z. Truman, a former graduate assistant in Civil Engineering at the University of Missouri-Rolla, is Assistant Professor of Civil Engineering at the Washinton University, St. Louis.

TABLE OF CONTENTS

LIST OF ILLUSTRATIONS

Figures Page

Figures Page

Figures Page

Figures Page

Figures Page

Figures Page

LIST OF TABLES

Tables Page

Tables Page

I. INTRODUCTION

In the past decade, a considerable amount of literature has been published in the area of optimum structural design. The increasing number of publications correspond closely to the rapid demand for economical and reliable structural design in virtually all fields of endeavor. Optimum design has been extensively used in aircraft structural engineering (1,2).

Various optimization techniques of linear, nonlinear, and dynamic programming have been developed for different types of static and dynamic structures (3,4,5). In general most of the techniques have some limitations and are best suited for certain classes of problems. The technique based on energy distribution as optimality criteria has been proven to be effective for large structures in aerospace engineering (6,7,8). Recently, Venkayya and Cheng (9), Cheng and Srifuengfung (10,11,12), and Cheng (13) extended the optimization algorithm for structures subjected to earthquake motions.

Previous studies of optimum seismic structural design were mostly based on the linearization technique and static equivalent seismic forces for simple structures and shear buildings (14,15). Cheng and Botkin (16,17) studied the feasible direction technique for the design of tall buildings and large frameworks. This included the geometric nonlinearity of P-Δ effect. The technique

was also studied by Ray et al (18), Walker and Pister (19), and Pister et al (20) for various optimal design cases. Cheng and his associates further studied the modern optimization technique of optimality criteria for various cost functions and nondeterministic structural systems (21,22). All the published references including these cited above are mainly for two dimensional structures.

Current design for three-dimensional seismic structures are mostly based on analysis computer programs for which one horizontal component of ground motion can be applied in any direction of the structural plane. The building codes do not indicate how the interactive earthquake components influence design parameters but only specify in general that the lateral seismic forces are assumed to act nonconcurrently in the direction of each of the main axes of a structure. Cheng, among others, studied the coupling effect of horizontal and vertical ground acceleration on plane structures (23,24,25), and he further investigated the effect of three-dimensional parametric earthquake motions on space frameworks and building systems (26,27,28). It was found that the response behavior of both plane and space structures can be significantly influenced by multicomponent earthquake motions.

A study of available information concerning seismic research activities around the world which appears in the

"Proceedings of the World Conferences on Earthquake Engineering," "Earthquake Prediction and Hazard Mitigation Options for USGS and NSF Programs," and others (29,30,31) indicates that the optimum design of three-dimensional building systems subjected to an interaction of earthquake motions is important but not available. Thus the work of optimum design of three-dimensional seismic structures was undertaken and an automated design computer program was developed for which the results are reported here.

II. SCOPE OF INVESTIGATIONS AND RELATED RESEARCH WORK

The emphasis of the research may be briefly summarized in the following six categories: 1) optimality criteria, 2) sensitivity analyses, 3) structural elements and models, 4) response spectra seismic forces, 5) ATC-03 seismic forces, and 6) critical structural parameters and recommendations.

A. OPTIMALITY CRITERIA

The development of optimality criteria methods (1) in the early 70's may be considered as a great contribution in the field of engineering optimization. It provides major improvements over other optimization methods currently in vogue. The significant advantage of the method is that the number of iterations required for convergence to an optimum (or psuedo-optimum) design is largely independent of the number of design variables which is, in fact, the downfall of pure mathematical programming techniques (4,16,18). For many single constraint optimization problems, the optimization principle may be simply stated as: the optimum structure is one in which the average strain energy density when combined with the kinetic energy density is the same for all of the constituent members. Most publications define the multiple constraint optimality criteria in simple terms based on an approximation of the energy density

calculations (8,10). The current project has extended the state-of-the-art of the optimization algorithm for multiple constraints.

Recursion relationships provide a means of using numerical procedures to resize the structural members based upon the aforementioned optimality principle. The early work indicated that the combined strain and kinetic energy densities could become quite inconsistent for individual members (13). This inconsistency has been eliminated, and the resizing procedures are now quite reliable.

B. SENSITIVITY ANALYSES

The optimality criteria approach to optimization is heavily dependent upon the accurate calculation of the constraint gradients. These gradients are determined numerically using several different methods. Within optimality criteria methods the virtual load technique is prevalent, whereas, the pseudo-load technique is used within most mathematical programming approaches (32,33). Also, certain types of constraint gradients are best handled through direct equations developed from differentiation of their structural response equations.

The majority of computing effort is concentrated in the determination of these gradients, therefore, these techniques were studied and modified in order to make the best use of the three-dimensional analysis package.

The work presented uses all three numerical procedures in order to find the constraint gradients. Depending on the type of constraint, an approach was chosen which would provide accurate gradients with the least computational effort.

C. STRUCTURAL ELEMENTS AND MODELS

The structural elements and models used were based upon the analysis package taken from INRESB-3D (34). This computer program was initially developed as a three dimensional, inelastic analysis program with time-step dynamic capabilities. The static, elastic analysis portion of the program, as well as the element types were used in the development of the presented work.

The structural elements can be divided into two categories: steel elements and concrete elements. There are three types of steel elements: the beam-column, the beam, and the brace; and there are two types of reinforced-concrete elements: the beam-column and the flexural panel. Each element type has its own set of allowable local degrees of freedom which are dictated by the structural model used.

The structural model used within INRESB-3D was developed with computational efficiency as its goal. Each structure uses a rigid (in plane) slab system in order to represent the planar response with three degrees of freedom. The slab is assumed to be flexible in the

out of plane directions in order to allow vertical deflections at each structural node. A reduced stiffness matrix is found by condensing the rotational degrees of freedom at each structural node, and this reduced stiffness matrix is used in order to reduce the required computer storage.

Therefore, each structure can be represented with three degrees of freedom in the plane of each floor and a vertical degree of freedom at each structural node. This model provides a means of studying three-dimensional structures subjected to a variety of loadings including multi-component ground motions.

D. RESPONSE SPECTRA SEISMIC FORCES

The time-step dynamic analysis within INRESB-3D was replaced with an elastic, modal response spectra algorithm. Optimization of structural systems within the time domain is not needed, since it becomes computationally inefficient and expensive. The work presented is intended to provide a means of producing preliminary designs which do not require the precision of the time step analysis.

The response spectra analysis was developed specifically for multi-component excitations. The computer algorithm allows the use of three different response spectra for each seismic analysis which allows both translational degrees of freedom and the vertical degrees of freedom to be excited through the use of their own

response spectra. Torsional ground motions were not considered.

E. ATC-03 SEISMIC FORCES

The ATC-03 (35) provisions provide two approaches for seismic analysis, the equivalent lateral force technique and the modal analysis approach. Both approaches are based upon finding a value for the base shear and distributing this total shear to the different levels. These seismic forces are developed from a two-dimensional representation of the structure for each of two orthogonal directions, as implied by the provisions. The forces for the two directions are then combined according to the ATC-03 provisions with 100 percent of the principal direction forces and 30 percent of the orthogonal direction forces. In addition a torsional force must be applied which is based upon a 5 percent (of the base dimension) accidental eccentricity with respect to the mass center. These forces are then applied as static loads. The optimization is also treated as a static optimization problem.

F. CRITICAL PARAMETERS AND RECOMMENDATIONS

Optimization provides a consistent means of studying and comparing the effects of different structural-related parameters. The results and recommendations presented in Chapters IX and X are based upon studies performed for

several of these structural-related parameters. In addition the effects of several optimization-related parameters are discussed.

The major objective of the work was to create a three-dimensional structural optimization program which could be used to study the effects of structural-related parameters. In the broadest sense, the algorithm includes several analysis capabilities including static, modal analysis and the ATC-03 analysis procedures. Within each type of analysis several parameters have been studied such as: types of constraints, combinations of constraints, objective functions, combinations of elements, structural plans, and structural elevations. Specifically, the modal analysis was used to study multi-component excitations, and the ATC-03 provisions were used to study the effects of ATC-03 parameters such as: soil profile, geographic location, plan and vertical irregularities, ATC-03 stability function, and ATC-03 analysis techniques. Each example is discussed in detail with a brief summary of the important observations within each example. These observations are then used to make recommendation based upon the results and discussions presented.

III. STRUCTURAL ELEMENTS

ODRESB-3D (Optimum Design of 3-Dimensional Reinforced-Concrete and Steel Buildings) is a computer program developed for this work. ODRESB-3D has the options of either optimizing or simply analyzing three-dimensional structures comprised of five different types of elements. These elements are based upon the analytical features of INRESB-3D. Each type of element is characterized by its local degrees of freedom, primary and secondary design variables, construction material, and orientation. The five types of elements can be classified as steel beam-columns, beams and braces as well as reinforced-concrete beam-columns (shear walls) and flexural panels.

A. STEEL ELEMENTS

The steel element cross-sections can be regular shapes (rectangular, tubular, or circular) or irregular shapes such as I-sections. The wide-flange cross-sections are the most useful in structural design for beams and beam columns, whereas the braces can be considered as single or double angles or rods.

The beam-columns are allowed twelve local degrees of freedom. Each element has three translational and three rotational degrees of freedom at each node as shown in Figure 1. Therefore, the analysis requires each beam-column to be represented by six geometric,

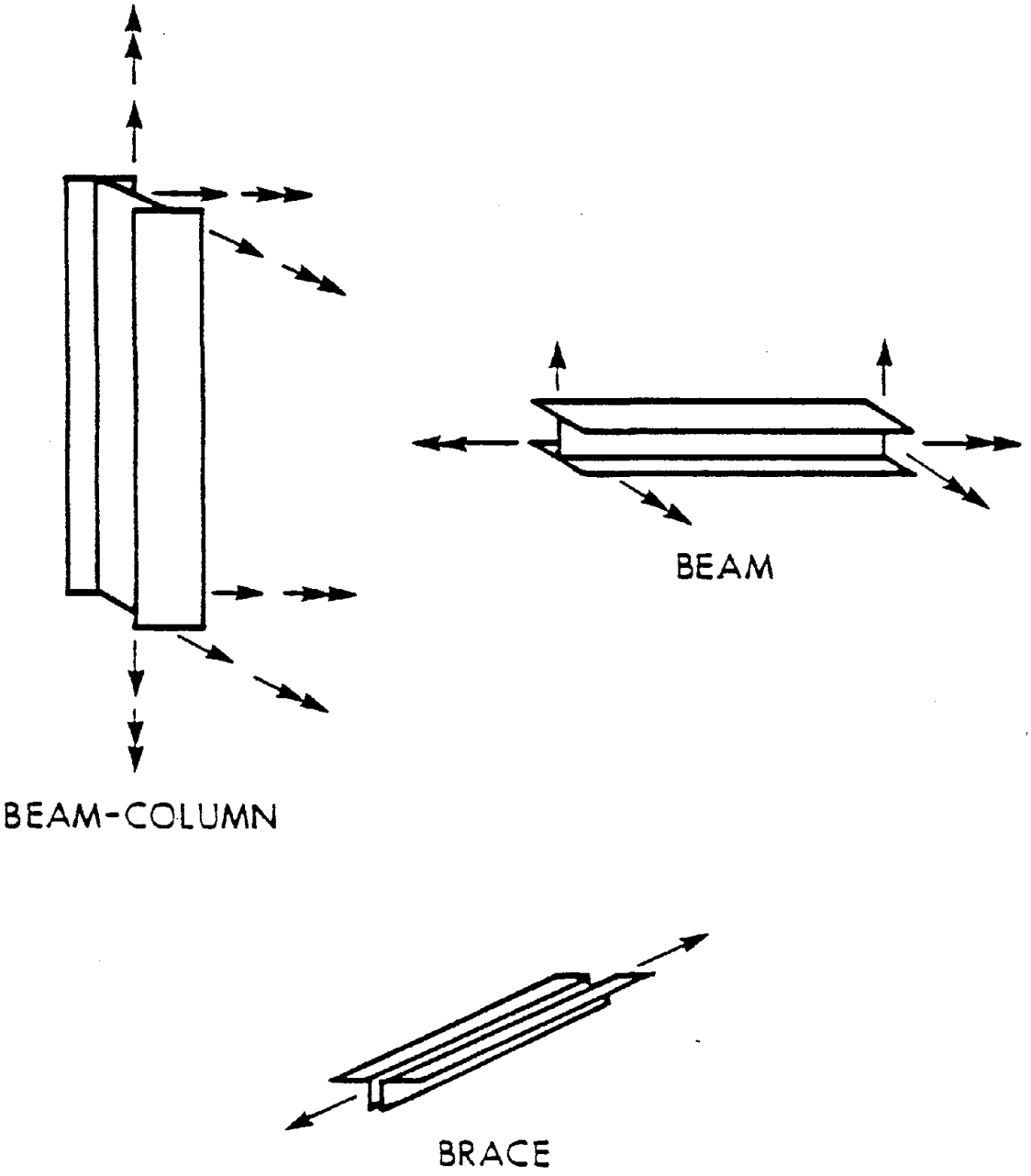

Figure 1. Steel Elements with the Elemental Degrees of Freedom

cross-sectional properties: the major-axis, minor-axis, and torsional moments of inertia, major-axis and minor-axis section modulii, and the cross-sectional area.

The beams are allowed six elemental degrees of freedom. Each beam has one degree of translation and two degrees of rotation at each node as shown in Figure 1. Therefore, the analysis requires each beam to be represented by three geometric properties: the major-axis moment of inertia, section modulus, and the torsional moment of inertia.

The steel braces have two degrees of freedom. Each element node is allowed to displace along the axis of the member as shown in Figure 1. Therefore, the cross-sectional area is the only geometric property required to represent a brace.

B. REINFORCED-CONCRETE ELEMENTS

The concrete elements are based upon the following assumptions. The elements must be rectangular (or square) with a fixed depth, h. The steel must be equally distributed along the major and minor axes with the amount of steel based upon the chosen value of ρ, the percentage of steel per the gross cross-sectional area. Also, the cracking depth is based upon the theory of working stress for bending about a single axis.

Both the concrete panels and beam-columns use the same working stress theory in order to determine their

cross-sectional properties (36). The panels have six degrees of freedom while the beam-columns are allowed twelve degrees of freedom as shown in Figure 2. Each corner of the panel is allowed to translate in the vertical direction, while the upper and lower faces of the panel are allowed to rigidly displace in the horizontal direction as sketched in the figure. This requires each panel to be represented by three geometric properties: the major-axis moment of inertia, the major-axis section modulus, and the cross-sectional area. The reinforced-concrete beam-columns have the same degrees of freedom as the steel beam-columns and require the same six geometric properties in order to represent the element.

The working stress model is based upon the transformed cross-sections shown in Figure 3. The transformed cross-sectional properties can be derived as

$$I_x = \frac{1}{3}b(kd)^3 + (n-1)\ A_s(kd-d')^2 + n\ A_s(d-kd)^2 \qquad (3.1)$$

$$I_y = \frac{1}{3}h(kb')^3 + (n-1)\ A_s(kb'-b")^2 + n\ A_s(b'-kb')^2 \qquad (3.2)$$

$$A_t = b(kd) + (n-1)\ A_s + nA_s \qquad (3.3)$$

where

$$A_s = \rho bd \qquad (3.4)$$

$$d = Ph \qquad (3.5)$$

$$d' = (1-P)h \qquad (3.6)$$

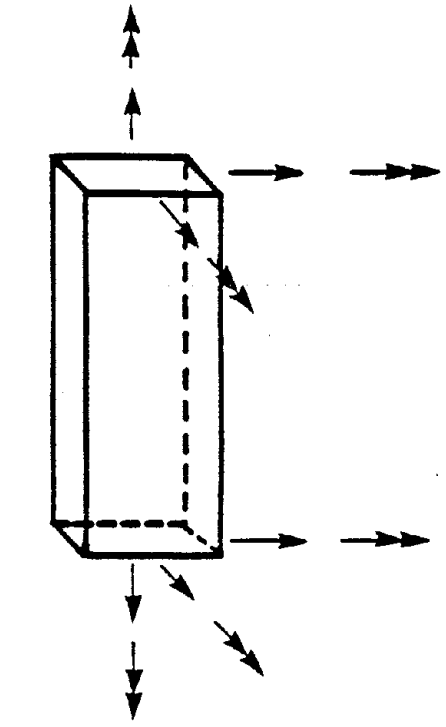

BEAM-COLUMN

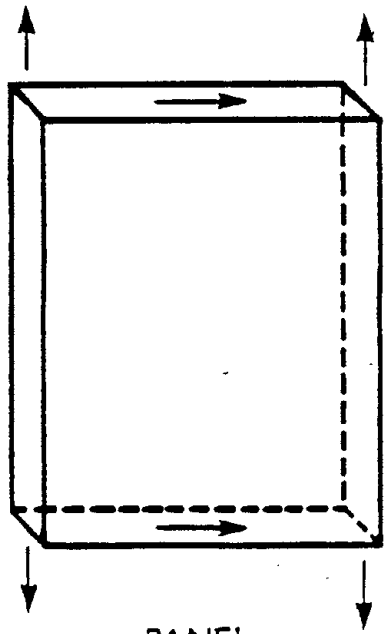

PANEL

Figure 2. Concrete Elements with the Elemental Degrees of Freedom

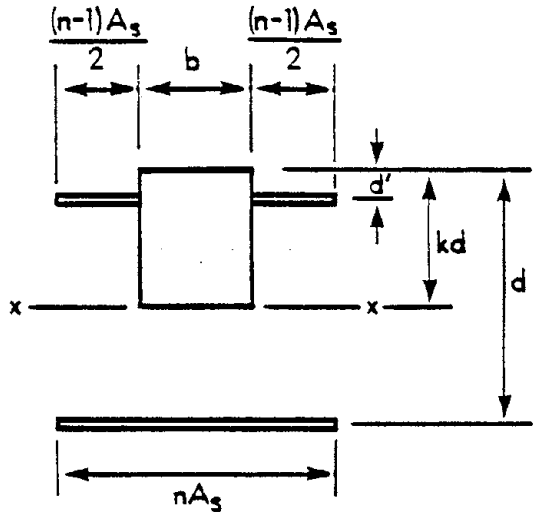

(a)

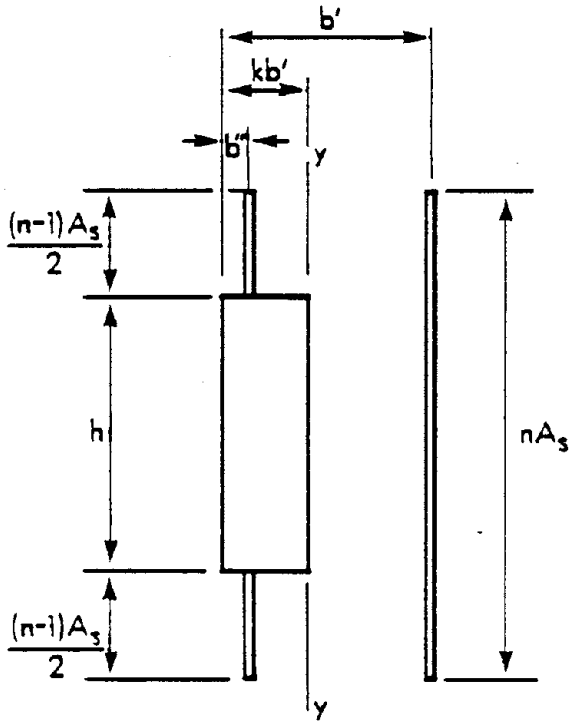

(b)

Figure 3. Transformed Concrete Elements with Respect to a) the Major-axis and b) the Minor-axis

$$k = \left(\frac{f_c}{f_c + f_s}\right) \tag{3.7}$$

$$n = E_s/E_c \tag{3.8}$$

in which E_s, is Young's modulus for steel, E_c, is Young's modulus for concrete, f_s, is the working stress for steel and, f_c, is the working stress for concrete which provides the following equation in terms of ρ, the percentage of steel, P, the percentage of the depth to the lumped steel, k, the percentage of the effective depth for the cracked section based upon the position of the lumped steel, n, the modular ratio, b, the variable width, and h, the fixed depth as

$$I_x = bh^3 \left[\tfrac{1}{3}(kP)^3 + (n-1)\rho P(P(k+1)-1)^2 + n\rho P^3(1-k)^2\right] \tag{3.9}$$

$$I_y = hb^3 \left[\tfrac{1}{3}(kP)^3 + (n-1)\rho P(P(k+1)-1)^2 + n\rho P^3(1-k)^2\right] \tag{3.10}$$

$$A_t = Pbh\,[k+2n\rho-\rho] \tag{3.11}$$

Note that the terms in the brackets are independent of the dimensions of the cross-section, therefore greatly simplifying the equations to a constant times the relationship between the depth and width. The assumptions required by this formulation are: 1) uniform distribution

of steel with respect to the major and minor axes, 2) no interaction with respect to the bending about both axes, 3) fixed depth with a variable width, and 4) no tensile strength associated with the concrete. These assumptions are somewhat restrictive, but do not hamper the use of the elements within the optimization.

C. PRIMARY VS. SECONDARY DESIGN VARIABLES

Pure mathematical optimization of a structural system would require each geometric property to be used as a design variable. In other words, this procedure would prefer to find the most efficient set of geometric properties for each element which would optimize the structural system while maintaining the structural response within the given limits. Although this might be the most efficient system for the given objective function, the set of geometric properties most likely will not represent a cross-section which is realistic. As an example, if the structure needed very little axial strength in most of the columns yet needed considerable bending resistance the optimization would produce columns with a very small cross-sectional area and a very large moment of inertia. As the optimization pushes these properties to their extreme, it would be difficult to find an appropriate wide-flange or reinforced-concrete cross-section to satisfy both conditions. Also, in the

optimization process each design variable is an unknown quantity, and just as in a structural problem a slight increase in the number of unknowns (degrees of freedom) can cause a much larger increase in computational efforts. Because of these reasons, a model was developed for both the steel and concrete elements which would allow each element to be represented by one geometric property called the primary design variable. All other geometric properties other than the primary design variable are defined as secondary design variables. The model provides a continuous relationship between the primary and secondary design variables. Similar approaches have been used for regular shapes which produce an exact relationship between the primary and secondary design variables (37), and for irregular shapes using polynomials as a psuedo-discrete approximation (38).

The model developed produces an exact relationship for regular shapes and the reinforced-concrete elements, while providing an approximate relationship for steel wide-flange sections. All element types except the braces use the major-axis moment of inertia as their primary design variables. Whereas, the brace uses its cross-sectional area. Each secondary design variable is represented in this form

$$S_{ij} = C_{1j} \, \delta_i^{C_{2j}} + C_{3j} \qquad (3.12)$$

where S_{ij} is the j^{th} secondary design variable for the i^{th} element, C_{1j}, C_{2j}, and C_{3j} are the appropriate constants, and δ_i is the i^{th} element primary design variable, (i.e., the major-axis moment of inertia, etc.).

1. Regular Cross-sections. Several different techniques can be used to determine the constants in Equation 3.12. For most regular cross-sections such as pipes, rectangular, and circular shapes these constants can be determined exactly. For example a rectangular cross-section with a fixed ratio of depth to width of R provides a set of equations for the minor-axis moment of inertia and the cross-sectional area as

$$I_y = \frac{1}{R^2} I_x \tag{3.13}$$

$$A = \left(\frac{12}{R}\right)^{1/2} I_x^{1/2} \tag{3.14}$$

2. Steel Wide-flange Sections. The primary and secondary design variables associated with steel wide-flange sections are of the psuedo-discrete variety. The actual values are discrete but are approximated with a continuous spectrum of sizes.

The constants for the steel wide-flange elements were determined in order to give an upper bound for each of the secondary design variables. It is important to note that these equations do not provide a one to one correspondence for the primary and secondary design variables with respect

to a specific wide-flange cross-section. In other words the final values for these primary and secondary design variables will not yield a specific wide-flange section as found in the American Institute of Steel Construction Manual (AISCM)(39). Reasonable judgement coupled with the optimization information must be used in order to select the appropriate wide-flange cross-section for each element. The equations determined from the AISC Manual for wide-flange shapes are

$$I_y = 0.0389\ I_x^{0.925} \tag{3.15}$$

$$J = 0.0221\ I_x^{0.958} \tag{3.16}$$

$$A = 0.5008\ I_x^{0.487} \tag{3.17}$$

$$S_x = 0.4531\ I_x^{0.774} \tag{3.18}$$

$$S_y = 0.0423\ I_x^{0.732} \tag{3.19}$$

for $I_x < 1550\ in^4$

$$I_y = 0.0265\ I_x + 20.47 \tag{3.20}$$

$$J = 0.0124\ I_x^{0.905} \tag{3.21}$$

$$A = 0.5008\ I_x^{0.487} \tag{3.22}$$

$$S_x = 0.0462\ I_x + 78.46 \tag{3.23}$$

$$S_y = 0.0041\ I_x + 7.64 \tag{3.24}$$

for $1550 \leq I_x < 12{,}100$ in^4

$$I_y = 0.0518\ I_x + 159.1 \tag{3.25}$$

$$J = 0.0124\ I_x^{0.905} \tag{3.26}$$

$$A = 0.5008\ I_x^{0.487} \tag{3.27}$$

$$S_x = 0.0520\ I_x + 56.00 \tag{3.28}$$

$$S_y = 0.0076\ I_x + 0.566 \tag{3.29}$$

for $12{,}100$ in$^4 \leq I_x$.

These equations were determined by plotting each secondary design variable with respect to the primary design variable on log-log paper where the slope of the straight line representation becomes the constant C_{2j} in Equation 3.12 and the other two constants C_{1j} and C_{3j} can be found from the coordinates of two points on the line by solving two simultaneous equations. The curves of these equations are shown in Figures 4 to 8. If the size of the elements is to correspond to a certain type of wide-flange section, such as W36 or W14, more exact sets of equations can be derived for any subregion of the available cross-sections. These equations are best derived using curve-fitting techniques.

3. Reinforced-concrete Sections. The reinforced-concrete element equations are based upon the working stress model and should be considered as a means of finding reasonable preliminary sizes. The form of the

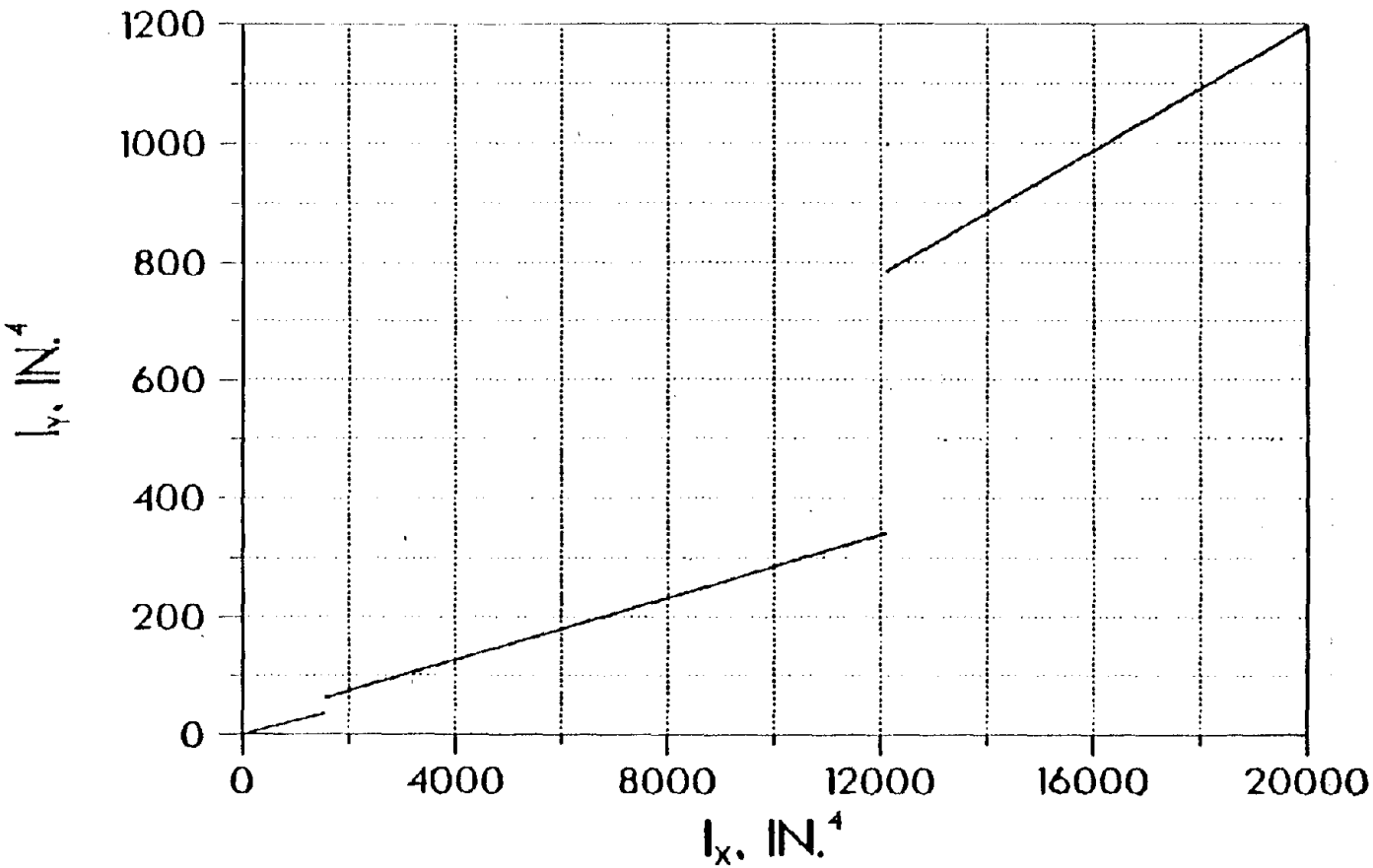

Figure 4. Minor-axis versus Major-axis Moments of Inertia for AISC Wide-flange Sections (1 in = 2.54 cm)

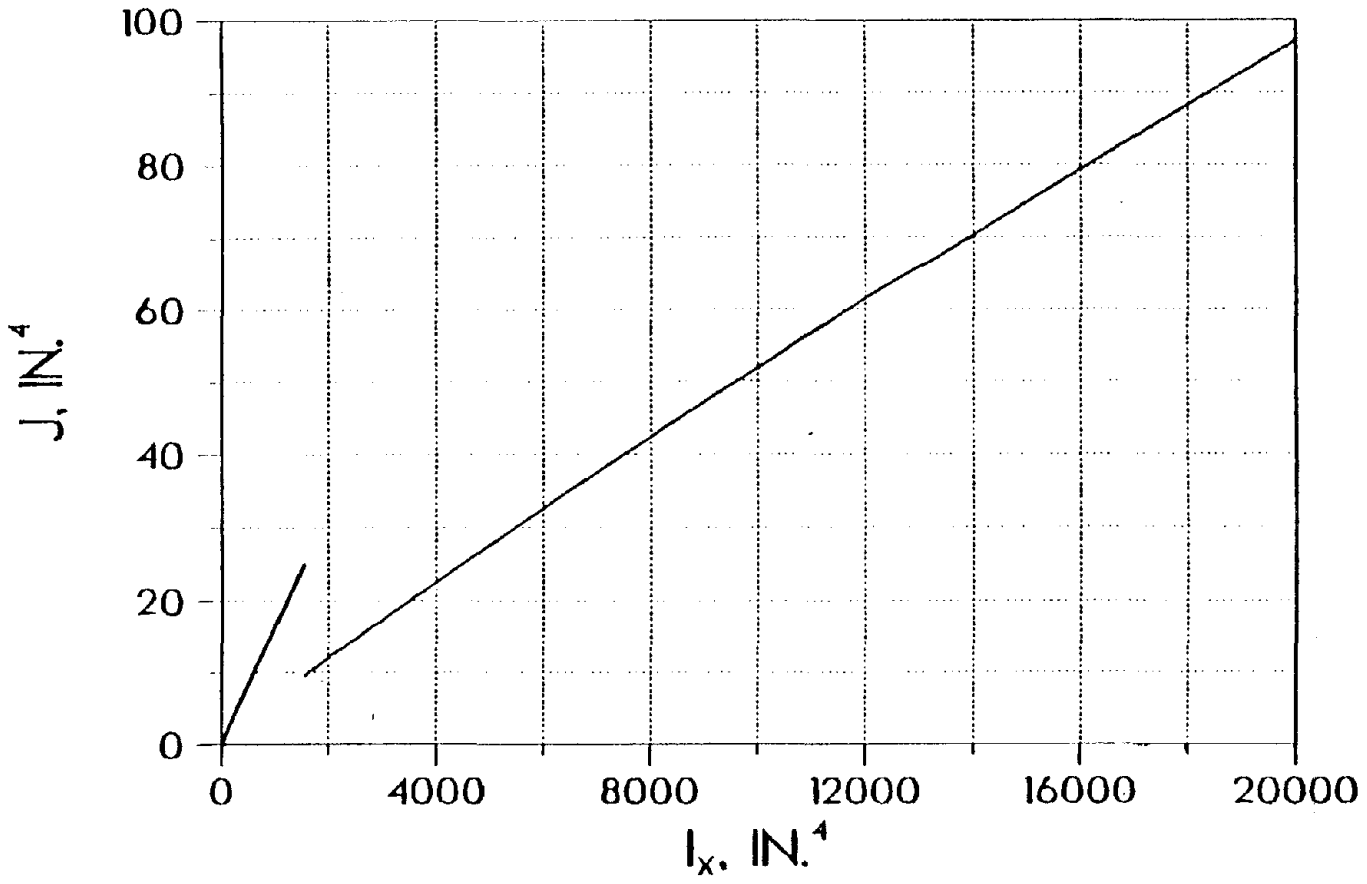

Figure 5. Torsional versus Major-axis Moments of Inertia for AISC Wide-flange Sections (1 in = 2.54 cm)

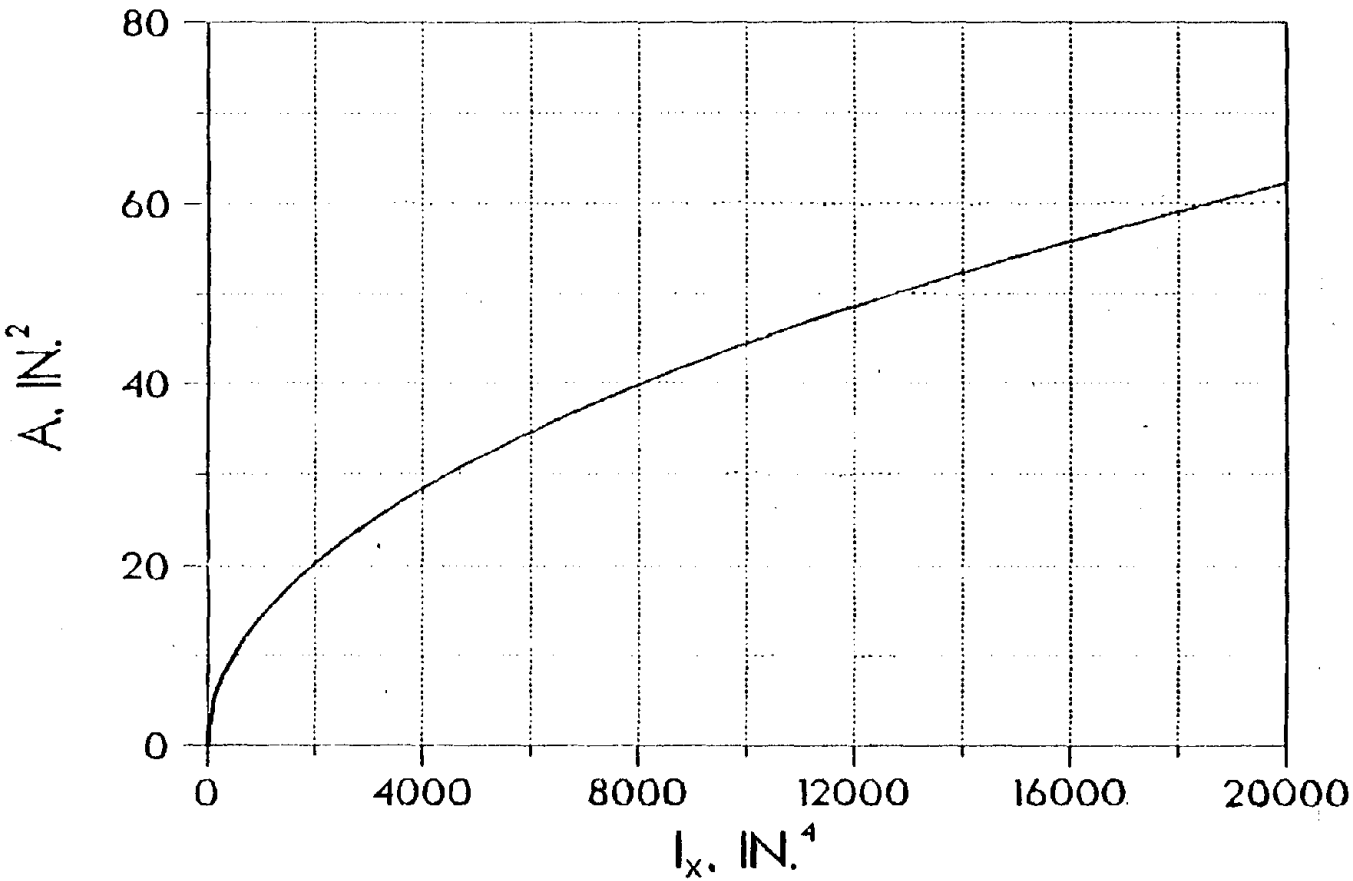

Figure 6. Cross-sectional Area versus Major-axis Moments of Inertia for AISC Wide-flange Sections (1 in = 2.54 cm)

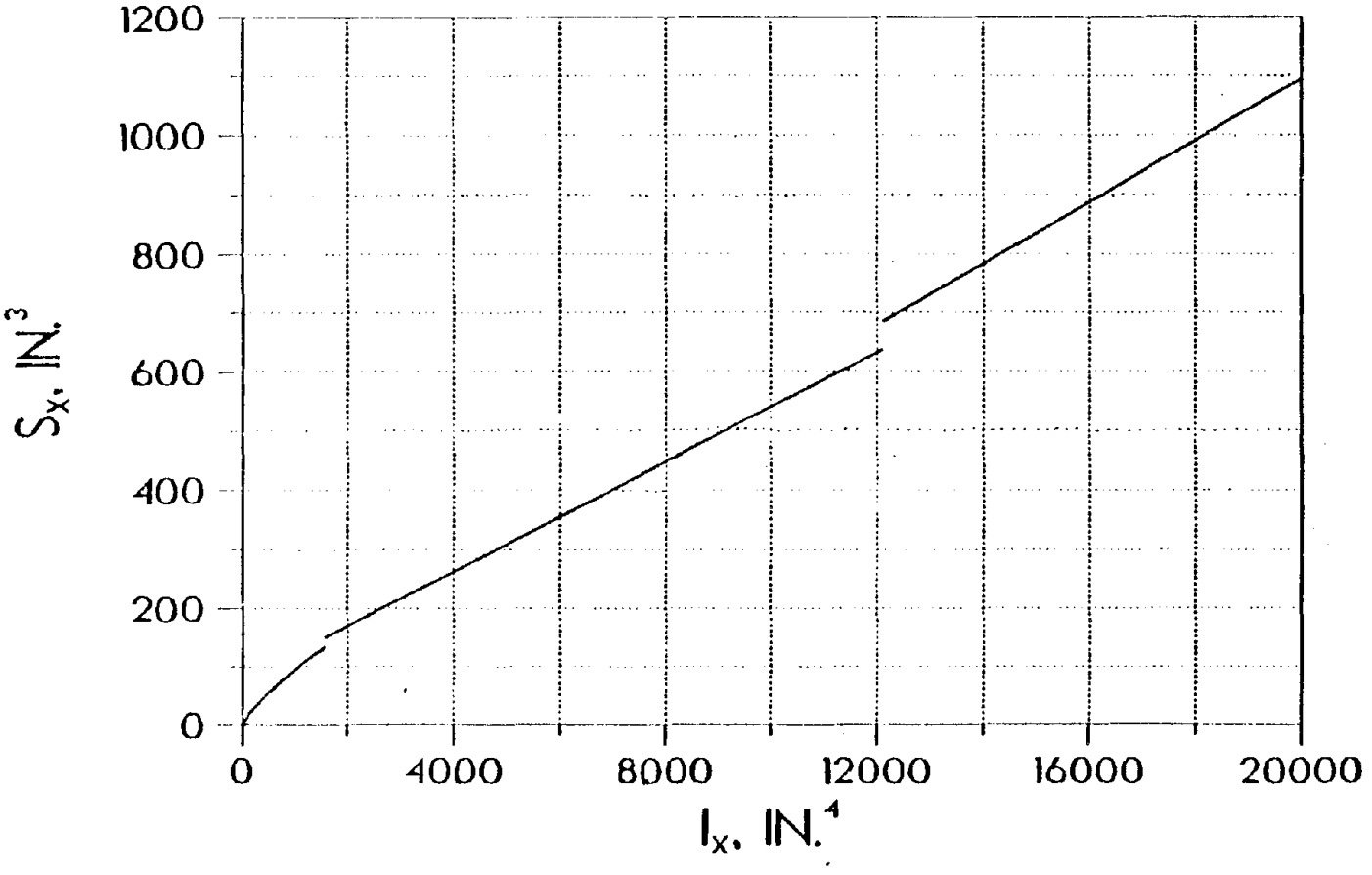

Figure 7. Major-axis Section Modulus versus Major-axis Moment of Inertia for AISC Wide-flange Sections (1 in = 2.54 cm)

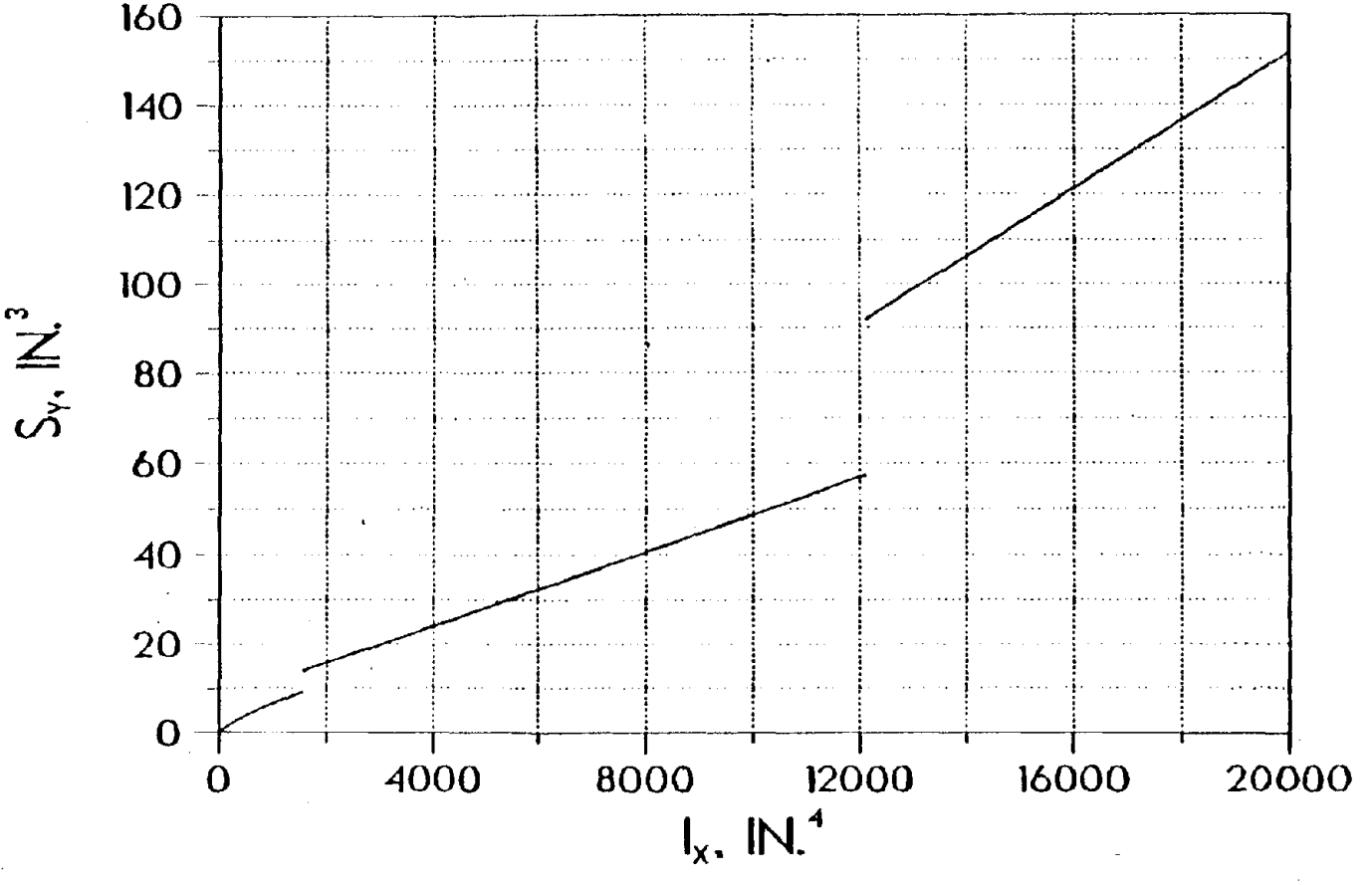

Figure 8. Minor-axis Section Modulus versus Major-axis Moment of Inertia for AISC Wide-flange Sections (1 in = 2.54 cm)

concrete equations is similar to that of Equation 3.12. The equations are based upon the theoretical derivation given in Equations 3.1 to 3.11 and are

$$I_y = \frac{1}{h^8 D^2} I_x^3 \tag{3.30}$$

$$J = \frac{1}{h^8 D^2} I_x^3 + I_x \tag{3.31}$$

$$A = (P(k+2n\rho-\rho)/h^2 D)\ I_x \tag{3.32}$$

$$A_N = \frac{1}{h^2 D} I_x \tag{3.33}$$

where I_x is the major-axis moment of inertia, A_N, is the gross concrete area, h, is the depth of the cross-section, P, is the percentage of depth to the lumped tensile reinforcement, k, is the percentage of depth for the cracked cross-section, n, is the modular ratio, ρ, is the percentage of steel, and D is a constant based on the given properties. The equation for D is

$$D = (Pk)^3/3 + \rho P(n-1)(P(k+1)-1)^2 + nP^3\rho(1-k)^2 \tag{3.34}$$

Equations 3.30 to 3.33 are derived by replacing the width b with its equivalent representation in terms of I_x as derived from Equation 3.9.

IV. STRUCTURAL MODEL AND ANALYSIS

A. ASSUMPTIONS AND MODELLING

Structural optimization is an iterative process due to the nonlinear expressions associated with the structural response, the objective function, and the design variables. It becomes important to generate a structural model which will provide an efficient solution with a reasonable amount of computing time. Therefore, using the elements as described previously and making several appropriate assumptions, a structure can be represented with a small number of global degrees of freedom.

1. Global Degrees of Freedom. The characteristics of the global degrees of freedom are consistent with the local degrees of freedom for each of the elements previously described. For instance, each floor is assumed to be rigid in its own plane, while being flexible in the planes perpendicular to the slab. This assumption is why the beams are assumed not to deform axially or bend about their minor axes. The rigid slab assumption (in its own plane) allows every floor to be represented by two translational and one rotational degree of freedom in the horizontal plane. By allowing the floor to remain flexible with respect to the vertical planes, each structural node is allowed to displace vertically and

to rotate about the two horizontal axes as shown in Figure 9. Eventually these rotational degrees of freedom are eliminated through static condensation leaving each structure with a vertical degree of freedom at each node along with two translational and one rotational degree of freedom at each story as shown in Figure 10. Therefore the total number of global degrees of freedom is given by

$$D.O.F. = NC * NS + 3 * NS = NS * (NC+3) \qquad (4.1)$$

where NC, is the number of column lines, and NS, is the number of stories. These assumptions and the condensation cause a large reduction in the amount of computer space with respect to the analysis, but has some drawbacks with respect to the optimization procedures.

2. Second-order Effects. Second-order (P-delta) effects are handled with two different approaches. The static and response spectrum analyses use a separate geometric stiffness matrix, while the ATC-03 analysis uses a stability factor in order to adjust the structural response. The ATC-03 stability factor and its general approach will be discussed in Section IV.D.2.

The geometric stiffness is based upon the string stiffness technique as shown in Figure 11. The string stiffness technique assumes that the given column with

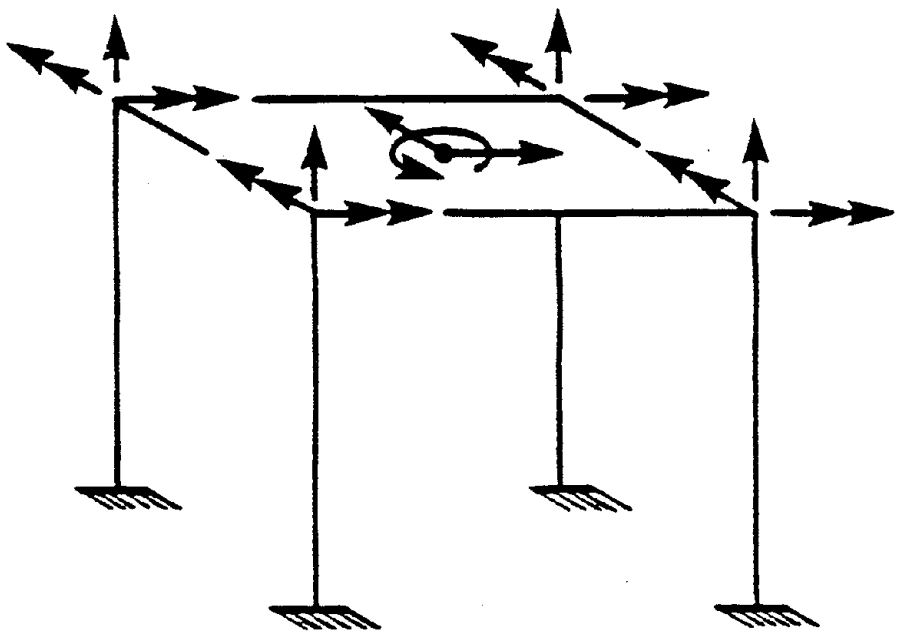

Figure 9. Global Degrees of Freedom per Floor Before Condensation

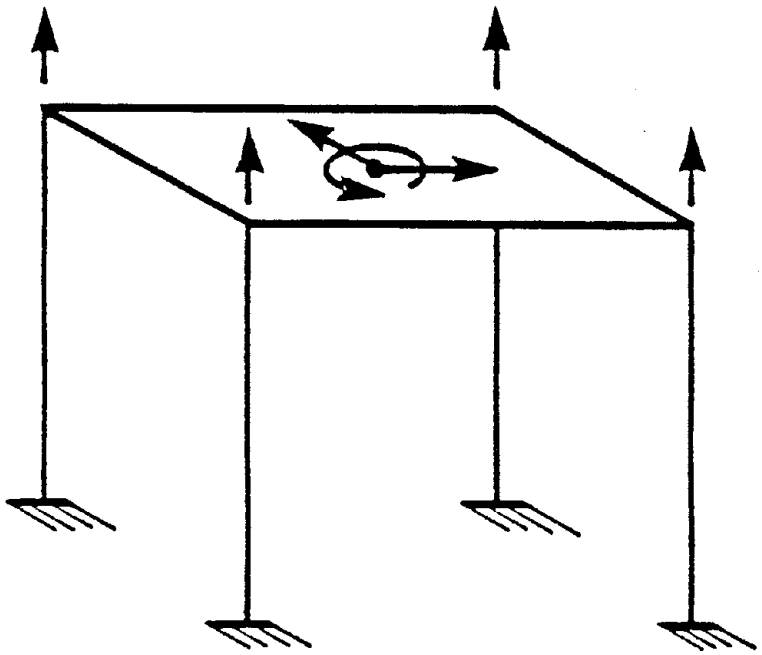

Figure 10. Global Degrees of Freedom per Floor After Condensation

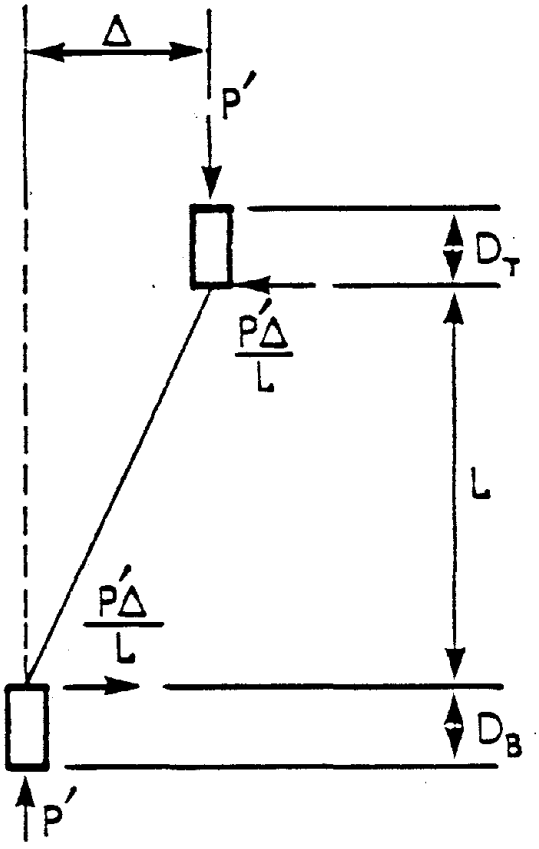

Figure 11. String Stiffness Approach to Second-order Effects

axial force, P', creates a second-order moment equivalent to the axial force multiplied by the drift, Δ. In order to enforce equilibrium an additional shear of P'/L is required, where L is the length of the flexible portion of the column. This term of P'/L is used to reduce the lateral stiffness of structure, therefore increasing the lateral deflections and increasing the internal moments. The elemental geometric stiffness becomes

$$\begin{Bmatrix} V_{xi} \\ V_{yi} \\ V_{xj} \\ V_{yj} \end{Bmatrix} = \begin{bmatrix} -P'/L & 0 & P'/L & 0 \\ 0 & -P'/L & 0 & P'/L \\ P'/L & 0 & -P'/L & 0 \\ 0 & P'/L & 0 & -P'/L \end{bmatrix} \begin{Bmatrix} x_i \\ y_i \\ x_j \\ y_j \end{Bmatrix} \qquad (4.2)$$

Note that D_T and D_B are rigid zones at the top and bottom of the column respectively. These rigid zones are included within the stiffness formulation although they were not shown in the previous description of the columns. This string stiffness is transformed and added directly to the global stiffness which is used for the static and response spectrum analyses.

3. External Stiffness. The computer program also has the option of adding external or nonstructural stiffness to the structural stiffness. These externally applied stiffnesses can be added to any one or combination of the floor degrees of freedom which act in the horizontal planes of the floors as shown in Figure 12. Therefore,

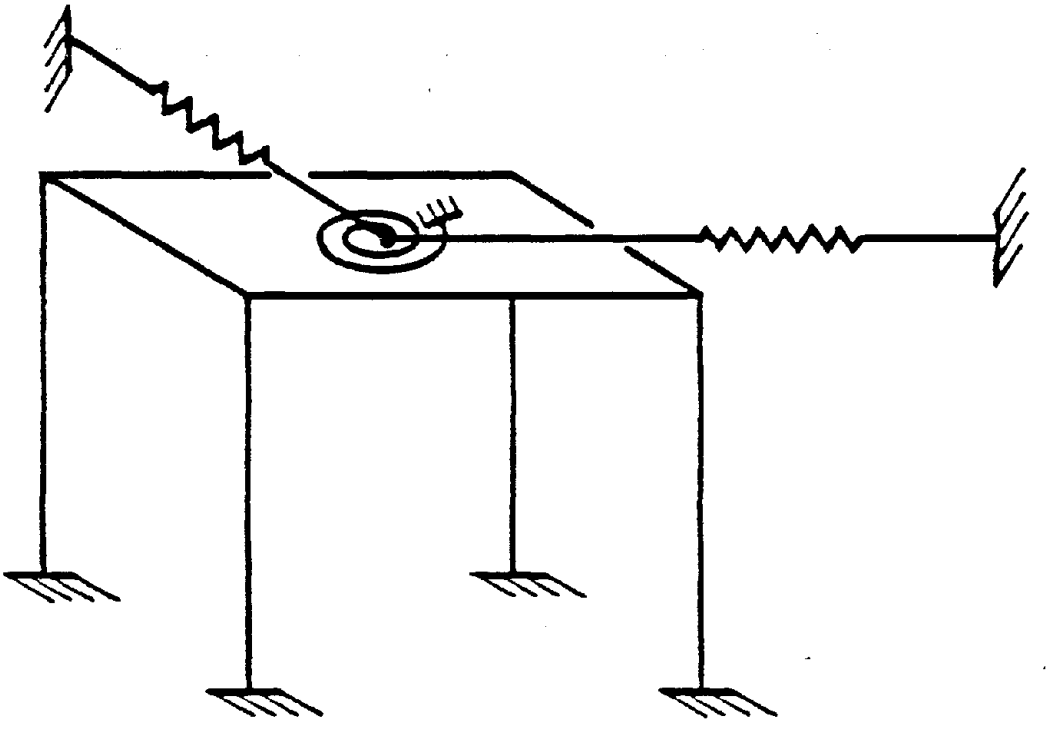

Figure 12. Allowable External Stiffnesses per Floor

the three-dimensional structures can be used to simulate two-dimensional structures by eliminating any rotational effects or by eliminating a translational component along with the rotational component of the structural response. These external stiffnesses are used when performing an ATC-03 seismic analysis as explained in Section IV.D.2.

4. Structural Mass. When a dynamic analysis is performed the structural mass matrix must be generated. A lumped mass system is used where there is mass associated with each of the global degrees of freedom. The analyses use both structural and nonstructural mass. The non-structural mass must be part of the input data, but the structural mass is generated within the program. The vertical masses are determined by summing the appropriate amounts of the total mass of each element connecting at that node and the nodal nonstructural mass. In equation form this becomes

$$M_{vk} = \frac{1}{2} \sum_{j=1}^{n} m_j + \frac{1}{4} \sum_{\ell=1}^{p} m_\ell + M'_{vk} \qquad (4.3)$$

where M_{vk} is the vertical nodal mass at node k, m_j, is the total mass of element j, n, is the total number of columns, beams, and braces joining at node k, m_ℓ is the mass of panel ℓ and p is the total number of panels joining at node k, and M'_{vk} is the nonstructural vertical mass (input data) at node k. Figure 13 shows how each type of element must

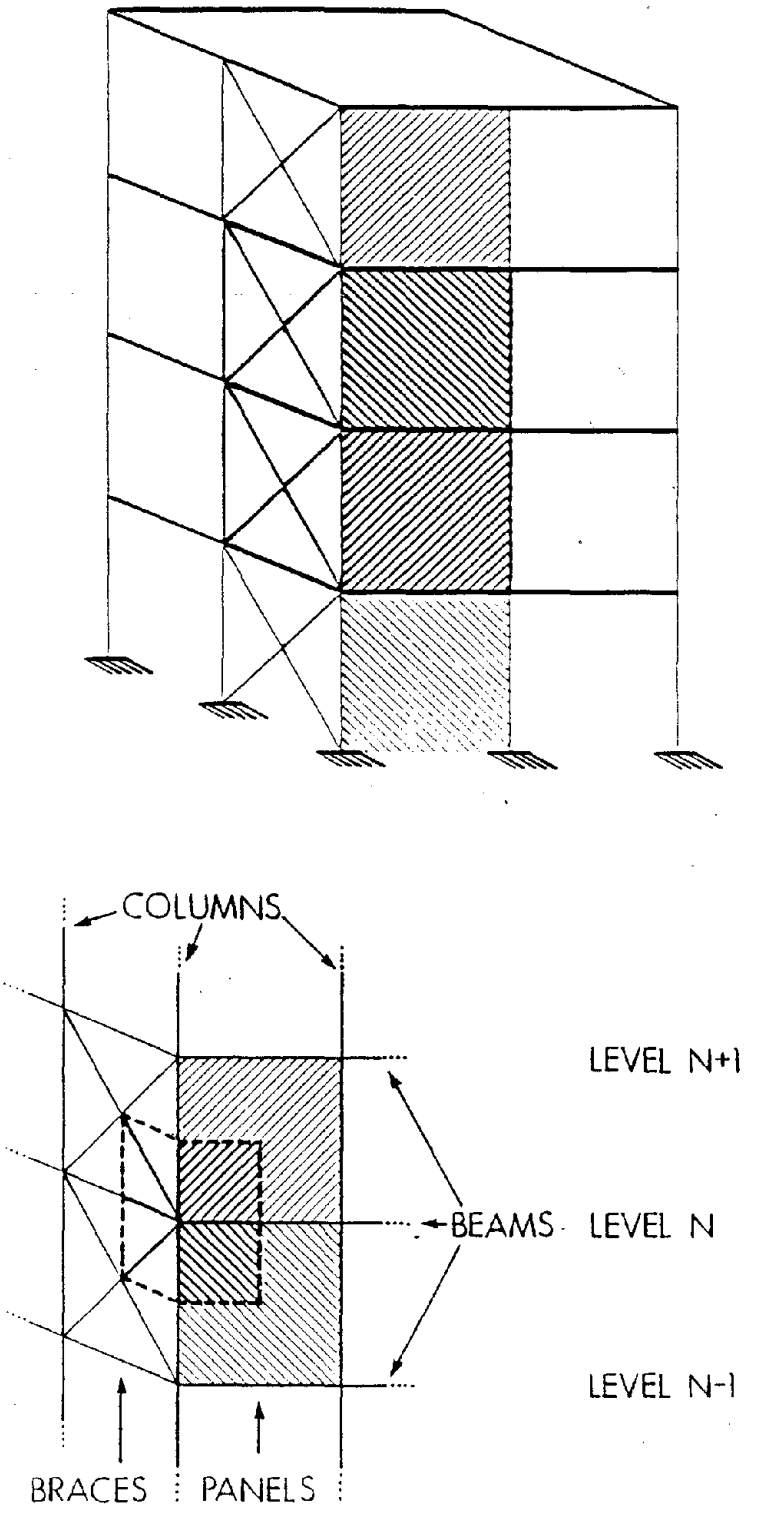

Figure 13. Elemental Contribution to the Nodal Lumped Mass

be included in the vertical lumped mass. The translational mass for each floor is the sum of the vertical structural masses and the total nonstructural mass which becomes

$$M_{Ti} = \sum_{k=1}^{q} M_{vk} + M_{Ni} = M_{Si} + M_{Ni} \qquad (4.4)$$

where M_{Ti}, is the translational mass for level i, q, is the total number of structural nodes on level i, M_{Si}, is the total structural mass for level i, and M_{Ni}, is the total nonstructural mass for level i.

The rotational mass inertia is dependent upon the distribution of the structural and nonstructural masses on each level. The structural mass is assumed to be lumped at each of the structural nodes as developed in the first two terms of Equation 4.3, and the nonstructural mass inertia is an input parameter. Therefore, the structural rotatory mass inertia is calculated within the program with this formula

$$M_{SRi} = \sum_{k=1}^{q} M_{vk}(x_k^2 + y_k^2) = \sum_{k=1}^{q} M_{vk} r_k^2 \qquad (4.5)$$

where M_{SRi} is the structural, rotatory mass inertia for level i, x_k and y_k, are the distances from the global mass center along the x and y axes for node k, and r_k is the magnitude of the position vector between the global mass center and node k. The rotatory inertia for the

nonstructural mass can be found by classical techniques as

$$M_{NR} = \int r^2 dm \tag{4.6}$$

where M_{NR} is the rotatory inertia, r, is the magnitude of the position vector from the mass center to the differential mass dm. Generally, the nonstructural mass can be assumed to be uniformly distributed over the floor which makes Equation 4.6 easier to solve since dm can be converted into a geometric property. Breaking each floor plan into regular shapes the total nonstructural, rotatory inertia can be found through a simple transformation which is similar to the parallel axis theorem and is given by

$$M_{NRi} = \sum_{e=1}^{c} (M'_{NRe} + d^2 M_{Ne}) \tag{4.7}$$

where M'_{NRe} is the rotatory inertia about element e's own mass center (these elements are the divided shapes of a floor plan), d, is the distance between the global mass center for level i and the mass center for element e, M_{Ne}, is the total mass for element e, and c, is the total number of shapes (elements) used to represent level i. The derivation of Equation 4.7 is given in Appendix A. For most structural plans the mass distribution can be represented by rectangles and triangles. This nonstructural, rotatory inertia must be given as input data.

Therefore, the total rotatory inertia about the global mass center can be given as

$$M_{Ri} = M_{SRi} + M_{NRi} \tag{4.8}$$

where M_{Ri}, represents the total rotatory inertia for level i. There is no mass associated with the condensed rotational degrees of freedom, therefore the mass matrix becomes a diagonal matrix with an associated mass for each global degree of freedom.

B. STATIC ANALYSIS

The elastic, global stiffness is assembled through a sequence of transformations. First the local degrees of freedom are transformed to member-end deformations which include the rigid zones effects. Secondly the member-end deformations are transformed to frame displacements which are located at a reference point which is a specific column line. This column line and frame coordinate system must be located such that the mass center is located in the first quadrant of the reference coordinate system. The last transformation is used to relocate the frame coordinates to a global coordinate system located at the mass center of each floor.

The transformations are handled at different stages of the analysis. The element stiffness is assembled

and transformed from local deformations to member-end deformations through this equation

$$[K]_E = [T]_E^T [K_e] [T]_E \tag{4.9}$$

where $[K]_E$ is the member-end stiffness, $[K_e]$ is the elastic-element stiffness, and $[T]_E$ is the transformation matrix which is element dependent. These element transformations are given in Reference 40.

The transformation from member-end displacements to reference coordinates is independent of the elements. This transformation converts all local degrees of freedom into two translational and a rotational degrees of freedom at the respective level. It has no effect on the vertical displacements or rotations located in the vertical planes as described earlier. This transformation becomes

$$[K]_{Ef} = [T]_{fE}^T [K]_E [T]_{fE} \tag{4.10}$$

where $[K]_{Ef}$, is the element frame stiffness and $[T]_{fE}$ is the transformation based on Figure 14 and given as

$$[T]_{fE}\left\{U^f\right\} = \begin{bmatrix} s & -c & a & 0 & 0 & 0 \\ c & s & b & 0 & 0 & 0 \\ 0 & 0 & 1 & 0 & 0 & 0 \\ 0 & 0 & 0 & s & -c & 0 \\ 0 & 0 & 0 & c & s & 0 \\ 0 & 0 & 0 & 0 & 0 & 1 \end{bmatrix} \begin{Bmatrix} U_x^f \\ U_y^f \\ U_\theta^f \\ \theta_x^f \\ \theta_y^f \\ U_z^f \end{Bmatrix} \tag{4.11}$$

where

$$a = -ys - xc$$

$$b = -yc + xs$$

$$c = \cos\theta$$

$$s = \sin\theta$$

Once this transformation has been performed for each element the stiffness for that level may be generated in terms of the reference or frame coordinates as

$$[K]_f = \sum_{i=1}^{m} [K]_{Efi} \tag{4.12}$$

where $[K]_f$ represents the stiffness in terms of the reference coordinates, and m signifies the total number of elements at floor i.

The last transformation required is to change the reference coordinates to global coordinates located at the mass center. This transformation is also element independent and becomes

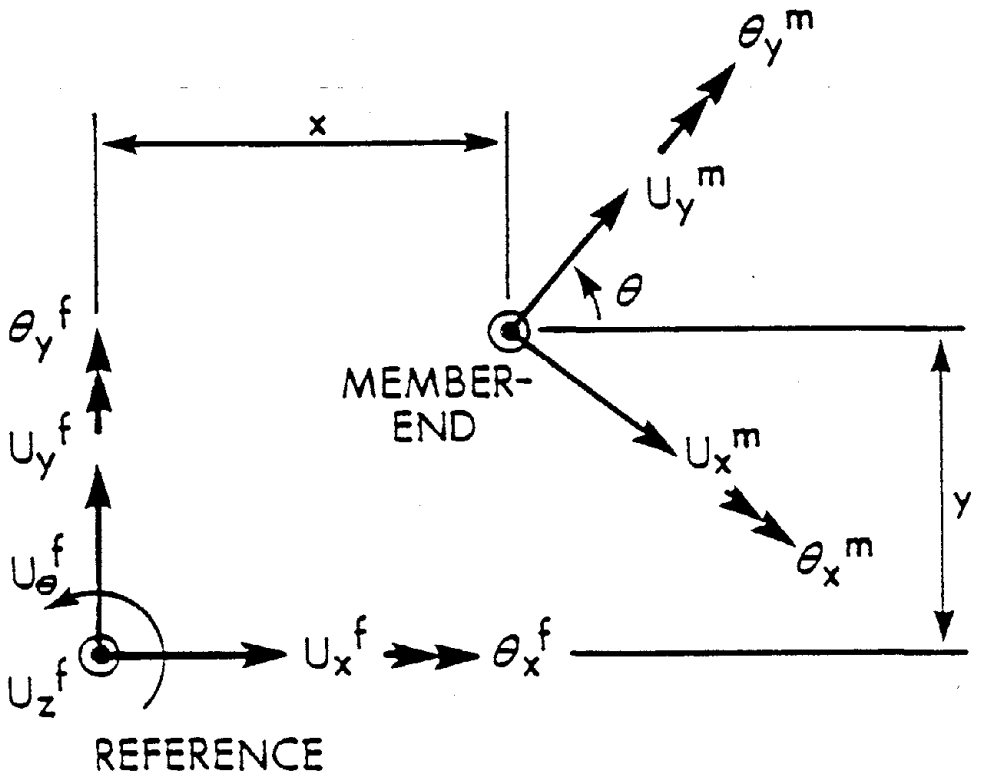

Figure 14. Transformation from Local to Reference Coordinates

$$[K]_G = [T]_G^T [K]_f [T]_G = [T]_G^T \left(\sum_{i=1}^{m} [K]_{Efi} \right) [T]_G$$

$$= \sum_{i=1}^{m} [T]_G^T [K]_{Efi} [T]_G \qquad (4.13)$$

where $[T]_G$, is formed using the transformation, $[A]_n$, based upon Figure 15 and is given by

$$[T]_G = \begin{bmatrix} A_1 & & & \\ & A_2 & & \\ & & \ddots & \\ & & & A_n \end{bmatrix} \qquad (4.14)$$

where

$$[A]_n = \begin{bmatrix} \cos\beta & \sin\beta & (-\Delta y\cos\beta + \Delta x\sin\beta) \\ -\sin\beta & \cos\beta & (\Delta x\cos\beta + \Delta y\sin\beta) \\ 0 & 0 & 1 \end{bmatrix}_n \qquad (4.15)$$

and n represents the number of levels. Note that the transformation, being element independent, can be applied to each elemental reference stiffness or to the total reference stiffness. This is important with respect to the numerical techniques employed for gradient determinations.

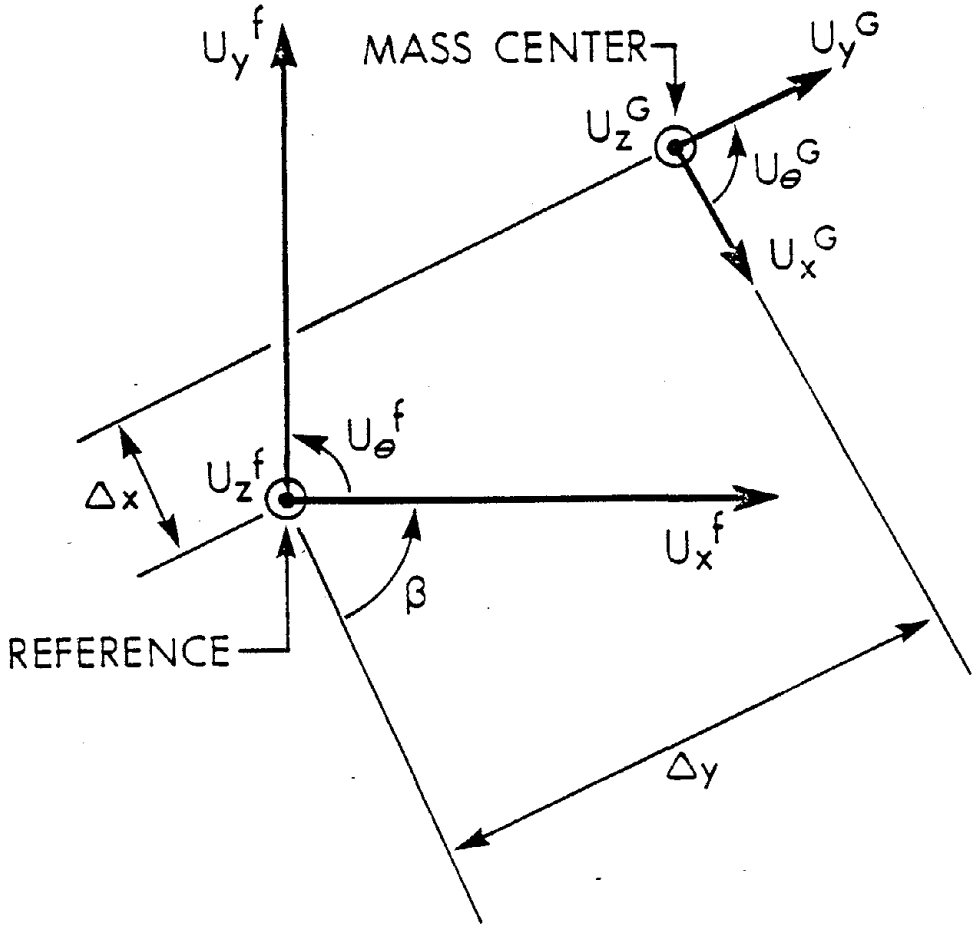

Figure 15. Transformation from Reference to Global Coordinates

The building systems considered are assumed to be linear-elastic structures. This allows each structure to be represented by the equation

$$[K][U] = [R] \tag{4.16}$$

where [K], represents the combined elastic stiffness and geometric stiffness as

$$[K] = [K]_G + [K]_g \tag{4.17}$$

[U], is the structural displacements, [R] is the matrix of loads, $[K]_G$ represents the global elastic stiffness, and $[K]_g$ is the global geometric stiffness.

Within the analysis the rotational degrees of freedom are eliminated prior to the solution of Equation 4.16. The static condensation can be performed prior to or after the global transformation and can be derived as shown

$$\begin{bmatrix} K_{11} & K_{12} \\ K_{21} & K_{22} \end{bmatrix} \begin{Bmatrix} U_1 \\ U_2 \end{Bmatrix} = \begin{Bmatrix} R_1 \\ R_2 \end{Bmatrix} \tag{4.18}$$

which forms the two equations

$$K_{11}U_1 + K_{12}U_2 = R_1 \tag{4.19}$$

and

$$K_{21}U_1 + K_{22}U_2 = R_2 \tag{4.20}$$

where U_1, is the rotational degrees of freedom, U_2, is the vertical and lateral degrees of freedom, R_1, is the fixed end forces and R_2, is the vertical and lateral loads. Since U_1 represents the rotational degrees of freedom, they can be eliminated by solving Equation 4.19 for U_1 as

$$U_1 = K_{11}^{-1}[R_1 - K_{12}U_2] \tag{4.21}$$

and substituting Equation 4.21 into Equation 4.20 gives

$$K_{21}K_{11}^{-1}[R_1 - K_{12}U_2] + K_{22}U_2 = R_2 \tag{4.22}$$

Rearranging Equation 4.22 provides

$$[K_{22} - K_{21}K_{11}^{-1}K_{12}][U_2] = [R_2 - K_{21}K_{11}^{-1}R_1] \tag{4.23}$$

where $[K_{22} - K_{21}K_{11}^{-1}K_{12}]$ represents the condensed stiffness and $[R_2 - K_{22}K_{11}^{-1}R_1]$ are the condensed loads. Since each level is only related to the levels above and below it, the assembly and reduction of the stiffness is handled story by story from the top to the bottom of the

structure (40). Back substitution is handled in the same fashion story by story from the bottom to the top of the structure.

The static load combinations are comprised of two sets of independent lateral forces and four sets of vertical forces. These six sets of forces can be combined to form at most ten loadings. The lateral loads consist of two orthogonal, concentrated loads for each level. A specific point of application must be given for each level and each set of lateral forces. The four sets of vertical forces are composed of one set of concentrated, vertical nodal loads and three sets of uniformly distributed loads. The vertical nodal loads have independent magnitudes, but must be located at a structural node producing axial loads on the columns. Each uniformly distributed load has its own magnitude and can be applied to any set of beams within a load combination. These uniformly distributed loads are considered to act along the length of the beams. Note that these uniformly distributed loads are reduced to their fixed-end forces which must be taken into account during the condensation, (R_1 in Equation 4.21). A variety of load combinations can be formed by applying load factors to the various types of forces. The typical formula would be

$$L_i = \gamma_{1i}V_1 + \gamma_{2i}V_2 + \gamma_{3i}V_3 + \gamma_{4i}V_4 + \gamma_{5i}R_5 + \gamma_{6i}R_6 \tag{4.24}$$

where L_i, is the ith load combination, γ_{1i}, ..., γ_{6i}, are the appropriate load factors, V_1, ...,V_4, are the vertical forces, and, R_5 and R_6, are the lateral forces.

C. NATURAL FREQUENCIES AND MODE SHAPES

The natural frequencies and mode shapes are needed in order to perform a modal analysis. Several points must be considered when determining which technique to be used to find the frequencies and modes. The efficiency, the flexibility, the accuracy, and programmability of the technique need to be considered when choosing an eigenvalue solver.

The natural frequencies and modes of vibration are the eigenvalues and eigenvectors associated with the generalized eigenproblem. The standard eigenproblem is of the form

$$[K][\Phi] = [\Phi][\omega^2] \tag{4.25}$$

whereas, the generalized eigenproblem is of the form

$$[K][\Phi] = [M][\Phi][\omega^2] \tag{4.26}$$

or in modal form

$$[K]\{\phi\}_j = \omega_j^2[M]\{\phi\}_j \tag{4.27}$$

where [K] is the stiffness matrix, [Φ] is the matrix of columns which represent the eigenmodes, $\{\phi\}_j$ the jth column of [Φ] or the jth eigenmode, $[\omega^2]$, is the diagonal matrix of the square of the natural frequencies, ω_j^2, is the jth row and jth column element of $[\omega^2]$ or the jth natural frequency associated with the jth mode $\{\phi\}_j$, and [M] is the mass matrix. The generalized eigenproblem becomes the standard eigenproblem if the mass matrix is taken as the identity matrix. Many methods for solving the eigensystems have been developed and reported in the literature.

Equations 4.25-4.27 suggest that the mode shape is defined only as a direction in n-dimensional space. In other words, the mode can be defined as having any magnitude with that given direction. Within the analysis presented the mode shapes are normalized with respect to the mass giving the relationship

$$\{\phi\}_i^T[M]\{\phi_j\} = \delta_{ij} \tag{4.28}$$

where δ_{ij} is the Kronecker delta. Equation 4.28 is based upon the orthonormality of mode shapes which also provides this relationship

$$\{\phi\}_i^T[K]\{\phi\}_j = \omega_i^2\delta_{ij} \tag{4.29}$$

Equations 4.28 and 4.29 can be written as

$$[\phi]^T[M][\phi] = [I] \tag{4.30}$$

and

$$[\phi]^T[K][\phi] = [\omega^2] \tag{4.31}$$

These relationships are necessarily valid with respect to eigenvalues and eigenvectors only if the $[\phi]$ matrix is of dimension equal to the total number of degrees of freedom.

It is important to note that the static condensation shown in Equation 4.23 has no effect on the eigenvalue solutions as long as no mass is associated with the condensed degrees of freedom. Partitioning Equation 4.27 provides

$$\begin{bmatrix} K_{12} & K_{12} \\ K_{21} & K_{22} \end{bmatrix} \begin{Bmatrix} \phi_1 \\ \phi_2 \end{Bmatrix} = \omega^2 \begin{bmatrix} 0 & 0 \\ 0 & M_{22} \end{bmatrix} \begin{Bmatrix} \phi_1 \\ \phi_2 \end{Bmatrix} \tag{4.32}$$

where $\{\phi_1\}$ are the modal components associated with the massless degrees of freedom and $\{\phi_2\}$ are the modal

components for the degrees of freedom with mass. Equation 4.32 provides the relationship

$$\{\phi_1\} = -[K_{11}]^{-1}[K_{12}]\{\phi_2\} \tag{4.33}$$

which can be substituted into Equation 4.32 to give

$$\left[[K_{22}]-[K_{21}][K_{11}]^{-1}[K_{12}]\right]\{\phi_2\} = \omega^2[M_{22}]\{\phi_2\} \tag{4.34}$$

or

$$[K]_R\{\phi_2\} = \omega^2[M_{22}]\{\phi_2\} \tag{4.35}$$

Unlike the static condensation, a further reduction is impossible since the right-hand side of Equation 4.35 is not given explicitly. In the static condensation presented previously the effect of the explicitly given loads can be accounted for with respect to the uncondensed degrees of freedom as shown in Equation 4.23. As shown in Equations 4.32-4.35, the accuracy of the natural frequencies and modes is not affected by the condensation but is dependent upon the distribution of the lumped mass. The mass matrix used is a diagonal mass matrix with the mass distributed as described in Section IV.A.4. One problem associated with static condensation is related to the fact that, $[K]_R$, the reduced stiffness matrix has

a larger bandwidth than the original stiffness. This increases the computational effort required for the solution of the natural frequencies and mode shapes.

Structural eigenvalue problems generally must be solved through an iterative technique, since the solution involves finding the roots of a polynomial of order equivalent to the order of the stiffness and mass. The iterative techniques can be grouped into five categories: 1) poly-vector iteration methods, 2) transformation methods, 3) polynomial iteration methods, 4) Sturm sequence property methods, and 5) combinations of the other four categories. A transformation method called the generalized Jacobi method was used (41).

The transformation methods make use of the relationships given in Equations 4.30 and 4.31 which diagonalize the stiffness and mass matrices. This diagonalization is achieved by successively pre- and postmultiplying [K] and [M] by transformation matrices $[T]_n$ which are devised in a manner to force [K] and [M] closer to a diagonal form. Therefore, the relationships become

$$[T]_n^T \ldots [T]_2^T [T]_1^T [K] [T]_1 [T]_2 \ldots [T]_n = [\omega^2] \quad (4.36)$$

and

$$[T]_n^T \ldots [T]_2^T [T]_1^T [M] [T]_1 [T]_2 \ldots [T]_n = [I] \quad (4.37)$$

where

$$[\phi] = [T]_1[T]_2 \ldots [T]_n \tag{4.38}$$

The explicit details of the generalized Jacobi method are given in Appendix B. The advantages of this technique are 1) the eigenproblem need not be transformed to the standard eigenproblem given in Equation 4.25 which is advantageous when the matrices are ill-conditioned, that is a possibility when considering the ATC-03 applied loads, 2) all eigenvalues and eigenvectors are determined (this can also be detrimental), and 3) it is simple in theory and easily programmed. The ability to handle ill-conditioned matrices was the primary reason for choosing this technique. A more effective technique might be to use one of the combination techniques such as the subspace iteration method (41) which uses the Jacobi iteration as one step in its solution. This could possibly be more effective due to the fact that it solves for any number of the lowest natural frequencies and mode shapes, whereas Jacobi iteration must solve for all eigenvectors and eigenvalues.

D. DYNAMIC ANALYSIS

1. Modal Analysis. The dynamic analysis is based upon an elastic stiffness and lumped mass system. Both

of these have been discussed in detail in Sections IV.B and IV.A.4 respectively. The basic dynamic equation for an earthquake excited structure is

$$[M]\{\ddot{U}\} + [C]\{\dot{U}\} + [K]\{U\} = -[M]\{\ddot{q}\} \qquad (4.39)$$

where [M], is the mass matrix, [C], is the damping matrix, [K], is the stiffness matrix, {U}, is the relative displacements vector, $\{\ddot{q}\}$, is the base acceleration vector, and each $\cdot$ represents one differentiation with respect to time. If the damping [C] is neglected and harmonic motion is assumed, Equation 4.39 produces the linear eigenvalue problem

$$[K][\Phi] = [M][\Phi][\omega^2] \qquad (4.40)$$

which is used to find the natural frequencies and associated mode shapes to be used within the following dynamic analyses.

Response spectrum or spectral analyses have been used with considerable success with respect to earthquake excitations of structures and structural components (42,43,44). The advantage is clearly due to the removal of the time dependence of Equation 4.39. The disadvantage is due to the conservative nature of the solution.

Response spectrums are based upon the response of a single degree of freedom system to a force which is considered to be a series of impulse loadings. This idea leads to Duhamel's integral with the form

$$U(t,\omega,\beta) = \frac{1}{\omega}\int_0^t \ddot{q}(\tau)\hat{h}(t-\tau)d\tau \qquad (4.41)$$

where ω, is the natural frequency, $\ddot{q}$, represents the base acceleration (any one of the three components), U, is the response of the structure, β, is the damping coefficient, and

$$\hat{h}(t-\tau) = e^{-\beta\omega(t-\tau)}\sin\omega(t-\tau) \qquad (4.42)$$

The different response spectra are found by taking the maximum value of the integral portion of Equation 4.41 and plotting that value with respect to ω and β. This maximum value of the integral is called the pseudo-velocity response which gives the maximum displacement as

$$q)_{max} = \frac{1}{\omega} S_v \qquad (4.43)$$

where

$$S_v = \left[\int_0^t \ddot{q}(\tau)\hat{h}(t-\tau)d\tau\right]_{max} \qquad (4.44)$$

the spectral displacement and spectral acceleration can be given in terms of the spectral or psuedo-velocity as

$$S_D = \frac{1}{\omega} S_v \tag{4.45}$$

and

$$S_a = \omega S_v \tag{4.46}$$

Since the response spectra are based on single degree of freedom systems, the multi-degree of freedom structures must be transformed into a series of single degree of freedom structures.

This transformation is accomplished by using generalized coordinates. Generalized coordinates make use of the individual mode contributions through this formula

$$\{U\} = [\Phi]\{P\} \tag{4.47}$$

where

$$\{P\} = \{P_1, P_2, \cdots P_n\} \tag{4.48}$$

are the generalized or normal coordinates. Substituting Equation 4.47 into Equation 4.89 and premultiplying by the transpose of mode shape j reduces Equation 4.39 to

$$m_j \ddot{p}_j + c_j \dot{p}_j + k_j p_j = -\{\phi\}_j^T [M] \{\ddot{q}\} \qquad (4.49)$$

which is a single degree of freedom system due to the fact that pre- and postmultiplying [M], [C], and [K] by the mode shape j provides diagonal matrices with only one element at the (j,j) location. Therefore, a set of uncoupled equations for single degree of freedom systems are formed which represent the multi-degree of freedom system.

This transformation of the multi-degree of freedom system to a set of single degree of freedom systems provides the means for using the response spectrum. Using Equations 4.43 and 4.49 the maximum response in terms of the generalized coordinates becomes

$$p_{j)max} = -\frac{\{\phi\}_j^T [M] \{\ddot{q}\}}{m_j} = -\frac{\{\phi\}_j^T [M]}{m_j \omega_j} \{S_{vj}\}$$

$$= -\frac{\{\phi\}_j^T [M]}{m_j \omega_j^2} \{S_{aj}\} \qquad (4.50)$$

Note that S_{vj} and S_{aj} can have different components for the two horizontal and vertical components. When the mode shapes, $\{\phi\}_j$, are normalized with respect to mass Equations 4.49 and 4.50 become

$$\ddot{p}_j + c_j\dot{p}_j + \omega_j^2 p_j = -\{\phi\}_j^T [M]\{\ddot{q}\} \tag{4.51}$$

and

$$p_{j)max} = - \frac{\{\phi\}_j^T [M]}{\omega_j^2} \{S_{aj}\} \tag{4.52}$$

Referring to Equation 4.47 the actual displacements can be written as

$$\{U\} = [\Phi]\{P\}_{max} \tag{4.53}$$

which is considered to be conservative since these maxima do not occur simultaneously for all modes in the multi-degree of freedom system. In order to reduce this conservative solution the square root of the sum of the squares of the contributing modes can be used to find the final displacements. The final dynamic displacements take the form

$$\{U\} = \left[\sum_{j=1}^{n} [\{\phi\}_j \ (p_j)_{max}]^2 \right]^{1/2} \tag{4.54}$$

where n is the number of contributing modes. These displacements are then used to find the elastic member forces.

As mentioned previously three separate response spectra can be used in the analysis; one for each

direction of horizontal acceleration and one for the vertical acceleration. The rotational degrees of freedom for each floor are assumed to be free of the dynamic excitation.

The computer program requires acceleration spectra to be input as polynomials of the fourth degree or less. These polynomials are of the form

$$S_{a_k}(T)/a_{max} = C_1(T-C_6)^4 + C_2(T-C_6)^3 + C_3(T-C_6)^2 + C_4(T-C_6) + C_5 \quad (4.55)$$

where $S_{a_k}(T)$, is the acceleration response at period T in the kth direction, a_{max} is the maximum ground acceleration, and $C_1,\ldots,C_6$ are appropriate constants. The equations for the acceleration response spectrum shown in Figure 16 are

$$(S_a/a_{max}) = -26.14T^2 + 13.94T + 0.935 \quad (4.56)$$

for $T \leq 0.4$ sec. and

$$(S_a/a_{max}) = 0.1606(T-0.4)^4 - 1.141(T-0.4)^3 + 2.996(T-0.4)^2 - 3.618(T-0.4) + 2.229 \quad (4.57)$$

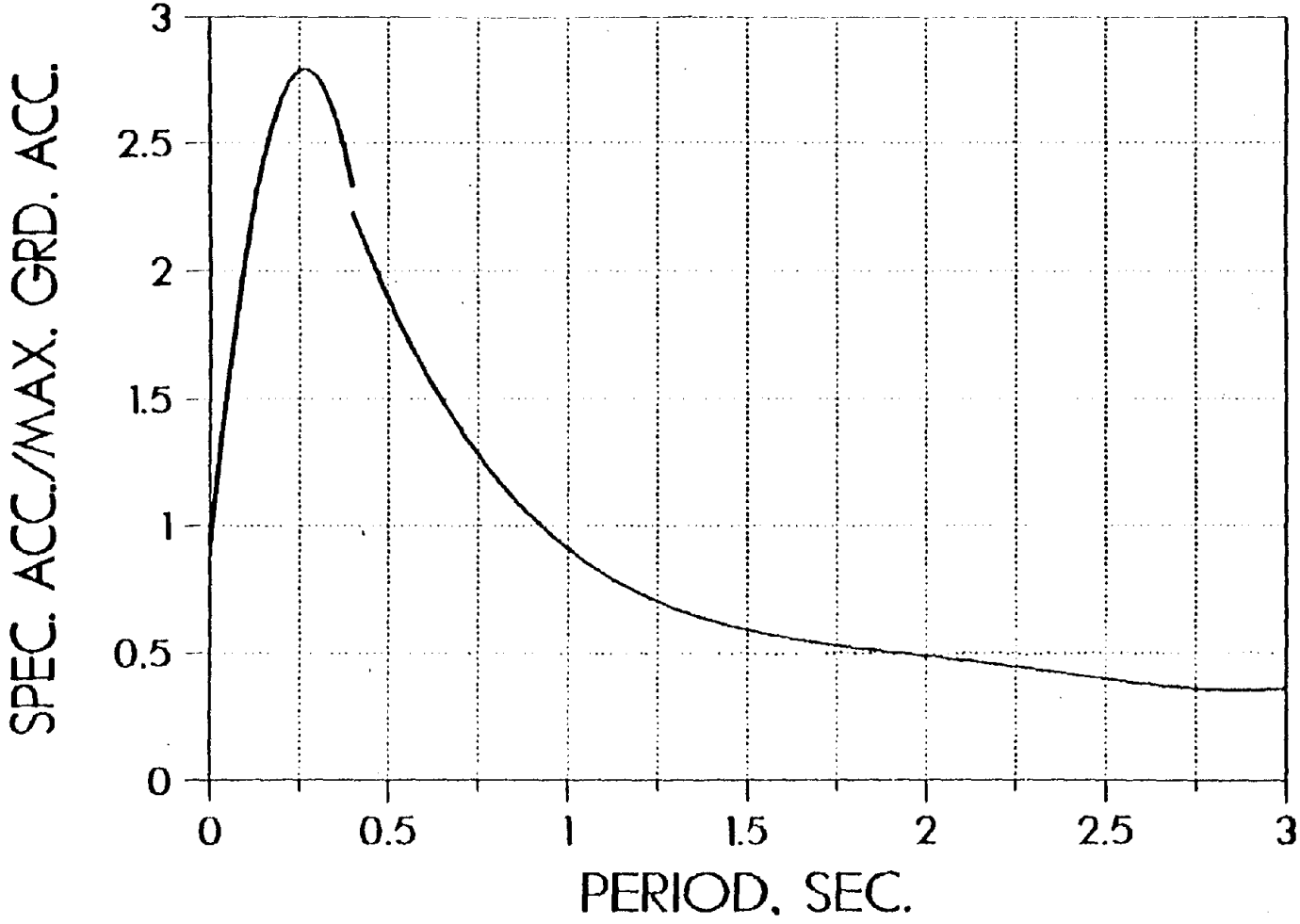

Figure 16. Typical Acceleration Response Spectrum

for T > 0.4 sec. This form was chosen in order to provide an adequate numerical representation of the spectrum and to provide a simple technique for finding the slope of the acceleration spectrum at a given period, which is needed within the optimization.

2. ATC-03 Analysis. The ATC-03 tentative provisions (35) provide two options for determining the lateral forces to be used for finding the seismic structural response. The two approaches are called the equivalent lateral force and modal analysis approaches. Both approaches assume the structures to be analyzed as two dimensional structures. This requires two analyses for each three-dimensional structure, one being in each of the two orthogonal directions. In order to simulate a two-dimensional system, a large external stiffness must be applied with respect to the torsional and a translational degree of freedom at each level, while allowing translation in one direction along with the vertical displacements at each node. The ATC-03 also requires that the principal direction of excitation have a five percent (of the base dimension) "accidental" eccentricity from the mass center. The final design is based upon the principal direction forces (including the eccentricity) plus thirty percent of the orthogonal direction forces. The ATC-03 also requires these load combinations

$$1.2Q_D + 1.0Q_L + 1.0Q_S \pm 1.0Q_E \quad (4.58)$$

or

$$0.8Q_D \pm 1.0Q_E \quad (4.59)$$

where Q_D, is the dead load, Q_L, is the live load, Q_S, is the snow load, and Q_E is the ATC-03 earthquake loads.

The equivalent lateral force technique is based upon the weight distribution coupled with the story height. The base shear, V, and mth level lateral force, F_m, are given as

$$V = C_S W_T \quad (4.60)$$

and

$$F_m = C_{vm} V \quad (4.61)$$

where C_S, is the seismic design coefficient which depends on the soil conditions, building site, fundamental period, and response modification factors as given in the ATC-03 provisions, W_T, is the gravity load of the building, and C_{vm}, is the shear distribution factor for the mth level. C_{vm} is given by this formula

$$C_{vm} = \frac{w_m h_m^k}{\sum_{i=1}^{n} w_i h_i^k} \tag{4.62}$$

where w_m and w_i are the portion of the weight assigned to level m or i, h_m and h_i, are the respective heights above the base to level m or i, and k is an exponent related to the building period ($1 \leq k \leq 2$). The lateral forces given in Equation 4.61 are used to find the displacements which are used to determine the elastic member forces.

The ATC-03 modal analysis procedure is based upon the weight distribution and mode shapes of the system being considered. The base shear for mode j, V_j, and the mth level lateral force for mode j, F_{mj}, are given as

$$V_j = C_{sj}\bar{W}_j \tag{4.63}$$

and

$$F_{mj} = C_{vmj}V_j \tag{4.64}$$

where C_{sj}, is the modal seismic design coefficient which depends upon the soil conditions, building site, fundamental period and response modification factor, $\bar{W}_j$, is the effective modal gravity load determined as

$$\bar{W}_j = \frac{\left[\sum_{i=1}^{n} \omega_i \phi_{ij}\right]^2}{\sum_{i=1}^{n} \omega_i \phi_{ij}^2} \tag{4.65}$$

and C_{vmj}, is the jth mode shear distribution factor for the mth level which is given by

$$C_{vmj} = \frac{W_m \phi_{mj}}{\sum_{i=1}^{n} W_i \phi_{ij}} \tag{4.66}$$

where ϕ_{mj} and ϕ_{ij} are the mth and ith level components of the jth eigenvector, and W_m and W_i are the portions of W_T assigned to level m or i. The final design values for base shear, story shears, and deflections are combined by using the square root of the sum of the squares of each modal value.

The ATC-03 provisions have their own method for including P-delta effects, called the stability coefficient, which is determined by using the formula

$$\theta = \frac{P_x \Delta}{V_x h_{sx} C_d} \tag{4.67}$$

where P_x, is the total gravity load above level x, Δ, is the story drift, V_x, is the seismic shear force acting between levels x and x-1, h_{sx}, is the story height below

level x, and, C_d, is the deflection amplication factor. If the stability coefficient is greater than one-tenth, the story drift is to be multiplied by the factor $(1+a_d)$ in order to take into account the second-order effects. The term a_d is found by using the formula

$$a_d = \theta/(1-\theta) \tag{4.68}$$

which produces a P-delta factor for the drift of the form

$$f_1 = (1 + \frac{\theta}{1-\theta}) = 1/(1-\theta) \tag{4.69}$$

The same factor is to be used for both ATC-03 analysis procedures.

The load combinations for seismic excitations include the static effects superimposed with the dynamic effects. The superposition is allowed since the building systems are assumed to remain in the elastic region. ATC-03 actually takes into account the inelastic effects through their deflection amplification factors and their response modification factors, but the ATC-03 still allows direct superposition as shown in Equations 4.58 and 4.59. The possible load combinations are the same as those given in Section IV.B for static analysis with the exception that the lateral force responses are replaced with the seismic responses. The only option this precludes is the case

where wind or some other lateral force cannot be applied simultaneously with a seismic load. This is a reasonable assumption as evidenced by most seismic codes.

V. STRUCTURAL OPTIMIZATION

Structural optimization can be defined as designing and constructing a structure at the lowest cost, with the objective of fulfilling a well-defined purpose. Research termed as structural optimization must be defined in a slightly different manner. In terms of structural research, optimization refers to the development and application of computer techniques for improving designs with respect to a distinct objective while staying within well-defined constraints. The objective can be the weight, cost, reliability, or any combination of these ideas. The constraints generally represent the structural response and member dimension limitations. No matter what objective function or constraints are chosen, the computer has become the means for finding a series of feasible designs.

The intent of this chapter is to outline the different topics associated with structural optimization. First, a general review of optimization theory will include the mathematical statement, the Lagrangian function, and the Kuhn-Tucker necessary conditions. These concepts will then be applied to the structural system previously described in order to develop an algorithm.

A. MATHEMATICAL STATEMENT

The general form of every optimization problem, be it structural or nonstructural, is the same. The mathematical problem is stated as

$$\text{minimize } O(\delta) \tag{5.1}$$

$$\text{subject to } g_j(\delta) \leq 0 \qquad \text{for } j = 1,\ldots,\ell \tag{5.2}$$

$$\underline{\delta}_i \leq \delta_i \leq \overline{\delta}_i \qquad \text{for } i = 1,\ldots,n \tag{5.3}$$

where $O(\delta)$, is the objective function, $g_j(\delta)$, are the structural response constraints, $\underline{\delta}_i$ and $\overline{\delta}_i$, are the minimum and maximum sizes for element i, ℓ, is the number of upper and lower bound constraints, n, is the total number of structural elements, and δ_i, is the primary design variable for element i.

B. LAGRANGIAN

The Lagrangian incorporates the constraints and objective into a single function. The Lagrangian is written as

$$L(\delta,\lambda) = O(\delta) + \sum_{j=1}^{\ell} \lambda_j g_j(\delta) \tag{5.4}$$

where λ_j is the Lagrange multiplier associated with the jth constraint. Mathematically, this formulation actually requires the constraints to be converted into equality

constraints. This does not require each constraint to become active (reach its upper or lower limit) but it removes the inequality associated with Equations 5.2 and 5.3.

C. KUHN-TUCKER CONDITIONS

The Lagrangian is used to derive the most important theorem of structural optimization the Kuhn-Tucker necessary conditions for an optimal solution which are given as

$$\frac{\partial L}{\partial \delta_i}(\delta^*, \lambda^*) = 0 \qquad i = 1, \ldots, n \qquad (5.5)$$

$$\lambda_j^* \geq 0 \qquad j = 1, \ldots, \ell \qquad (5.6)$$

$$g_j(\delta^*)\ \lambda_j^* = 0 \qquad j = 1, \ldots, \ell \qquad (5.7)$$

in which the * refers to a set of primary design variables, δ, and Lagrange multipliers, λ, which are associated with an optimal solution (33,45). These conditions are necessary but not sufficient conditions for a globally optimal solution. The sufficient conditions of optimality which are used in addition to the necessary conditions can be found in Reference 45.

D. OBJECTIVE FUNCTION

The objective function is the actual function to be minimized such as cost or weight of the structures. The objective function used in the computer program takes the form

$$O(\delta) = \sum_{i=1}^{n} \gamma_i V_i \tag{5.8}$$

where γ_i, is the appropriate constants of object value per unit volume for element i, V_i, is the volume of element i which is a function of the primary design variable, and n, is the total number of structural elements. The volume is related to the primary design variables through Equation 3.12 giving the relationship

$$V_i(\delta_i) = \ell_i A_i = \ell_i (C_{1A} \delta_i^{C_{2A}} + C_{3A}) \tag{5.9}$$

where ℓ_i, is the length of element i, C_{1A}, C_{2A}, and C_{3A} are the appropriate constants for the area, A_i, of element i. The constant γ_i is most often used as the specific weight or the cost per unit volume. The values for γ_i used within the examples are given in each of the respective examples. These values were determined from References 46 and 47.

E. CONSTRAINTS

Constraints represent the restrictions that the structural designer would like to impose while trying to find the optimal structural system. These constraints can be of several different types such as equality, inequality, side or linkage constraints. The equality constraints find very little use in building systems since they are generally used to enforce equilibrium and compatibility which are already enforced due to the stiffness formulation. The inequality constraints are used to place limits on structural response such as displacements, frequencies, stresses, and buckling loads. Side constraints are also inequality constraints but are generally not handled in the same mathematical manner as the structural responses. These side constraints are used to limit the size of the structural elements within a practical range. The linkage constraints (called linking) are used to force certain structural elements to have primary design variables of the same size. Linking is also handled in a different fashion than the inequality constraints. In theory any combination of these constraints can be applied to a structure, but numerically this can be difficult. This is one area in which state-of-art research is being applied. The work presented has been performed with combinations of multiple constraints with good results.

F. OPTIMALITY CONDITIONS

The optimality criteria used in the optimization algorithm is derived from the Kuhn-Tucker conditions. Using Equations 5.4, 5.5, 5.6 and 5.7 the optimality criteria becomes

$$\frac{\partial L}{\partial \delta_i} = \frac{\partial O}{\partial \delta_i} + \sum_{j=1}^{\ell} \lambda_j \frac{\partial g_j}{\partial \delta_i} = 0 \qquad i = 1,\ldots,n \qquad (5.10)$$

with

$$\lambda_j \geq 0 \qquad j = 1,\ldots,\ell \qquad (5.11)$$

$$\lambda_j g_j = 0 \qquad j = 1,\ldots,\ell \qquad (5.12)$$

Rearranging Equation 5.10 gives

$$-\sum_{j=1}^{\ell} \lambda_j \left(\frac{\partial g_j}{\partial \delta_i}\right) / \left(\frac{\partial O}{\partial \delta_i}\right) = 1 \qquad i = 1,\ldots,n \qquad (5.13)$$

which must be true along with Equations 5.11 and 5.12 when a locally or globally optimal solution is obtained. Equations 5.8 and 5.9 provide

$$\frac{\partial O}{\partial \delta_i} = \gamma_i \frac{\partial V_i}{\partial \delta_i} = \gamma_i \ell_i \frac{\partial A_i}{\partial \delta_i} = \gamma_i \ell_i C_{1A} C_{2A} \delta_i^{(C_{2A}-1)} \qquad (5.14)$$

which allows Equation 5.13 to become

$$T_i = - \left(\sum_{j=1}^{\ell} \lambda_j \frac{\partial g_j}{\partial \delta_i} \right) / \left(\gamma_i \ell_i \, C_{1A} C_{2A} \delta_i^{(C_{2A}-1)} \right)$$

$$i = 1,\ldots,n \qquad (5.15)$$

In the past structures composed of single design variable elements, such as braces, have shown that the optimality criteria represents a condition where the virtual strain energy densities become equivalent for all members. This idea cannot be supported by Equation 5.15 since the stiffness matrix is not linear with respect to a single type of design variable. This nonlinearity prohibits the development of this concept for elements which must be represented by primary and secondary design variables.

The optimality criteria shown in Equation 5.15 is the basis used to derive a convergent algorithm. As an optimal solution is approached the values of T_i, for the ith element, will approach unity giving for an optimal solution

$$T_i = 1 \qquad i = 1,\ldots,n \qquad (5.16)$$

This value of T_i provides a measure of the solution at that iteration. With this idea, it becomes logical to use T_i as a measure to help resize the elements with the use of recurrence relations. The difficulty with using the T_i values is that they are dependent upon the Lagrange

multipliers which are unknown, as well as, which constraints are to be considered active. If a reasonable method for determining the Lagrange multipliers can be found, they will help sort the active and nonactive constraints by using Equation 5.11. Assuming the Lagrange multipliers to be known, the resizing of the elements can be handled through recursive relationships.

Side constraints, which limit the size of the structural elements, are handled in a different manner than the constraints associated with the structural response. Equation 5.10 requires only the optimality criteria for those elements whose side constraints are non-active providing

$$\frac{\partial L}{\partial \delta_i} = \frac{\partial O}{\partial \delta_i} + \sum_{j=1}^{\ell} \lambda_j \frac{\partial g_j}{\partial \delta_i} = 0 \qquad i = 1,\ldots,n_1 \qquad (5.17)$$

and

$$T_i = 1 \qquad i = 1,\ldots,n_1 \qquad (5.18)$$

where n_1 represents the number of elements which are considered active (not at a maximum or minimum value). These passive elements (elements at a maximum or minimum value) are forced to take the maximum or minimum value, therefore the continuity required by the optimality criteria is no longer valid for these design variables.

Linking of elements also has an effect on Equation 5.10. Linking is used to force the primary design variables of several elements to have the same value which implies that all of these elements can be represented by one design variable. In matrix form this becomes

$$\{\delta\} = [A] \{\Lambda\} \qquad (5.19)$$
$$(nx1) = (nxm)(mx1)$$

in which $\{\Lambda\}$ is the vector of m global design variables required to represent the problem, [A], is the matrix of zeros and ones which relates each δ_i for the ith element to the appropriate global design variable, and $\{\delta\}$ is the vector of primary design variables for each element. Equation 5.17 is required for each active global design variable and can be written as

$$\frac{\partial L}{\partial \Lambda_v} = \frac{\partial O}{\partial \Lambda_v} + \sum_{j=1}^{\ell} \frac{\partial g_j}{\partial \Lambda_v} = 0 \qquad v = 1,\ldots,n_2 \qquad (5.20)$$

but the $\frac{\partial L}{\partial \Lambda_v}$ becomes

$$\frac{\partial L}{\partial \Lambda_v} = \sum_{i=1}^{s} \frac{\partial L}{\partial \delta_i} = \sum_{i=1}^{s} \left(\frac{\partial O}{\partial \delta_i} + \sum_{j=1}^{\ell} \frac{\partial g_j}{\partial \delta_i}\right)$$

$$v = 1,\ldots,n_2 \qquad (5.21)$$

where n_2 is the total number of active global design variables, and s, is the number of elemental design variables linked to Λ_v. The total effect of the global design variable is simply the sum of the effects of each elemental design variable associated with that global design variable. Note that a one to one correspondence between the global and elemental design variables (s=1) causes Equation 5.21 to degenerate to Equation 5.10 for the non-linking case.

G. RECURRENCE RELATIONS

Recurrence relations generally have been divided into two categories. The first category requires the use of an exponential form (48). For any given design variable an exponential recurrence relation can be derived by multiplying δ_i to the rth power times Equation 5.16 and taking the rth root to give

$$\delta_i^{(k+1)} = \delta_i^k (T_i)_k^{1/r} \qquad i = 1,\ldots,n \qquad (5.22)$$

where k represents the values for the kth iteration. Equation 5.22 can be rewritten as

$$\delta_i^{(k+1)} = \delta_i^k \, (1+(T_i-1))_k^{1/r} \qquad i = 1,\ldots,n \qquad (5.23)$$

The parameter r is a convergence control parameter or step size which determines how large of a change will occur

per element. The second category is to use a linear form for recurrence. A linear form can be derived by multiplying the optimality criteria in Equation 5.16 by $\delta_i(1-\alpha)$ to give

$$\delta_i^{(k+1)} (1-\alpha) = \delta_i^k (1-\alpha)T_i \qquad i = 1,\ldots,n \qquad (5.24)$$

or

$$\delta_i^{(k+1)} = \delta_i^k (\alpha + (1-\alpha)T_i)_k \qquad i = 1,\ldots,n \qquad (5.25)$$

which ignores the change in δ_i^{k+1} and δ_i^k and α is called a relaxation parameter. The value of α is used as the convergence control parameter for these relationships (32). The most widely used approach for a linear form is derived by writing the binomial expansion of Equation 5.23 and retaining only the linear terms giving

$$\delta_i^{k+1} = \delta_i^k (1 + \frac{1}{r}(T_i-1))_k \qquad i = 1,\ldots,n \qquad (5.26)$$

where the term (T_i-1) measures the error in the solution at iteration k. Note that Equation 5.25 and Equation 5.26 are related by

$$\alpha = (1 - \frac{1}{r}) \qquad (5.27)$$

The recurrence relationships given above need several pieces of information prior to their use. The convergence control parameters or relaxation parameters (r or α) must be chosen, the constraint gradients must be found, and a reasonable estimate of the Lagrange multipliers must be determined. The convergence control parameter, r, can be set equivalent to two for most applications. Certain problems which are numerically sensitive might require a larger value which in turn reduces the amount of change in the element size per iteration. This increase is also likely to increase the number of iterations for convergence, but will produce a more stable history. The gradients of the constraints and the determination of the Lagrange multipliers will be discussed in the following sections.

H. LAGRANGE MULTIPLIERS

Prior to using Equations 5.22 to 5.26 to resize the primary design variables the Lagrange multipliers needed for the optimal solution must be provided. Except for the simplest of cases, the optimal Lagrange multipliers can only be approximated. The recursive techniques generally require an initial estimate which can be difficult to assess. Other techniques can be devised in order to find Lagrange multipliers which will satisfy the optimality criteria as long as a set of probable active constraints have been chosen. The Lagrange multiplier

determination can be divided into two categories: 1) exponential recurrence relations or 2) linear equations based upon linear recurrence relations. This process is very important to the convergence, stability, and accuracy of the solution.

The first category of numerical techniques for Lagrange multiplier determination is based upon the same recurrence relationships in Equations 5.22 to 5.26. If the constraints are rewritten in two forms

$$g_j = (u_j - \bar{u}_j) \leq 0 \qquad j = 1,\ldots,\ell \qquad (5.28)$$

or

$$g_j = (\underline{u}_j - u_j) \leq 0 \qquad j = 1,\ldots,\ell \qquad (5.29)$$

where Equation 5.28 represents an upper limit constraint with $\bar{u}_j$ being that upper limit and Equation 5.29 represents a lower limit constraint with $\underline{u}_j$ being the lower limit associated with structural response u_j, and ℓ is the number of constraints. These two relationships can be written as

$$D_j = \frac{u_j}{\bar{u}_j} \leq 1 \qquad j = 1,\ldots,\ell \qquad (5.30)$$

or

$$D_j = \frac{u_j}{u_j} \leq 1 \qquad j = 1,\ldots,\ell \qquad (5.31)$$

If only active constraints are considered the inequalities become strictly equalities. Only the active constraints have non-zero Lagrange multipliers as shown by Equations 5.11 and 5.12. Equations 5.30 and 5.31 can be multiplied by the Lagrange multiplier to the zth power and then taking the zth root gives

$$\lambda_j^{(k+1)} = (D_j)^{1/z} \lambda_j^k \qquad j = 1,\ldots,\ell \qquad (5.32)$$

Note that the first iteration requires an initial estimate for $\lambda^{(1)}$. Using the same approach as was used to find Equations 5.23 and 5.26, the Lagrange multipliers can be found using

$$\lambda_j^{k+1} = \lambda_j^k \left(1 + \frac{1}{z}(D_j - 1)\right)_k \qquad j = 1,\ldots,\ell \qquad (5.33)$$

which also requires an initial estimate for the Lagrange multipliers.

The second category for finding the Lagrange multipliers requires the use of the linear recurrence relationships given in Equations 5.25 and 5.26. Using these relationships provides a means for producing a set of linear equations which can be solved for the Lagrange multipliers. The change in the jth constraint can be

written as

$$g_j(\delta+\Delta\delta)-g_j(\delta) = \sum_{i=1}^{n} \frac{\partial g_j}{\partial \delta_i} \Delta\delta_i \qquad j = 1,\ldots,\ell \qquad (5.34)$$

If g_j is assumed to be an active constraint, the change, $\Delta\delta$, should force $g_j(\delta+\Delta\delta)$ to become zero giving

$$-g_j = \sum_{i=1}^{n} \frac{\partial g_i}{\partial \delta_i} \Delta\delta_i \qquad j = 1,\ldots,\ell \qquad (5.35)$$

The change in the design variable, $\Delta\delta_i$, can be written in two forms by using Equations 5.25 and 5.26 to give

$$\Delta\delta_i = \delta_i^{k+1} - \delta_i^k = (1-\alpha)(T_i-1)_k \delta_i^k$$

$$i = 1,\ldots,n \qquad (5.36)$$

and

$$\Delta\delta_i = \delta_i^{k+1} - \delta_i^k = \frac{1}{r}(T_i-1)_k \delta_i^k$$

$$i = 1,\ldots,n \qquad (5.37)$$

Substituting Equations 5.13, 5.25. and 5.26 into Equation 5.35 gives these equations

$$-g_j = \sum_{i=1}^{n} \frac{\partial g_j}{\partial \delta_i} (1-\alpha) \left(- \sum_{p=1}^{\ell} \lambda_p \left(\frac{\partial g_p}{\partial \delta_i} \Big/ \frac{\partial O}{\partial \delta_i}\right)-1\right) \delta_i^k$$

$$j = 1,\ldots,\ell \qquad (5.38)$$

$$-g_j = \sum_{i=1}^{n} \frac{\partial g_j}{\partial \delta_i} \frac{1}{r} \left(- \sum_{p=1}^{\ell} \lambda_p \left(\frac{\partial g_p}{\partial \delta_i} \Big/ \frac{\partial O}{\partial \delta_i}\right) - 1\right) \delta_i^k$$

$$j = 1, \ldots, \ell \qquad (5.39)$$

where p represents a constraint which is within the set of active constraints. Once again the relationship between r and α as given in Equation 5.27 is apparent. Rearranging Equation 5.39 gives

$$r g_j - \sum_{i=1}^{n} \frac{\partial g_j}{\partial \delta_i} \delta_i^k = \sum_{p=1}^{\ell} \lambda_p \left(\sum_{i=1}^{n} \frac{\partial g_j}{\partial \delta_i} \frac{\partial g_p}{\partial \delta_i} \Big/ \frac{\partial O}{\partial \delta_i}\right)_k \delta_i^k$$

$$j = 1, \ldots, \ell \qquad (5.40)$$

Equation 5.38 provides the same equation if $(1-\alpha)$ is substituted for r. These equations are desirable since an initial estimate of the Lagrange multipliers is not needed, but a fairly accurate set of active constraints is needed in order to reduce the number of calculations. These equations also take into account the dependence of one constraint upon another, where the exponential recurrence relations do not. If only the diagonal terms associated with $\left(\frac{\partial g_j}{\partial \delta_i}\right)\left(\frac{\partial g_p}{\partial \delta_i}\right)$ are considered, the recurrence and linear equations can be proven to be the same as long as $\frac{1}{z}$ is equivalent to r.

The recurrence methods are not effected by linking and side constraints, but the linear techniques are

effected. The effect of side constraints must be added to the linear equations, since the T_i's (optimality criteria) do not consider side constraints. Rewriting Equation 5.35 yields the following form

$$-g_j = \sum_{i=1}^{n_1} \frac{\partial g_j}{\partial \delta_i} \Delta\delta_i^k + \sum_{i=n_1+1}^{n} \frac{\partial g_j}{\partial \delta_i} (\delta_i^P - \delta_i^k)$$

$$j = 1,\ldots,\ell \qquad (5.41)$$

where δ_i^P represents an element which becomes passive during the kth iteration, and n_1 is the number of active elements. Using Equation 5.13 and the same formulation as presented earlier Equation 5.41 becomes

$$rg_j - \sum_{i=1}^{n_1} \frac{\partial g_j}{\partial \delta_i} \delta_i^k + r \sum_{i=n_1+1}^{n} \frac{\partial g_j}{\partial \delta_i} (\delta_i^P - \delta_i^k) =$$

$$\sum_{p=1}^{\ell} \lambda_p \left(\sum_{i=1}^{n_1} \frac{\partial g_j}{\partial \delta_i} \frac{\partial g_p}{\partial \delta_i} \Big/ \frac{\partial O}{\partial \delta_i} \right) \delta_i^k$$

$$j = 1,\ldots,\ell \qquad (5.42)$$

These passive elements are generally not known until the recursive relations for the design variables are used and the new variables are checked for violation of the minimum or maximum size. This creates an iterative procedure within the kth iteration for determining the Lagrange multipliers.

Linking effects Equation 5.42 also. The optimality criteria from Equation 5.21 becomes

$$T_v = - \left(\sum_{i=1}^{s} \sum_{j=1}^{\ell} \frac{\partial g_j}{\partial \delta_i} \Big/ \sum_{i=1}^{s} \frac{\partial O}{\partial \delta_i} \right)$$

$$v = 1, \ldots, n_2 \qquad (5.43)$$

Using Equations 5.21, 5.34, and 5.43 the linear equations become

$$rg_j - \sum_{i=1}^{n_2} \left(\sum_{q=1}^{s} \frac{\partial g_j}{\partial \delta_q} \right)_i \Lambda_i^k =$$

$$\sum_{p=1}^{\ell} \lambda_p \left(\sum_{i=1}^{n_2} \left(\sum_{q=1}^{s} \frac{\partial g_j}{\partial \delta_q} \frac{\partial g_p}{\partial \delta_q} \Big/ \sum_{q=1}^{s} \frac{\partial O}{\partial \delta_q} \right) \Lambda_i^k \right)$$

$$j = 1, \ldots, \ell \qquad (5.44)$$

or

$$rg_j - \sum_{i=1}^{n_2} \frac{\partial g_j}{\partial \delta_i} \delta_i^k =$$

$$\sum_{p=1}^{\ell} \lambda_p \left(\sum_{i=1}^{n_2} \left(\sum_{q=1}^{s} \frac{\partial g_j}{\partial \delta_q} \frac{\partial g_p}{\partial \delta_q} \Big/ \sum_{q=1}^{s} \frac{\partial O}{\partial \delta_q} \right) \Lambda_i^k \right)$$

$$j = 1, \ldots, \ell \qquad (5.45)$$

Combining the linking and side constraints Equation 5.34 becomes

$$rg_j - \sum_{i=1}^{n_1} \frac{\partial g_j}{\partial \delta_i} \delta_i^k + r \sum_{i=n_1+1}^{n} \frac{\partial g_j}{\partial \delta_i} (\delta_i^p - \delta_i^k) =$$

$$\sum_{p=1}^{\ell} \lambda_p \left(\sum_{i=1}^{n_2} \left(\sum_{q=1}^{s} \frac{\partial g_j}{\partial \delta_q} \frac{\partial g_p}{\partial \delta_q} \Big/ \sum_{q=1}^{s} \frac{\partial O}{\partial \delta_q} \Lambda_i^k \right) \right.$$

$$j = 1, \ldots, \ell \qquad (5.46)$$

Equation 5.46 provides equations corresponding to the active constraints which have non-zero, positive Lagrange multipliers. If the equations yield a negative Lagrange multiplier, this constraint should be considered non-active, according to the Kuhn-Tucker conditions. This requires the solution of a new set of equations which is identical to the previous set with all terms associated with that Lagrange multiplier removed. (In terms of a matrix solution, the row and column of coefficients associated with this constraint would be removed.) It is important to have a good estimate of active constraints in order to avoid having negative Lagrange multipliers which will cause a resolution of reduced equation sets. Also a poor choice of constraints can cause the linear equations, which do take into account the dependence of one constraint upon another, to eliminate active constraints from the considered active set.

Each category of methods have their advantages and their disadvantages. The advantages associated with the

recurrence techniques are: 1) there is no need to predict an active set of constraints since Equation 5.32 will force the Lagrange multipliers associated with a passive constraint to become small, 2) very little computational effort is required for these techniques, and 3) these techniques are unaffected by side constraints or linking. The disadvantages of the recurrence relations are: 1) the initial value for the Lagrange multipliers must be given, 2) convergence can be slow and unstable, and 3) no dependence between active constraints are considered. The advantages of the linear equations techniques are: 1) no initial values for the Lagrange multiplier are needed, 2) convergence is "usually" more stable, 3) the interdependence of the constraints are taken into account. The disadvantages of the linear techniques are: 1) the large computational effort required to form and solve the simultaneous equations, 2) an accurate estimate of the active constraints is required, 3) an algorithm for eliminating the equations and coefficients of negative Lagrange multipliers is required, and 4) the equations must be reformed when passive elements are encountered. The linear equation technique was chosen to be used since it is more stable and provides a reasonable means for checking the set of active constraints. Also, certain three-dimensional structures can become sensitive to design change which can cause unstable convergence if the recurrence relations are used and a poor choice for the

initial set of Lagrange multipliers is made. The Lagrange multipliers for the three-dimensional problems have been elusive in the fact that they range in value from 10^{-1} to 10^{5} within the examples studied. With this large range it becomes difficult to choose the initial set of Lagrange multipliers. A possible algorithm might be to use the linear equations for the first two to three iterations to find a reasonable set of Lagrange multipliers and then revert to using the recurrence relations in order to save computer time.

I. ACTIVE CONSTRAINTS

In order to save computational time, it is important to choose a reasonably accurate set of active constraints. The active constraints are considered to be any constraints which are "close" to the constraint surfaces. This can be translated into a condition where Equations 5.30 and 5.31 are nearly equal to unity. The algorithm checks these values and compares them to a specific acceptable range as designated by the user. The choice of active constraints is based upon these equations

$$(1-P_1) \leq \frac{u_j}{\bar{u}_j} \leq (1+P_2) \tag{5.47}$$

for upper bound constraints and

$$(1-P_1) \leq \frac{\underline{u}_j}{u_j} \leq (1+P_2) \tag{5.48}$$

for lower bound constraints. These equations allow the user the flexibility of establishing a region along the constraint surface which can be as large or as small as desired. The value $(1-P_1)$ provides the thickness of the region on the feasible side of the constraint and the value $(1+P_2)$ provides the acceptable region of constraint violation, if any, for the nonfeasible side of the constraint surface.

J. SCALING OF THE DESIGN

It has been established that there must be a set of active constraints before the optimization algorithm can be used. Generally, a preliminary design will be either conservative (no active constraints) or nonconservative (a violation of one or more constraints). Therefore, some technique must be used to adjust these design variables such that a set of active constraints, as justified by Equations 5.47 and 5.48, will be satisfied. In the past, structures which were linear with respect to their design variables used a technique called scaling to adjust the designs (32,48). Scaling uses a factor to adjust the design variable which is the maximum value of either of these two values

$$f_j = \frac{u_j}{\bar{u}_j} \qquad j = 1,\ldots,\ell_1 \qquad (5.49)$$

for upper limit constraints or

$$f_j = \frac{\underline{u}_j}{u_j} \qquad j = 1,\ldots,\ell_2 \qquad (5.50)$$

for lower limit constraints where ℓ_1 and ℓ_2 are the numbers of possible upper and lower limit constraints, respectively. For a stiffness matrix which is linear with respect to the design variable, the response is adjusted by a simple factor, too. For example, the stiffness for a truss would provide this equation

$$f_j[K]\{u\}_s = \{R\} \qquad (5.51)$$

which in turn would produce $\{u\}_s = \{u\}/f_j$; which would force u_j to become $\overline{u}_j$ or $\underline{u}_j$ which is the criteria for an active constraint. This is not the case for a stiffness matrix which is nonlinear with respect to the primary design variable.

The use of scaling for the nonlinear (in terms of the primary design variable) stiffness and response becomes an iterative procedure. Once the primary design variable is scaled, the secondary design variables are scaled according to Equation 3.12 which gives

$$S_{ij} = C_{1j} (f\delta_i)^{C_{2j}} + C_{3j} \qquad (5.52)$$

Depending on which constraint is being scaled and the effect of the secondary element on that constraint, the scaling can take several cycles to reach an active value. For instance, the concrete elements have a fixed depth but variable width, the minor axis moment of inertia uses the cube of the factor as shown by using Equation 3.22 to produce

$$I_y = \frac{1}{h^8 D^2} (fI_x)^3 \tag{5.53}$$

Therefore, the orientation of these concrete elements becomes critical with respect to scaling. The natural frequencies are also affected in a strange manner since both the stiffness and mass changes when scaling is used. The structural mass and stiffness are changed according to Equations 4.8 and 4.13. When the concrete elements are used the structural mass can become fairly significant. Thinking of the frequency in terms of the Rayleigh quotient it can be written as

$$\omega^2 = \frac{\{\phi\}^T [K]_f \{\phi\}}{\{\phi\}^T [M]_f \{\phi\}} \tag{5.54}$$

where $[K]_f$ and $[M]_f$ represent the nonlinear scaling of the terms in the stiffness and mass. The effect of this is highly problem dependent. Scaling can also became divergent for steel structures if the system which provides an active constraint approaches a point of discontinuity

of the secondary design variables with respect to the primary design variable as seen in Figures 4 to 8. Despite this instability most problems can be adjusted to eliminate this problem by reorienting or resizing certain elements within the problem. Another alternative is to open the range for active constraints in order to force certain constraints to become active at an earlier stage. Rarely does the instability occur after the first cycle of optimization.

Scaling also has a problem with a combination of frequency and displacement constraints. This is due to the fact that the factor becomes counterproductive. The displacements are affected by Equation 5.49 or the inverse of the factor, whereas the frequencies, in most cases, are affected in a greater sense by the direct multiplication of the factor f. Therefore, an oscillation between potentially active constraints can take place where the structural system forces the displacements to become active while violating the frequencies and this resulting violation causes the frequency to become active while violating the displacements in the next cycle of scaling. Because of this oscillatory effect, frequency and displacement constraint combinations are handled differently. The scaling is only allowed to affect the displacements, and the frequencies are forced to their active values through the use of Equation 5.46. The term rg_j is a means of adjusting the

Lagrange multipliers to force the constraints to become active. This term forces g_j to become zero.

Scaling is important for two different operations during the optimization algorithm. The first is to find the initial set of active constraints by using the maximum factor to change the primary design variables, which in turn changes the secondary design variables. The second is to force the design back within the region for active constraints as defined by Equations 5.47 and 5.48. It is also possible for constraints to be added to the active set through this technique. For example, an optimization cycle has been performed and has resized the elements; this new design could allow a new constraint to be violated. This violation could be due to the numerical process or the fact that the constraint was not in the original set of active constraints. It then becomes necessary to scale the new design to a value within the acceptable region. Once a set of active constraints has been determined a constraint will not be removed from the active set unless it has a negative Lagrange multiplier. This is true regardless if the addition of a new constraint causes the constraint value to leave the range provided in Equations 5.47 and 5.48 but the scaling will never let any constraint go beyond the upper limit of $(1+P_2)$, which corresponds to a constraint violation.

K. TERMINATION CRITERIA

Due to the iterative techniques used for the non-linear, structural optimization problem, termination criteria must be developed. The criteria have to be able to handle several distinct conditions. The primary condition is to check for convergence or divergence of the objective function. Secondary conditions are to limit the amount of allowed computing time and to check for divergent scaling. These criteria must be flexible yet easily handled within the iterative algorithm.

The secondary criteria are important since these are used to terminate an optimization sequence which is either diverging or converging at a very slow rate. Limiting the allowable number of optimization cycles and the allowable number of analyses will stop the procedure from using excessive computing resources due to a slowly converging or slowly diverging solution. (The slowly diverging system usually occurs near the optimal solution where there might be a slight constraint violation in the range of 1 to $(1+P_2)$). Divergent scaling can occur in two modes, the first being an ever increasing or decreasing set of factors or, most often, a generation of an oscillatory set of factors. These divergent scalings are handled by limiting the number of optimizations and analyses. These secondary criteria are used to stop an excessive use of the computer resources.

The primary criteria are involved with the actual optimization of the structure. The validity of the optimization is measured with respect to the T_i values given in Equation 5.18, but tend to be an unrealistic measure to the structural designer. In the latter stages of optimization there are very small changes made to the structural elements which provide a very small change in the value of the objective function. The pure mathematician would be interested in the final system with the T_i values as close to unity as possible, but the structural designer would be satisfied with the design if it is within a certain range of the optimal solution. Therefore, convergence is considered by comparing the values for the objective function at successive optimization cycles to a specified percentage of change, P_3, in these values which can be written as

$$\frac{|O^{k-1} - O^k|}{O^k} \leq P_3 \tag{5.55}$$

If Equation 5.55 is satisfied the algorithm is terminated. Divergence of the algorithm must also be considered. After several cycles of optimization it is possible that a new set of constraints will be chosen which will cause a divergent trend. The algorithm will allow only two successive iterations in which the objective function increases in value. The algorithm will terminate after the second divergent cycle. In certain instances this

new set of constraints could eventually optimize to a smaller objective value, but in most cases it appears to produce larger or nearly equivalent solutions. The primary criteria must be carefully considered with respect to the condition of computing resources versus the closeness to an optimal solution. A good range for P_3 seems to be 0.5% to 5%. A smaller percentage of change in the objective function requires more computing time but provides a near optimal solution, whereas a larger percentage saves computing time at the expense of optimization.

VI. SENSITIVITY ANALYSIS

As seen by Equations 5.10 to 5.15 an important part of the optimization procedure is to determine the gradients of the constraints with respect to the primary design variables. This portion of the optimization is generally the most time consuming, yet it is very important. As will be seen, these gradients must be found through the use of numerical techniques. The most common techniques include direct, virtual load, and psuedo-load techniques. The direct techniques are developed from direct differentiation of the equations related to the structural response, while the psuedo-load and virtual load techniques are developed numerically.

A. CONSTRAINT GRADIENTS

First the constraint gradients must be written in terms of the structural responses. Equations 5.28 and 5.29 give the constraints in these two forms

$$g_j = (u_j - \bar{u}_j) \leq 0 \tag{6.1}$$

for an upper bound constraint and

$$g_j = (\underline{u}_j - u_j) \leq 0 \tag{6.2}$$

for a lower bound constraint where $\bar{u}_j$ and $\underline{u}_j$ are the upper and lower bounds, respectively, and u_j is the structural

response (i.e. static displacement or stress, natural frequency, or dynamic displacement or stress, etc.). Therefore, the gradients of the jth constraint can be written as

$$\frac{\partial g_j}{\partial \delta_i} = \frac{\partial u_j}{\partial \delta_i} \qquad i=1,\ldots,n \qquad (6.3)$$

for an upper bound constraint and

$$\frac{\partial g_j}{\partial \delta_i} = - \frac{\partial u_j}{\partial \delta_i} \qquad i=1,\ldots,n \qquad (6.4)$$

for a lower bound constraint, since $\bar{u}_j$ and $\underline{u}_j$ are constants, where δ_i represents the ith primary design variable and n is the total number of elements. Keep in mind that the structural problem generally has several load cases associated with each response which would change u_j to u_{jl} and g_j to g_{jl} where l represents the lth load case. For clarity in the development of this section the equations will be derived for a single load case.

B. STIFFNESS AND MASS DERIVATIVES

All three approaches will make use of the fact that the stiffness and mass are directly differentiable with respect to the primary and secondary design variables. Using the chain rule and Equations 4.4, 4.8, and 4.13, the stiffness and mass gradients with respect to the primary design variables can be derived. Equation 3.12 is the key

to an easy solution of the gradients for these stiffnesses and masses which are nonlinear with respect to the primary design variables.

1. Stiffness. The total stiffness can be broken into the elemental stiffness matrices which can then be broken into the contributions for the different geometric properties. The total stiffness can be written as

$$[K]_T = \sum_{i=1}^{n} [K]_i \tag{6.5}$$

where $[K]_T$ represents the total stiffness, and $[K]_i$ represents that portion of the total stiffness supplied by the ith element. Each elemental stiffness can then be written as

$$[K]_i = \sum_{j=1}^{t} [K]_{ij} \tag{6.6}$$

where $[K]_{ij}$, represents the portion of the ith elemental stiffness supplied by the jth geometric property, and t is the total number of geometric properties required to represent element i, as discussed in Section III.A. For example a beam-column stiffness, which requires the most geometric properties, can be written as

$$[K]_i = [K]_{iA} + [K]_{iI_x} + [K]_{iI_y} + [K]_{iJ} \tag{6.7}$$

where A, I_x, I_y, and J represent the area, major-axis, minor-axis and torsional moments of inertia, respectively. Note that the beam-column uses the major-axis moment of inertia as the primary design variables and the other geometric properties are the secondary design variables given by Equation 3.12. Using Equation 6.5, the derivative of the stiffness can be written as

$$\frac{\partial [K]_T}{\partial \delta_i} = \frac{\partial [K]_i}{\partial \delta_i} \qquad i=1,\ldots,n \tag{6.8}$$

since $[K]_i$ is the only portion of the total stiffness which is dependent upon the ith primary design variable, δ_i. Equations 6.5, 6.6 and 6.8 give

$$\frac{\partial [K]_T}{\partial \delta_i} = \frac{\partial}{\partial \delta_i} \left(\sum_{j=1}^{t} [K]_{ij} \right) = \sum_{j=1}^{t} \left(\frac{\partial [K]_{ij}}{\partial \delta_i} \right) \tag{6.9}$$

where

$$\frac{\partial [K]_{ij}}{\partial \delta_i} = \frac{\partial [K]_{ij}}{\partial S_{ij}} \frac{\partial S_{ij}}{\partial \delta_i} \tag{6.10}$$

and

$$\frac{\partial S_{ij}}{\partial \delta_i} = C_{1j} C_{2j} \delta_i^{(C_{2j}-1)} \tag{6.11}$$

Note that $[K]_{ij}$ is linear in terms of the secondary design variable S_{ij}, so that

$$\frac{\partial [K]_{ij}}{\partial S_{ij}} = \frac{[K]_{ij}}{S_{ij}} \tag{6.12}$$

and the final form for the derivative of the total stiffness becomes

$$\frac{\partial [K]_T}{\partial \delta_i} = \sum_{j=1}^{t} \left(\frac{[K]_{ij}}{S_{ij}}\right) C_{1j} C_{2j} \delta_i^{(C_{2j}-1)} \tag{6.13}$$

For the beam-columns this would be written as

$$\frac{\partial [K]_T}{\partial I_{xi}} = \frac{[K]_{iA}}{A_i} \frac{\partial A_i}{\partial I_{xi}} + \frac{[K]_{iI_x}}{I_{xi}} + \frac{[K]_{iJ}}{J_i} \frac{\partial J_i}{\partial I_{xi}} + \frac{[K]_{iI_y}}{I_{yi}} \frac{\partial I_{yi}}{\partial I_{xi}} \tag{6.14}$$

or

$$\frac{\partial [K]_T}{\partial I_{xi}} = \frac{[K]_{iA}}{A_i} \left(C_{1A} C_{2A} I_{xi}^{(C_{2A}-1)}\right) + \frac{[K]_{iI_x}}{I_{xi}} + \frac{[K]_{iJ}}{J_i} \left(C_{1J} C_{2J} I_{xi}^{(C_{2J}-1)}\right) + \frac{[K]_{iI_y}}{I_{yi}} \left(C_{1I_y} C_{2I_y} I_{xi}^{(C_{2I_y}-1)}\right) \tag{6.15}$$

Now it is easily seen why the form of Equation 3.12 was used to relate the primary and secondary design variables. In the case where the stiffness is linear with respect to

only the primary design variable the derivative of the total stiffness is written in the form of Equation 6.12, where S_{ij} is the primary design variable. This form greatly simplifies the optimization procedures, but unfortunately it is not possible to represent a three-dimensional system other than a truss in this form.

2. Mass. The derivative of the mass is simpler due to the fact that the structural mass is strictly dependent upon the cross-sectional area, and the non-structural mass is independent of the elemental geometric properties. Writing the total mass as

$$[M]_T = \sum_{i=1}^{n} [M]_i + [M]_{NS} \tag{6.16}$$

where $[M]_T$, represents the total mass, $[M]_i$, represents the ith elemental mass, and $[M]_{NS}$ represents the non-structural mass. Using Equation 6.16, the derivative of the mass becomes

$$\frac{\partial [M]_T}{\partial \delta_i} = \frac{\partial [M]_i}{\partial \delta_i} \qquad i=1,\ldots,n \tag{6.17}$$

since $[M]_i$ is the only portion of the mass which is dependent upon the ith primary design variable. The elemental mass, $[M]_i$, is related to the primary design variable through the cross-sectional area which changes Equation 6.17 to

$$\frac{\partial [M]_T}{\partial \delta_i} = \frac{\partial [M]_i}{\partial A_i} \frac{\partial A_i}{\partial \delta_i} \tag{6.18}$$

or

$$\frac{\partial [M]_T}{\partial \delta_i} = \frac{[M]_i}{A_i} \left(C_{1A} C_{2A} \delta_i^{(C_{2A}-1)}\right) \tag{6.19}$$

since the mass is linear in terms of the area, A_i, and the cross-sectional area is related to the primary design variable through Equation 3.12. Equation 6.19 is very simple for the bracing elements as the term in the parantheses is equivalent to unity. Once again the truss problem or the problem where the mass and stiffness are linear in terms of the primary design variables becomes a much simpler problem. The interdependence of the geometric properties causes a problem in terms of finding the derivatives of the mass and stiffness.

C. STRUCTURAL RESPONSE GRADIENTS

1. Static Response Gradients. Static response gradients are generally found using one of two numerical techniques called the virtual load and psuedo-load techniques. The psuedo-load approach has been used primarily within mathematical programming algorithms, whereas the virtual load approach has been used for most of the optimality criteria algorithms. The chosen algorithm uses the virtual load technique for static response gradients, but

it also uses the general idea associated with the psuedo-load technique for determining the dynamic response gradients.

The virtual load technique is based upon the premise that the static displacements and stresses can be written as a linear combination of the structural displacements. This can be written as

$$u_j = \{b\}_j^T \{U\} \tag{6.20}$$

where, $\{b\}_j^T$, is the appropriate vector to enforce this relationship, u_j, is the jth global displacement or stress, and $\{U\}$ is the vector of global displacements. The vector $\{b\}_j$ will be examined in detail with respect to each type of response in later sections. Using Equation 6.20, the gradient for the jth displacement or stress can be written as

$$\frac{\partial u_j}{\partial \delta_i} = \frac{\partial \{b\}_j^T}{\partial \delta_i} \{U\} + \{b\}_j^T \frac{\partial \{U\}}{\partial \delta_i} \tag{6.21}$$

The first term in Equation 6.21 is generally assumed to be zero. In other words, the vector $\{b\}_j$ is assumed to be a vector of constants. This is valid for the displacement gradients, but it is not valid for the stress gradients unless the stress is associated with a truss element. This assumption generally does not cause a problem within the algorithm after the first few cycles of optimization.

Therefore, Equation 6.21 becomes

$$\frac{\partial u_j}{\partial \delta_i} = \{b\}_j^T \frac{\partial \{U\}}{\partial \delta_i} \tag{6.22}$$

which requires the term $\frac{\partial \{U\}}{\partial \delta_i}$. Taking the partial derivatives of Equation 4.16 provides this equation

$$\frac{\partial [K]_T}{\partial \delta_i} \{U\} + [K]_T \frac{\partial \{U\}}{\partial \delta_i} = \frac{\partial \{R\}}{\partial \delta_i} = 0 \tag{6.23}$$

since the static loads are independent of the design variables. Rearranging Equation 6.23 gives

$$\frac{\partial \{U\}}{\partial \delta_i} = - [K]_T^{-1} \frac{\partial [K]_T}{\partial \delta_i} \{U\} \tag{6.24}$$

where $\frac{\partial [K]_T}{\partial \delta_i}$ is given in Equation 6.13.

Defining $\{b\}_j$ as the virtual load

$$\{b\}_j = [K]_T \{v\}_j \tag{6.25}$$

a virtual displacement vector, $\{v\}_j$ for the jth constraint becomes

$$\{v\}_j = [K]_T^{-1} \{b\}_j \tag{6.26}$$

and using symmetry of the stiffness, Equation 6.26 becomes

$$\{v\}_j^T = \{b\}_j^T [K]_T^{-1} \tag{6.27}$$

Substituting Equation 6.24 into Equation 6.22 gives

$$\frac{\partial u_j}{\partial \delta_i} = - \{b\}_j^T [K]_T^{-1} \frac{\partial [K]_T}{\partial \delta_i} \{U\} \tag{6.28}$$

and substituting Equation 6.27 into Equation 6.28 provides

$$\frac{\partial u_j}{\partial \delta_i} = - \{v\}_j^T \frac{\partial [K]_T}{\partial \delta_i} \{U\} = - \{v\}_j^T \frac{\partial [K]_i}{\partial \delta_i} \{U\} \tag{6.29}$$

which is the component of the gradient for the jth static displacement or stress constraint. Everything needed for Equation 6.29 is known except the values of $\{v\}_j^T$. In order to find $\{v\}_j^T$, it is necessary to find $\{b\}_j^T$.

a. Displacement. The virtual loads, $\{b\}_j$, as noted are dependent upon the jth constraint, and if they are stress constraints also become element dependent. The virtual load vector for a displacement constraint is

$$\{b\}_j^T = [0...,0,1,0,...,0] \tag{6.30}$$

where there is a unit value at the jth location. The virtual load vectors for the stresses must be developed for each type of element.

b. Beam-column Stress. The beam-column stress constraint virtual load vectors are based upon a

biaxial-bending and axial stress combination. The stresses considered for the beam-column elements are

$$\sigma = \frac{P}{A} \pm \frac{M_x c}{I_x} \pm \frac{M_y d}{I_y} \tag{6.31}$$

where P, is the axial load, M_x and M_y, are the moments about the x and y axes respectively, c and d, are the appropriate distances from the neutral axes to the outer most fibers, and A, I_x, and I_y are the geometric properties as previously defined. The signs are needed to represent the stress in each quadrant of a cross section. Torsional stresses were assumed to be negligible and were not considered within the development of the stress constraints. Equation 6.31 is the basis for developing the virtual load vector using the beam-column stiffness coefficients along with Figure 17 gives P, M_x, and M_y at end i in these forms

$$P = \frac{EA}{L} (U_i^1 - U_j^1) \tag{6.32}$$

$$M_{x_i} = \frac{6EI_x}{L^2} (U_i^2 - U_j^2) + \frac{4EI_x}{L} (U_i^6 + \frac{1}{2} U_j^6) \tag{6.33}$$

$$M_{y_i} = \frac{6EI_y}{L^2} (U_j^3 - U_i^3) + \frac{4EI_y}{L} (U_i^5 + \frac{1}{2} U_j^5) \tag{6.34}$$

where E is Young's modulus and L is the length of the elastic portion of the beam-column. Substituting

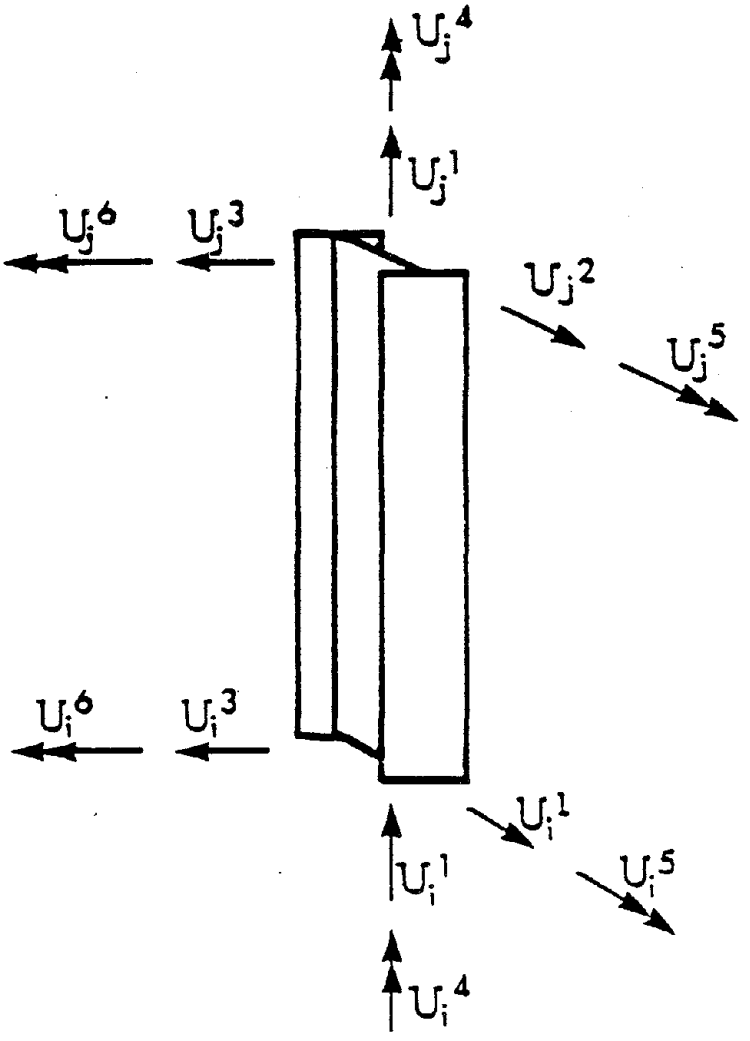

Figure 17. Column Degrees of Freedom for Determination of the Column Stress Vector

Equations 6.32, 6.33, and 6.34 into Equation 6.31, the stress in terms of the displacements can then be written as

$$\sigma = \frac{E}{L}\left(U_i^1 - U_j^1\right) \pm \left[\frac{6Ec}{L^2}\left(U_i^2 - U_j^2\right) + \frac{4Ec}{L}\left(U_i^6 + \frac{1}{2}U_j^6\right)\right]$$

$$\pm \left[\frac{6Ed}{L^2}\left(U_j^3 - U_i^3\right) + \frac{4Ed}{L}\left(U_i^5 + \frac{1}{2}U_j^5\right)\right] \qquad (6.35)$$

or

$$\sigma_i = \left[\frac{E}{L} - \frac{E}{L}\right]\begin{Bmatrix} U_i^1 \\ U_j^1 \end{Bmatrix} \pm \begin{bmatrix} \frac{6Ec}{L^2} & \frac{4Ec}{L} & \frac{-6Ec}{L^2} & \frac{2Ec}{L} \end{bmatrix}\begin{Bmatrix} U_i^2 \\ U_i^6 \\ U_j^2 \\ U_j^6 \end{Bmatrix}$$

$$\pm \begin{bmatrix} \frac{-6Ed}{L^2} & \frac{4Ed}{L} & \frac{6Ed}{L^2} & \frac{2Ed}{L} \end{bmatrix}\begin{Bmatrix} U_i^3 \\ U_i^5 \\ U_j^3 \\ U_j^5 \end{Bmatrix} \qquad (6.36)$$

therefore, $\{b\}_j$ for the stress at end i of the beam column becomes

$$\{b\}_j^T = \left[\frac{E}{L}\ 0\ 0\ 0\ 0\ 0\ -\frac{E}{L}\ 0\ 0\ 0\ 0\ 0\right]$$

$$\pm \frac{Ec}{L^2}\left[0\ \ 6\ \ 0\ \ 0\ \ 0\ \ 4L\ \ 0\ \ -6\ \ 0\ \ 0\ \ 0\ \ 2L\right]$$

$$\pm \frac{Ed}{L^2}\left[0\ \ 0\ \ -6\ \ 0\ \ 4L\ \ 0\ \ 0\ \ 0\ \ 6\ \ 0\ \ 2L\ \ 0\right] \qquad (6.37)$$

where the signs are chosen according to the active stress found by Equation 6.31 and j represents the jth active constraint.

c. Beam Stress. The beam stress constraints are based strictly upon the model given in Figure 18, considering pure bending stresses. These stresses at end i can be written as

$$\sigma_i = \pm \frac{M_{x_i} c}{I_x} \tag{6.38}$$

where M_x is the moment about the major axis, c, is the distance from the major axis to the outer most fiber, and I_x is the major axis moment of inertia. Using the beam stiffness coefficients along with Figure 18 gives the moment at end i as

$$M_{x_i} = \frac{EI_x}{L^2} \begin{bmatrix} 6 & 4L & -6 & 2L \end{bmatrix} \begin{Bmatrix} U_i \\ \theta_i \\ U_j \\ \theta_j \end{Bmatrix} \tag{6.39}$$

and the moment at end j as

$$M_{x_j} = \frac{EI_x}{L^2} \begin{bmatrix} 6 & 2L & -6 & 4L \end{bmatrix} \begin{Bmatrix} U_i \\ \theta_i \\ U_j \\ \theta_j \end{Bmatrix} \tag{6.40}$$

where E is Young's modulus and L is the length of the elastic portion of the beam. Substituting Equation 6.39

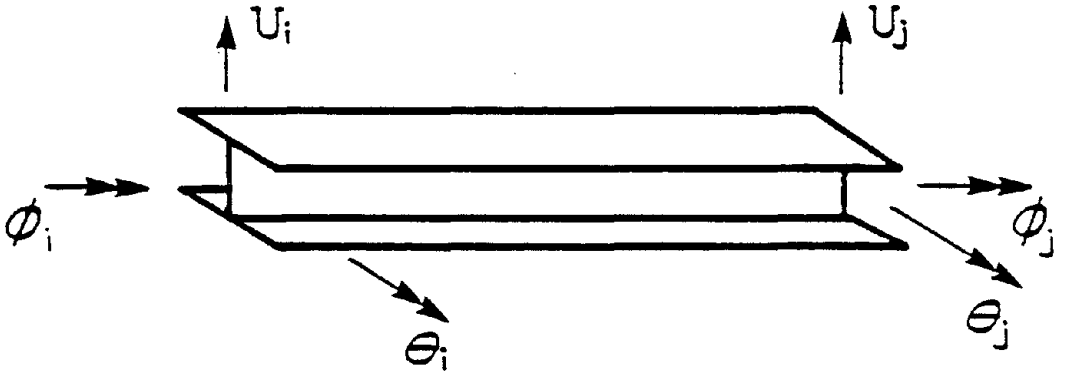

Figure 18. Beam Degrees of Freedom for Determination of the Beam Stress Vector

into Equation 6.38 the stresses can be written in terms of the displacements as

$$\sigma_i = \pm \frac{Ec}{L^2} [6 \quad 4L \quad -6 \quad 2L] \begin{Bmatrix} U_i \\ \theta_i \\ U_j \\ \theta_j \end{Bmatrix} \tag{6.41}$$

and

$$\sigma_j = \pm \frac{Ec}{L^2} [6 \quad 2L \quad -6 \quad 4L] \begin{Bmatrix} U_i \\ \theta_i \\ U_j \\ \theta_j \end{Bmatrix} \tag{6.42}$$

which gives $\{b\}_k$, the virtual load vector for the kth beam stress constraint, as

$$\{b\}_{ki} = \frac{Ec}{L} [6 \quad 4L \quad -6 \quad 2L] \tag{6.43}$$

and

$$\{b\}_{kj} = \frac{Ec}{L} [6 \quad 2L \quad -6 \quad 4L] \tag{6.44}$$

where only the positive sense is chosen since the same level of stress is used for tension and compression for the beam model (infinite axial stiffness).

d. Brace Stress. The brace stress constraints are based strictly upon the axial stress. The stress can be written as

$$\sigma = P/A \tag{6.45}$$

where P, is the axial load, and A is the cross-sectional area. Using the axial stiffness coefficients along with Figure 19 gives the axial load as

$$P = \{\frac{EA}{L} \quad -\frac{EA}{L}\} \begin{Bmatrix} U_1 \\ U_2 \end{Bmatrix} \tag{6.46}$$

where E, A, and L have been previously defined. Substituting Equation 6.46 into Equation 6.45 the stresses can be written as

$$\sigma = \{\frac{E}{L} \quad -\frac{E}{L}\} \begin{Bmatrix} U_1 \\ U_2 \end{Bmatrix} \tag{6.47}$$

which gives $\{b\}_j$ as

$$\{b\}_j^T = \{E/L \quad -E/L\} \tag{6.48}$$

where the tensile or compressive sense of the stress is determined strictly by the elemental displacements. This may be achieved since the stress is assumed to be uniform over the cross-section and is based upon only one type of elemental loading, the axial load.

e. Panel Stress. The panel stress constraint virtual load vectors are based upon axial stress combined with bending about one axis. The stresses considered are

$$\sigma_i = \frac{P}{A} \pm \frac{M_{x_i} c}{I_x} \tag{6.49}$$

and

$$\sigma_j = \frac{P}{A} \pm \frac{M_{x_j} c}{I_x} \tag{6.50}$$

where i and j represent ends i and j and the other terms are previously defined. Using the panel stiffness coefficients along with Figure 20, the values for P and M_{xi} are given as

$$P = [E/L \quad -E/L] \begin{Bmatrix} U_1 \\ U_2 \end{Bmatrix} \tag{6.51}$$

$$M_{x_i} = \frac{Ec}{L^2} [6 \quad 4L \quad -6 \quad 2L] \begin{Bmatrix} U_3 \\ U_4 \\ U_5 \\ U_6 \end{Bmatrix} \tag{6.52}$$

$$M_{x_j} = \frac{Ec}{L^2} [6 \quad 2L \quad -6 \quad 4L] \begin{Bmatrix} U_3 \\ U_4 \\ U_5 \\ U_6 \end{Bmatrix} \tag{6.53}$$

where E is Young's modulus and L is the height of the panel. Substituting Equations 6.51, 6.52, 6.53 into 6.49 and 6.50 gives the stresses in terms of the displacements as

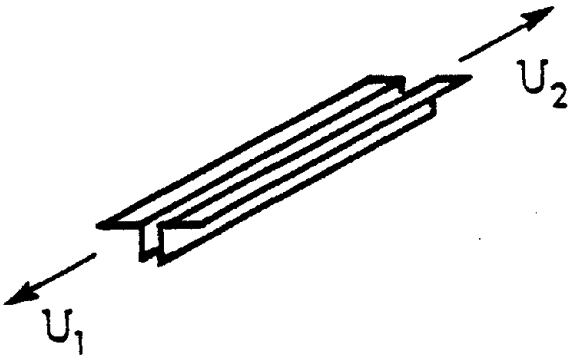

Figure 19. Brace Degrees of Freedom for Determination of the Brace Stress Vector

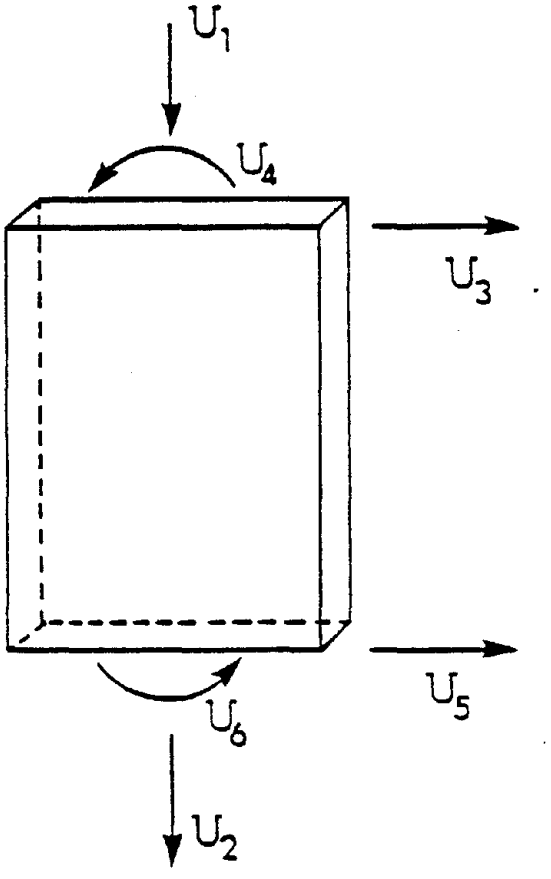

Figure 20. Panel Degrees of Freedom for Determination of the Panel Stress Vector

$$\sigma_i = \{E/L \quad -E/L\} \begin{Bmatrix} U_1 \\ U_2 \end{Bmatrix} \pm \frac{Ec}{L^2} [6 \quad 4L \quad -6 \quad 2L] \begin{Bmatrix} U_3 \\ U_4 \\ U_5 \\ U_6 \end{Bmatrix} \tag{6.54}$$

and

$$\sigma_j = \{E/L \quad -E/L\} \begin{Bmatrix} U_1 \\ U_2 \end{Bmatrix} \pm \frac{Ec}{L^2} [6 \quad 2L \quad -6 \quad 4L] \begin{Bmatrix} U_3 \\ U_4 \\ U_5 \\ U_6 \end{Bmatrix} \tag{6.55}$$

Therefore, the virtual load vectors can be given as

$$\{b\}^T_{ki} = [E/L \quad -E/L \quad 0 \quad 0 \quad 0 \quad 0] \pm \frac{Ec}{L^2} [6 \quad 4L \quad -6 \quad 2L] \tag{6.56}$$

and

$$\{b\}^T_{kj} = [E/L \quad -E/L \quad 0 \quad 0 \quad 0 \quad 0] \pm \frac{Ec}{L^2} [6 \quad 2L \quad -6 \quad 4L] \tag{6.57}$$

where the signs are chosen according to the active constraint being tensile or compressive.

f. Effects of Coordinate Transformations. The virtual load vectors given in Equations 6.30, 6.37, 6.44, 6.48, 6.56, and 6.57 are coordinate system dependent. The displacement response, virtual load vector is given in the global system, but the stress virtual load vectors are

presented in the local or elemental system. The virtual displacements are eventually calculated in the global system. The stress virtual load vectors, however, should be transformed from local to the global coordinates for which the vectors $\{b\}_j$ must first be transformed into the reference coordinate system as

$$\{b\}_{jREF} = [T]^T \{b\}_{jE} \tag{6.58}$$

and then be transferred to the global system as

$$\{b\}_j^G = [T']^T \{b\}_{jREF} = [T']^T[T]^T \{b\}_{jE} \tag{6.59}$$

where [T] and [T'] are the appropriate transformations and $\{b\}_j^G$, $\{b\}_{jREF}$, and $\{b\}_{jE}$ are the virtual load vectors in global, reference, and elemental forms respectively. These transformations are the same transformations as discussed in Section III.

Although the virtual displacements are found in the global system, the static response gradients are best found using the elemental or local coordinates. This is due largely to the fact that the elemental force subroutines can easily calculate the vector $\frac{\partial [K]_i}{\partial \delta_i} \{U\}$. As long as $\{U\}$, $[K]_i$, and $\{U\}_j$ are all transformed to the local system, the gradient calculated by Equation 6.29 will be identical in any reference system. This is due to the fact that transformations are orthogonal or $[T]^T = [T]^{-1}$.

Therefore, any coordinate system can be used, as long as, each component of the calculation is consistent with that frame of reference.

g. Reduction Effects. Also, prior to using Equation 6.29, the components of $\{b\}_j$ associated with the rotational degrees of freedom must be condensed. This requires the virtual load vector to be modified and reduced as shown in Equation 4.23 giving the reduced virtual load as

$$\{b\}_{jRED} = \{b_2\}_j - [K_{21}][K_{11}]^{-1}\{b_1\}_j \tag{6.60}$$

where $\{b_2\}_j$, is the portion of the $\{b\}_j$ vectors which correspond to vertical and translational global degrees of freedom, and $\{b_1\}_j$ is the portion of the $\{b\}_j$ vector corresponding to the rotational, global degrees of freedom. Using Equation 6.26 and $\{b\}_{jRED}$, the $\{v_2\}_j$ terms corresponding to the vertical and translational, global, virtual displacements are found. Equation 4.21 can be used to find $\{v_1\}_j$, the corresponding rotational, global, virtual displacements as

$$\{v_1\}_j = [K_{11}]^{-1}[\{b_1\}_j - [K_{12}]\{b_2\}_j] \tag{6.61}$$

These values are needed since Equation 6.29 is evaluated at the elemental level, as shown by Equation 6.8, which needs the rotational degrees of freedom. Therefore, the virtual displacements, including the rotational degrees of

freedom, are transferred into local virtual displacements and used to find the gradients. The local level is used since the derivative of the stiffness requires only the portion of the stiffness supplied by element i as seen in Equations 6.8 and 6.13.

h. Effects of the Primary Assumption. Equation 6.29 was derived by assuming the virtual load vector to be independent of the primary design variable which is not true except for the brace elements. Each of the bending elements have a term which is related to the depth and/or width of the elements. The values for c and d, the depths, are determined through Equation 3.12 and are given as

$$c = \frac{I_x}{S_x} = I_x/(C_{1S_x} I_x^{C_{2S_x}} + C_{3S_x}) \tag{6.62}$$

and

$$d = \frac{I_y}{S_y} = (C_{1I_y} I_x^{C_{2I_y}} + C_{3I_y})/(C_{1S_y} I_x^{C_{2S_y}} + C_{3I_y}) \tag{6.63}$$

The algorithm chosen uses the assumption based Equation 6.22 instead of 6.21 with very little effect after the first one to two cycles of optimization for the stress constraints. The values for d and c can cause a violation of the stress constraints after an optimization cycle, but is corrected through iterative scaling. If this problem

persists a larger convergence factor (smaller step size) can be chosen to reduce this violation. Generally, this assumption has proven to be reasonable, saving computing time and space.

2. Frequency Constraint Gradients. Frequency constraint gradients are found by a direct differentiation of the free-vibration equation used to find the natural frequencies. Equation 4.27 for a single natural frequency can be written as

$$[[K]_T - \omega_j^2 [M]_T]\{\phi\}_j = 0 \tag{6.64}$$

Differentiating Equation 6.64 with respect to the primary design variable, δ_i, yields

$$\left[\frac{\partial [K]_T}{\partial \delta_i} - \frac{\partial \omega_j^2}{\partial \delta_i} [M]_T - \omega_j^2 \frac{\partial [M]_T}{\partial \delta_i}\right] \{\phi\}_j + [[K]_T - \omega_j^2 [M_T]] \frac{\partial \{\phi\}_j}{\partial \delta_i} = 0 \tag{6.65}$$

Since the stiffness and mass are symmetric, premultiplying Equation 6.65 by $\{\phi\}_j^T$ eliminates the second bracketed term and gives

$$\{\phi\}_j^T \left[\frac{\partial [K]_T}{\partial \delta_i} - \frac{\partial \omega_j^2}{\partial \delta_i} [M]_T - \omega_j^2 \frac{\partial [M]_T}{\partial \delta_i}\right] \{\phi\}_j = 0 \tag{6.66}$$

Rearranging this equation provides the gradient of the natural frequency as

$$\frac{\partial \omega_j^2}{\partial \delta_i} = \frac{\{\phi\}_j^T \left[\frac{\partial [K]_T}{\partial \delta_i} - \omega_j^2 \frac{\partial [M]_T}{\partial \delta_i} \right] \{\phi\}_j}{\{\phi\}_j^T [M]_T \{\phi\}_j} \tag{6.67}$$

or

$$\frac{\partial \omega_j^2}{\partial \delta_i} = \{\phi\}_j^T \left[\frac{\partial [K]_T}{\partial \delta_i} - \omega_j^2 \frac{\partial [M]_T}{\partial \delta_i} \right] \{\phi\}_j \tag{6.68}$$

when the eigenvector is normalized with respect to the mass as in the presented algorithm. Using Equations 6.13 and 6.19, a direct solution to the gradient of the squared, natural frequency can be obtained. A form very similar to Equation 6.68 can be derived for linear buckling loads, but were not considered for this algorithm.

3. Dynamic Response Gradients. The dynamic gradients are derived by direct differentiation of the generalized displacement equation, and applying a technique similar to the last step of a psuedo-load approach. The psuedo-load approach uses Equation 6.22 to find the gradients. As mentioned previously, the first term of Equation 6.21 is assumed to be independent of the primary design variable such that Equation 6.22 can be used directly. Once all of the displacement derivatives are found the $\{b\}_j$ vector of appropriate values as given in Section VI.C.1 can be used

to find the stress and displacement gradients. First these displacement derivatives must be calculated.

a. Dynamic Displacement. The form shown in Equation 4.53 for the dynamic displacement is for a direct linear superposition of the modal contributions. The square root of the sum of the squares can be used in this algorithm and can be written as

$$U_j = \left[\sum_{k=1}^{t} (\phi_{jk} p_j)^2 \right]^{1/2} = \left[\sum_{k=1}^{t} x_k^2 \right]^{1/2} \tag{6.69}$$

where k represents the kth eigenvector, x_k, represents the kth modal component of U_j, and t is the total number of eigenvectors used in the modal analysis. Using the chain rule, the gradient can be written as

$$\frac{\partial U_j}{\partial \delta_i} = \sum_{\ell=1}^{t} \frac{\partial U_j}{\partial x_\ell} \frac{\partial x_\ell}{\partial \delta_i} \tag{6.70}$$

or

$$\frac{\partial U_j}{\partial \delta_i} = \sum_{\ell=1}^{t} \frac{1}{2} \left[\sum_{k=1}^{t} x_k^2 \right]^{-1/2} 2(x_\ell) \frac{\partial x_\ell}{\partial \delta_i} \tag{6.71}$$

This is the same as

$$\frac{\partial U_j}{\partial \delta_i} = \sum_{\ell=1}^{t} \frac{x_\ell}{U_j} \frac{\partial x_\ell}{\partial \delta_i} = \frac{1}{U_j} \sum_{\ell=1}^{t} x_\ell \frac{\partial x_\ell}{\partial \delta_i} \tag{6.72}$$

where

$$\frac{\partial x_\ell}{\partial \delta_i} = \frac{\partial \phi_{j\ell}}{\partial \delta_i} p_\ell + \phi_{j\ell} \frac{\partial p_\ell}{\partial \delta_i} \tag{6.73}$$

in which $j\ell$ represents the jth component of the ℓth eigenvector and p_ℓ is the ℓth eigenvector generalized displacement as given in Equation 4.52. Equation 6.72 states that the gradient of the jth global displacement is the sum of the change in the modal components times a weighting factor of the modal component divided by the total displacement.

The use of direct modal superposition calls for a slightly different form for the dynamic displacement gradients. These gradients are found directly from the equations by using Equation 4.53 as

$$\{U\} = [\phi] \{P\}_{max} \tag{6.74}$$

or

$$U_j = \sum_{\ell=1}^{t} \phi_{j\ell} p_\ell = \sum_{\ell=1}^{t} x_\ell \tag{6.75}$$

The gradients can then be found as

$$\frac{\partial U_j}{\partial \delta_i} = \sum_{\ell=1}^{t} \left(\frac{\partial \phi_{j\ell}}{\partial \delta_i} p_\ell + \phi_{j\ell} \frac{\partial p_\ell}{\partial \delta_i} \right) \tag{6.76}$$

which is identical to Equation 6.71 with the exception of the summation. In a sense the direct superposition becomes a subset of the root sum of the squares procedure. Both techniques require the gradients of the eigenvectors $\{\phi\}$, and the gradients of the generalized displacement $\{p\}$.

The generalized displacement gradients can be derived using Equation 4.52 for the jth component which takes the form

$$p_j)_{max} = \frac{\{\phi\}_j^T [M]}{m_j \omega_j^2} \{S_a\}_j \tag{6.77}$$

where the negative sign has been removed. Taking the partial derivative of Equation 6.77 gives

$$\frac{\partial p_j}{\partial \delta_i} = \frac{\partial \{\phi\}_j^T}{\partial \delta_i} \frac{[M]}{m_j \omega_j^2} \{S_a\}_j + \{\phi\}_j^T \frac{\partial [M]}{\partial \delta_i} \frac{\{S_a\}_j}{m_j \omega_j^2}$$

$$+ \{\phi\}_j^T \frac{[M]}{m_j \omega_j^2} \frac{\partial \{S_a\}_j}{\partial \delta_i} + \{\phi\}_j^T \frac{[M]}{\omega_j^2} \frac{\partial (\frac{1}{m_j})}{\partial \delta_i} \{S_a\}_j$$

$$+ \{\phi\}_j^T \frac{[M]}{m_j} \frac{\partial (\frac{1}{\omega_j^2})}{\partial \delta_i} \{S_a\}_j \tag{6.78}$$

where

$$m_j = \{\phi\}_j^T [M] \{\phi\}_j \tag{6.79}$$

and $\{S_a\}_j$ is given by Equation 4.55. Once again this equation requires the gradients of the eigenvectors, as well as, the gradients for the reciprocal generalized mass, m_j, the spectral accelerations, $\{S_a\}_j$, the total mass, [M], and the reciprocal squared natural frequencies, ω_j^2.

Using the chain rule the gradient for the reciprocal, generalized mass can be defined as

$$\frac{\partial \frac{1}{m_j}}{\partial \delta_i} = \frac{\partial \frac{1}{m_j}}{\partial m_j} \frac{\partial m_j}{\partial \delta_i} = -m_j^{-2} \frac{\partial m_j}{\partial \delta_i} \tag{6.80}$$

and Equation 6.79 provides

$$\begin{aligned} \frac{\partial m_j}{\partial \delta_i} &= \frac{\partial \{\phi\}_j^T}{\partial \delta_i} [M] \{\phi_j\} + \{\phi\}_j^T \frac{\partial [M]}{\partial \delta_i} \{\phi\}_j \\ &\quad + \{\phi\}_j^T [M] \frac{\partial \{\phi\}_j}{\partial \delta_i} \\ &= 2 \frac{\partial \{\phi\}_j^T}{\partial \delta_i} [M]\{\phi\}_j + \{\phi\}_j^T \frac{\partial [M]}{\partial \delta_i} \{\phi\}_j \end{aligned} \tag{6.81}$$

Equation 6.80 can then be written as

$$\frac{\partial \frac{1}{m_j}}{\partial \delta_i} = -\frac{1}{m_j^2} \left[2 \frac{\partial \{\phi\}_j^T}{\partial \delta_i} [M]\{\phi\}_j + \{\phi\}_j^T \frac{\partial [M]}{\partial \delta_i} \{\phi\}_j \right] \tag{6.82}$$

where once again the gradients of the eigenvectors are required.

The spectral acceleration gradients can be found from Equation 4.55, and the chain rule. Since the spectral acceleration is written in terms of the period the chain rule must be applied as

$$\frac{\partial\{S_a\}_j}{\partial\delta_i} = \frac{\partial\{S_a\}_j}{\partial T_j}\frac{\partial T_j}{\partial\omega_j}\frac{\partial\omega_j}{\partial\omega_j^2}\frac{\partial\omega_j^2}{\partial\delta_i} \tag{6.83}$$

where the period can be written in terms of the natural frequency as

$$T_j = \frac{2\pi}{\omega_j} \tag{6.84}$$

The derivative of the spectral acceleration, with $a_{max} = C_7$, with respect to the period is

$$\frac{\partial S_{aj}}{\partial T_j} = [4C_1(T_j-C_6)^3 + 3C_2(T_j-C_6)^2 + 2C_3(T_j-C_6) + C_4]C_7 \tag{6.85}$$

The second term in Equation 6.83 is found by using Equation 6.84 giving

$$\frac{\partial T_j}{\partial\omega_j} = -\frac{2\pi}{\omega_j^2} \tag{6.86}$$

and the third term can be written as

$$\frac{\partial\omega_j}{\partial\omega_j^2} = \frac{\partial(\omega_j^2)^{1/2}}{\partial\omega_j^2} = \frac{1}{2}\frac{1}{\omega_j} \tag{6.87}$$

The last term $\frac{\partial \omega_j^2}{\partial \delta_i}$ is given in Equation 6.67. Equation 6.85 is the reason a polynomial was chosen to represent the spectral acceleration, although any technique where the slope of the spectral acceleration could be determined could be used. Equation 6.83 can be rewritten as

$$\frac{\partial S_{aj}}{\partial \delta_i} = - \{\eta_j\} \frac{\pi}{\omega_j^3} \frac{\partial \omega_j^2}{\partial \delta_i} \tag{6.88}$$

where η_j represents the slope of Equation 4.55, the spectral acceleration or the value associated with Equation 6.85.

The gradient of the reciprocal, square of the natural frequency can be developed similarly to that of the reciprocal generalized mass. The chain rule can be used to produce

$$\frac{\partial \frac{1}{\omega_j^2}}{\partial \delta_i} = \frac{\partial \frac{1}{\omega_j^2}}{\partial \omega_j^2} \frac{\partial \omega_j^2}{\partial \delta_i} \tag{6.89}$$

which gives

$$\frac{\partial \frac{1}{\omega_j^2}}{\partial \delta_i} = - \left(\frac{1}{\omega_j^2}\right)^2 \frac{\partial \omega_j^2}{\partial \delta_i} = - \frac{1}{\omega_j^4} \frac{\partial \omega_j^2}{\partial \delta_i} \tag{6.90}$$

where the $\frac{\partial \omega_j^2}{\partial \delta_i}$ is given in Equation 6.67.

Using the information provided in Equations 6.82, 6.87, 6.88 and 6.90 the jth generalized displacement gradient can be written as

$$\frac{\partial p_j}{\partial \delta_i} = \frac{\partial \{\phi\}_j^T}{\partial \delta_i} \frac{[M]}{m_j \omega_j^2} \{S_a\}_j + \{\phi\}_j^T \frac{\partial [M]}{\partial \delta_i} \frac{\{S_a\}_j}{m_j \omega_j^2}$$

$$- \{\phi\}_j^T \frac{[M]}{m_j^2 \omega_j^2} \left[2 \frac{\partial \{\phi\}_j^T}{\partial \delta_i} [M] \{\phi\}_j \right.$$

$$\left. + \{\phi\}_j^T \frac{\partial [M]}{\partial \delta_i} \{\phi\}_j \right] \{S_a\}_j - \{\phi\}_j^T \frac{[M]}{m_j \omega_j^2} \left[\frac{\pi}{\omega_j^3} \{\eta\}_j \right.$$

$$\left. + \frac{\{S_a\}_j}{\omega_j^2} \right] \frac{\partial \omega_j^2}{\partial \delta_i} \qquad (6.91)$$

where $\frac{\partial [M]}{\partial \delta_i}$ is given in Equation 6.19 and the gradients of the eigenvectors will be discussed in the next Section. If the eigenvectors are "always" orthogonalized with respect to the mass, the generalized mass will always be unity. Therefore the term associated with the $\partial \frac{1}{m_j} / \partial \delta_i$ becomes zero, in other words this will be unaffected by a change in the design variable. For the case of eigenvectors normalized with respect to the mass, Equation 6.91 becomes

$$\frac{\partial p_j}{\partial \delta_i} = \frac{\partial \{\phi\}_j^T}{\partial \delta_i} \frac{[M]}{\omega_j^2} \{S_a\}_j + \{\phi\}_j^T \frac{\partial [M]}{\partial \delta_i} \frac{\{S_a\}_j}{\omega_j^2}$$

$$- \{\phi\}_j^T \frac{[M]}{\omega_j^2} \left[\frac{\pi}{\omega_j^3} \{\eta\}_j + \frac{\{S_a\}_j}{\omega_j^2} \right] \frac{\partial \omega_j^2}{\partial \delta_i} \qquad (6.92)$$

where the m_j terms are set to one and the third term of Equation 6.91 becomes zero. The effects of this term, when there is mass normalization, are absorbed into the first term which provides the effect of the change in the eigenvectors. If this normalization procedure is not used, Equation 6.91, in its entirety, should be used.

The use of the previously derived equation to find the gradient of the generalized displacement hinges on finding a numerical technique to provide the gradients of the eigenvectors. The most common technique is to write the eigenvectors as a linear combination of all the eigenvectors (49,50,51). A more direct approach was chosen based upon a direct differentiation of the free vibration equation (51,52). This differentiation of Equation 4.27 gives

$$\left[\frac{\partial [K]_T}{\partial \delta_i} - \frac{\partial \omega_j^2}{\partial \delta_i} [M]_T - \omega_j^2 \frac{\partial [M_T]}{\partial \delta_i}\right]\{\phi\}_j + \left[[K]_T - \omega_j^2 [M]_T\right] \frac{\partial \{\phi\}_j^T}{\partial \delta_i} = 0 \qquad (6.93)$$

Rearranging Equation 6.93, it becomes

$$\left[[K]_T - \omega_j^2 [M]_T\right] \frac{\partial \{\phi\}_j^T}{\partial \delta_i} = -\left[\frac{\partial [K]_T}{\partial \delta_i} - \frac{\partial \omega_j^2}{\partial \delta_i} [M]_T - \omega_j^2 \frac{\partial [M]_T}{\partial \delta_i}\right]\{\phi\}_j \qquad (6.94)$$

Since the matrix

$$\left[[K]_T - \omega_j^2 [M]_T\right] \tag{6.95}$$

is singular, a simple inversion cannot be performed in order to solve for $\partial\{\phi\}_j^T/\partial\delta_i$. The rank of this matrix is less than the number of degrees of freedom by the formulation of Equation 4.27. This also states that the eigenvector is only valid within a multiple due to this singularity, which provides the key to solving Equation 6.94. Forcing the change of one component of the eigenvector to be zero is the same as always forcing that component to take on a specific value such as unity. This provides a boundary condition for the elimination of the row and column associated with the component whose change or gradient component is assumed to be zero, and provides a matrix which is non-singular and can be inverted. Therefore the eigenvector derivative will take this form

$$\frac{\partial\{\phi'\}_j^T}{\partial\delta_i} = \left\{ \frac{\partial\phi'_{ij}}{\partial\delta_i}, \frac{\partial\phi'_{2j}}{\partial\delta_i} \ldots, 0, \ldots \frac{\partial\phi'_{nj}}{\partial\delta_i} \right\} \tag{6.96}$$

where the zero term has been chosen as the component associated with the degree of freedom defined by the jth natural frequency. Therefore, the eigenvector gradients can be written as

$$\left(\frac{\partial\{\phi'\}_j^T}{\partial\delta_i}\right)_R = -\left[[K]_T - \omega_j^2[M]\right]_R^{-1}\left[\frac{\partial[K]_T}{\partial\delta_i} - \frac{\partial\omega_j^2}{\partial\delta_i}[M]_T - \omega_j^2\frac{\partial[M]_T}{\partial\delta_i}\right]_R(\{\phi'\}_j)_R \tag{6.97}$$

where R stands for the reduced system and the prime stands for the eigenvector which has the jth component removed.

There is a problem associated with the use of Equation 6.97. If the eigenvector is normalized with respect to the mass or some other quantity, the change in the jth component will not be zero from one iteration to the next. Therefore, a correction term must be applied. The correction is found by writing the eigenvector which is normalized with respect to the mass in terms of the eigenvector with the jth component equal to unity as

$$\{\phi''\}_j^T = \frac{\{\phi'\}_j}{m_j^{1/2}} \tag{6.98}$$

where m_j is the normalized mass given as

$$m_j = \{\phi'\}_j^T[M]\{\phi'\}_j \tag{6.99}$$

The gradient of $\{\phi\}_j^T$ can be derived as

$$\frac{\partial\{\phi''\}_j^T}{\partial\delta_i} = \frac{1}{(m_j)^{1/2}}\frac{\partial\{\phi'\}_j^T}{\partial\delta_i} + \{\phi'\}_j^T\frac{\partial\left(\frac{1}{m_j}\right)^{1/2}}{\partial\delta_i} \tag{6.100}$$

Using the chain rule and Equation 6.82, Equation 6.100 becomes

$$\frac{\partial\{\phi''\}_j^T}{\partial\delta_i} = \frac{1}{m_j}^{1/2} \frac{\partial\{\phi'\}_j^T}{\partial\delta_i}$$

$$- \frac{1}{2}\{\phi'\}_j^T \frac{1}{m_j}^{3/2} \left[2 \frac{\partial\{\phi'\}_j^T}{\partial\delta_i} [M]\{\phi'\}_j \right.$$

$$\left. + \{\phi'\}_j^T \frac{\partial[M]}{\partial\delta_i} \{\phi'\}_j \right] \qquad (6.101)$$

where the prime stands for the reduced unnormalized eigenvector and the double prime represents the reduced normalized eigenvector.

Solving for the gradients of the eigenvectors requires a large portion of the total computational time. The inversion of the matrix shown in Equation 6.97 is required for each mode used in the modal analysis. The gradients of the eigenvectors should be in storage in order to be accessible as they are needed in several phases of the dynamic gradient approach presented. In fact, these equations need be solved for only the eigenvectors required. The combination of this technique along with a subspace iteration eigenvalue solver would be very efficient.

b. Dynamic Stress. The dynamic stress gradients are determined by using Equations 6.22 and 6.72. Making the assumption that the $\{b\}_j$ vectors are independent of the

design variables and the fact that Equation 6.72 produces all of the dynamic displacement gradients with respect to both the primary design variables and the displacements, the stress gradients can be written as

$$\frac{\partial u_j}{\partial \delta_i} = \{b\}_j^T \frac{\partial \{U\}}{\partial \delta_i} \tag{6.102}$$

where the vectors $\{b\}_j$ have been defined for each element type in Section VI.C. This is very similar to the psuedo-load techniques as used for mathematical programming. This calculation in Equation 6.102 can be performed since all of the terms of $\frac{\partial \{U\}}{\partial \delta_i}$ can be found from the equations presented in the previous section. Just as in the static response gradients the transformations have no effect as long as $\{b\}_j^T$ and $\frac{\partial \{U\}}{\partial \delta_i}$ are in the same coordinate system.

One difficulty is due to the need for the gradients of the rotational degrees of freedom associated with $\{U\}$. Since the $\{b\}_j$ vectors presented in Section III.C are dependent upon these rotational degrees of freedom in the elemental level, they are also dependent upon the rotational degrees of freedom in the global system. The first inclination is to use a reduced vector for $\{b\}_j$ as given in Equation 6.60, but this is not possible due to the relationship presented in Equation 6.21 restated as

$$\frac{\partial u_j}{\partial \delta_i} = \frac{\partial \{b\}_{j\ RED}^T}{\partial \delta_i} \{U\} + \{b\}_{j\ RED}^T \frac{\partial \{U\}}{\partial \delta_i} \tag{6.103}$$

The term $\frac{\partial \{b\}^T_{j\ RED}}{\partial \delta_i}$ requires the derivative of Equation 6.60 stated as

$$\frac{\partial \{b\}_{j\ RED}}{\partial \delta_i} = \frac{\partial}{\partial \delta_i}\left[\{b_2\}_j - [K_{21}][K_{11}]^{-1}\{b_1\}_j\right] \qquad (6.104)$$

Eventually this would require the partial derivative of $[K_{11}]^{-1}$ which is quite difficult to find. Therefore the gradients for the eliminated rotational degrees of freedom must be found.

These gradients can be found numerically using the relationship

$$\begin{bmatrix} K_{11} & K_{12} \\ K_{21} & K_{22} \end{bmatrix} \begin{Bmatrix} U_1 \\ U_2 \end{Bmatrix} = \begin{Bmatrix} 0 \\ R_D \end{Bmatrix} \qquad (6.105)$$

where U_1 represents the rotational displacements prior to reduction and R_D represents the dynamic forces. Taking the partial derivative with respect to the primary design variable gives

$$\begin{bmatrix} \frac{\partial K_{11}}{\partial \delta_i} & \frac{\partial K_{12}}{\partial \delta_i} \\ \frac{\partial K_{21}}{\partial \delta_i} & \frac{\partial K_{22}}{\partial \delta_i} \end{bmatrix} \begin{Bmatrix} U_1 \\ U_2 \end{Bmatrix} + \begin{bmatrix} K_{11} & K_{12} \\ K_{21} & K_{22} \end{bmatrix} \begin{Bmatrix} \frac{\partial U_1}{\partial \delta_i} \\ \frac{\partial U_2}{\partial \delta_i} \end{Bmatrix} = \begin{Bmatrix} 0 \\ \frac{\partial R_D}{\partial \delta_i} \end{Bmatrix} \qquad (6.106)$$

Rearranging the top line of Equation 6.106 gives

$$[K_{11}] \frac{\partial\{U_1\}}{\partial\delta_i} + [K_{12}] \frac{\partial\{U_2\}}{\partial\delta_i} = 0 - \frac{\partial[K_{11}]}{\partial\delta_i}\{U_1\}$$

$$- \frac{\partial[K_{12}]}{\partial\delta_i}\{U_2\} \tag{6.107}$$

or

$$\frac{\partial\{U_1\}}{\partial\delta_i} = [K_{11}]^{-1}\left[- \frac{\partial[K_{11}]}{\partial\delta_i}\{U_1\} - \frac{\partial[K_{12}]}{\partial\delta_i}\{U_2\}\right.$$

$$\left. - [K_{12}] \frac{\partial\{U_2\}}{\partial\delta_i}\right] \tag{6.108}$$

This is very similar to Equation 6.61 if it is rewritten as

$$\frac{\partial\{U_1\}}{\partial\delta_i} = [K_{11}]^{-1}\left[\{R'\} - [K_{12}] \frac{\partial\{U_2\}}{\partial\delta_i}\right] \tag{6.109}$$

where

$$\{R'\} = -\left\{\frac{\partial[K_{11}]}{\partial\delta_i}\{U_1\} + \frac{\partial[K_{12}]}{\partial\delta_i}\{U_2\}\right\} \tag{6.110}$$

The similarity of Equation 6.61 and Equation 6.109 allows the use of the previously defined subroutines for expansion of the reduced set of displacements to that of the total set of displacements. Once the gradient terms associated with the rotational degrees of freedom are found using Equation 6.109, and the appropriate transformations are used to place the $\frac{\partial\{U\}}{\partial\delta_i}$ and $\{b\}_j$ into a common reference

system Equation 6.102 can be used to find the dynamic stress gradients.

The gradient calculations are generally the most time consuming portion of an optimization algorithm. The developed algorithm is no exception. Each static constraint generates a virtual load vector which must be used to find the virtual displacements, requiring one inversion of the stiffness matrix, and each response spectrum analysis requires the inversion of "m" matrices of order one degree smaller than the stiffness for the "m" modes required by the modal analysis. The ATC-03 dynamic portion is treated as a static problem using the virtual load technique with very good results.

VII. OPTIMIZATION ALGORITHM

Chapters III, IV, V, and VI have all of the needed information to develop the algorithm used in finding the results presented within Chapters VIII and IX. Any optimization algorithm used has at least four major parts: the analysis, constraint determination, optimization, and termination. Within these four major areas there are a range of techniques and procedure some of which were mentioned in the previous Chapters. This Chapter will break the algorithm into each important operation while citing the section or equations that are appropriate for that operation. The major steps within the algorithm are:

1) Inputing the initial data.
2) Determining the secondary design variables.
3) Analyzing the structures.
4) Determining the primary, active constraints.
5) Scaling of the primary design variables.
6) Checking of the termination criteria.
7) Calculating the gradients.
8) Determining the Lagrange multipliers.
9) Resizing of the primary design variables.
10) Checking for active and passive elements.
11) Finalizing output and plot information.

These topics have all been discussed in detail in the preceding chapters, but need to be brought together in a unified algorithm.

Inputing the data is the first step. The input includes all of the dimensions pertaining to the structural layout, the element material properties, the element primary design variables, the load combinations, the upper and lower constraint values, the termination criteria, and the convergence control parameter. The input also includes either the specific weights or costs per unit volume for the objective function, as well as, the type of analyses to be performed. There are several options for the type of analyses coupled with optimization constraints:

1) Static stress constraints.
2) Static displacement constraints.
3) Static displacement and stress constraints.
4) Frequency constraints.
5) Static displacement and stress, frequency, and dynamic displacement and stress constraints.

The input structure is outlined in the computer manual (53).

The second operation is to determine the secondary design variables for each element. These are determined by using Equation 3.12. For a single analysis the option to input the secondary design variables is available.

As mentioned in the input data there are several options with respect to analysis. The static analysis is performed as given in Equation 4.16. The natural frequency analysis is performed by using the Jacobi iteration approach given in Equation 4.26 and Appendix B. The

dynamic analysis is performed by using modal analysis with the root sum of the squares for the modal contributions or direct superposition as given in Equations 4.54 and 6.75, or it is performed using the ATC-03 provisions. The ATC-03 allows the use of two approaches: the equivalent lateral force technique presented in Equations 4.60 to 4.62 and the modal analysis procedure presented in Equations 4.63 to 4.66. Keep in mind that the dynamic responses replace the static lateral loads in the load combination given in Equation 4.24. The static and dynamic loads are linearly superimposed with no initial effects of the static analysis taken into account for the dynamic analysis.

After the analyses are performed, the constraints must be separated into potentially active and passive sets. These active constraints are chosen by using Equations 5.45 and 5.46 and are used in the development of the equations for the Lagrange multipliers. If an incorrect set of active constraints are chosen, the optimization algorithm will have to adjust. This adjustment is made in the scaling step or during the Lagrange multiplier determination.

Scaling is used in several instances during the optimization. As defined in Section V.I, scaling is used to force the most violated constraint within the active region defined by Equations 5.45 and 5.46 by using the factors given in Equations 5.47 and 5.48. After scaling

is performed, steps 2-4 must be performed again. Since these three-dimensional problems are nonlinear with respect to the primary design variable, the scaling is an iterative process. Any time there are no constraints in the active region or whenever a constraint is violated a scaling will take place.

At this point, if a scaling was not needed the termination criteria is checked. The algorithm will not terminate if a scaling is required to bring a constraint into the active region unless the total number of analyses exceeds the input limit. Otherwise, the other termination criteria are checked for percentage of weight change and/or the total number of analyses. If the termination criteria are not satisfied another cycle of optimization (steps 7-10) will occur.

The optimization phase begins by calculating the gradients of the active constraints with respect to the primary design variables. These gradient calculations were discussed in great detail in Chapter VI. The virtual load technique was used for the static and ATC-03 gradients, whereas direct differentiation provides the numerical procedures for the frequency and modal analysis gradients.

These gradients are then used to create a set of linear equations used for the determination of the Lagrange multipliers. These linear equations are defined in Equation 5.44. Once the equations have been solved, the Lagrange multipliers must be checked with respect to the

optimality criteria stated in Equations 5.5, 5.6 and 5.7. If all of the Lagrange multipliers are positive a valid set of active constraints were chosen in step 4. If one or more of the Lagrange multipliers are negative, the constraints associated with those negative Lagrange multipliers are removed from the active set and the reduced set of equations are resolved until all Lagrange multipliers are positive. If all of the Lagrange multipliers are negative, all but the last added active constraint is kept for the optimization procedure. This allows the algorithm a chance to continue and pick a new set of active constraints in step 4 during the next complete cycle starting at step 2. This rarely occurs except when frequency constraints are coupled with displacement and/or stress constraints. Equation 5.44 also takes into account the effect of side constraints or passive elements (those elements that have reached their maximum or minimum values).

Once the Lagrange multipliers have been determined as all positive values, the optimization proceeds to the resizing of the elements. This is accomplished by using the linear recurrence relation in Equation 5.26. These equations make use of only those active constraints which were left after the determination of the Lagrange multipliers. If Equation 5.26 forces any of the elements to violate the side constraints, the algorithm must go back to step 8 and regenerate the equations for the Lagrange multipliers. Once these are all positive the recursive

relationships can be used again. Therefore, steps 8 and 9 are iterative in nature. Once there are no new passive elements generated by Equation 5.26, the first cycle of optimization is finished.

After this first cycle of optimization is finished the algorithm begins with step 2 and continues in this fashion until step 6 is satisfied. Once step 6 is satisfied, the algorithm jumps to step 11 for processing of the output. The output provides the input data, the optimum cycle data such as: elemental forces and stresses, the displacements, the natural frequencies, final sizes, final value for the objective function, number of cycles of optimization, and active constraints. The option also exists to print all data for every cycle.

VIII. ALGEBRAIC AND NUMERICAL ILLUSTRATION OF THE OPTIMIZATION ALGORITHM

This chapter has been designed to provide a transition from the theoretical development to actual computer generated solutions. Several topics presented within the previous sections are best developed and understood by illustration. Therefore, selected topics, as well as, two simple examples will be presented.

A. ALGEBRAIC EXAMPLE FOR MULTIPLE CONSTRAINTS

The equations and derivations in Chapters IV, V, and VI were given in concise mathematical form. Therefore, this section will be used to illustrate the specific use of these equations.

Each constraint must be written such that its value will always be less than zero. The constraint equations for displacement, U_j, become

$$g_j = (U_j - \overline{U}_j) \leq 0 \tag{8.1}$$

or

$$g_j = (\underline{U}_j - U_j) \leq 0 \tag{8.2}$$

where $\overline{U}_j$ is the upper bound and $\underline{U}_j$ is the lower bound for displacement U_j. The constraint g_j can be used to represent

any type of constraint by replacing U_j, $\bar{U}_j$, and $\underline{U}_j$ with the appropriate response, upper bounds, and lower bound values for the stress, σ_j, the square of the natural frequency, ω_j^2, and the drift, Δ_j. Therefore, the Lagrangian, represented by Equation 5.4, becomes

$$L = \sum_{i=1}^{n} \gamma_i \ell_i (C_{1A} \delta_i^{C_{2A}} + C_{3A}) + \sum_{j=1}^{\ell_1} \lambda_j (U_j - \bar{U}_j) +$$

$$\sum_{j=1}^{\ell_2} \lambda_j (\underline{U}_j - U_j) + \sum_{j=1}^{\ell_3} \lambda_j (\sigma_j - \bar{\sigma}_j) + \sum_{j=1}^{\ell_4} \lambda_j (\underline{\sigma}_j - \sigma_j) +$$

$$\sum_{j=1}^{\ell_5} \lambda_j (\omega_j^2 - \bar{\omega}_j^2) + \sum_{j=1}^{\ell_6} \lambda_j (\underline{\omega}_j^2 - \omega_j^2) + \sum_{j=1}^{\ell_7} \lambda_j (\Delta_j - \bar{\Delta}_j) +$$

$$\sum_{j=1}^{\ell_8} \lambda_j (\underline{\Delta}_j - \Delta_j) \qquad (8.3)$$

Using the Kuhn-Tucker conditions in Equations 5.5 to 5.7, the optimality criteria in Equation 5.15 becomes

$$T_i = \left[\pm \sum_{j=1}^{\ell_1+\ell_2} \lambda_j \frac{\partial U_j}{\partial \delta_i} \pm \sum_{j=1}^{\ell_3+\ell_4} \lambda_j \frac{\partial \sigma_j}{\partial \delta_i} \pm \sum_{j=1}^{\ell_5+\ell_6} \lambda_j \frac{\partial \omega_j^2}{\partial \delta_i} \pm \sum_{j=1}^{\ell_7+\ell_8} \lambda_j \frac{\partial \Delta_j}{\partial \delta_i} \right] \Big/ \left[\gamma_i \ell_i C_{1A} C_{2A} \delta_i^{(C_{2A}-1)} \right] = 1$$

$$i = 1, \ldots, n \qquad (8.4)$$

where the upper bound constraints use the positive sign and the lower bound constraints use the negative sign.

In order to reduce the number of Lagrange multiplier equations and the number of coupled terms, two equations will be derived. The first will consider an upper bound displacement constraint as active, and the second will consider an upper bound drift as active. The simultaneous equations to be solved for the Lagrange multipliers are derived from Equation 5.42 as

$$r(U-\bar{U}) - \sum_{i=1}^{n_1} \frac{\partial U}{\partial \delta_i} \delta_i + r \sum_{i=n_1+1}^{n} \frac{\partial U}{\partial \delta_i} (\delta_i^P - \delta_i) =$$

$$\lambda_U \left(\sum_{i=1}^{n_1} \left(\frac{\partial U}{\partial \delta_i}\right)^2 / (\lambda_i \ell_i C_{1A} C_{2A} \delta_i^{(C_{2A}-1)}) \right) +$$

$$+ \lambda_\Delta \left(\sum_{i=1}^{n_1} \left(\frac{\partial U}{\partial \delta_i} \frac{\partial \Delta}{\partial \delta_i}\right) / (\lambda_i \ell_i C_{1A} C_{2A} \delta_i^{(C_{2A}-1)}) \right) \tag{8.5}$$

and

$$r(\Delta-\bar{\Delta}) - \sum_{i=1}^{n_1} \frac{\partial \Delta}{\partial \delta_i} \delta_i + r \sum_{i=n_1+1}^{n} \frac{\partial \Delta}{\partial \delta_i} (\delta_i^P - \delta_i) =$$

$$\lambda_U \left(\sum_{i=1}^{n_1} \left(\frac{\partial \Delta}{\partial \delta_i} \frac{\partial U}{\partial \delta_i}\right) / (\gamma_i \ell_i C_{1A} C_{2A} \delta_i^{(C_{2A}-1)}) \right)$$

$$+ \lambda_\Delta \left(\sum_{i=1}^{n_1} \left(\frac{\partial \Delta}{\partial \delta_i}\right)^2 / (\gamma_i \ell_i C_{1A} C_{2A} \delta_i^{(C_{2A}-1)}) \right) \tag{8.6}$$

where all quantities on the left side of Equations 8.5 and 8.6 are known and all quantities on the right side of the Equations are known except λ_U and λ_Δ, the Lagrange multipliers associated with the displacement constraint and drift constraints, respectively. Equations 8.5 and 8.6 show that the simultaneous equations to be solved are symmetric, and they do account for constraint interaction through the off-diagonal terms. These equations are rigorous and time consuming to generate, but provide a reliable means for finding the Lagrange multipliers. Many algorithms use only the diagonal terms of these equations which ignore the constraint interaction. Including this interaction seems to provide an algorithm which provides better constraint control between cycles of optimization.

From Equations 8.4, 8.5, and 8.6, it is imperative to have the correct or good approximations of the constraint gradients. The gradients are found by using the virtual load technique for the static response gradients, Equation 6.20, an approach similar to the psuedo-load technique for the dynamic response gradients, Equation 6.102, and a direct numerical technique for the square of the natural frequency, Equation 6.68.

The drift constraint will be used to explain the derivation of the virtual load technique. First, the drift between levels m and n can be written in terms of the displacements as

$$\Delta_{mn} = \{b\}_{mn}^{T} \{U\} = [0\ldots,0,1,0\ldots,0,-1,0,\ldots,0]\{U\} \tag{8.7}$$

where the positive 1 is in the nth location and the negative 1 is in the mth location. The virtual load approach would then find the component of the gradient of the drift as

$$\frac{\partial \Delta_{mn}}{\partial \delta_i} = - \{v\}_{mn}^{T} \frac{\partial [K]_T}{\partial \delta_i} \{U\} \tag{8.8}$$

where

$$\{v\}_{mn} = [K]_T^{-1} \{b\}_{mn} \tag{8.9}$$

If a psuedo-load approach were used the gradient would be written as

$$\frac{\partial \Delta_{mn}}{\partial \delta_i} = \{b\}_{mn}^{T} \frac{\partial \{U\}}{\partial \delta_i} \tag{8.10}$$

in which the gradient of the displacements would have to be found.

Once the gradients and the Lagrange multipliers are found, the optimality criteria can be used to resize the primary design variables. Then the new secondary design variables are determined from the new primary design variable using Equation 3.12. These new geometric quantities are then used to calculate the new response and to start the optimization once again.

B. THE CHOICE FOR PRIMARY DESIGN VARIABLES

Classical optimization techniques are generally developed for convex systems. If the convexity of the constraints can be relaxed to a near linear situation, the solution techniques become more efficient. Unfortunately, structural optimization problems are nonlinear and nonconvex. These effects can be minimized by using certain geometric properties for the primary design variables.

Since the objective function is linear in terms of the cross-sectional areas, and the dominant stiffness parameters for the bending elements are the major-axis moments of inertia, these quantities were considered the best possibilities for the primary design variables. In addition to these quantities, the inverse cross-sectional area and the inverse major-axis moment of inertia were considered. The inverse of these quantities can reduce the nonlinearity of the constraints (this effect is most pronounced for mathematical programming techniques which travel along the constraint boundaries). When referring to the use of the major-axis moment of inertia as the primary design variable this applies to only the bending elements and the concrete panel. The brace was always represented by its cross-sectional area and its inverse.

The comparison of primary design variables was made using the two-dimensional structure shown in Figure 21. The frame consists of two rectangular cross-sectional beam-column elements and a brace. All elements were made of

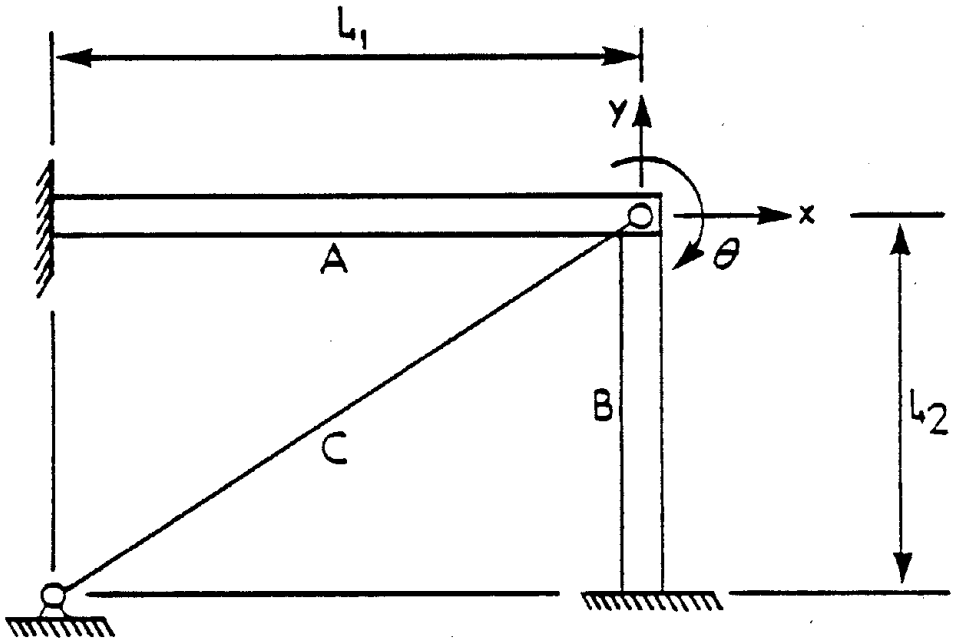

Figure 21. Two Dimensional Structure Consisting of Two Beam-columns and a Brace

steel with a modulus of elasticity of 30,000 ksi (20,700 kN/cm^2). The beam-column crossections were forced to have a depth to width ratio of 2.0 which provides the major-axis moment of inertia, I, in terms of the cross-sectional area, A, as

$$I = \frac{1}{6} A^2 \tag{8.11}$$

The lengths L_1 and L_2 were both 15.0 ft. (4.58 m). Each element started with an initial area of 30.0 in^2 (194 cm^2). The analysis was considered similar to a steady state problem such that the load vector was 50.0 kip (223 kN) in the x-direction, -100 kip (445 kN) in the y-direction, and 1000 k-in (113 kN-m) in the θ-direction. It was similar to a steady state situation in that the solution was based upon this equation

$$[[K] - \bar{\omega}^2[M]]\{U\} = \{P\} \tag{8.12}$$

where, [K], is the stiffness matrix, $\bar{\omega}$, is the frequency of the applied load, [M], is the mass matrix, {U} is the displacement vector, and {P} is the constant load vector. The fact that a constant load vector was used, creates a situation which is not purely steady state. This procedure was used in order to test the gradient calculations of the stiffness and mass within a structural situation. The value for $\bar{\omega}$ was 100 rad/sec. Each element was constrained

to have its stress below 22 ksi (15 kN/cm^2); while the bending elements were to have cross-sectional areas above 0.1 in^2 (0.6 cm^2) and the brace was to have a cross-sectional area above 2.0 in^2 (12.9 cm^2). The x-displacement was to remain below 0.020 in. (0.05 cm), and the y-displacement was to remain below 0.026 in. (0.066 cm). Small displacement constraints were chosen in order to have the displacements close to their active values concurrently with the stress constraints.

The results are presented in Table I. All of the results in Table I correspond to two cycles of optimization. All four solutions provide similar sizes for the bending elements, but the inverse geometric properties provide considerably larger values for the brace element. Each design was controlled by the stress in element B. Within the first cycle of each problem the stress in each bending element was within 95 percent of the active value, therefore, both of these stresses were considered as active constraints. In each case the Lagrange multipliers for the stress in element A was negative (approximately -4.0×10^{-3}) while the Lagrange multiplier for the stress in element B was positive (approximately 4.2×10^{-3}). Since the constraint for element A provided a negative Lagrange multiplier, it was dropped from the active set of constraints, and the Lagrange multiplier equations were resolved providing a value for the remaining constraint of approximately 1.7×10^{-4}. Note that there is considerable difference in

TABLE I. Results for a Two Dimensional Frame with Different Primary Design Variables after Two Cycles of Optimization (1 in = 2.54 cm, 1 kip = 4.45 kN)

	Design Variable			
	Area	Moment of Inertia	Inverse Area	Inverse Moment of Inertia
A_A (in^2)	26.13	25.81	26.13	25.83
A_B (in^2)	26.28	26.07	26.28	26.71
A_C (in^2)	13.10	11.68	17.37	15.48
Wt. (kip)	3.62	3.52	3.93	3.80
No. Scalings	5	2	5	2
No. Analyses	7	4	7	4

the values for the Lagrange multipliers after one constraint is removed.

Optimality criteria approaches are sensitive to the set of constraints chosen to be active. Making the correct choices for this active set is still being studied by the structural optimization researchers. Using the major-axis moment of inertia for the bending elements and the cross-sectional area for the brace provides the lowest weight with the least amount of computational effort. The cross-sectional area produced similar results to those produced by the major-axis moment of inertia problem except that the analyses required was considerably larger. As seen from Table I this is due to the number of scalings required to reach a set of active constraints. (Reaching an active constraints requires the response to be "close" to the limiting value.) The large number of scalings is due to the nonlinear factoring associated with the moment of inertia when using the area as the primary design variable. From Equation 8.11 it is seen that a linear scaling of the area provides a moment of inertia factor which is one-sixth of the square of the factor for the area. Therefore, it was decided to use the major-axis moment of inertia as the primary design variable for the bending elements and the concrete panels and to use the cross-sectional area for the brace elements. The use of these primary design variables also enhances the control of the constraint values within the optimization. In other words, the constraint responses

tend to remain close to their limits after optimization which reduces the need for scaling which requires a re-analysis.

The cases where the area of each element and the moment of inertia of the bending elements coupled with the area for the brace were taken one cycle further. This was to verify that the major-axis moment of inertia did provide a better approach to the problem. The final results are presented in Table II. The distribution is very similar for each case, but the major-axis moment of inertia problem provides the lesser final weight with fewer analyses required. As in the previous two cycles only the stress constraint for element B was active.

C. THREE DIMENSIONAL DESIGN EXAMPLE

A one-story, one-bay, three-dimensional frame, as shown in Figure 22, was thoroughly examined with several numerical techniques and constraint cases. One of these cases will be presented here in order to help the overall understanding of the algorithm. An in depth look at the first cycle will be presented along with the results of the entire design. This example includes every element type, and it will include static stress and displacement constraints.

The three-dimensional structure was used to test the use of mixed element types as well as mixed constraints. The frame consists of a square, rigid-slab which was

TABLE II. Results for a Two Dimensional Frame with Different Primary Design Variables after Three Cycles of Optimization (1 in = 2.54 cm, 1 kip = 4.45 kN)

	Design Variable	
	Area	Moment of Inertia
A_A (in^2)	25.5	25.2
A_B (in^2)	27.8	27.4
A_C (in^2)	6.7	5.9
Wt (kip)	3.21	3.11
No. Scalings	6	2
No. Analyses	9	5

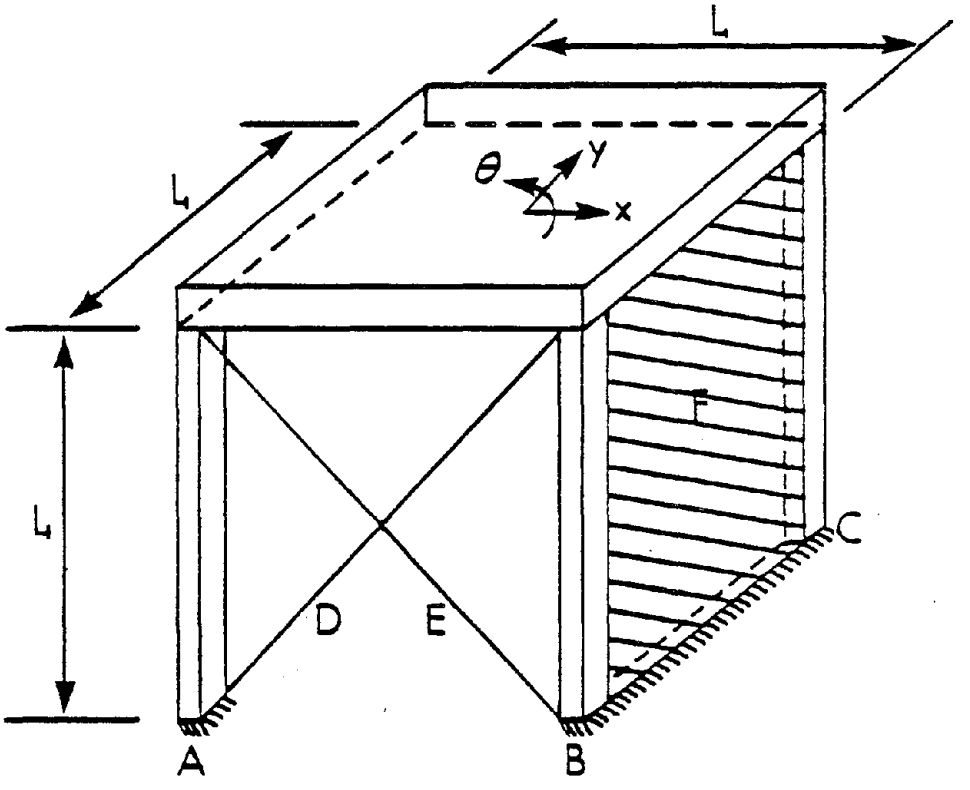

Figure 22. Three Dimensional, Multi-element Structure

10.0 ft. by 10.0 ft. (3.05 m by 3.05 m) which was supported by three 10 ft. (3.05 m) rectangular, steel columns (A, B, and C). The rectangular cross sections are assumed to have a depth to width ratio of 1.5, and the concrete panel is assumed to have a fixed depth which spans between columns B and C. The column depths are parallel to the y-direction. Steel X-bracing (D and E) are in one vertical plane with a concrete flexural panel (F) in another plane as shown in Figure 22. The concrete panel does not include steel. The loading consists of 300 kips (1335 kN) in the x-direction, 100 kips (445 kN) in the y-direction, and 3000 kip-in (339 kN-m) in the θ-direction.

The constraints consist of static displacement and stress constraints. The maximum allowable deflection is 0.5 in. (1.27 cm) for both the x- and y-directions. The maximum allowable stresses are 30 ksi (20.7 kN/cm^2) for the steel elements, and 3.0 ksi (2.1 kN/cm^2) for the concrete panel. Three side constraints are used; 864,000 in^4 (0.359 m^4) is the lower limit for the concrete panel's moment of inertia, 35.0 in^4 (1451 cm^4) is the lower limit for the steel columns, and 5.0 in^2 (32.3 cm^2) is the lower limit for the steel braces. Moduli of elasticity of 30,000 ksi (20,700 kN/cm^2) and 3,000 ksi (2,070 kN/cm^2) were used for the steel and concrete elements, respectively. The final results of each iteration are shown in Table III.

This example has two exceptions with respect to the algorithm presented in Chapter VII. A psuedo-scaling was

used. When this solution was generated a scaling based upon the cross sections and constraints was developed which used the largest ratio of the actual response to the constraint limit to the 4/3 power. This type of scaling could not be justified within later examples, therefore the standard scaling using a power of 1.0 was used. Secondly a scaling was performed at the end of each optimization cycle. Later this was not found to be necessary, therefore, a scaling only occurs when the constraints violate the upper limit or when there is no violation, but all constraints are below the lower active limit of $(1-P_1)$.

A step by step procedure of how the first cycle was generated will be given:

Step 1 - The initial values for the element sizes were chosen as 1500 in^4 (62,400 cm^4) for elements A, B and C, 100 in^2 (645 cm^2) for elements D and E, and 2,000,000 in^4 (0.832 m^4) for the concrete panel.

Step 2 - The static displacements were determined as $x = 0.19$ in (0.49 cm), $y = 0.17$ in (0143 cm), and $\theta = -0.003$ rad.

Step 3 - The maximum normal stress was determined for each element as $\sigma_A = 28.8$ ksi (19.9 kN/cm^2), $\sigma_B = 0.76$ ksi (0.52 kN/cm^2), $\sigma_C = 19.4$ ksi (13.4 kN/cm^2), $\sigma_{D,E} = 1.74$ ksi (1.20 kN/cm^2), and $\sigma_F = -0.02$ ksi (-0.014 kN/cm^2).

Step 4 - The largest ratio of structural response to constraint value was determined and used to find the scaling factor as

$$f = \left(\frac{28.8}{30}\right)^{4/3} = 0.947 \qquad (8.13)$$

Step 5 - The initial sizes were adjusted by the factor given in Equation 8.13. A lower limit of 95% of the constraint limit was set as the acceptable limit. Within the current algorithm the ratio within the parenthesis of Equation 8.13 would have provided an acceptable factor (above 0.95) and a scaling would not have taken place. The new values are 1418 in^4 (59,000 cm^4) for elements A, B, and C, 94.7 in^2 (610 cm^2) for elements D and E, 1,891,180 in^4 (0.787 m^4) for element F. Then all secondary design variables were determined from the new primary design variable.

Step 6 - Solve the new problem for the new displacements. None of the displacements are close to the active value.

Step 7 - Solve the new problem for the new stresses. Only the stress for element A has a stress which is near the active value. Element A was a maximum stress of 30.0 ksi (20.7 kN/cm^2).

Step 8 - All constraints were checked for violation (was the scaling factor above $(1+P_2)$). None of the constraints were violated. All constraints were then checked to see if any constraints were active (was the scaling factor between $(1-P_1)$ and $(1+P_2)$). The stress for element A was chosen as an active constraint.

Step 9 - The gradient of the stress for element A was determined using this equation

$$\frac{\partial \sigma_A}{\partial \delta_i} = - \{v\}_A^T \frac{\partial [K]}{\partial \delta_i} \{U\} \qquad i = A,\ldots,F \qquad (8.14)$$

where δ_i represents the primary design variable for each element, $\{U\}$ is the vector of displacements, and $\{v\}_A^T$ is a vector of virtual displacements determined from

$$\{v\}_A = [K]^{-1}\{b\}_A \qquad (8.15)$$

where $\sigma_A = \{b\}_A^T \{U\}$.

Step 10 - The linear equations for the determination of the Lagrange multiplier was developed. Since there is only one active constraint, there is only one Lagrange multiplier to be found and one equation to be formed. This equation was determined using Equation 5.42. The Lagrange multiplier was 0.118. If there were more than one active constraint providing a set of Lagrange multipliers which were not all positive, the constraints associated with the negative Lagrange multipliers would be removed from the active set. The new set of equations would be resolved, and this process would continue until all of the Lagrange multipliers were positive.

Step 11 - The optimality criteria would be determined for each element as shown in Equation 5.15. The optimality criteria for this cycle were $T_A = 1.25$, $T_B = 0.06$, $T_C = 0.61$, $T_{D,E} = 0.006$, and T_F was a negative quantity which was nearly zero. An optimal solution is obtained when all active elements (elements not at their upper or lower

limits) have optimality criteria near unity. From the optimality criteria it is seen that elements D, E, and F are trying to rapidly reduce their size.

Step 12 - The optimality criteria are used within the linear recurrence relationship given as

$$\delta_i^{k+1} = (1 + \frac{1}{r}(T_i - 1))\,\delta_i^k \qquad i = A,\ldots,F \qquad (8.16)$$

with a convergence control parameter, r, of 2.0 to produce the second cycle element sizes. The new sizes are I_{xA} = 1598 in^4 (66500 cm^4), I_{xB} = 748.4 in^4 (31,100 cm^4), I_{xC} = 1143 in^4 (47,600 cm^4), $I_{D,E}$ = 47.55 in^2 (307 cm^2), and I_{xF} = 864,000 in^4 (0.360 m^4). Since the optimality criteria for element F was negative, it was reduced to its lower limit (passive value) without the use of Equation 8.16.

Step 13 - The new structural responses are determined and checked for constraint violation. If violation occurs the design is scaled. If there is no violation the termination criteria of percentage weight change, number of optimization cycles and number of analyses are checked. The percentage weight change for this cycle was approximately 37.5 percent. This is largely due to the large decrease in size associated with the concrete panel. If none of the termination criteria are satisfied the problem is shifted back to step 4 for this problem, but generally it goes to step 6.

The final results are shown in Table III. This problem was terminated due to the number of cycles of optimization which had a maximum of ten cycles. Realistically, this problem could have been terminated earlier due to the small change in weight after the sixth or seventh cycle. Note that elements B and F reached these passive values and the braces stabilized at a value of 10.5 in^2 (67.7 cm^2). Since only the stress for element A remained an active constraint throughout this problem, the global optimum result would most likely force all elements except A to become passive.

D. ILLUSTRATION OF EIGENVECTOR GRADIENTS WITHIN A DYNAMIC RESPONSE CONSTRAINT PROBLEM

A dynamically constrained structure is optimized with exactly the same steps as the previous static problem with the exception of the gradient determination. The dynamic displacement gradients are found by using Equation 6.76 and the dynamic stress gradients are determined in a manner similar to a psuedo-load technique as shown in Equation 6.102. From Equation 6.102 it is apparent that the dynamic displacement gradients must be found. Equation 6.76, to find the dynamic displacement gradients, requires the natural frequency and eigenvector gradients.

An illustration of these calculations will be presented for a structure with the same configuration as the static problem presented in Section VIII.C. The calculations

TABLE III. Results for a Three Dimensional Static Constraint Problem

Cycle	A ($in.^4$)	B ($in.^4$)	C ($in.^4$)	D,E ($in.^2$)	F ($in.^4$)	Weight (k)
0	1500.0	1500.0	1500.0	100.0	2,000,000	--
0*	1418.4	1418.4	1418.4	94.5	1,891,180	36.39
1†	1683.9	788.5	1205.0	50.1	910,334	22.72
2	2009.7	436.6	987.5	27.4	921,852	19.99
3	2492.2	233.4	722.3	15.7	958,700	18.79
4	2988.7	128.0	603.6	11.6	926,560	17.87
5	3343.8	67.4	438.0	10.5	893,500	17.14
6	3553.4	35.8	295.4	10.4	877,810	16.59
7	3688.0	35.4	187.8	10.4	872,890	16.32
8	3770.5	35.2	113.4	10.5	868,810	16.06
9	3810.6	35.0	65.3	10.5	864,000	15.80

* The 0* values are found by scaling the initial values given in 0.
† Element F has become passive in this step but takes the value 910,334 due to a scaling factor of 1.053. This example uses scaling after each iteration.

are performed for $I_A = 1576\ in^4$ ($65{,}600\ cm^4$), $I_B = 743\ in^4$ ($30{,}900\ cm^4$), $I_C = 1121\ in^4$ ($46{,}700\ cm^4$), $A_{D,E} = 47.1\ in^2$ ($304\ cm^2$), and $I_F = 955{,}130\ in^4$ ($0.398\ m^4$). The first natural frequency is 92.14 rad/sec, and the first eigenmode is $x = 1.0$, $y = 0.951$, and $\theta = -0.016$. The actual calculations will then be compared to the numerically generated gradients found by making a small change in the variable.

Several quantities are needed to find both the gradients for the natural frequency and the eigenvectors with respect to element A. From Equations 6.94 and 6.97, the important quantities are:

$$\frac{\partial [K]}{\partial I_A} \{\phi\} = \begin{Bmatrix} 4.32 \times 10^{-3} \\ 3.96 \times 10^{-1} \\ -2.57 \times 10^{1} \end{Bmatrix} \tag{8.17}$$

and

$$\frac{\partial [M]}{\partial I_A} \{\phi\} = \begin{Bmatrix} 1.57 \times 10^{-6} \\ 1.49 \times 10^{-6} \\ -1.79 \times 10^{-4} \end{Bmatrix} \tag{8.18}$$

and

$$[M]\{\phi\} = \begin{Bmatrix} 7.08 \times 10^{-2} \\ 6.73 \times 10^{-2} \\ -4.3 \times 10^{0} \end{Bmatrix} \tag{8.19}$$

From Equation 6.68

$$\frac{\partial \omega^2}{\partial I_A} = \frac{7.90\times10^{-1} - 8490\ (5.84\times10^{-6})}{0.203} = 3.647 \qquad (8.20)$$

and the numerically calculated value for a 0.01 change in the moment of inertia for element A gives $\Delta\omega^2/\Delta I_A = 3.648$ which is very close to the actual value. From Equation 6.94

$$\left[[K] - \omega^2[M]\right] \frac{\partial\{\phi\}}{\partial I_A} = -\begin{Bmatrix} 4.32 \times 10^{-3} \\ 3.96 \times 10^{-1} \\ -2.57 \times 10^{1} \end{Bmatrix} + 8490 \begin{Bmatrix} 1.57 \times 10^{-6} \\ 1.49 \times 10^{-6} \\ -1.79 \times 10^{-4} \end{Bmatrix}$$

$$+ 3.647 \begin{Bmatrix} 7.08 \times 10^{-2} \\ 6.73 \times 10^{-2} \\ -4.31 \times 10^{0} \end{Bmatrix} = \begin{Bmatrix} 2.67 \times 10^{-1} \\ -1.39 \times 10^{-1} \\ 8.51 \times 10^{0} \end{Bmatrix} \qquad (8.21)$$

Once the right side of the equation is generated a boundary condition is applied in order to generate a solution. Since the matrix $\left[[K] - \omega^2[M]\right]$ is singular, the eigenvector provides only a direction. As seen in the eigenvector, the first term can always be set to one with the other terms taking the appropriately scaled quantities. Therefore, if this term can always be unity there will never be a change in this term. The boundary condition becomes $\partial\phi_1/\partial I_A = 0$ similar to a constrained direction with respect to a stiffness formulation. This allows the reduction of $\left[[K] - \omega^2[M]\right]$

to a nonsingular matrix. For this problem the solution is found from this equation

$$\left[[K] - \omega^2[M]\right] \begin{Bmatrix} 0 \\ \partial\phi_2/\partial I_A \\ \partial\phi_3/\partial I_A \end{Bmatrix} = \begin{Bmatrix} 0 \\ -1.39 \times 10^{-1} \\ 8.51 \times 10^{0} \end{Bmatrix} \tag{8.22}$$

and gives

$$\begin{Bmatrix} \partial\phi_2/\partial I_A \\ \\ \partial\phi_3/\partial I_A \end{Bmatrix} = \begin{Bmatrix} -3.85 \times 10^{-5} \\ \\ 5.28 \times 10^{-7} \end{Bmatrix} \tag{8.23}$$

The numerically generated quantities for $\Delta I_A = 0.01$ were $\Delta\phi_2/\Delta I_A = -3.85 \times 10^{-5}$ and $\Delta\phi_3/\Delta I_A = 5.32 \times 10^{-7}$ which show that the equation evaluated gradients are correct. As explained in Section V.C.3.a a correction term can be applied to these gradients if the eigenvectors are normalized with respect to the mass. This term must be included since none of the eigenvectors will be constants any longer. These quantities would be used, in the previously presented equations, to generate the gradient of the dynamic displacements with respect to element A. This type of calculation must be performed for each element, therefore it is easily seen why the gradient calculations are one of the most time consuming processes.

E. EFFECTS OF A UNIFORM LOAD ON STRESS GRADIENTS

The stress gradients for elements with uniformly distributed loads as calculated using Equation 6.29 must be combined with an additional term. Equation 6.29 finds the stress for the element with the applied local displacements, but it does not include the fixed-end force terms. The actual stress for a uniformly loaded beam is calculated as

$$\sigma_j = \frac{Mc}{I} \pm \frac{M_F c}{I} \tag{8.24}$$

where M is the elastically calculated moment, M_F, is the fixed-end moment, c, is the distance from the neutral axis to the farthest fiber of the cross section, and, I, is the major-axis moment of inertia. Therefore, the stress gradients for a uniformly loaded beam must include an additional term as

$$\frac{\partial (\sigma_j)_F}{\partial I} = - \frac{M_F c}{I^2} \tag{8.25}$$

where $(\sigma_j)_F$, represents the fixed-end moment stress, and the stress gradients for a static, uniformly loaded beam becomes

$$\frac{\partial \sigma_j}{\partial I} = - \{v\}_j^T \frac{\partial [K]}{\partial I} \{U\} \pm (- \frac{M_F c}{I^2}) \tag{8.26}$$

This additional term can be a large or small percentage of the total gradient depending on the effect of the fixed-end moment and the size of the moment of inertia.

In addition to this correction, it is important to note that the first term of Equation 8.26 is developed with an assumption which prevents it from representing the complete stress gradient. The assumption is to neglect the effects of the term $\frac{\partial\{b\}_j}{\partial\delta_i}\{U\}$ (assuming $\frac{\partial\{b\}_j}{\partial\delta_i} = 0$). This in effect assumes that the depth of the element is fixed or independent of the moment of inertia. In reality this is not true and Equation 3.12 is used to provide the distance, c, as

$$c = I/S \tag{8.27}$$

for a symmetric section where S is calculated using the secondary design variable relationships for the section modulii.

F. EFFECTS OF CONDENSATION ON GRADIENT CALCULATIONS

When using the psuedo-load approach to calculate the gradients, as with the dynamic stress constraints, the first term of Equation 6.21, $\frac{\partial\{b\}_j}{\partial\delta_i}$, cannot be assumed to be zero. This term cannot be assumed to be zero because $\{b\}_j$ is a reduced or condensed vector which is dependent

upon the stiffness matrix through the condensation process. Two approaches were attempted to solve this problem.

The first attempt was to find the dependence of $\{b\}_{j\ RED}$ (Reduced $\{b\}_j$) with respect to the primary design variable. The direct differentiation of Equation 6.104 provides an equation which is quite complicated as

$$\frac{\partial\{b\}_{j\ RED}}{\partial\delta_i} = \frac{\partial\{b_2\}_j}{\partial\delta_i} - \frac{\partial[K_{21}]}{\partial\delta_i}[K_{11}]^{-1}\{b_1\}_j$$

$$- [K_{21}]\frac{\partial[K_{11}]^{-1}}{\partial\delta_i}\{b_1\}_j - [K_{21}][K_{11}]^{-1}\frac{\partial\{b_1\}_j}{\partial\delta_i} \tag{8.28}$$

The problem with this equation is the need for $\frac{\partial[K_{11}]^{-1}}{\partial\delta_i}$ which is quite difficult to obtain.

The second approach is the same as that used in Equations 6.105 to 6.109. These equations provide a means of finding the gradients of the previously condensed displacements as

$$\frac{\partial\{U_1\}}{\partial\delta_i} = [K_{11}]^{-1}\left[-\frac{\partial[K_{11}]}{\partial\delta_i}\{U_1\} - \frac{\partial[K_{12}]}{\partial\delta_i}\{U_2\}\right.$$

$$\left. - [K_{12}]\frac{\partial\{U_2\}}{\partial\delta_i}\right] \tag{8.29}$$

and allows the use of the full psuedo-load vector $\{b\}_j^T$ multiplied with the full displacement gradient vector. This also uses the assumption that the gradient of the full $\{b\}_j^T$ vector is zero. This second approach has produced results within a few percent of the values calculated by the gradient approximation using a small change in the design variable as seen in the previous examples.

G. REMARKS

This is a sample of the type of calculations and concepts which had to be explored in detail prior to and during the development of the computational algorithm. The gradient calculations are very time consuming and they were studied very closely with respect to ways of efficiently computing exact and approximate gradients. The displacement and frequency constraints are exact numerical solutions, whereas, the stress gradients have the assumption that the gradient of the psuedo-load vector is zero which provides a very good approximation. It is important to the algorithm to have good approximations to the gradients. Without reasonable values the optimization algorithm cannot maintain the constraint values. If these are not maintained, scalings must be performed between cycle, which rapidly increases the total number of analyses.

IX. DESIGN RESULTS FOR ASSESSMENT OF CODE PROVISION, COST, AND MULTIPLE-COMPONENT SEISMIC INPUT

A. COMMON STRUCTURAL AND OPTIMIZATION PARAMETERS

Several structures, loadings, analyses, and constraints will be used to explore and verify the use and results of the proposed algorithm and computer program. A majority of the examples will be structural systems subjected to dynamic loads with static and dynamic displacement constraints. A few examples will be presented for the static response, frequency, and dynamic stress constraint problems, but most of the examples will be concerned with dynamic displacement constraints. This set of constraints was used in order to interpret the effect of seismic loading on the structural systems, and the optimal stiffness distribution for drift control with respect to seismic loads.

Many of the structural examples use common parameters during the optimization. In order to prevent repetition, common parameters or default parameters will be given and can be assumed for each problem unless stated otherwise within that specific example. The convergence control parameter, r, used is 2. This value is acceptable for most structural problems. The range for choosing an active constraint is to have, P_1, the lower bound active constraint limit to be 10% and, P_2, the upper bound active constraint limit to be 5%. These limits are slightly restrictive and could be expanded for the lower limit. The chances of

numerical instability can be reduced by increasing the acceptable region for active constraints. This increase in the active region will also reduce the number of scalings required within the optimization problem. The objective function of weight is based upon the specific weights of steel and concrete as 0.490 k/ft^3 (7.82 Mg/m^3) and 0.150 k/ft^3 (2.39 Mg/m^3), respectively. The equations relating the secondary design variables with respect to the primary design variables are given by Equations 3.15 to 3.29 for the wide-flange cross-sections, and by Equations 3.30 to 3.34 for the concrete elements. The most common response spectrum used is given by Equations 4.56 and 4.57 which simulates the actual response spectrum given by Seed (54) as a stiff-soil site response spectrum. The modulus of elasticity for the steel and concrete elements were 30,000 k/in^2 (20,700 kN/cm^2) and 3,000 k/in^2 (2,070 kN/cm^2), respectively. The story or level numbers increase from base (0) to the top of the structure (n = number of stories). Note that the column lines and bays will generally be designated by letters or numbers as shown in each of the respective figures. All other pertinent details or changes from these default parameters will be given for each individual or set of problems which are discussed. During the course of this research a number of examples have been examined, this chapter provides a few typical examples.

B. STEEL STRUCTURE SUBJECT TO STATIC CONSTRAINTS

A two story all steel, setback structure will be used to illustrate a problem with active static displacement constraints. This structure is shown in Figure 23. The displacement constraints are chosen as 0.25 in. (0.64 cm) for the first level and 0.50 in. (1.27 cm) for the second level displacements. These values are used with respect to both the x and y directions as shown in Figure 24. Stress constraints of 36 ksi (25 kN/cm^2) were applied for all elements, columns, beams, and braces. The termination criteria were 15 cycles of optimization, 20 cycles of analysis or less than a 2 percent change in weight. A set of lateral loads of 400 kips (1780 kN) and 450 kips (2003 kN) were applied at the upper and lower mass centers, respectively. These lateral loads were applied in both the x and y directions. Along with the lateral loads, a set of 5 kips (22 kN) nodal forces were applied at each column node. The initial sizes used for the column were 56.6 in^4 (2356 cm^4), for the beams were 146.0 in^4 (6077 cm^4), and for the braces were 3.63 in^2 (23.4 cm^2). No linking was assumed for the design variables. After the first cycle of analysis, a scaling factor of approximately 121 was obtained for which the initial sizes of 6849 in^4 (285,100 cm^4) for the columns, 17,667 in^4 (735,400 cm^4) for the beams, and 439 in^2 (2832 cm^2) for the braces was required in order to satisfy the constraints.

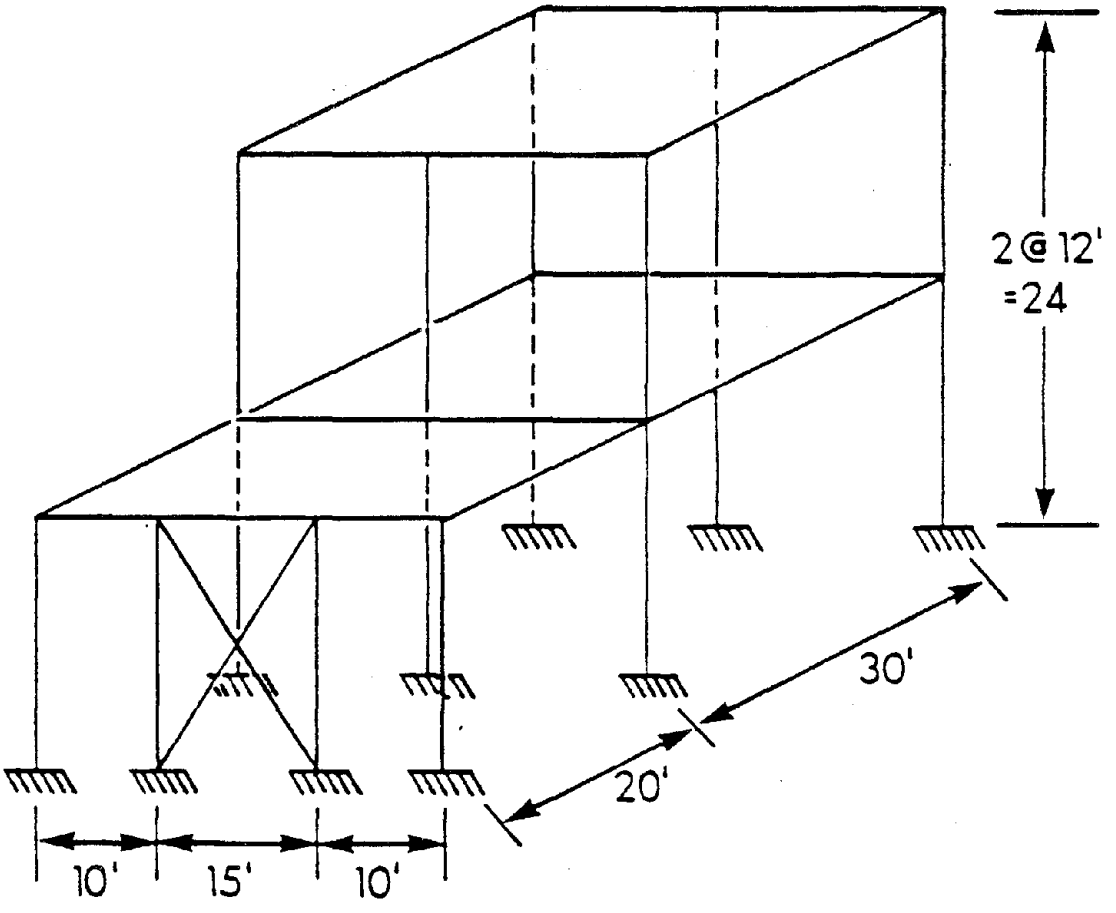

Figure 23. Two Story Steel Setback Structure
(1' = .305m)

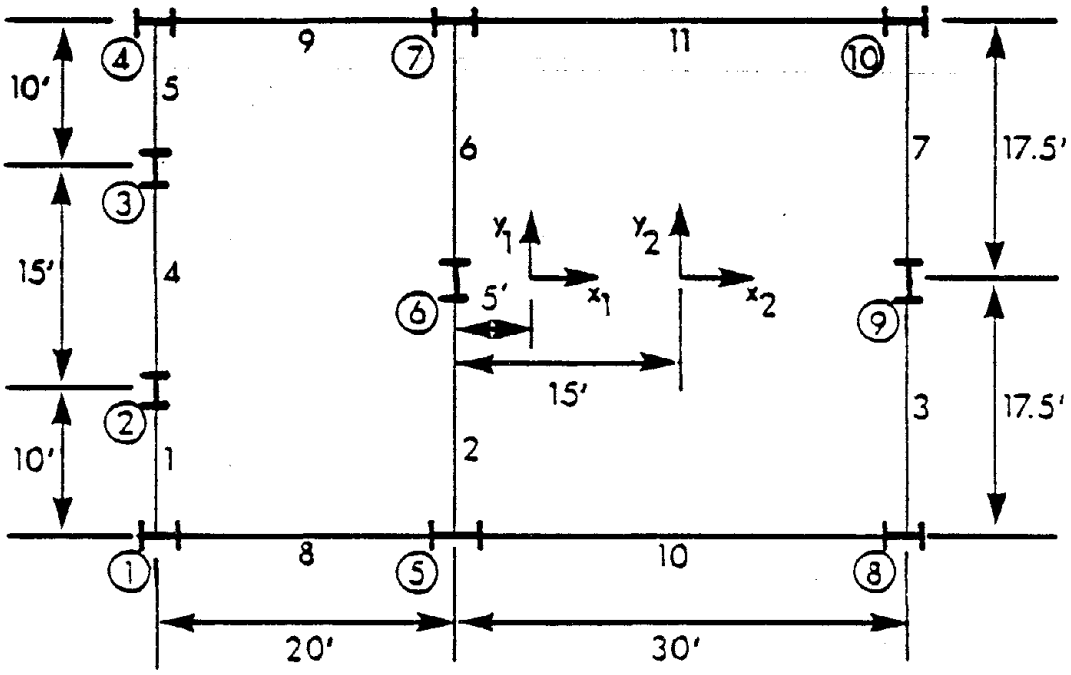

Figure 24. Two Story Steel Setback Structure - Plan View (1' = .305m)

The actual optimization requires 10 cycles of optimization, 12 analyses, and was terminated due to a 1.8 percent change in weight between the last two cycles. The initial weight after the scaling was 588.5 kips (266.6 Mg) and the final weight was 321.7 kips (1457. Mg) a reduction of approximately 45 percent based on the initial weight. As shown in Figure 25. Of course this weight is based upon the relationship between the area and the major-axis moment of inertia for the beams and columns and the initial assumption of all columns and all beams starting with the same relative stiffness, respectively. The initial set of active constraints chosen included only the x-displacement on the second level (x_2 = 0.461 in.)(1.17 cm). The next cycle included the x-displacements on both levels with x_1 = 0.228 in. (0.579 cm) and x_2 = 0.507 in. (1.29 cm), but x_1 was eliminated from the active set since its Lagrange multiplier was -375.2 (a negative Lagrange multiplier violates the Kuhn-Tucker Conditions). After three cycles the active set of constraints stabilized and consisted of the x and y displacement on the second level. The final values for the displacements are given in Table IV. The final size for each member along with the value for, T_i, the optimality criteria are given in Tables V and VI, respectively. The optimality criteria have quite a large range of values. The values which are less than 0.5 generally indicate that eventually those elements would reach their minimum values while those values above 0.5

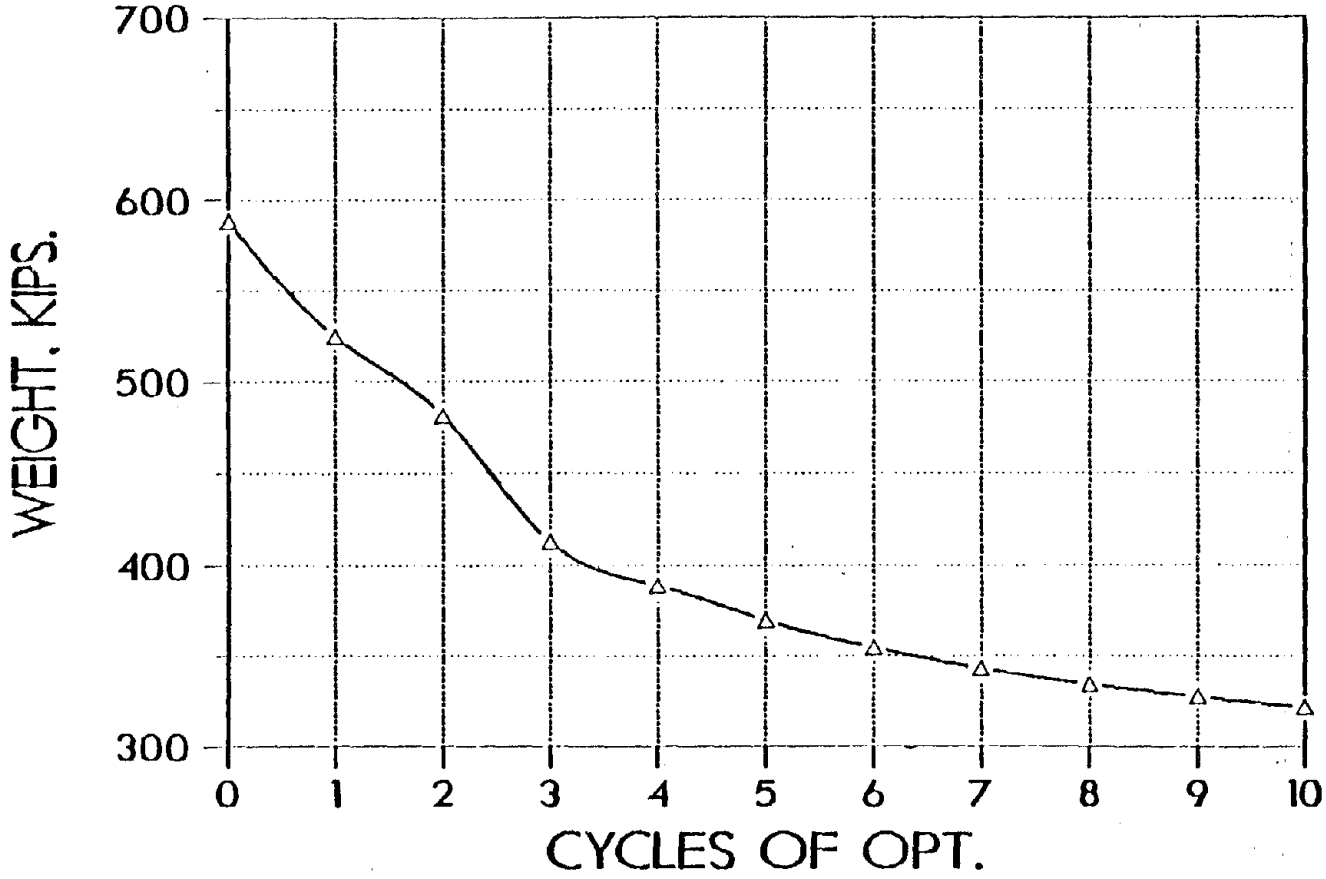

Figure 25. Weight versus Cycles of Optimization for a Two Story Steel Setback Structure with Static Response Constraints (1 kip = 4.45 kN)

TABLE IV. Final Displacement for the All Steel, Two Story Setback Structure (1 in = 2.54 cm)

Level, i	2	1
x_i (in)	0.501	0.12
y_i (in)	0.499	0.200
ϕ_i (rad)	3.8×10^{-4}	3.9×10^{-4}

TABLE V. Optimal Sizes for the All Steel Two Story Setback Structure Subject to Static Displacement and Stress Constraints (1 in = 2.54 cm)

Column Major-Axis Moments of Inertia (in^4)

Level \ Line	1	2	3	4	5	6	7	8	9	10
2	-	-	-	-	11,789	7624	8708	6235	6202	6161
1	45,079	702	555	1270	27,284	689	893	4755	2195	1205

Beam Major-Axis Moments of Inertia (in^4)

Level \ Bay	1	2	3	4	5	6	7	8	9	10	11
2	-	2060	1809	-	-	2081	1734	-	-	6814	6155
1	894	2383	2986	758	919	2212	2096	21,257	2447	5446	3636

Brace Cross-sectional Areas (in^2)

Upper Column	Lower Column	Area
3	2	47.2
2	3	48.2

TABLE VI. Optimality Criteria for the All Steel Two Story Setback Structure Subject to Static Displacement and Stress Constraints

Columns

Level \ Line	1	2	3	4	5	6	7	8	9	10
2	-	-	-	-	1.225	1.438	0.835	0.932	1.094	0.887
1	1.410	0.212	0.196	0.166	1.146	0.224	0.363	0.732	1.035	0.703

Beams

Level \ Bay	1	2	3	4	5	6	7	8	9	10	11
2	-	0.942	0.678	-	-	0.904	0.644	-	-	0.910	0.854
1	0.100	1.023	0.963	0.006	0.053	0.852	0.686	1.223	0.363	0.519	0.644

Braces

Upper Column	Lower Column	T_i
3	2	0.865
2	3	0.887

are members which will eventually converge to an optimality criterion of unity. Once a large portion of the dominating elements have optimality criteria close to unity, the objective function shows little change and the design is terminated.

This solution illustrates the tendency for the optimization to produce strong bays or frames in order to provide the most efficient stiffness with the smallest amount of material. On the lower level columns 1 and 5 along with beam 8 provide most of the stiffness required to limit the lower level x-displacement, which also helps reduce the effect of the first level displacement and ultimately the total displacement at the second level. This is the reason for column sizes on the second level which are considerably smaller than the first floor columns of 1 and 5. In other words, this large lower level stiffness creates a situation where the drift of the second level can be larger than 0.25 in (0.64 cm) (difference between the second level constraint and the first level constraint). The second level y-displacements are mostly controlled by columns 5, 6 and 7 and beams 2 and 6 on the second level.

This example shows the need for several different types of constraints in order to provide realistic results. Side constraints in order to place minimum and maximum allowable sizes on elements are needed. Coupled with this is the need for linking of elements. Most designs will force certain

elements to maintain the same sizes and in this case most likely all columns would be forced to have the same size and all beams would be forced to have the same size. Both of these types of constraints will be considered in later examples. Drift control would be another desirable constraint.

Observations:

1. The proposed algorithm and computer program provide a means of controlling structural response. Every applied constraint is satisfied when the algorithm is terminated. A set of final active constraints consist of the displacements x_1, x_2, and y_2.
2. The algorithm produces a series of ten designs; all of which are feasible solutions. In other words, each design satisfies the constraints. Each design also decreases in weight as expected due to the minimization of the objective function which was the structural weight function.
3. The optimality criteria can vary significantly from the optimal value of unity while still providing a small change in the objective function. Therefore, the optimization can terminate prior to reaching a globally optimal solution.
4. The optimization of a structure tends to produce sets of strong bents. These are determined as the most efficient means of resisting lateral loads.

5. The distribution of large amounts of stiffness in several bents is generally an unrealistic situation. These results show the need for linking of the elements, as well as, side constraints.

C. STEEL AND CONCRETE STRUCTURE SUBJECT TO STATIC CONSTRAINTS

A two story setback structure similar to Figure 23 comprised of every element type will be used to illustrate a statically constrained response problem. The structure is shown in Figure 26. Due to the large amount of stiffness supplied by the panels and the shear walls, the deflection constraints were considered to be small. The upper level displacement constraints were 0.20 in. (0.51 cm) and the lower level displacement constraints were 0.60 in. (1.52 cm). These values apply to both the x and y directions. The maximum allowable stresses for the steel columns were 20.0 k/in^2 (13.8 kN/cm^2), for the steel beams were 16.5 k/in^2 (11.4 kN/cm^2), for the steel braces were 15.0 k/in^2 (10.4kN/cm^2), for the concrete columns were 3.0 k/in^2 (2.10 kN/cm^2) in compression and 50.0 k/in^2 (34.5 kN/cm^2) in tension, and for the concrete panels were 3.0 k/in^2 (2.10 kN/cm^2) in compression and 3.0 k/in^2 (2.10 kN/cm^2) in tension. The concrete elements were assumed to have a steel ratio of 0.025 and a modular ratio of 10.0 for the columns and 1.0 for the panels. The steel columns were

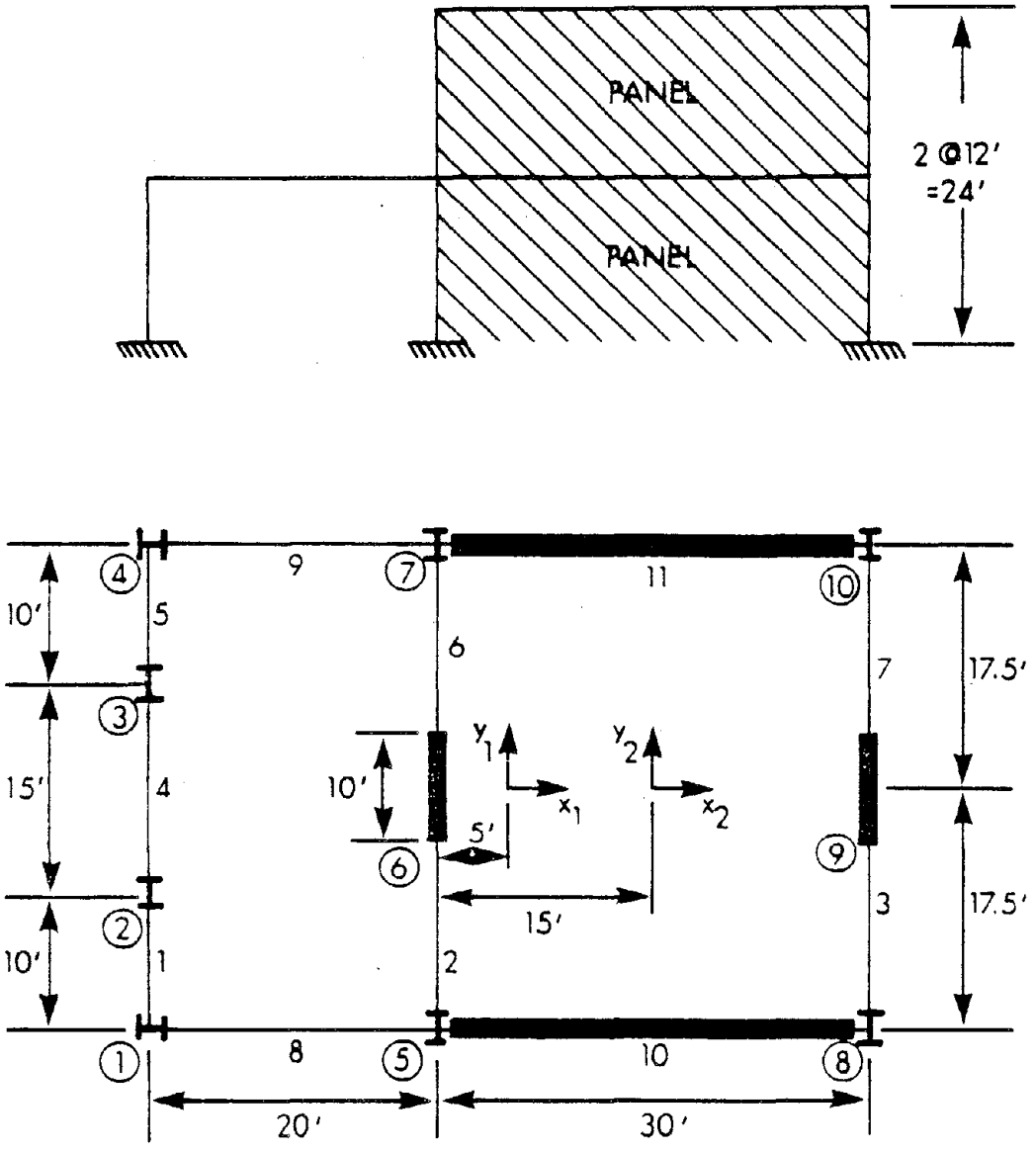

Figure 26. Two Story Setback Structure with Steel and Concrete Elements (1' = .305m)

constrained to be within a range of 7.0 in^4 (291 cm^4) to 50.0 in^4 (2080 cm^4), the beams were to be within 5.0 in^4 (208 cm^4) to 50.0 in^4 (2080 cm^4), the braces were constrained to be within 1.0 in^2 (6.5 cm^2) to 15.0 in^2 (96.8 cm^2), the concrete columns were to have widths within the range of 5.0 in. (12.5 cm) to 20.0 in. (50.8 cm), and the panels were to have widths in the range of 4.0 in. (10.2 cm) to 10.0 in. (25.4 cm). The loading consisted of 400 kips (1780 kN) concentrated, lateral loads on the top level applied in both the x and y directions at the mass center, 450 kips (2003 kN) concentrated, lateral loads on the lower level in both the x and y directions at the mass center, and 5 kips (22 kN) concentrated load per column node in the downward direction. The convergence control parameter was set at 4.0, and the termination criteria was 15 cycles of optimization, 20 cycles of analysis, or a 2 percent change in weight. The convergence control parameter was changed from the usual value of 2 due to the many different types of elements and stress constraints. No linking was applied to this structure.

The actual optimization of this structure requires six cycles of optimization and nine cycles of analysis. The initial weight was 391 kips (177 Mg) and the final weight was 131 kips (59.3 Mg) as shown in Figure 27. Initial and final design sizes are given in Table VII. The final solution produces optimality criteria which range in value

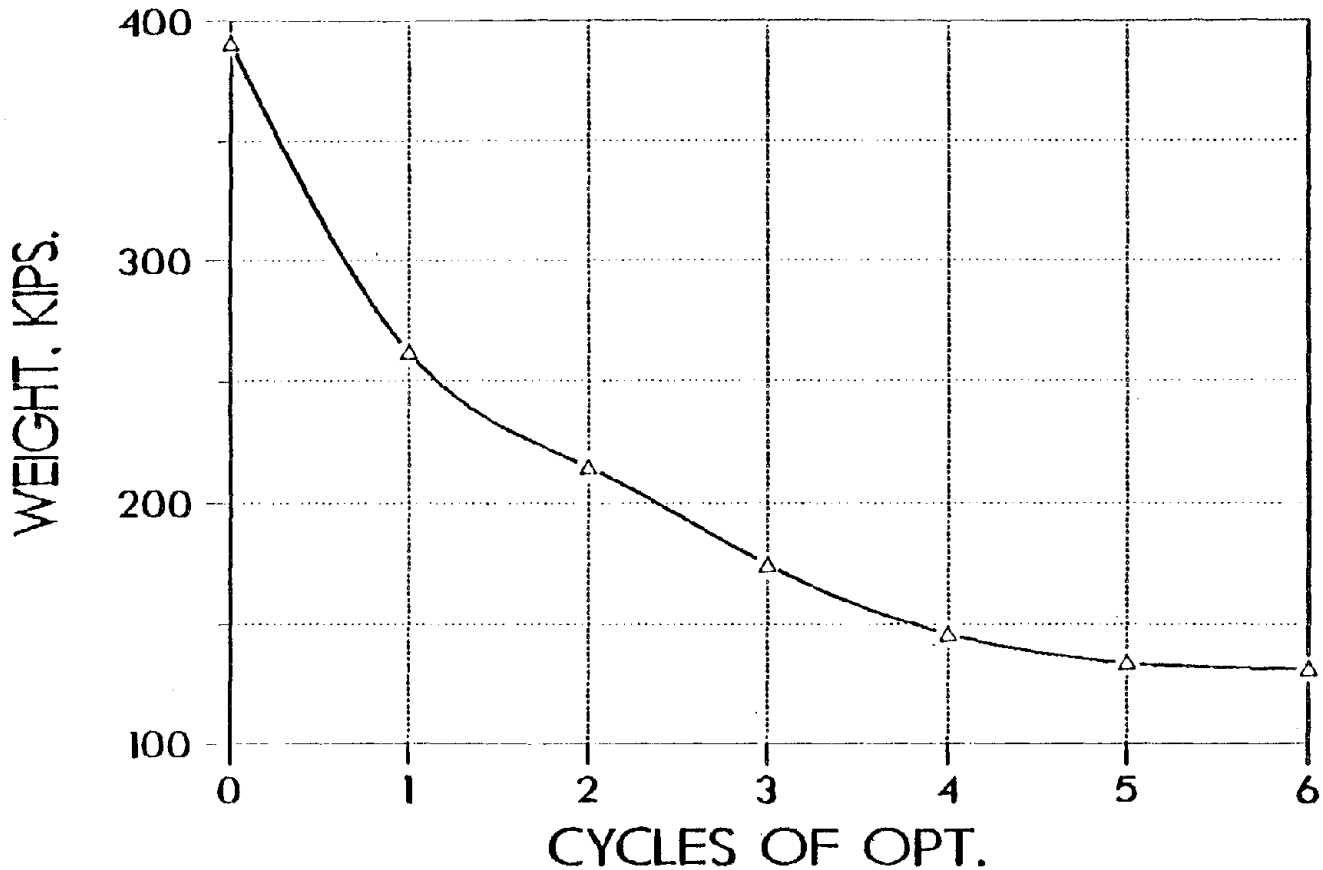

Figure 27. Weight versus Cycles of Optimization for a Two Story Setback Structure with Steel and Concrete Elements with Static Response Constraints (1 kip = 4.45 kN)

TABLE VII. Initial and Final Sizes and Maximum Stresses for the Two Story Setback (1 in = 2.54 cm, 1 k = 4.45 kN)

Columns

Level	Line	Initial (in^4)	Final (in^4)	Max. Stress (ksi)
2	5	56.6	15.1	14.9
	6	8.0 in.	5.0 in.*	28.3 (-1.7)
	7	56.6	29.0	14.2
	8	56.6	15.3	-18.5
	9	8.0 in.	5.0 in.*	27.3 (-1.6)
	10	56.6	19.7	-13.6
1	1	56.6	12.9	5.2
	2	56.6	28.1	12.6
	3	56.6	27.4	-12.0
	4	56.6	12.9	4.6
	5	56.6	7.8	17.0
	6	8.0 in.	8.8 in.	39.0 (-2.3)
	7	56.6	49.2	8.4
	8	56.6	7.0*	-17.1
	9	8.0 in.	7.8 in.	42.8 (-2.5)
	10	56.6	25.2	-8.9

Beams

Level	Bay	Initial (in^4)	Final (in^4)	Max. Stress (ksi)
2	2	146.0	24.5	13.4
	3	146.0	25.3	17.4***
	6	146.0	34.8	16.4***
	7	146.0	22.9	15.8***
	10	146.0	12.6	0.0
	11	146.0	12.6	0.1

TABLE VII. (cont.) Initial and Final Sizes and Maximum Stresses for the Two Story Setback (1 in = 2.54 cm, 1 k = 4.45 kN)

Beams

Level	Bay	Initial (in^4)	Final (in^4)	Max. Stress (ksi)
1	1	146.0	12.8	4.9
	2	146.0	17.9	10.6
	3	146.0	18.5	15.0
	4	146.0	12.6	1.4
	5	146.0	12.8	4.9
	6	146.0	21.7	14.0
	7	146.0	17.5	13.4
	8	146.0	12.6	1.0
	9	146.0	12.6	0.5
	10	146.0	12.6	0.3
	11	146.0	12.6	0.0

Panels

Level	Bay	Initial (in)	Final (in)	Max. Stress (ksi)
2	10	12.0	4.0*	0.9
2	11	12.0	4.0*	0.6
1	10	12.0	4.0*	3.0***
1	11	12.0	4.0*	-0.9

Braces

Top Line	Bot. Line	Initial (in^2)	Final (in^2)	Max. Stress (ksi)
3	2	3.63	15.0**	12.7
2	3	3.63	15.0**	-12.5

* Minimum Allowable Sizes
** Maximum Allowable Sizes
*** Active Stress Constaints

from 0.4 to 1.4. These values should be equivalent to one for all active members when an optimal solution is reached. The reason these values are not closer to one is due to the fact that the concrete elements have stabilized close to their minimum values providing little change in the weight which in turn terminated the process. If a true optimal solution was to be obtained, a smaller percentage weight change for termination would be required. The trend for this optimization is to reduce columns 5 (possibly to a passive value) and 8 to a small value and use the concrete columns 6 and 9 along with steel columns 8 and 10 and beams 6 and 7 for the y-displacement resisting system. Along with these frames, columns 2 and 3 on the first level coupled with the x-bracing provide a system which helps resist the torsion of the first level which in effect reduces the y-displacement on the second level due to the offset of the first and second level mass centers.

The final set of active constraints include stresses, displacements, and side constraints. The second level y-displacement is active with a value of 0.58 in.(1.47 cm). The stresses for the beams on level 2, bays 3, 6, and 7 are active, as well as, the stress in the panel on the lower level between column 5 and 8. The stresses are shown in Table VII. The stresses in the parenthesis are the maximum compressive stresses for the concrete columns. Note that there is a slight overstress of approximately 5%

for the beam on level 2, bay 3, which was allowed by the feasible range for an active constraint as discussed previously. All stresses, displacements, and sizes are within the acceptable regions and do produce a feasible design although a wide range of member sizes was obtained because no linking was assumed. The panels are so rigid that the x-displacements are approximately 10% of the constraint values, but it is interesting to note that the optimal solution tries to reduce the original structure to a set of one bay frames parallel to the direction of the active displacement in order to stop this displacement. This is a common trend for the pure optimization where every element is free to reach its own specific value at the optimal solution. For the simplest cases of one loading condition where there are no side constraints, the problems will reach a statically determinate system.

Observations:

1. The proposed algorithm and computer program are capable of optimizing a structure composed of a mixture of elements. This example includes every type of element allowed within the program.
2. The proposed algorithm is also capable of mixed constraint problems. The solution includes beam stress, displacements, and side constraints within the final set of active constraints.

3. The concrete elements tend to dominate the design since the structure is only two stories tall. Even the smallest concrete panel size provides enough stiffness to control the x-displacements, while the concrete columns along with the steel elements resist the y-displacements.
4. The optimization is smooth and rapid. It requires six cycles of optimization to reach the final solution.

D. FIVE STORY STRUCTURE SUBJECT TO FREQUENCY CONSTRAINTS

A five story L-shaped structure, shown in Figure 28, with seven column lines and seven beams all made of steel wide-flange sections will be used to provide an example of frequency (period) constraints. This structure does not include linking of elements but does use side constraints along with the frequency constraints. Each level has a translational mass of 0.31 k-s^2/in (54.3 Mg) and a rotational mass of 16,403 k-s^2-in (1854 Mg-m^2). Initially the columns have a moment of inertia of 9,500 in^4 (395,400 cm^4) while the beams have a moment of inertia of 9,000 in^4 (374,600 cm^4). This produces an initial weight of 206 kips (93.3 Mg). The optimization was to be terminated within 20 cycles of optimization, 20 cycles of analysis or less than a 5% reduction in weight between cycles. The constraints consist of keeping the first period between the values of 0.75 and 1.0 sec., the second period below 0.50

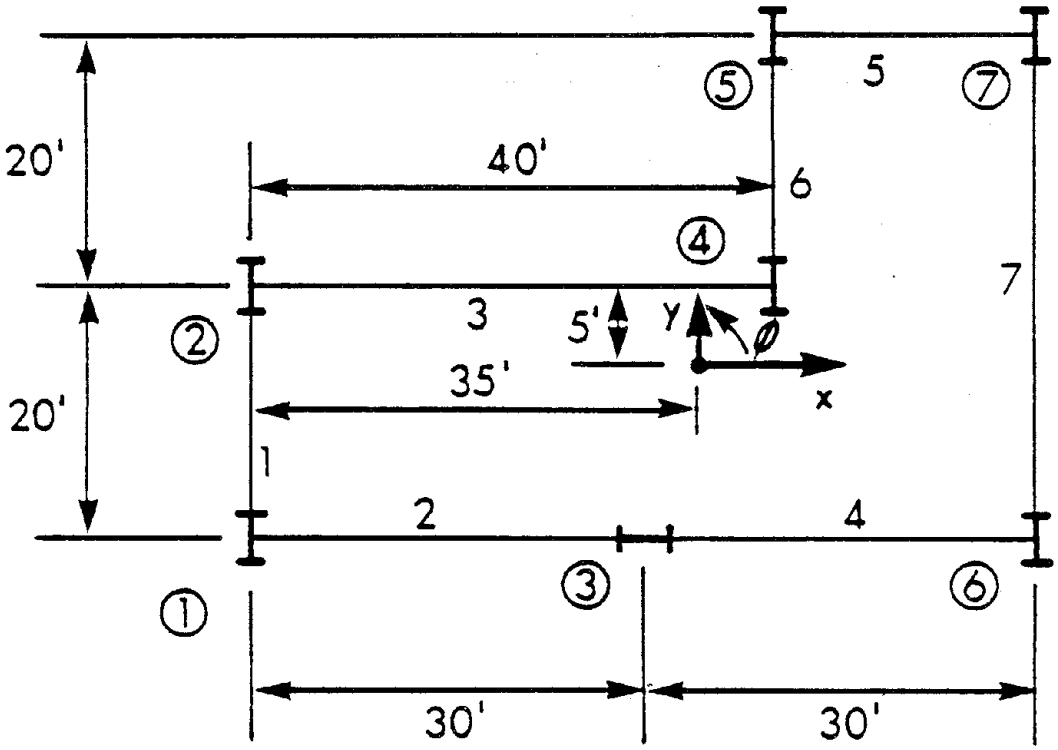

Figure 28. Five Story L-shaped Structure - Plan
(1' = .305m)

sec. and the third period below 0.40 sec. while keeping each element size between 10.0 in^4 (416 cm^4) and 20,000.0 in^4 (832,400 cm^4).

The optimization was terminated due to less than a 5% change in weight between cycles. The final weight was given as 104 kips (47.1 Mg) or nearly a 50% reduction of the initial weight, as shown in Figure 29. All three of the period constraints became active with T_1 = 1.02 sec., T_2 = 0.50 sec., and T_3 = 0.41 sec., as shown in Figure 30, while none of the side constraints became active. The final element sizes are given in Table VIII. Note that the beams increase in size from top to bottom except at the lowest level. This is a direct reflection of the added resistance provided to the bottom columns by having a fixed base and is common in most of the optimization problems which do not have stress constraints. This will also generally occur with stress constraints unless these beams are loaded with a uniformly distributed load in order to generate an active stress in these beams. Note that the modes are coupled since the rigidity center and mass center do not coincide. The mode shapes are shown in Figures 31, 32, and 33. Each mode must be represented with the x, y, and ϕ components since the modes are coupled. Certain components can be considered dominate in each mode, but the coupling precludes the use of stating whether the modes are x, y or rotational modes. The large value of the first

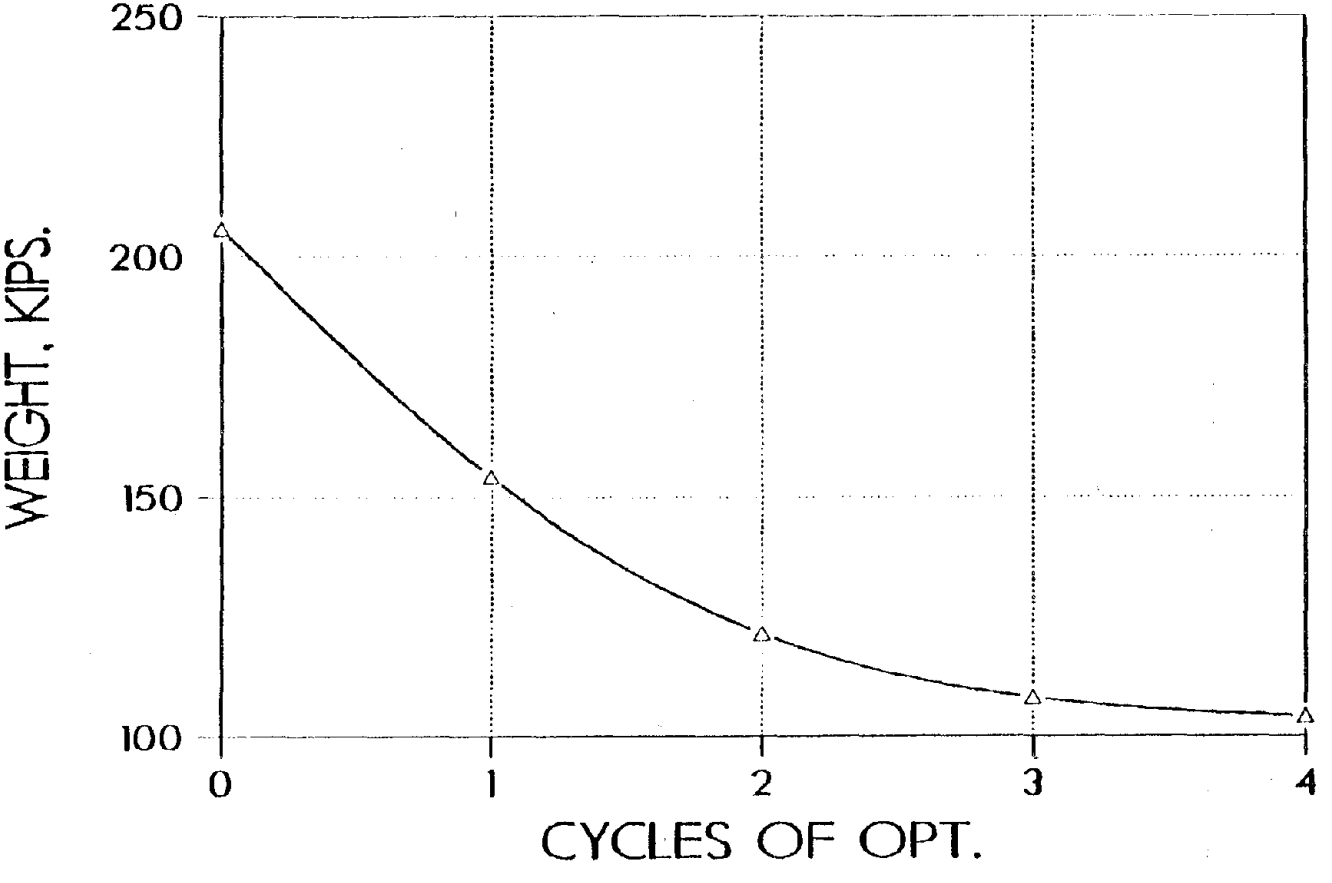

Figure 29. Weight versus Cycles of Optimization for the Five Story L-shaped Structure with Frequency Constraints (1 kip = 4.45 kN)

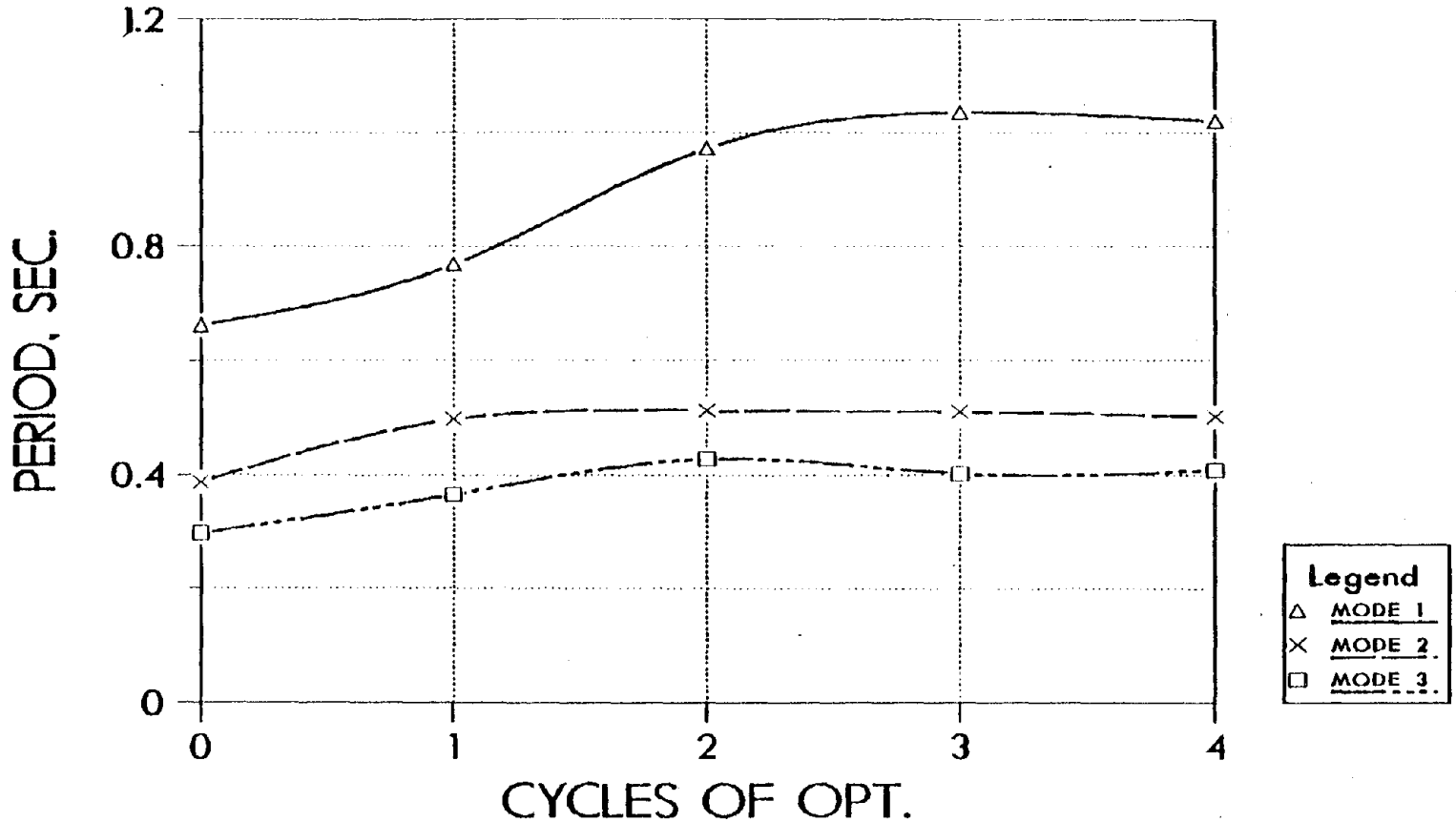

Figure 30. Period versus Cycles of Optimization for the Five Story L-shaped Structure with Frequency Constraints

TABLE VIII. Results for the Five Story L-shaped Building Subjected to Frequency Constraints (1 in = 2.54 cm)

Column (in^4)

Level \ Line	1	2	3	4	5	6	7
5	1158	944	1235	1161	1261	1471	1251
4	2710	1898	2036	2576	3147	3075	2656
3	4492	2873	3009	4298	5459	4790	3889
2	5420	3591	4324	5625	7262	5342	4508
1	5370	4493	18127	6309	7274	9522	9092

Beams (in^4)

Level \ Bay	1	2	3	4	5	6	7
5	661	543	348	592	338	857	846
4	1932	1139	506	1246	571	2821	2212
3	3608	1939	699	2041	904	5898	3896
2	4888	2488	813	2588	1115	8364	4613
1	4061	1702	737	1805	982	5747	2649

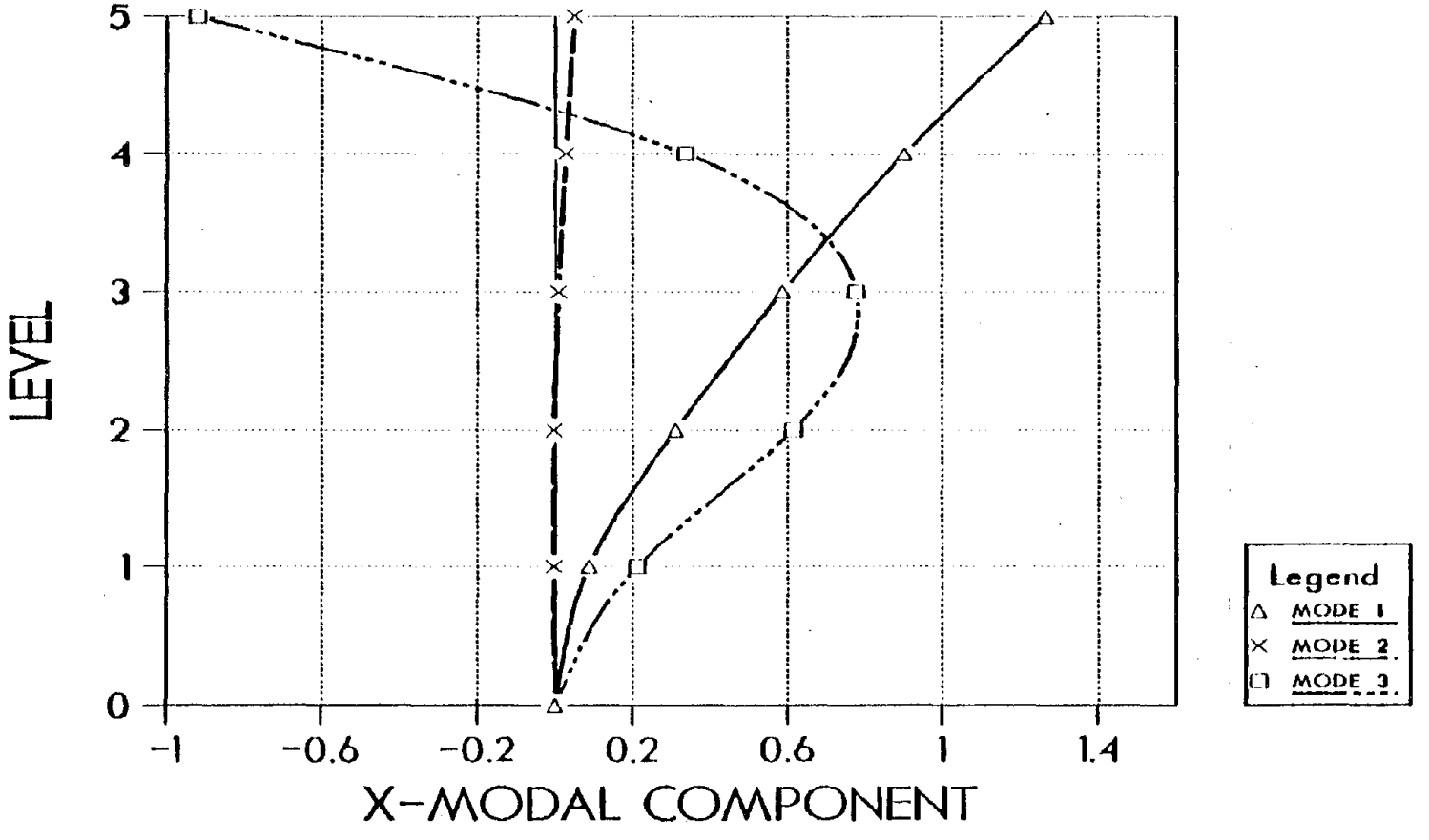

Figure 31. X-components of the Final Eigenmodes for the Five Story L-shaped Structure with Frequency Constraints

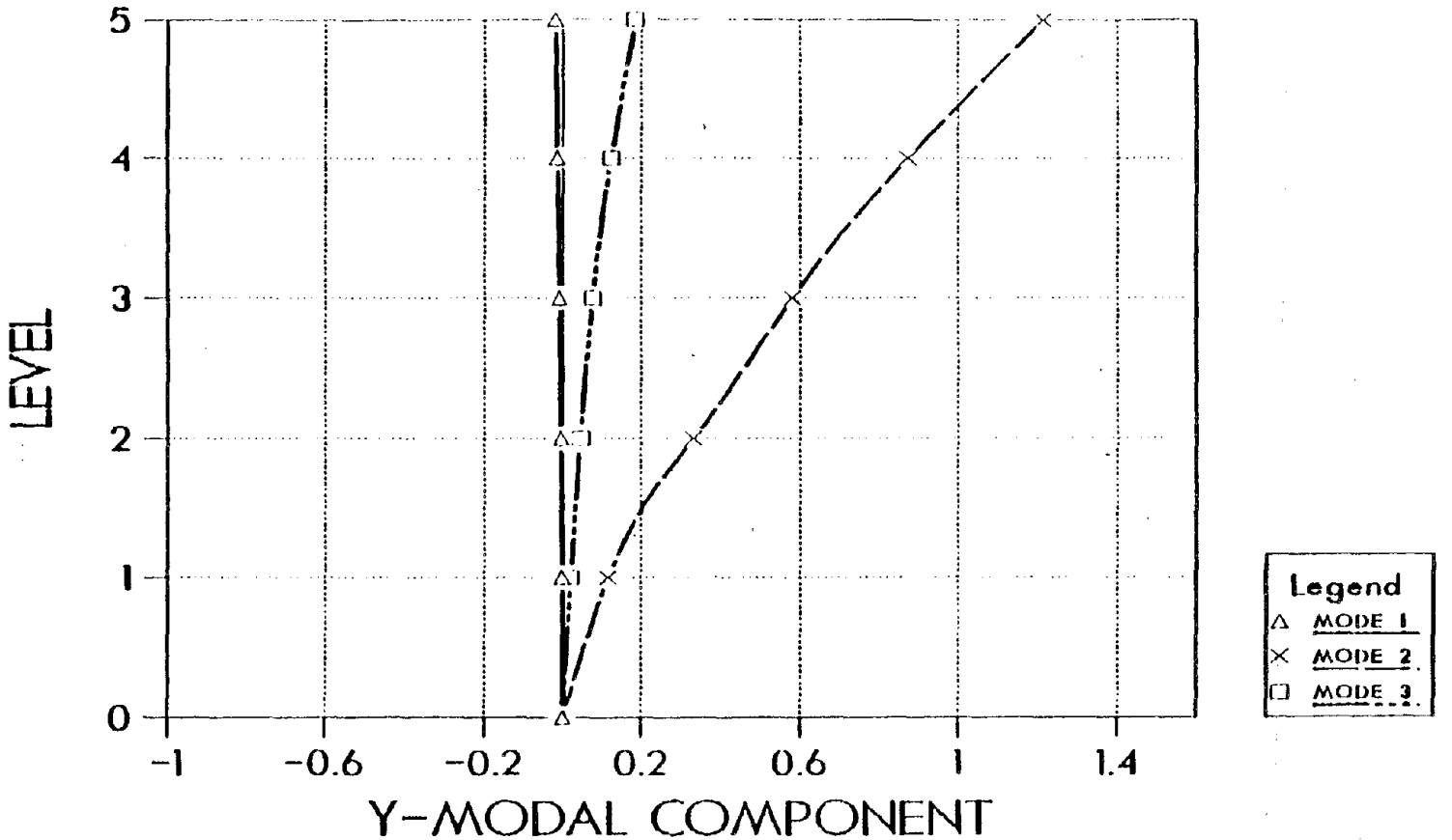

Figure 32. Y-components of the Final Eigenmodes for a Five Story L-shaped Structure with Frequency Constraints

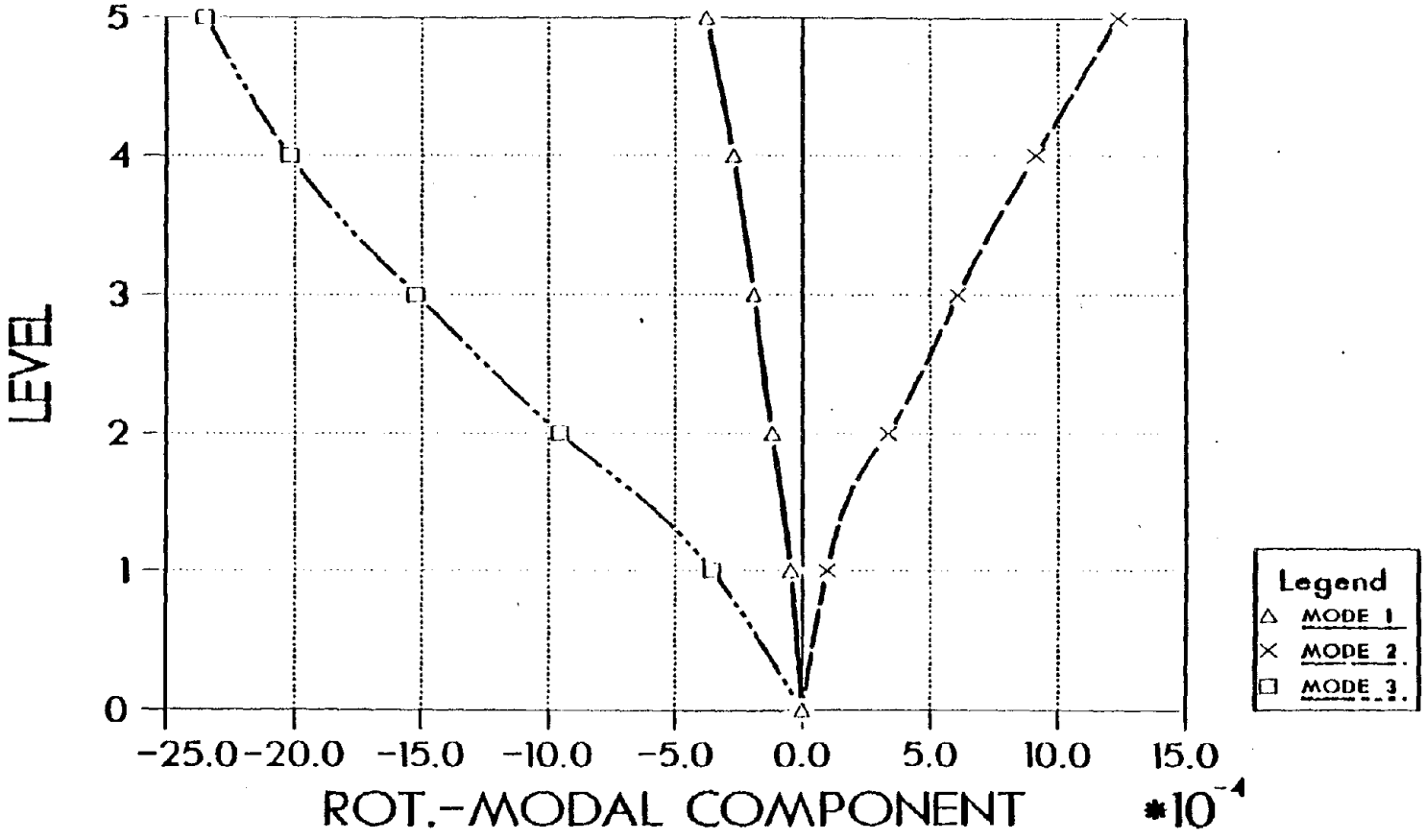

Figure 33. Φ-components of the Final Eigenmodes for a Five Story L-shaped Structure with Frequency Constraints

level, third column line is most likely due to the need to increase the stiffness in the x-direction in order to keep the first mode frequency under one second. Since column 3 is the only column oriented with the major-axis moment of inertia in the x-direction, the optimization can provide the most stiffness with the least area (weight) with this element. It also appears that the y-direction modes (frequencies) are resisted or increased by producing a strong frame with columns 4 and 5 and beam 6. This is not as easily seen as the reason for a large column 3. The ability to maintain certain frequencies or periods is in order that structures can be forced into specific regions of the response spectrums during a modal analysis.

Observations:

1. The proposed algorithm and computer program was able to control the first three natural frequencies of the five-sotry structure. This can be quite beneficial when designing for dynamic loads.
2. The optimization produces a series of designs which satisfy the frequency constraints. Each design reduced in weight while redistributing the stiffness in order to control the constraints.
3. The interpretation of the final distribution is hampered by the coupled nature of the vibration problem.

4. As in the previous example, dominant members and frames are generated which provide the optimal means for maintaining the constraints. Column 3 along with the bent formed by columns 4 and 5 and beam 6 are the primary members.

E. ATC-03 PARAMETER STUDY FOR A SYMMETRIC STRUCTURE USING THE EQUIVALENT LATERAL FORCE PROCEDURE

A ten story symmetric structure was used to perform a parameter study for the ATC-03 Equivalent Lateral Force method (35) for seismic analysis and design. The parameters which were varied consist of the effective peak acceleration, A_a, the effective peak velocity-related acceleration, A_v, and the soil type, S. The commentary in the ATC-03 provision provides this discussion relating to A_a and A_v (35):

> To best understand the meaning of EPA [A_a] and EPV[A_v], they should be considered as normalizing factors for construction of smoothed elastic response spectra for ground motions of normal duration. The EPA is proportional to spectral ordinates for periods in the range of 0.1 to 0.5 seconds, while EPV is proportional to spectral ordinates at a period of 1.0 second. ... The constant of proportionality (for a 5 percent damping spectrum) is set at a standard value of 2.5 in both cases.

This statement reflects the fact that structures farther from the epicenter of the earthquake could very well be more sensitive to the effective peak velocity-related acceleration due to the fact that ground motions tend to have an increase in duration and become more periodic with this distance. Therefore, the two terms were incorporated to take into account the resonance and distance effects associated with the seismic activity for any given structure. The map areas for A_a and A_v range from zero to seven which correspond to different areas within the United States. Area seven is the worst situation with respect to seismic activity (this corresponds roughly to a maximum ground acceleration of 0.4g). There are three soil types: Soil 1, rock or stiff soil conditions where the soil depth is less than 200 feet (61 m); Soil 2, deep cohesionless or stiff clay where the soil depth exceeds 200 feet (61 m); and Soil 3, soft to medium-stiff clays and sand. A recommendation is given to use soil type 2 if the soil properties are unknown. When performing these parameter studies actual situations were explored as shown in Table IX or a total of twenty-one combinations. These are the basic parameters which can be varied with respect to a given structure which is designed by the ATC-03 provisions.

Other than these ATC-03 parameters all other initial data and geometry as given here and in Figure 34 were held

TABLE IX. Combinations of A_a, A_v, and S Used for the ATC-03 Parameter Studies

A_a*	A_v*	Soil
7	7	1, 2, 3
6	6	1, 2, 3
5	6	1, 2, 3
	5	1, 2, 3
4	6	1, 2, 3
	5	1, 2, 3
	4	1, 2, 3

*Map Area Numbers

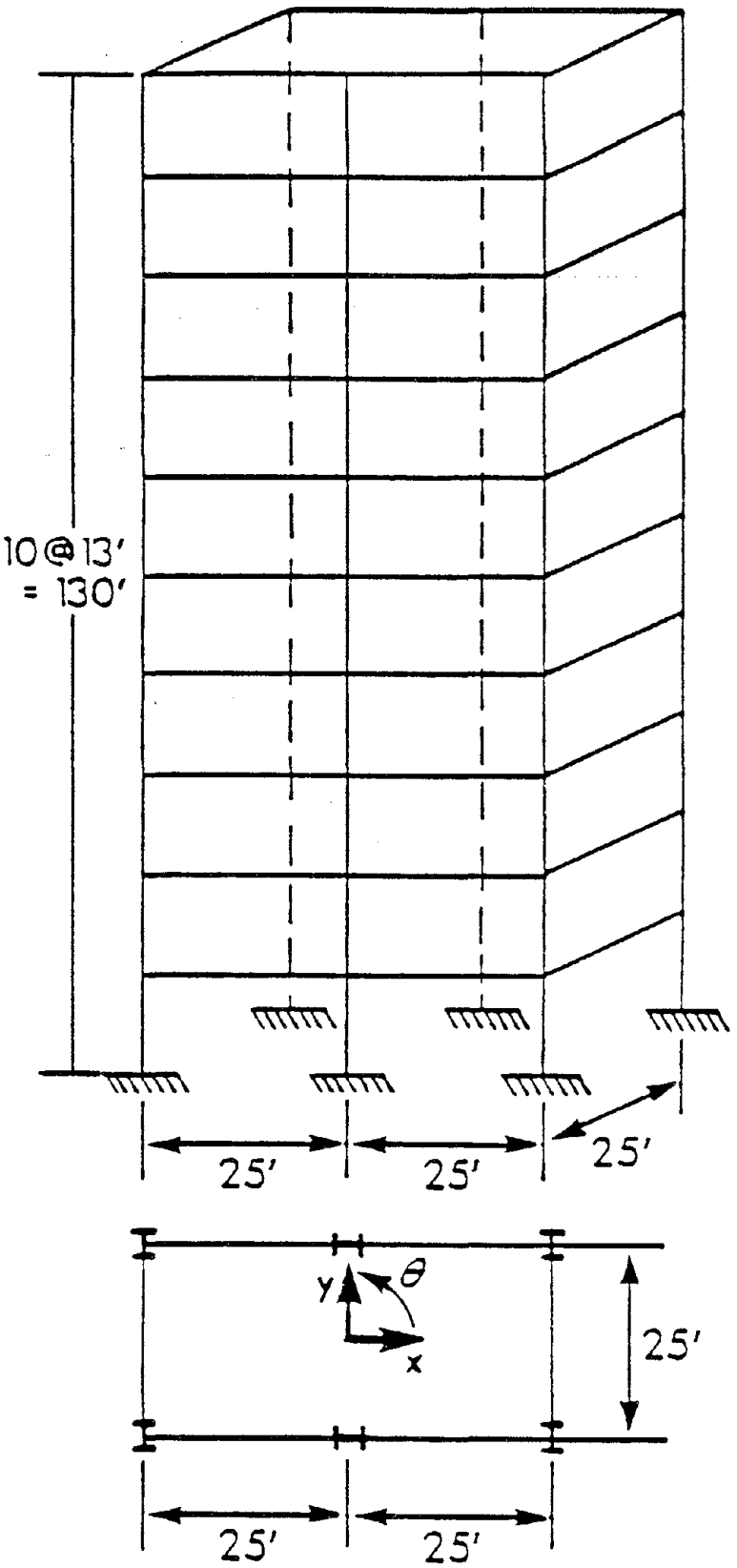

Figure 34. Ten Story Symmetric Structure
(1' = .305m)

constant. The convergence control parameter was 2, while the termination criteria was 25 cycles of optimization, 30 cycles of analysis, or a 0.5 percent weight change. This small percentage was chosen in order to insure a near optimal solution for each case. Only displacement constraints were considered and are given in Table X. These displacements are given with respect to an elastic analysis and have been based upon the drift criteria given within the ATC-03 provisions which states that the drift for this building cannot exceed 0.015 times the story height of 156 in (396 cm). This includes the ductility and nonlinear effects, therefore this ATC drift value is reduced. It is reduced in accordance with the deflection amplification factor, C_d. This is the applied ATC-03 factor which converts the linear elastic analysis to a pseudo-nonlinear analysis. A deflection amplification factor of 4.0, a response modification factor of 4.5, a seismic hazard exposure group of 2, and a location away from an active fault were used for the ATC-03 analysis (These factors are frame and material dependent). Note that the first level allowable deflection is less than the value just described. This is to force the first level deflection to become active as well as the other nine stories which will force the ATC-03 drift requirements to be satisfied.

TABLE X. Maximum Allowable Displacements (1 in = 2.54 cm)

Level	Max. Displ. (in)
10	5.520
9	4.940
8	4.360
7	3.780
6	3.200
5	2.620
4	2.040
3	1.460
2	0.880
1	0.300

The entire structure used steel, wide-flange sections and Equations 3.15 to 3.29 to represent the relationship between the secondary and primary design variables. Linking was used for both the columns and the beams. Every level was forced to maintain one size of columns and one size of beams. This provides a more realistic design and allows a reasonable approach to comparing relative stiffnesses of the different structures. Each level height was chosen to be 156 in. (396 cm) with each level having a translational mass of 0.647 k-s^2/in (113 Mg) and a rotational mass of 24,263 k-s^2-in (2742 Mg-m^2). The structure was subjected to only the lateral forces required by ATC-03 in order to see the effects of these loads. This does require two load cases. The first requires a five percent eccentricity in the positive y-direction and the second requires a five percent eccentricity in the negative y-direction for the x-direction lateral force. The primary direction of excitation is in the x-direction. Each load combination consists of 30 percent of the y-direction lateral force superimposed with 100 percent of the x-direction, eccentric lateral loads. The initial design sizes were 9500 in^4 (395,400 cm^4) for all columns and all beams, but could be changed by scaling prior to the first optimization cycle. Therefore, each structure starts with equivalent column and beam sizes but not necessarily 9500 in^4 (395,400 cm^4).

The results of these analyses provide several interesting observations. The major quantities associated with these results are given in Table XI. These results can be further reduced into twelve categories which produce Table XII. From Table XII, the final design seems to be most heavily related to the value of peak velocity-related acceleration and soil conditions. Categories III, VI, VII, and X show that identical results will be obtained for a range of effective peak accelerations as long as the effective peak velocity-related accelerations and soil conditions are held constant. This holds true because of two reasons. First, the base shear for this structure is based upon Equation 4.60 which is dependent upon the values A_v, S, R, and T. R, the response modification factor is a constant, the value of A_v and S are constants within their appropriate categories which leaves the period, T, which is also constant for this problem. The value of the period used in the calculations is not the value calculated and given in Table XII, but is the value found by

$$T_a = 0.035\ (h_n)^{0.75} \qquad (9.1)$$

where h_n is the total height of the structure. The ATC-03 provisions states:

TABLE XI. Effects of A_a, A_v, and S on a Symmetric Structure Subjected to ATC-03 Equivalent Lateral Forces (1 kip = 4.45 kN)

Soil	A_a*	A_v*	Init. Wt. (kip)	Final Wt. (kip)	Period (sec)	No. of Cycles
1	7	7	310.5	228.0	1.890	5
	6	6	269.9	196.7	2.153	5
	5	6	269.9	196.7	2.153	5
	5	5	221.5	159.0	2.614	5
	4	6	269.9	196.7	2.153	5
	4	5	221.5	159.0	2.614	5
	4	4	181.4	135.7	2.984	8
2	7	7	336.7	250.8	1.739	5
	6	6	295.0	216.9	1.974	5
	5	6	295.0	216.9	1.974	5
	5	5	242.1	174.0	2.402	6
	4	6	295.0	216.9	1.974	5
	4	5	242.1	174.0	2.402	6
	4	4	199.7	147.2	2.735	19
3	7	7	395.2	277.3	1.535	5
	6	6	336.7	243.0	1.789	5
	5	6	336.7	243.0	1.789	5
	5	5	269.9	196.7	2.153	5
	4	6	316.8	237.3	1.826	5
	4	5	269.9	196.7	2.153	5
	4	4	234.6	168.4	2.475	5

*Map Area Numbers

TABLE XII. Condensed Results for a Symmetric Structure Subjected to ATC-03 Equivalent Lateral Forces (1 kip = 4.45 kN)

Category	Wt. (kip)	Period (sec.)	A_a^*, A_v^*, S
I	277.3	1.535	7, 7, 3
II	250.8	1.739	7, 7, 2
III	242.9	1.789	6, 6, 3
			5, 6, 3
IV	237.1	1.826	4, 6, 3
V	228.0	1.890	7, 7, 1
VI	216.9	1.974	6, 6, 2
			5, 6, 2
			4, 6, 2
VII	196.7	2.153	6, 6, 1
			5, 6, 1
			4, 6, 1
			5, 5, 3
VIII	174.0	2.402	5, 5, 2
			4, 5, 2
IX	168.4	2.475	4, 4, 3
X	159.0	2.614	5, 5, 1
			4, 5, 1
XI	147.2	2.735	4, 4, 2
XII	135.7	2.984	4, 4, 1

*Map Area Numbers

> The fundamental period of the building, T, ... shall not exceed 1.2 T_a. Alternatively, the value of, T, may be taken equal to the approximate fundamental period of the building, T_a, ...

For the given structure T_a = 1.347 seconds and 1.2 T_a = 1.617 seconds. This statement and Equation 9.1 controls in every case except Category I, as seen in Table XII. Even in this case the actual period is greater than T_a. Category VII provides a similar trend except the same final design is valid for two different combinations of A_v and soil type. This is due to the fact that the product of A_v and S are equivalent for these two cases. The coefficient C_s in Equation 4.60 uses the product of A_v and S in its determination. A map area number of 6, provides A_v = 0.30 and a map area number of 5 provides A_v = 0.20. Soil type 1 gives a factor S of 1.0 and soil type 3 provides a factor S of 1.5. These terms then provide the same value for C_s, which in turn provides the same results with respect to the optimization.

The convergence properties of the twelve different categories is shown in Figure 35. Eleven of the twelve categories optimized within eight cycles with most finishing within five cycles. One case took nineteen cycles to finish. This eleventh case (Category XI) had a period of fluctuation begin after approximately six cycles. These fluctuations were strictly due to the small

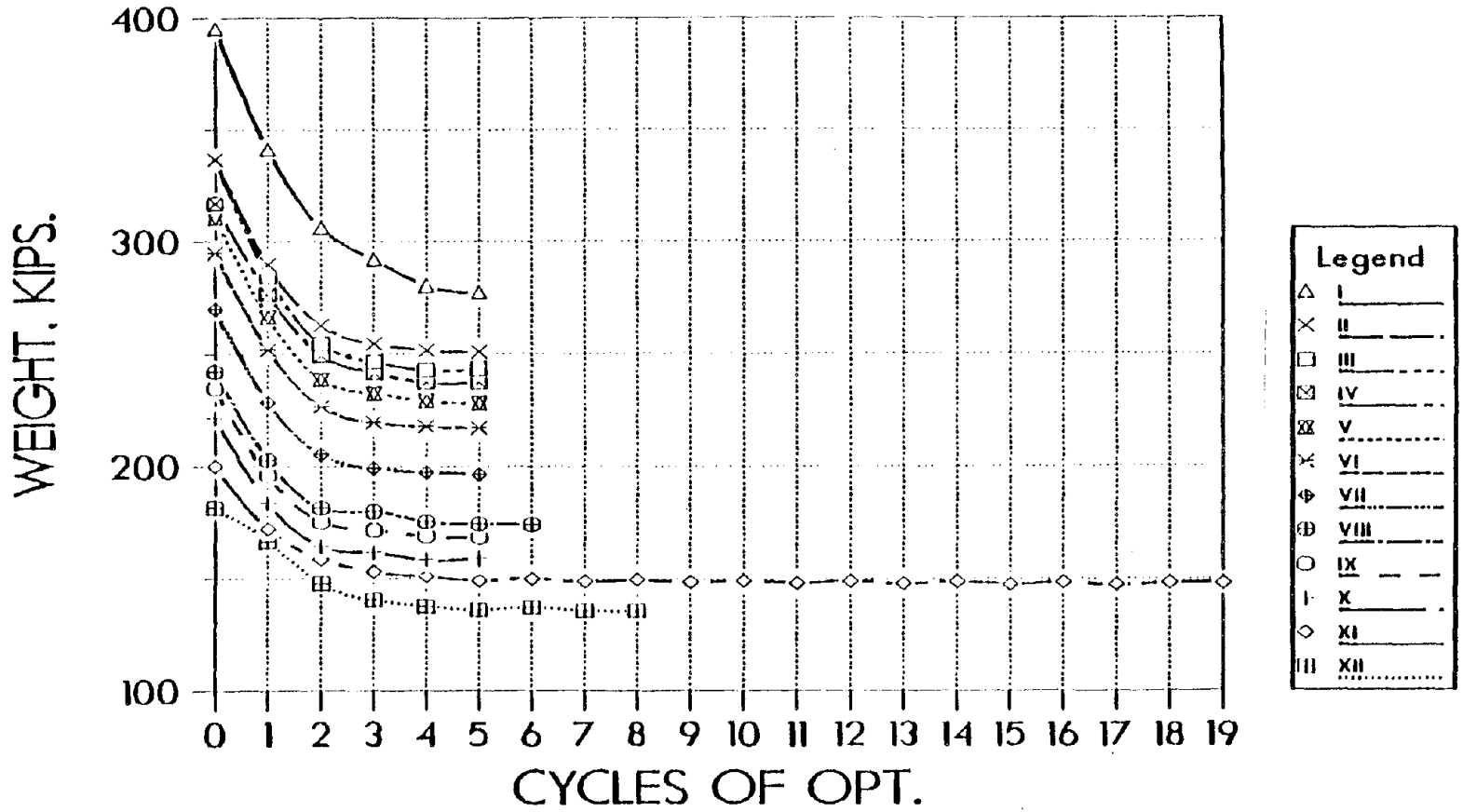

Figure 35. A Comparison of Weights for a Ten Story Symmetric Structure Subjected to ATC-03 Parameters; A_a, A_v, and S (1 kip = 4.45 kN)

percentage of weight change required for termination. This is a common occurence near an optimal solution. All of the structures had a final active constraint set which consisted of the x-displacements for each level. The maximum y-displacements ranged from approximately 1.6 in. (4.1 cm) to 2.0 in. (5.1 cm). The level versus column and beam major axis moments of inertia for the twelve categories are shown in Figures 36 and 37. The trends for all of the examples are similar as would be expected. All of the beams and columns tend to increase in stiffness in a regular fashion from the top level down to the first or second level. At the first level the beams change dramatically from the previously established pattern and at the second and first levels, respectively, the columns are slightly decreased then greatly increased. There are two reasons why this occurs. First the reduced displacement constraint at the first level requires a large stiffness for the first level columns. Secondly, the fixity at the base coupled with the strong first level column causes the optimization to place a relatively small beam at the first level. In other words, this set of beams has little effect on the first level or any subsequent displacements since the fixed base helps limit the first level rotations at the column nodes and the relative displacement between the column ends. The small reduction in the column stiffness at level two is most

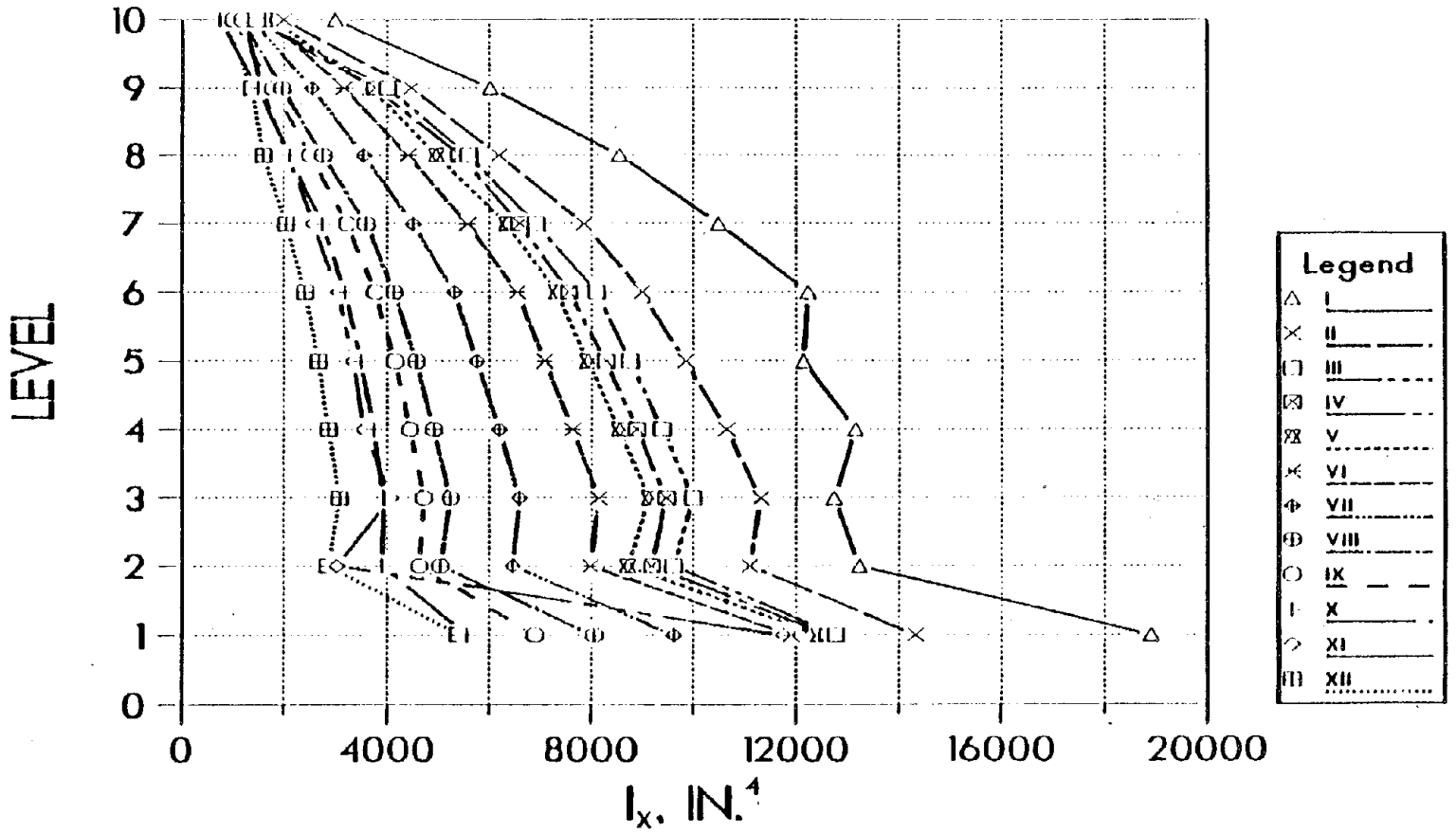

Figure 36. Column Stiffness Distribution for a Ten Story Symmetric Structure Subjected to ATC-03 Parameters; A_a, A_v, and S (1 in = 2.54 cm)

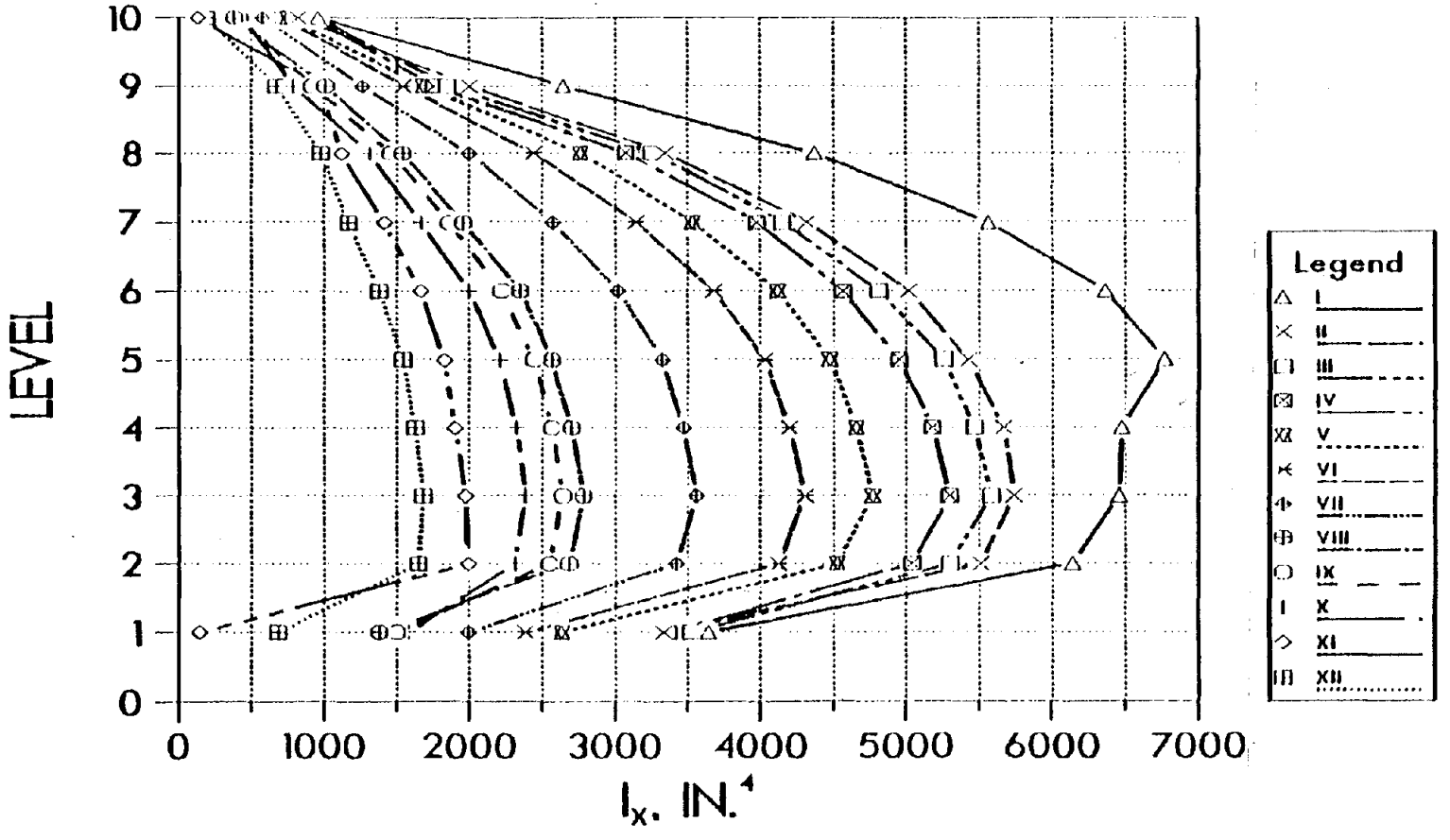

Figure 37. Beam Stiffness Distribution for a Ten Story Symmetric Structure Subjected to ATC-03 Parameters; A_a, A_v, and S (1 in = 2.54 cm)

likely due to the numerical procedure. With the first column being relatively large, the numerical solution sees a lesser need for stiffness at the level above it. This set of examples provides some information with respect to the ATC-03 provisions which should be explored further.

Observations:

1. The optimal structure is dependent upon A_v, the effective peak velocity-related acceleration and, S, the soil condition. Since the effective peak acceleration was noncontrolling, the original 21 categories could be reduced to 12 separate solutions. This result is due to the ATC-03 provisions for determining the base shear.
2. Each structure was designed using the ATC-03 period T_a, except Category I. Every other category produced periods which were above the ATC-03 limit of 1.2 T_a.
3. All categories except Category XI converged to an optimal solution within 8 cycles, and each category converged smoothly. Category XI had a fluctuating constraint due to the small percentage of weight change required for termination. This fluctuation could also be avoided by enlarging the width of the active constraint region.

4. Most categories optimized quickly and smoothly within 5 cycles. The optimal weights ranged from 135 kips (60 kN) to 277 kips (1233 kN).
5. The proposed algorithm and computer program can use linking to provide reasonable stiffness distribution.
6. The x-displacements on all levels formed the set of active constraints.
7. A large change in column stiffness occurs between the first and second levels. This large increase in stiffness is due to the fixity at the base and the small allowable displacement at the first level.
8. As long as all displacements become active the drift can be controlled through the displacement constraints.
9. With the exception of the first level, the columns and beams have a regular pattern with respect to stiffness distribution. Each category produces a system with increasing stiffness from top to bottom with nearly identical patterns.
10. Softer soil conditions coupled with large effective peak-velocity related accelerations produce larger variations in the stiffness.

F. ATC-03 PARAMETER STUDY FOR AN UNSYMMETRIC STRUCTURE USING THE MODAL ANALYSIS PROCEDURE

This ten story structure, shown in Figures 38 and 39, was used for several different parameter studies. The first study varies the values of the effective peak acceleration and the effective peak velocity-related acceleration while holding the soil type constant (soil type 1). These combinations were considered through the ATC-03 modal analysis procedure. Second, the soil type was varied while using map areas for the effective peak acceleration and effective peak velocity-related acceleration of seven. Third, the soil type, the effective peak acceleration and the effective peak velocity-related acceleration were held constant and the type of ATC-03 analysis was varied. The map areas were considered to be 7, the soil type was chosen as 1, and the analyses were the equivalent lateral force and the modal analysis procedures. Fourth and last, a different linking scheme was used. The first three examples consider each level to have all of its columns linked and all of its beams linked, respectively. The fourth case uses a more realistic approach of linking all of the columns on the levels one to three, all of the columns on levels four to six, all of the columns on levels seven and eight, and finally all of the columns on the levels nine and ten with a similar arrangement for the beams. These examples

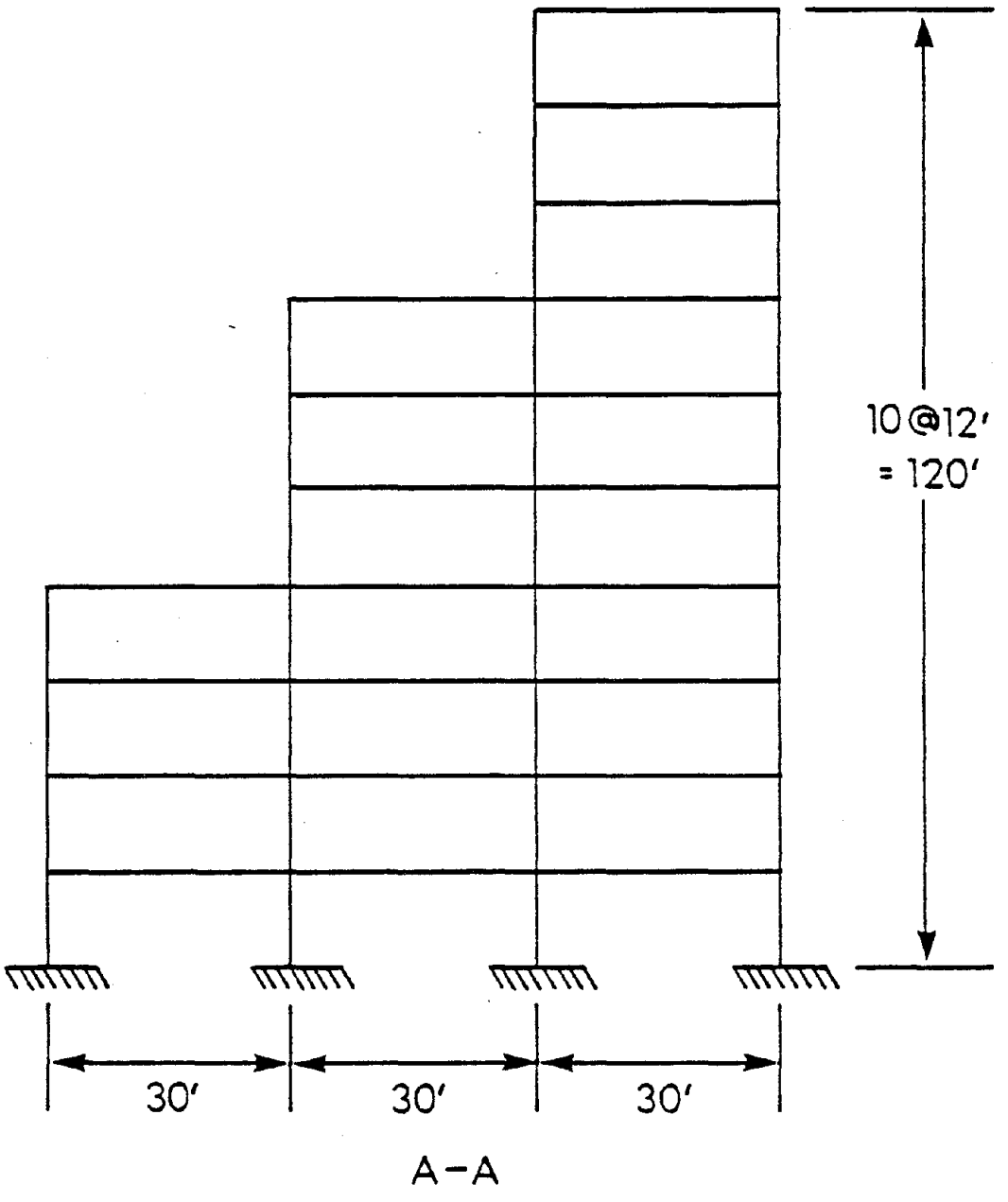

Figure 38. Ten Story Setback Structure - Elevation (1' = .305m)

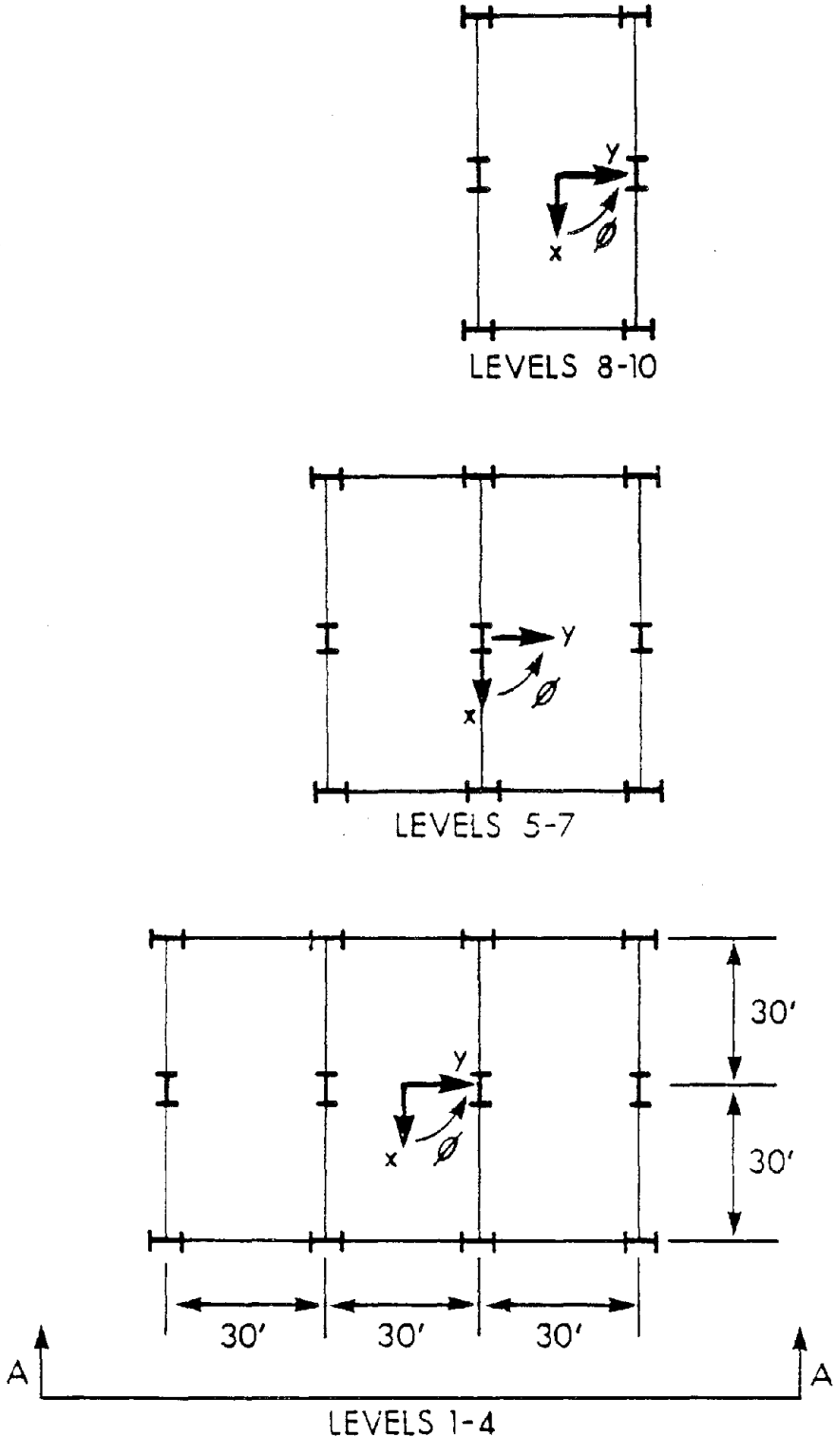

Figure 39. Ten Story Setback Structure - Plan (1' = .305m)

provide a means of exploring the ATC-03 provisions with respect to a vertically irregular structure while also exploring the optimization procedures.

There are several common parameters for these cases. All columns and beams are considered to be wide-flange elements controlled by Equations 3.15 to 3.29. These studies considered the structure to be within seismic hazard exposure group 2, to be near an active fault, to have a response modification factor of 4.5 and, to have a deflection amplification factor of 4.0. The translational and rotational masses for levels 8-10 were 0.839 k-s^2/in (147 Mg) and 45,280 k-s^2-in (5116 Mg-m^2), for levels 5-7, 1.678 k-s^2/in (294 Mg) and 144,895 k-s^2-in (16,373 Mg-m^2), for levels 1-4 2.516 k-s^2/in (441 Mg) and 353,180 k-s^2/in (39,910 Mg-m^2). All beams and columns had equivalent, initial values for the major axis moments of inertia for each problem. Each structure started with moments of inertia of 5500 in^4 (228,939)cm^4, but were then scaled within the program to a value which would produce an active constraint so the optimization could begin. The lower range control for active constraints was slightly relaxed to values of ten percent to fifteen percent while the upper range was maintained at five percent. This was done in order to control a slight fluctuation in scaling that was occurring due to the discontinuous nature of the secondary to

primary design variable relationships. Dynamic displacement constraints were considered and the two loadings consisted of the ATC-03 forces, determined by one of the two analysis techniques. The two loadings are required to check the effects of the five percent eccentricity with respect to the major-axis loading. This structures primary excitation was directed in the x-direction at each level's mass center plus or minus the five percent eccentricity while the y-direction loading was considered to be thirty percent of the lateral loads determined for that direction. The dynamic displacement constraints were chosen as 0.45 in. (1.14 cm) per floor level. This was based on the ATC-03 drift limit of 2.16 in. (5.49 cm) per floor, after inelastic effects are considered, or 2.16/4 = 0.54 in. (1.37 cm) for an elastic analysis. This was further reduced for all levels by a factor of 1.2 in order to insure that the first level drifts would remain less than 2.16 in. (5.49 cm). (This has been discussed in detail in Section IX.B). The other parameters are consistent with the common parameters given in Section IX.A or will be discussed with respect to each individual study.

1. Variation in Map Areas for Effective Peak Acceleration and Effective Peak Velocity-related Acceleration. This parameter study was used to explore the effects that the different combinations of effective peak accelerations and effective peak velocity-related accelerations have on the

optimal solutions. This is similar to the study performed on the ten story regular structure and provides similar results. Seven combinations were considered with map areas ranging from 4 to 7. These seven combinations provide actual allowed combinations of these map areas. The results are given in Figures 40 to 43. Within the legend the three digit numbers provide the map area for the effective peak acceleration, A_a, then the map area for the effective peak velocity-related acceleration, A_v, and the soil type, S. Each of these structures was analyzed using the ATC-03 modal analysis procedure using the first four modes. Each structure was analyzed using the period of 1.777 seconds for the first mode which is 1.4 T_a where T_a was defined by Equation 9.1. This portion of the ATC-03 states that no base shear will be less than that calculated for a period of 1.4 T_a and it need not exceed the value based upon the equivalent lateral force which is generally dominated by 1.2 T_a. Key values are also given in Table XIII.

Tables XIII and Figure 40 show similar results to those seen in the ten story regular structures. The effective peak velocity-related acceleration appears to be the dominate parameter. A map area of six for A_v provides optimal weights of 476.4 kips (215.8 Mg), 454.9 kips (206.1 Mg) and 473.6 kips (214.5 Mg) and a map area of five for A_v gives 387.3 kips (175.4 Mg) and 387.4 kips

TABLE XIII. Ten Story Setback Results with Respect to ATC-03 Map Areas (1 kip = 4.45 kN)

A_a*	A_v*	Init. Wt. (kip)	Final Wt. (kip)	Period (sec)	Active Constraints Load 1**	Load 2**
7	7	594.2	515.8	1.477	–	x_{10}-x_8***
6	6	516.5	476.4	1.717	x_{10}-x_8	x_{10}-x_5
5	6	516.6	454.9	1.716	x_{10}-x_8, x_6-x_5	x_{10}-x_5
5	5	423.9	387.3	2.206	x_{10}-x_3	x_{10}-x_3
4	6	515.9	473.6	1.725	x_{10}-x_8, x_6-x_5	x_{10}-x_5
4	5	424.1	387.4	2.116	x_{10}-x_8, x_6-x_5	x_{10}-x_5
4	4	368.5	314.4	2.489	x_{10}-x_5	x_{10}-x_5

*These numbers represent the map area numbers for A_a and A_v.

**Load 1 refers to a positive 5% eccentricity and Load 2 refers to a negative 5% eccentricity in the y-direction.

***x_{10}-x_8 indicates the the displacements in the x-direction at the 8th through 10th floors are active.

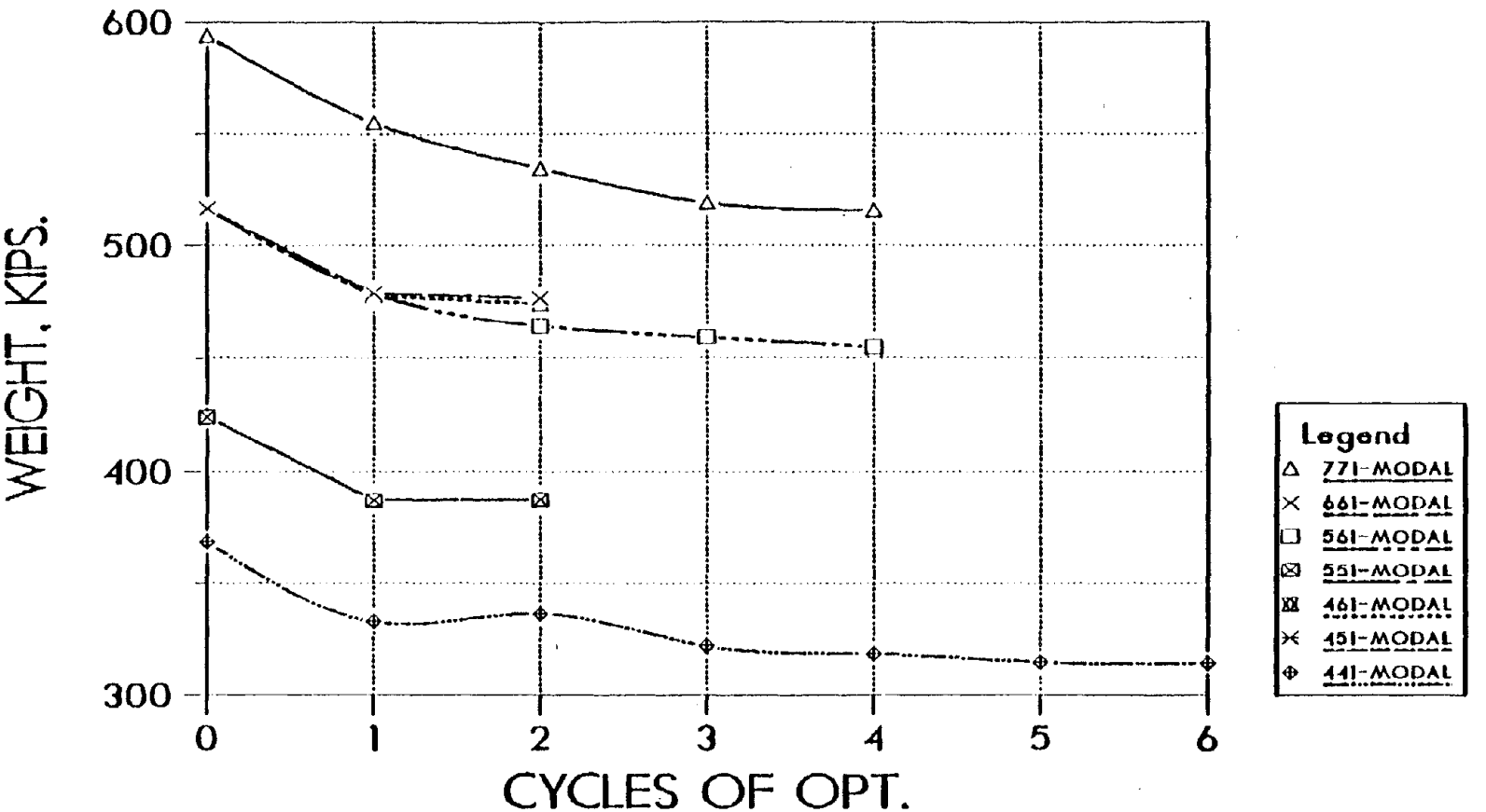

Figure 40. A Comparison of Weights for a Ten Story Setback Structure Subjected to Combinations of A_a and A_v (1 kip = 4.45 kN)

(175.5 Mg). Since these values are similar, Figure 39 can be broken into four regions which represent the effects of A_v. The difference in weights for the 561 case versus the 661 and 461 is due to a slight difference in mode shapes which produces slightly different displacements. These differences affect the optimal solution in terms of gradients and Lagrange multiplier calculations which allows this structure to generate slightly lower results. Looking at Figures 41 and 42 the 561 case provides larger columns but smaller beams than either of the two cases 661 and 461. These latter two cases are nearly identical. If case 561 were terminated at optimization cycle 2, it would have had beams and columns of similar size to those of 661 and 461. This indicates that there are several local minima in this region. Note that cases 551 and 451 lie exactly on top of each other in Figure 40, but they do differ with respect to column and beam stiffness.

When using wide-flange sections it is possible to have a significant difference in stiffness with little difference in weight or cost due to the relationship between the area and the major-axis moment of inertia, but in the same sense the final stiffness values are generally not as important as the stiffness trends from level to level. For all of these cases the general trend is for the columns to be larger than the beams and to be substantially larger near

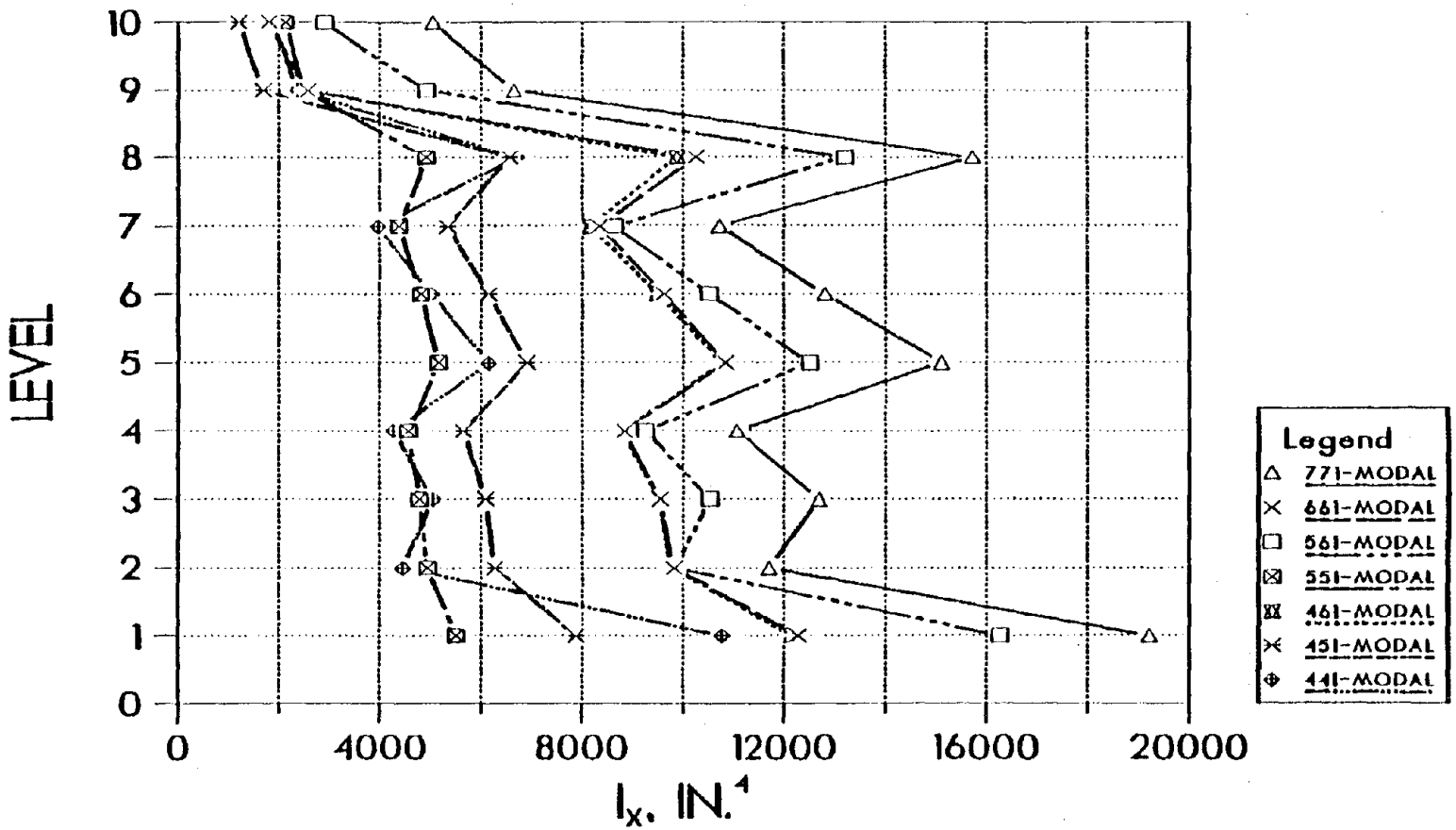

Figure 41. Column Stiffness Distributions for a Ten Story Setback Structure Subjected to Combinations of A_a and A_v (1 in = 2.54 cm)

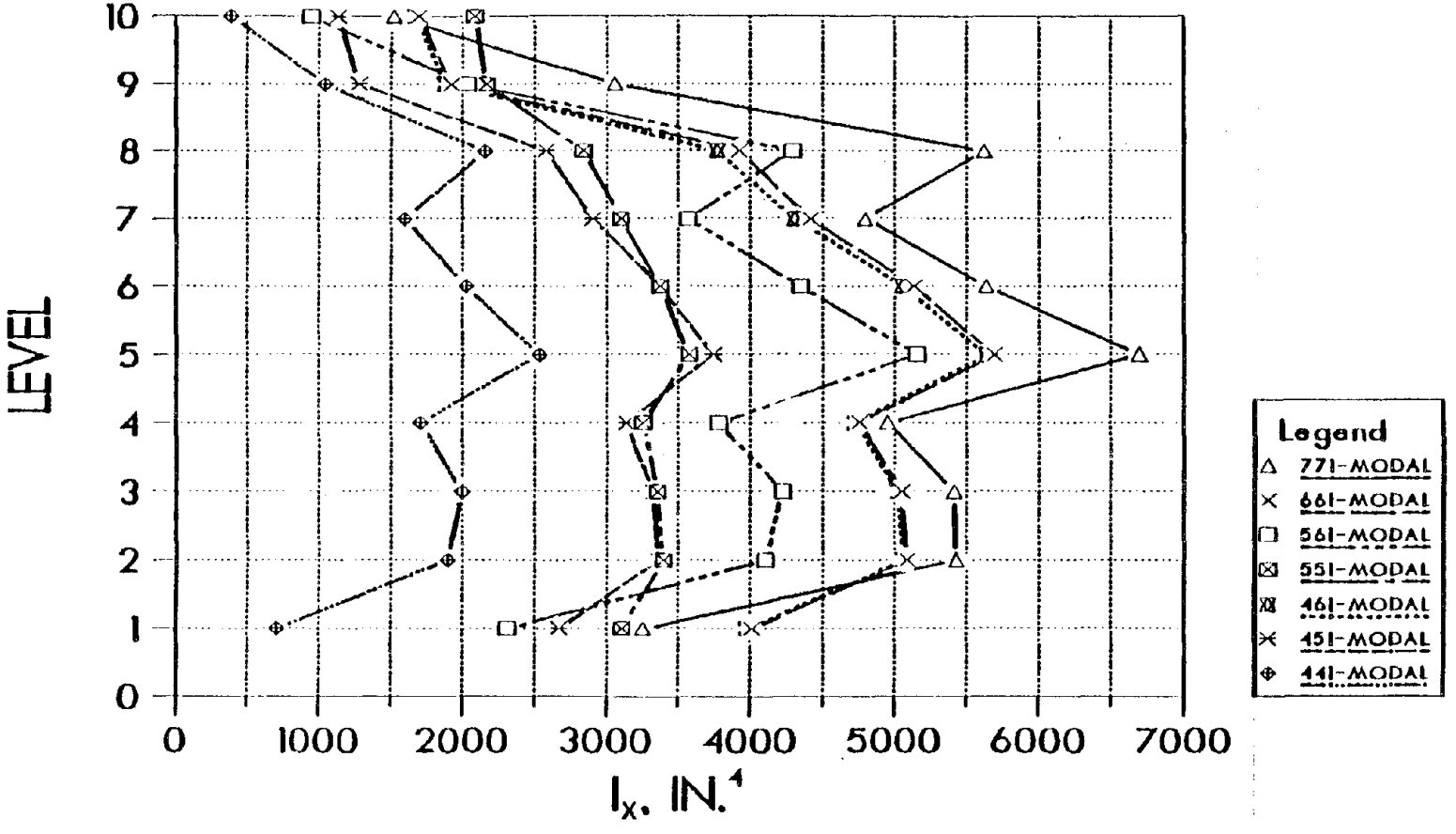

Figure 42. Beam Stiffness Distributions for a Ten Story Setback Structure Subjected to Combinations of A_a and A_v (1 in = 2.54 cm)

the lower levels. None of these distributions are smooth which is due to the irregularities in the vertical stiffness and mass center location for this structure. The general trend for these structures is to have increasing column sizes from the top of the setback to the bottom of a setback, then to reduce the column size at the top of the next lower setback. Looking at levels eight and five shows this trend quite well. This is due to the need to recoup a portion of the stiffness which is lost at that lower level of each setback. Keep in mind that the displacement constraints form a straight line from the base to the top, and the optimization is going to provide a structure which at least reaches several of these constraint values. Therefore, each setback reduces in stiffness from the bottom of the discontinued level to the top and the next setback has to compensate for the lost stiffness of the missing elements. The lower two levels have a slightly different trend due to the fixity at the base. This fixed base forces the lower column to become very stiff (making use of this stiffness and the fixity reduces the total displacement of nine upper levels which is very efficient with respect to the optimization). In the same sense, the optimization sees this as overkill and sometimes reduces the second column to a value smaller than the third level. This trend is seen in all of the columns

where the first column is much larger than the third level columns.

This base fixity is also responsible for providing smaller beams at the first level. Since the first level columns are generally very stiff, little resistance is required by the beams (If stress constraints were applied quite often the lower beams are controlled by stress constraints). Overall, the general trend for three of the seven cases is similar to that for the columns, large beams are required for the lower levels of each setback portion with a decrease in beam size at each level directly below the setback. All of the cases fulfill this general statement at level five, but do not satisfy this trend at level eight. The four cases are 661, 461, 551, and 451. Three of these cases can be attributed to the fact that x_1 is not considered an active constraint, and the fourth case 551 considers x_1 active until the Lagrange multipliers is found to be negative and it is removed. By not considering this constraint as active and the fact that these four cases used only two optimization cycles, these structures did not have a chance to try and reduce these beams. As seen with 561, the additional cycles causes this system to reach a solution similar to that of 771 and 441. It is also important to see that the beams are generally much smaller than columns. Most examples with displacement

constraints only will produce a system with strong columns and weak beams.

The ATC-03 provisions also provide stability and drift requirements. As mentioned previously the drifts are controlled by forcing the displacement constraints to be approximately eighty percent of the allowable drift. Since the drift at the level below the active constraints is generally the only controlling drift in an optimal solution, the other floors are forced to have approximately eighty percent of the allowable drift which allows the design to be somewhat stiffer than the ATC-03 provisions require. The largest drift for these seven cases was 2.157 in. (5.479 cm) which is slightly below the allowable value of 2.16. (5.486 cm), and it occurs at the top level of case 451. Only five levels within three cases had drifts above 2.00 in. (5.08 cm), therefore many of the cases could possibly be reevaluated with a displacement constraint slightly larger than the one used if a final design was required.

The stability factors are shown in Figure 43 for each of the seven cases and are found by using Equation 4.67. All seven of the curves tend to show a similar smooth transition from small theta values at the top to large values at the bottom. Several of the structures have a slight break in this trend at the second level.

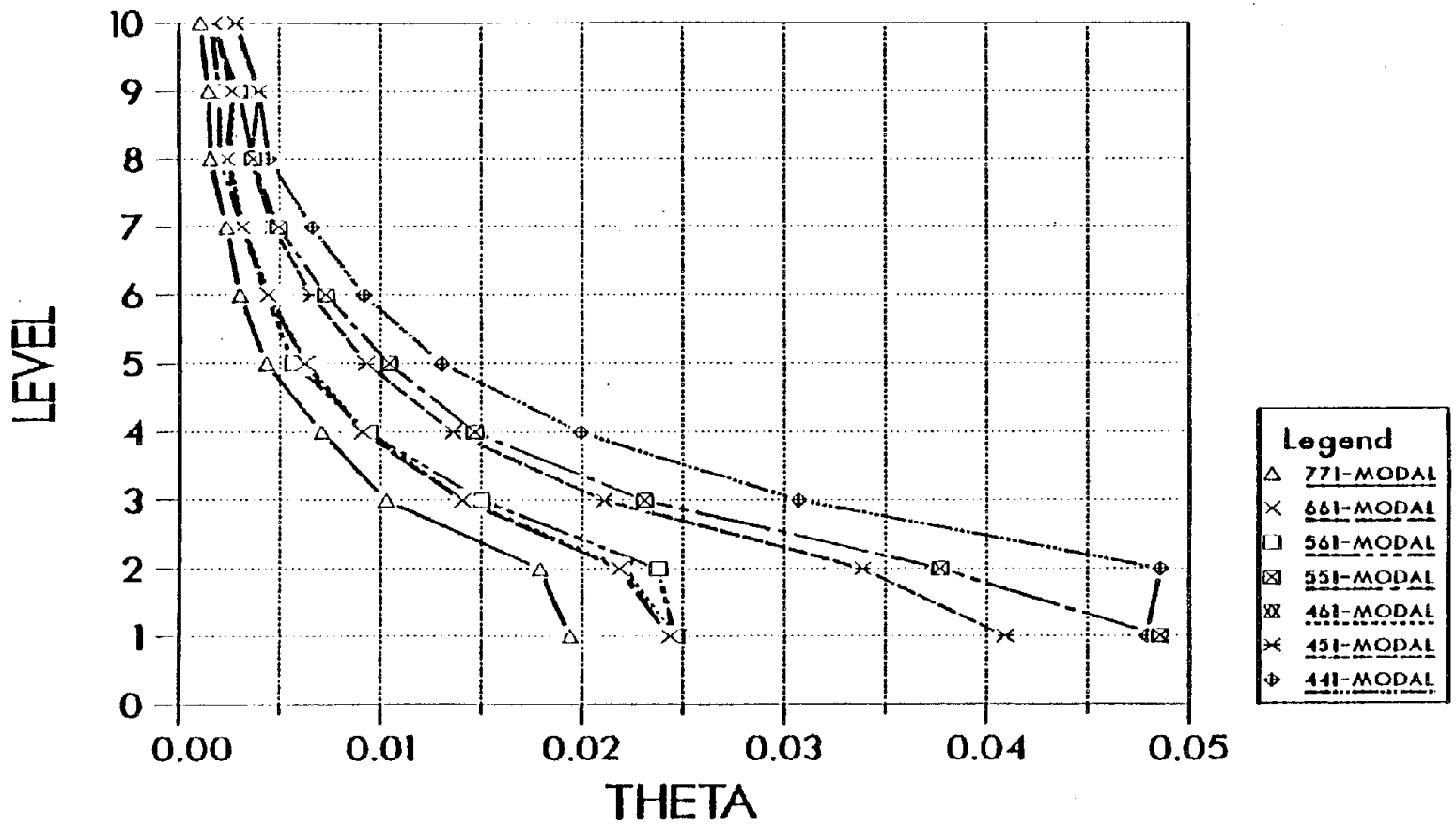

Figure 43. ATC-03 Stability Factors for a Ten Story Setback Structure Subjected to Combinations of A_a and A_v

Once again this is due to the very large columns at the base which allow small deflections and very little P-delta effects. The P-delta effect need not be considered if the stability factor, theta, is less than 0.1 which is the case for all seven structures. The largest factors are just below the value of 0.05. Note that as the structures become lighter (lower map numbers) the stability factor tends to increase. It is interesting that the structures are optimized into a stiffness distribution such that the theta factors do not reflect the setbacks. This is due to the fact that the drift was maintained through the displacement constraints which were used to distribute the stiffness.

Observations:

1. The effective peak velocity-related acceleration is the dominant factor. As seen in Figure 40, the optimal solutions can be grouped according to A_v. Due to the period of these structures, the effective peak acceleration has no effect on the ATC-03 analysis.
2. The stiffness distributions are no longer smooth. This is due to the vertical irregularities associated with each setback.
3. The general trend is for the stiffness, of the columns and beams, to decrease from bottom to top

between each set of discontinuities, and to have a large increase in stiffness within the first level of the next discontinuous section.

4. The ATC-03 stability factors are less than 0.05 which is well below the limit of 0.1. The larger stability factors occur within the lighter structures (lower effective peak acceleration values) as expected.
5. The stability factor curves do not reflect the vertical discontinuities. Their distribution is quite smooth. This is due to the linear variation of the constraint values.
6. The x-displacements form the final sets of active constraints as shown in Table XIII. Load case 2 which represents a positive five percent eccentricity in the y-direction provides the critical set of active constraints.
7. The maximum drift occurred at the top level within case 451. The drift was 2.157 in. (5.479 cm) which is slightly below the allowable value of 2.160 in. (5.486 cm).

2. Variation of Soil Type. The ten story setback structure was then subjected to ATC-03 modal analysis with a variation in soil type. The map areas for the effective peak acceleration and effective peak velocity-related accelerations were held constant at 7. All

other parameters were consistent with those presented in the proceeding section. The different soil types vary the optimal designs by the factors used in determining the base shear. Equation 4.60 has a term, C_s, which includes a term, s, that represents the soil condition and takes on the values of 1.0 for soil 1, 1.2 for soil 2, and 1.5 for soil 3. This is reflected by the response spectrum shown in Figure 44 which is the response spectrum used by the ATC-03 to produce the Equation for C_s as

$$C_s = 1.2\ A_v\ S/RT^{2/3} \qquad (9.2)$$

This is not the only equation used to find the base shear, it is the most predominant. There are three other equations to be used if certain criteria are satisfied (per mode basis). Therefore, it is not reasonable to assume the designs to be related strictly to these factors. Although it is not a direct factorization by S, the results were expected.

The results are shown in Table XIV and Figures 45 to 47. Soil condition 3 provides the largest weight of 598.4 kips (271.1 Mg) while soil condition 1 gives the lowest weight of 515.8 kips (233.7 Mg). Soil condition 2 provides a structure with a weight of 538.8 kips (244.1 Mg). Each structure required four cycles of optimization to have a weight change of less than one percent. Due to

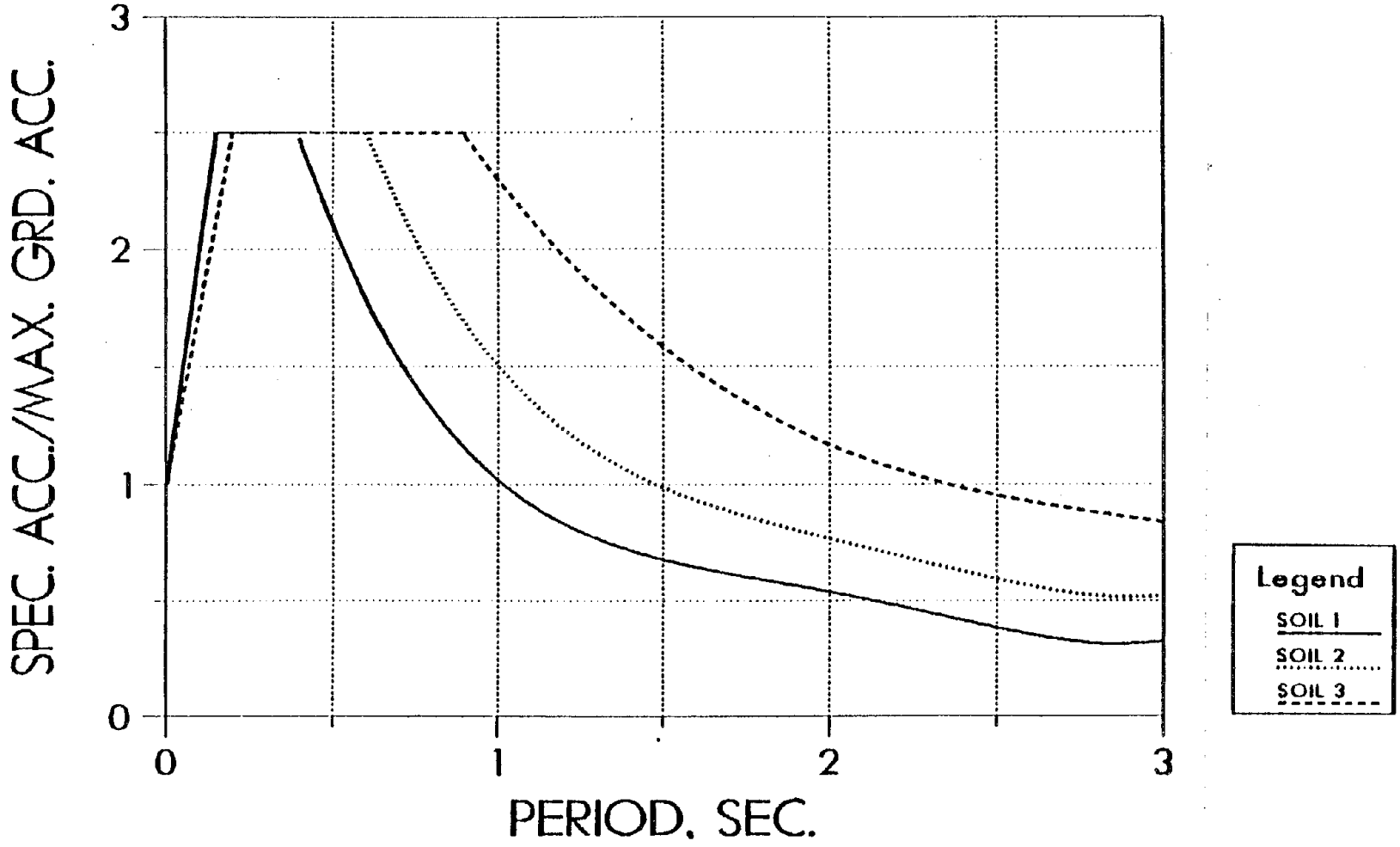

Figure 44. Response Spectra Used in the ATC-03 Provisions

TABLE XIV. Results for Variation in Soil Conditions for the Ten Story Setback Structure

Soil	Init. Wt. (kip)	Final Wt. (kip)	Period (sec)	Active Constraints Load 1*	Load 2*
1	594.2	515.8	1.477	-	$x_{10}-x_8$**
2	666.6	538.8	1.415	$x_{10}-x_4$	$x_{10}-x_4$
3	723.5	598.4	1.242	$x_{10}-x_5$	$x_{10}-x_5$

*Load 1 and Load 2 refer to the positive and negative 5% eccentricity in the y-direction respectively.

**$x_{10}-x_8$ indicates that the x-displacements are active from the 8th floor to the 10th floor.

scaling they all start a different weights which represent a structure with beams and columns of the same size initially.

The final stiffness distribution has essentially the same characteristics as those presented in the previous section. Levels eight and five require larger columns and beams than the preceeding levels due to the setback. Each system also needs large columns at the base with small beams at the first level. Soil condition 3 requires the maximum allowable column size at levels eight and one and nearly the maximum column at level five. Also, soil condition 3 requires larger beams and columns at every level of the structure. Soil condition 2 requires larger beams than soil condition 1, but the column sizes for soil condition 1 tend to be slightly larger than soil condition 2 for most levels. There is no apparent reason why this might occur other than the different initial designs might have provided a different path of optimization. This would be a numerical situation not related to the ATC-03 provisions other than through the four mode shapes used in the modal analysis. As seen from Figure 46 the beams are smaller than the columns providing a strong column - weak beam situation which helps in reducing the drift and in controlling the P-delta effect.

The drift and stability factor results are similar in characteristics to those of the previous section. The

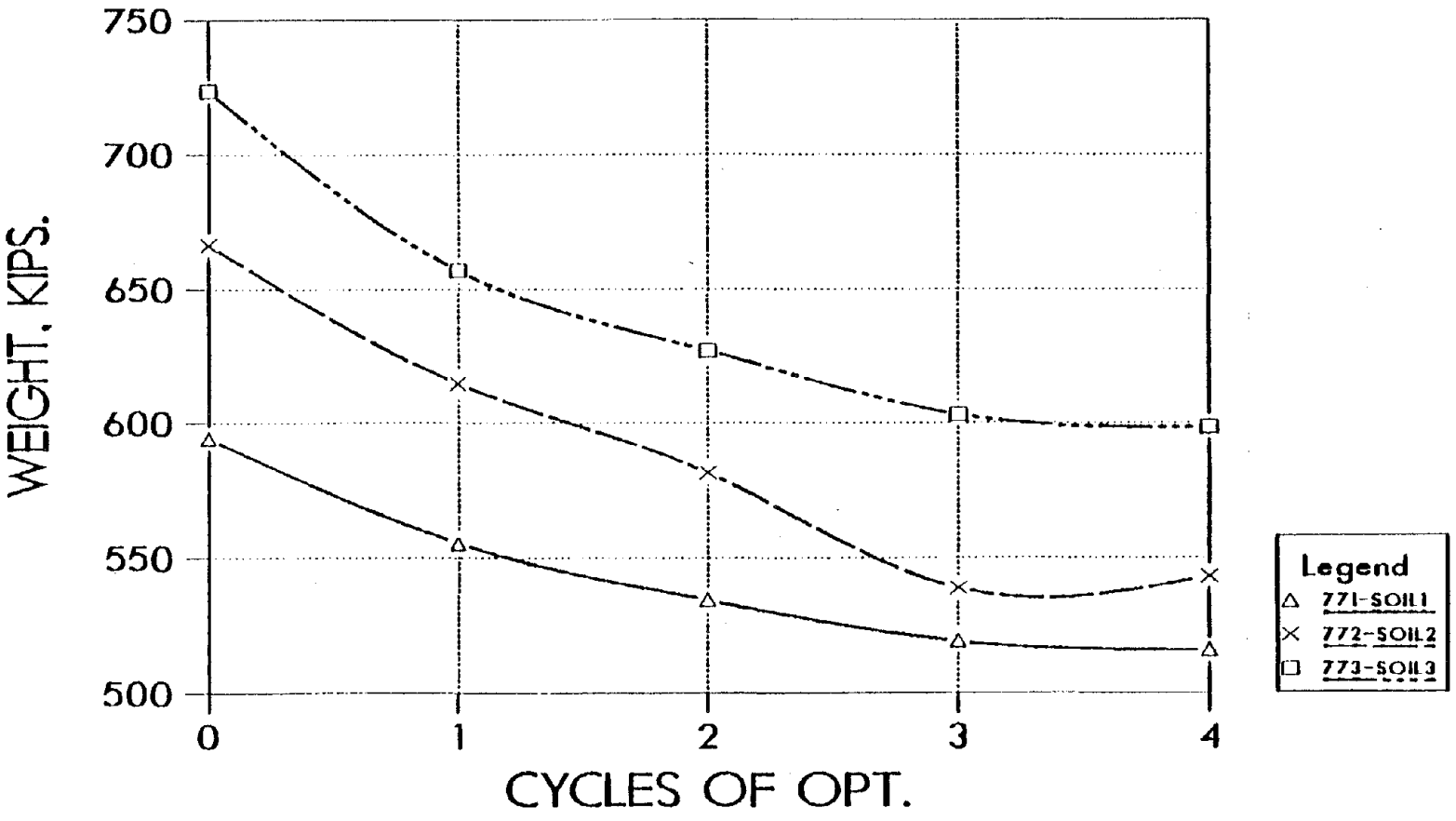

Figure 45. A Comparison of Weights for the Ten Story Setback Structure with a Variation in Soil Conditions (1 kip = 4.45 kN)

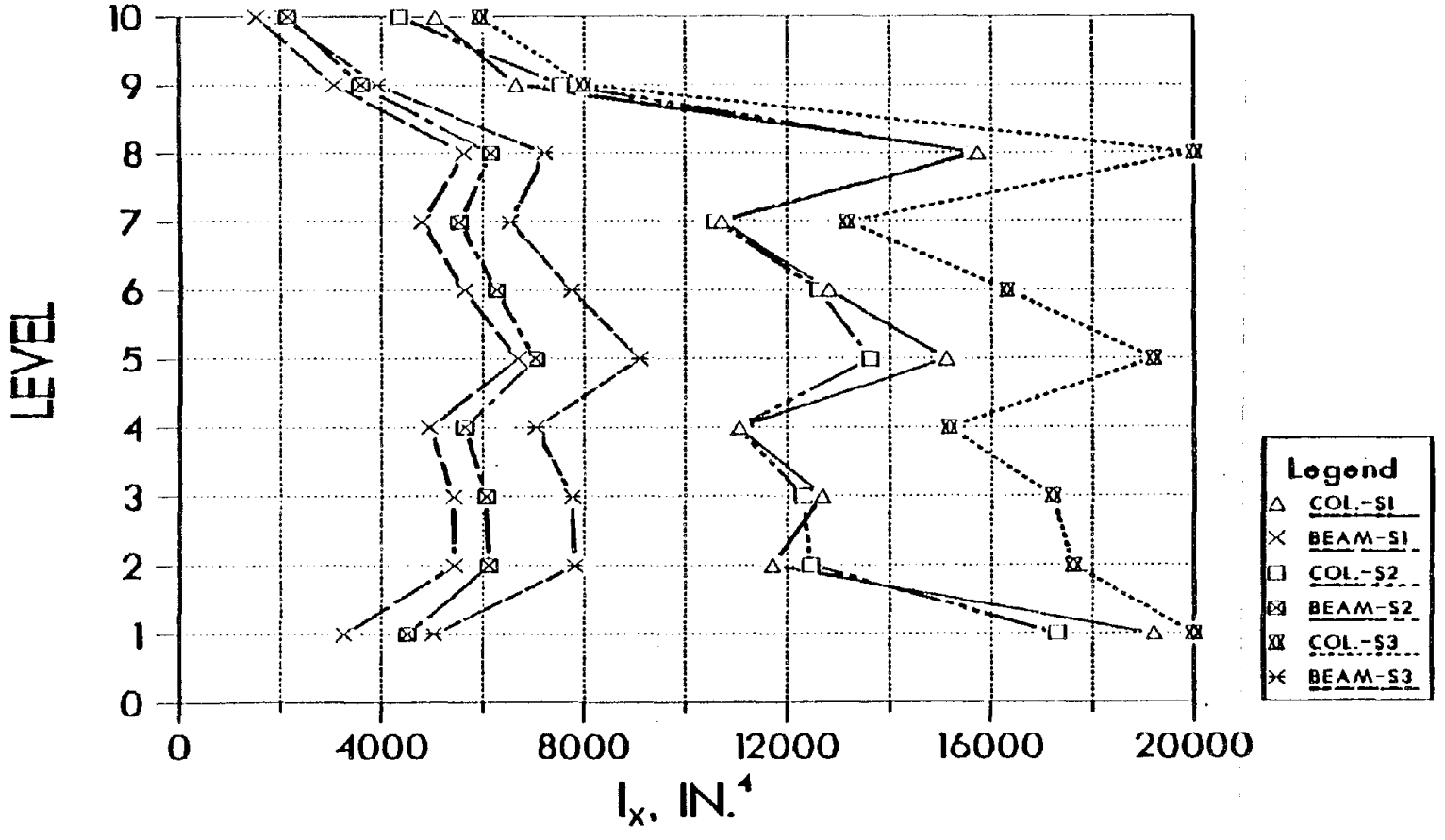

Figure 46. Column and Beam Stiffness Distributions for the Ten Story Setback Structure with a Variation in Soil Conditions (1 in = 2.54 cm)

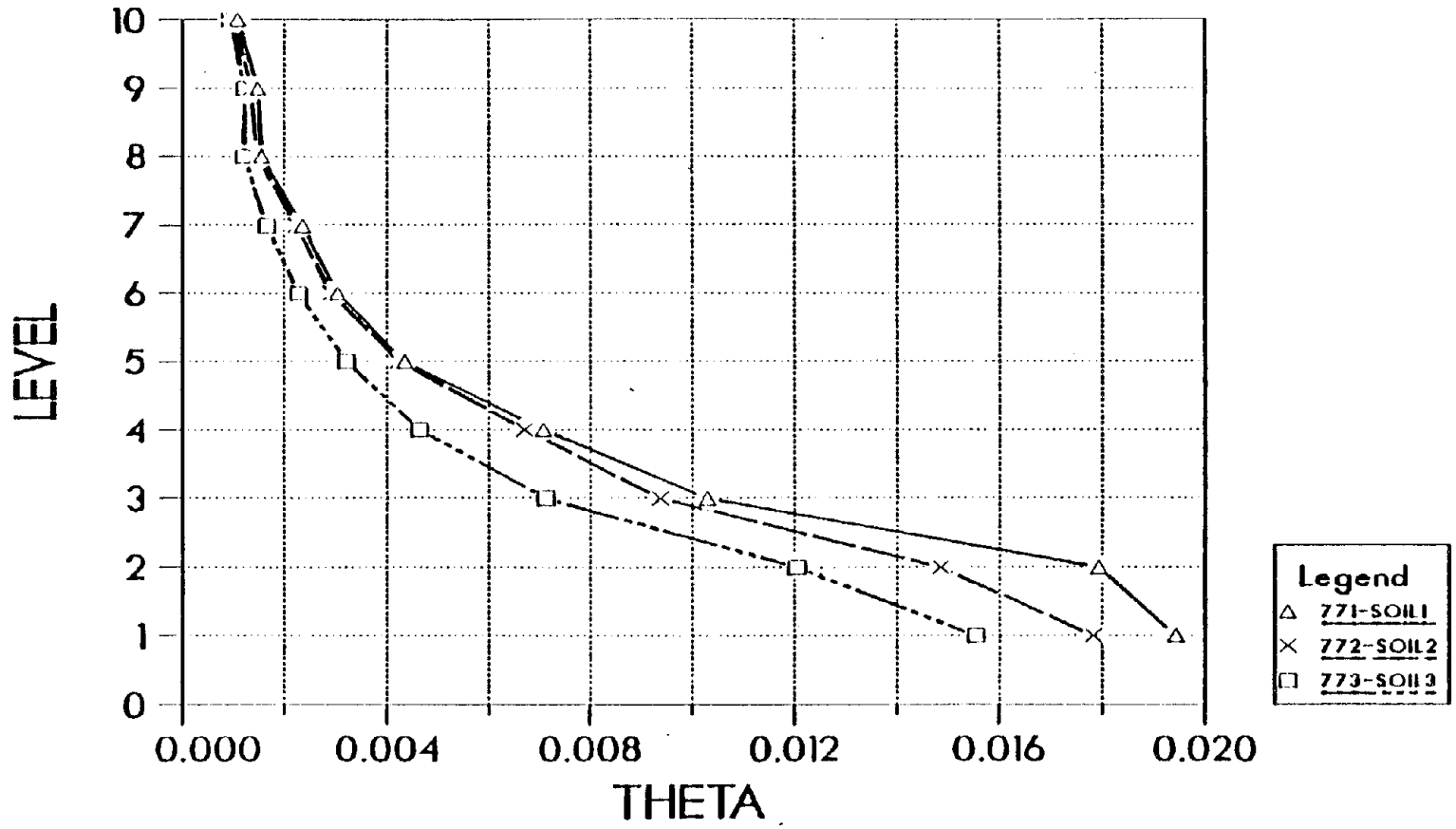

Figure 47. ATC-03 Stability Factors for the Ten Story Setback Structure with a Variation in Soil Conditions

maximum value of drift was 1.775 in (4.509 cm) for the top level of soil condition 2 and the largest value for the stability factor, that was 0.019 for soil condition 1. Both values are far below the allowable values. Table XIV shows the active constraints which are quite different for soil condition 1 as compared to the other two soil conditions. This is due to the smaller lateral forces being applied to the structure for soil condition 1. These active constraints are also reflected by the fact that the column stiffness for soil condition 1 is greater than that for soil 2 which provides more lateral restraint. Most likely if the termination criteria were identical, these columns would reduce to values below that for soil condition 2 and would allow more of the x-displacements to become active. These results provide the insight into the different soil conditions and their these effects with respect to the ATC-03 provisions.

Observations:

1. Soil condition 1 (rock) provides the smallest optimal weight with soil condition 3 (soft) providing the largest optimal weight.
2. The maximum stability factor is 0.019 for soil condition 1. As in the previous section this value is well below the maximum of 0.1. Also, the stability factors do not reflect the vertical irregularities.

3. The stiffness distributions are similar to those of the previous section.
4. The x-displacements form the set of active constraints as shown in Table XIV.
5. The maximum drift is 1.775 in (4.509 cm) at the top lead for soil condition 2. This is well below the maximum value of 2.160 in (5.486 cm).

3. Equivalent Lateral Force Versus Modal Analysis.

This section is used to provide some insight into the use of the ATC-03 equivalent lateral force procedure and the ATC-03 modal analysis procedure. For this purpose one case was studied. This case is for soil condition 1 and map areas 7 for the effective peak acceleration, A_a, and the effective peak velocity-related acceleration, A_v. All other parameters are as described in Section IX.F. The ATC-03 provisions say that a building will be classified as irregular if:

> "The building does not have an approximately symmetrical geometric configuration about the vertical axes or has horizontal offsets with significant dimensions."

and it says that buildings with only vertical irregularities should be analyzed with the ATC-03 modal analysis procedure. Therefore, an analysis by equivalent lateral force techniques would be considered inappropriate. This setback structure which has significant offsets was

analyzed with both techniques to see what differences would occur.

The results do not necessarily substantiate the need for the more detailed analysis for this structure. The results are given in Table XV and Figures 48 to 50. The modal analysis provides a lesser weight of 515.8 kips (233.7 Mg) as compared to the equivalent lateral force weight of 552.9 kips (250.5 Mg). With respect to the actual optimization it required four cycles for the modal analysis and seven cycles for the equivalent lateral force, although the last three cycles essentially provided no decrease in weight. The increase in weight for the fifth cycle is due to the addition of several new constraints during this cycle. Looking at Table XV, the set of active constraints is considerably different. The equivalent lateral force has active displacement at levels five to seven for both loading conditions whereas the modal analysis does not have any active constraints for loading condition one. These active constraints are dependent upon the rotational displacements at each level. A positive rotational displacement helps reduce the upper level x-displacement, whereas a negative rotation increases the x-displacement. Therefore, the load case with less positive rotational displacements will provide the first sets of active constraints. These constraints are difficult to predict due to the fact that both the translation and

TABLE XV. Results for Comparison of ATC-03 Analysis Techniques for the Ten Story Setback Structures (1 kip = 4.45 kN)

Analysis	Init. Wt. (kip)	Final Wt. (kip)	Period (sec)	Active Constraints Load 1*	Load 2*
ELF	686.7	552.9	1.343	x_9-x_5	$x_{10}-x_5$**
MODAL	594.2	515.8	1.477	-	$x_{10}-x_8$

*Load 1 and Load 2 refer to the positive and negative 5% eccentricity in the y-direction.

**$x_{10}-x_5$ indicates the x-displacements are active for the 5th through the 10th floors.

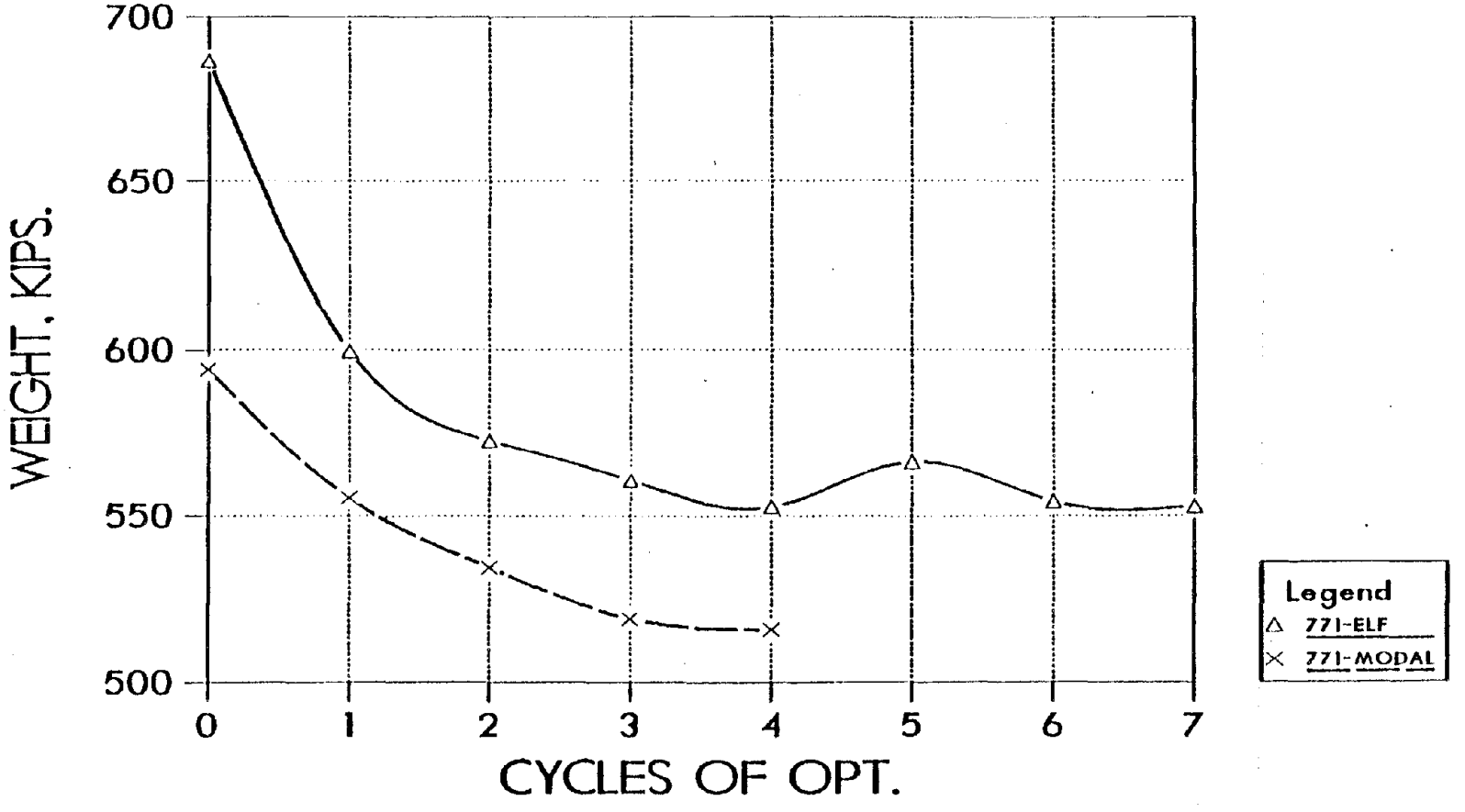

Figure 48. A Comparison of Weights for the Ten Story Setback Structure Subjected to the ATC-03 Equivalent Lateral Forces and Modal Analysis (1 kip = 4.45 kN)

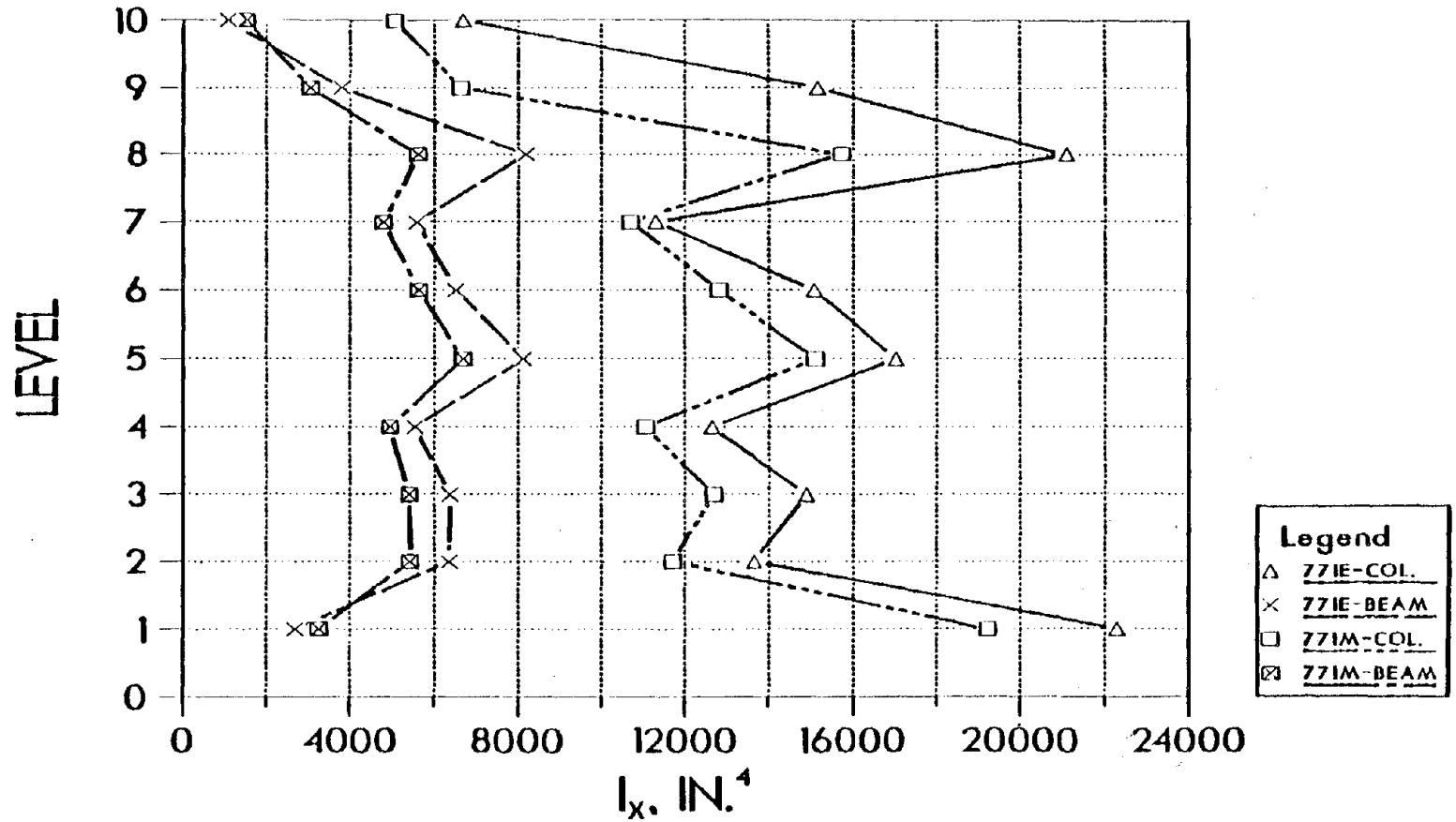

Figure 49. Column and Beam Stiffness Distributions for the Ten Story Setback Structure Subjected to the ATC-03 Equivalent Lateral Forces and Modal Analysis (1 in = 2.54 cm)

rotational displacement play a part in deciding the active constraints. Depending on the stiffness distribution these rotational effects can be large or small and independent of overall strength or weight.

Once again the stiffness distribution for the columns and beams has similar characteristics as the first two sets of results. Levels five and eight has increased sizes with the next levels below being smaller. They both have large first level columns and small lower level beams. In fact due to a scaling the equivalent lateral force analysis is asking for two columns which are above the maximum value. The stiffness required for the equivalent lateral force procedure is larger than that required by the modal analysis in all cases except for the beams on levels one and ten. Also, the general distribution is similar, except for some relatively large changes in the column stiffness within the top levels for the equivalent lateral force method.

The most prominent differences in the optimal solution is seen in the drift and stability criteria. The equivalent lateral force method has two drift values which violate the allowable drift of 2.16 in. (5.49 cm). Level eight has a drift of 2.39 in. (6.07 cm) and level five has a drift of 2.42 in. (6.15 cm) with the rest of the drifts being below 1.75 in. (4.45 cm). This violation is due to the fact that the level above these levels have an active displacement

while the level with the violated drift did not. The modal analysis has a maximum drift of 1.69 in. (4.29 cm) at the second level. These drifts in turn affect the stability factor, theta, as seen in Figure 50. There is a larger (relatively) change in the theta factors between levels nine and eight and between levels six and five which is due to these large drifts. The modal stability factors tend to provide a smooth transition from the tenth level to the second level. Neither design violates the 0.1 maximum value for the stability criteria. The drift and theta values would tend to substantiate the use of the modal analysis procedure for design along with the fact that it provides a lighter design. The unexpected result was that both analysis procedures provided similar stiffness distributions.

Observations:

1. Both analysis procedures provide similar stiffness distributions. This was not expected and contradicts the requirement of the ATC-03 provisions to use the modal analysis procedure for any vertically irregular structure.
2. The modal analysis procedure produces a lighter structure with less cycles.

3. The final sets of active constraints are quite different. The modal anlaysis produces a smaller set of active constraints as seen in Table XV.
4. The equivalent lateral force method has two drift violations. These both occur at levels where the displacement was not active but the next level displacement was active. The modal analysis procedure provides a maximum drift of 22% less than the maximum allowable drift.
5. These large drifts cause an irregularity in the stability factor distributions. Both analysis procedures provide stability factors below 0.02 which is 20% of the maximum allowable value, but the modal procedure provides a smooth distribution. Whereas, the equivalent lateral force procedure has a discontinuity at the levels of excessive drift.
6. The lesser weight (smaller sizes), the lower drifts, and the smooth stability factor curve tend to support the use of the modal analysis procedure. The use of less computational effort and the similarity in the final stiffness distributions tend to support the use of the equivalent lateral force technique even for vertically irregular structures.

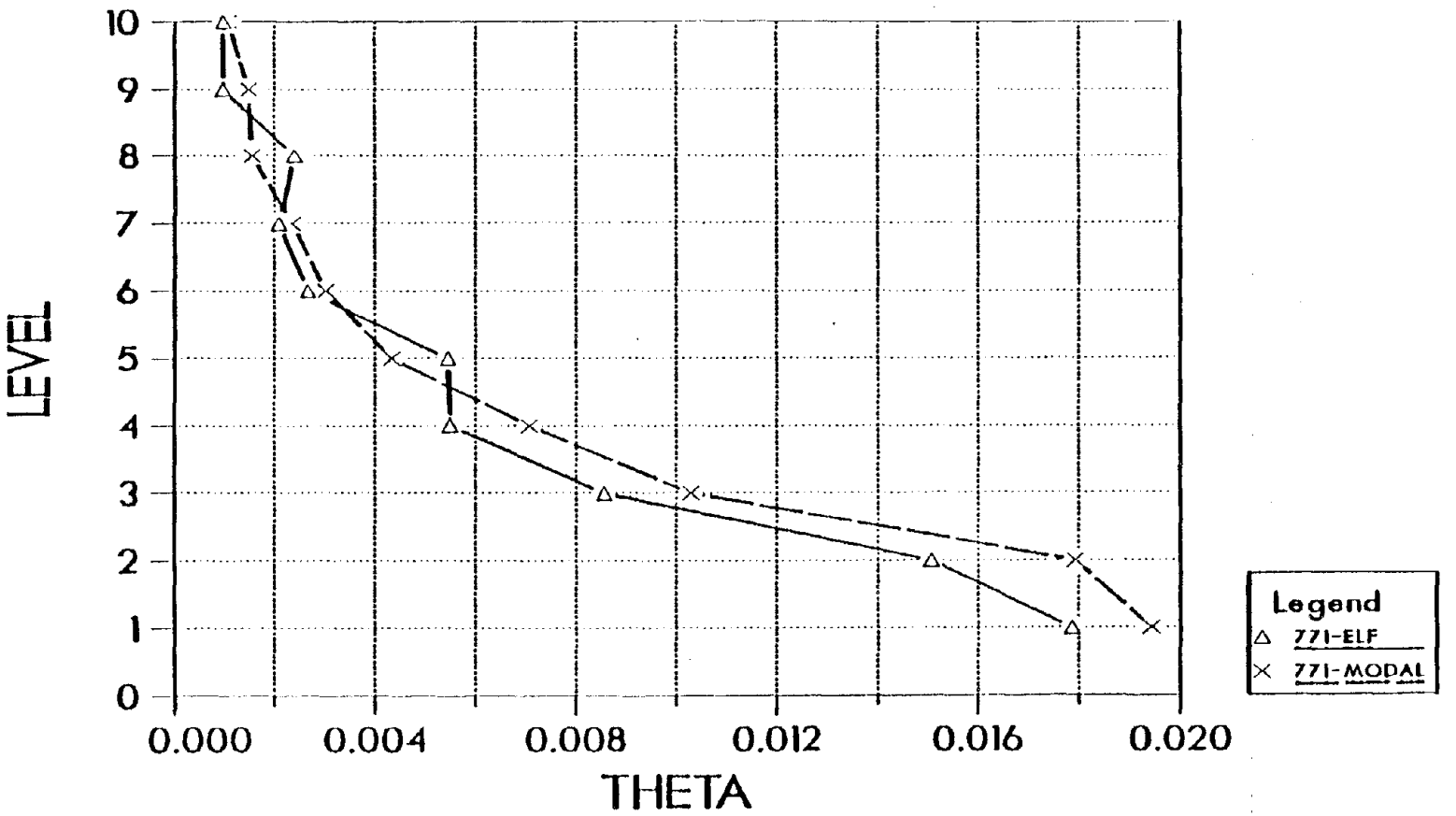

Figure 50. ATC-03 Stability Factors for the Ten Story Setback Structure Subjected to the ATC-03 Equivalent Lateral Forces and Modal Analysis

4. Linking of Multiple Levels Versus Linking of One Level. The effects of multiple story linking is to be discussed within this section. In order to provide continuity at the offset junctures linking of the columns and beam for several levels was considered. All of the columns on levels one to three were linked, all of the columns on levels four to six were linked, all of the columns on levels seven and eight were linked, and all of the columns on levels nine and ten were linked. A similar arrangement was used for the beams. Two extreme cases were considered. First map area 7 and then map area 4 for both the effective peak acceleration and effective peak velocity-related acceleration were used with soil condition 1. The ATC-03 modal analysis procedure was used. All other parameters are identical to those given in Section IX.F.1. Note this structure is subjected to lateral forces only.

The results for the multiple story linking and the single story linking structures are given in Table XVI and Figures 51 to 54. Within the legend, nolink refers to the single story linked case while link refers to the multi-story linking. From Table XVI, the percentage change in weight ranges from a 2.6 to 5.7 percent increase for the multi-story linked case which is relatively small. The ease of erection and detailing associated with the multi-story linking in a realistic situation could easily absorb

TABLE XVI. Results for Multiple Story Linking Versus Single Story Linking for the Setback Structure (1 kip = 4.45 kN)

	A_a^*	A_v^*	Init. Wt. (kip)	Final Wt. (kip)	% Difference	Period (sec)	Active Constraints Load 1**	Load 2**
Link	7	7	594.2	545.3	5.7	1.457	-	x_{10}-x_8, x_5***
No Link	7	7	594.2	515.8		1.477	-	x_{10}-x_8
Link	4	4	368.5	322.5	2.6	2.254	x_{10}-x_5	x_{10}-x_5
No Link	4	4	368.5	314.4		2.489	x_{10}-x_5	x_{10}-x_5

*Map Area Numbers

**Load 1 and Load 2 refer to the positive and negative 5% eccentricity in the y-direction, respectively.

***x_{10}-x_8, x_5 indicates that the x-displacements are active on the 8th through the 10th floors and on the 5th floor.

the cost of six percent of the total weight of steel. In addition to achieving a better distribution of stiffness as seen in Figure 52 and 53. The final weight comparisons are 545.3 kips (247.0 Mg) for the multi-story linking to 515.8 kips (233.7 Mg) for the single story linking for map area seven and 322.5 kips (146.1 Mg) for the multi-story linking compared to 314.4 kips (142.4 Mg) for the single story linking. In both cases the optimization of the multi-story linked case terminated with less optimization cycles than the single story linked case. This is to be expected due to the decrease in the number of design variables used to provide the same constrained response, and in the same vain this is the reason for larger weights. The active constraints for both sets of cases remain nearly the same except for the additional displacement constraint at the fifth level for map area 7. It would be reasonable to assume that the other five cases explored in Section IX.F.1 would provide solutions which would fit between the curves in Figure 51, and would have percentage changes within the range of 2.6 to 5.7 percent as long as several additional constraints did not become active.

Using multi-story linking improves the design considerably. The multi-story linking cases tend to average the single story linking results. For map area 7 it appears that the beams are on the high side of the average stiffness while the columns are slightly on the low side

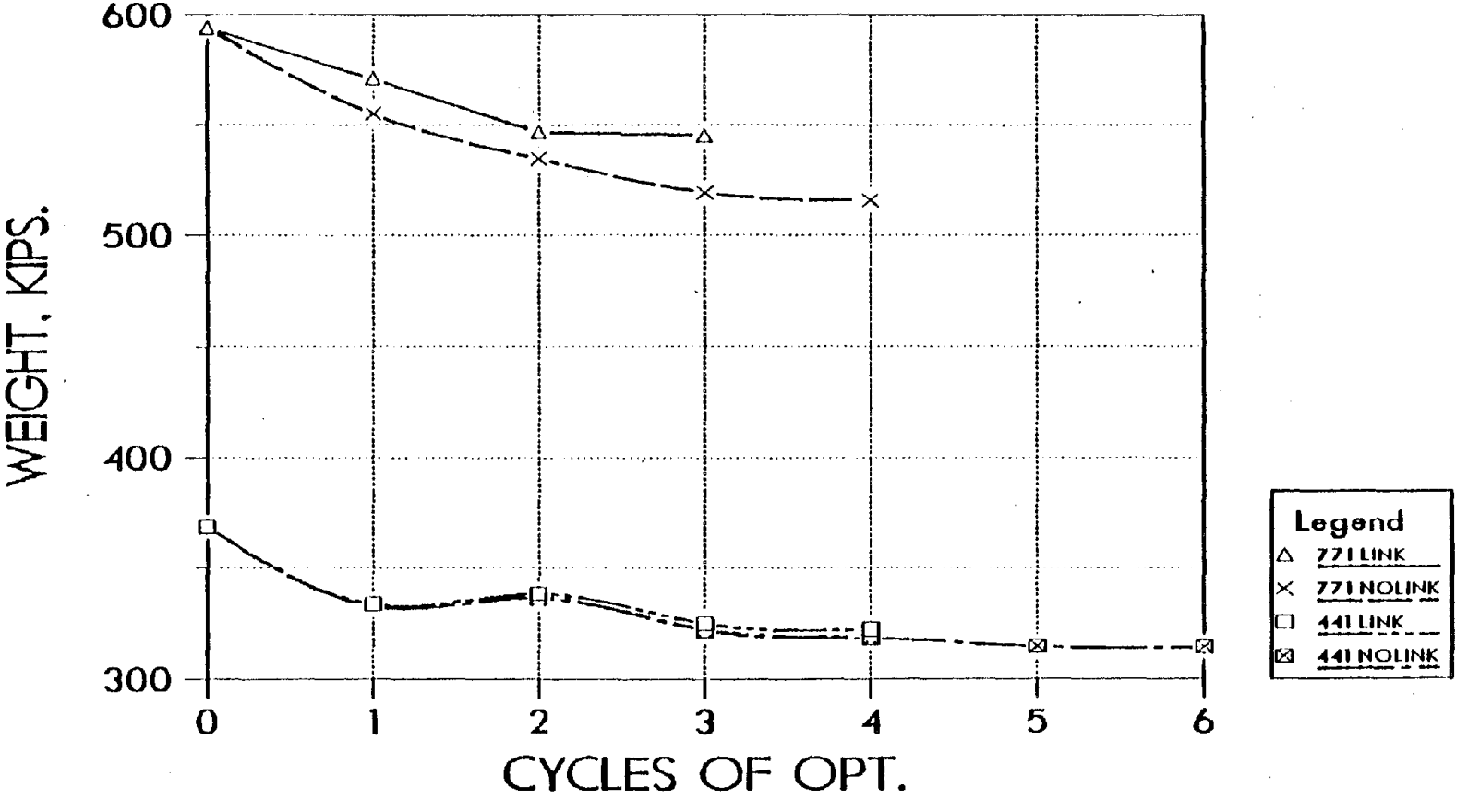

Figure 51. A Comparison of Weights for the Ten Story Setback Structure with and without Multiple Story Linking (1 kip = 4.45 kN)

except at the top two levels as compared to the single story linking. The results for map area 4 seem to be of similar nature. One of the main objectives was to eliminate the large changes in stiffness at the lower level of each setback which was accomplished as seen in Figures 52 and 53. Looking at these two figures, it appears that a possible linking would be to link the middle five levels (levels four to eight) with one design variable for the columns and one for the beams with little loss in terms of the optimal weight; and for map area 7 it appears that the first eight levels (one to eight) could have their columns linked without much loss. The upper levels still have a large reduction in stiffness which is due to the smaller total mass at the top and the fact that the optimization is forcing those upper level displacements to become active. It is important to notice the large reduction in the lowest level column moment of inertia. For map area 7 there is approximately a one third reduction in size, and for map area 4 there is approximately a one-half reduction in size. Both cases provide beam to column stiffness ratio's of approximately forty percent for all levels. This type of information would be useful for designers if an entire series of frames and possibilities were explored.

The drift and stability factors are slightly different. The maximum drifts for the multi-story linked cases are 1.77

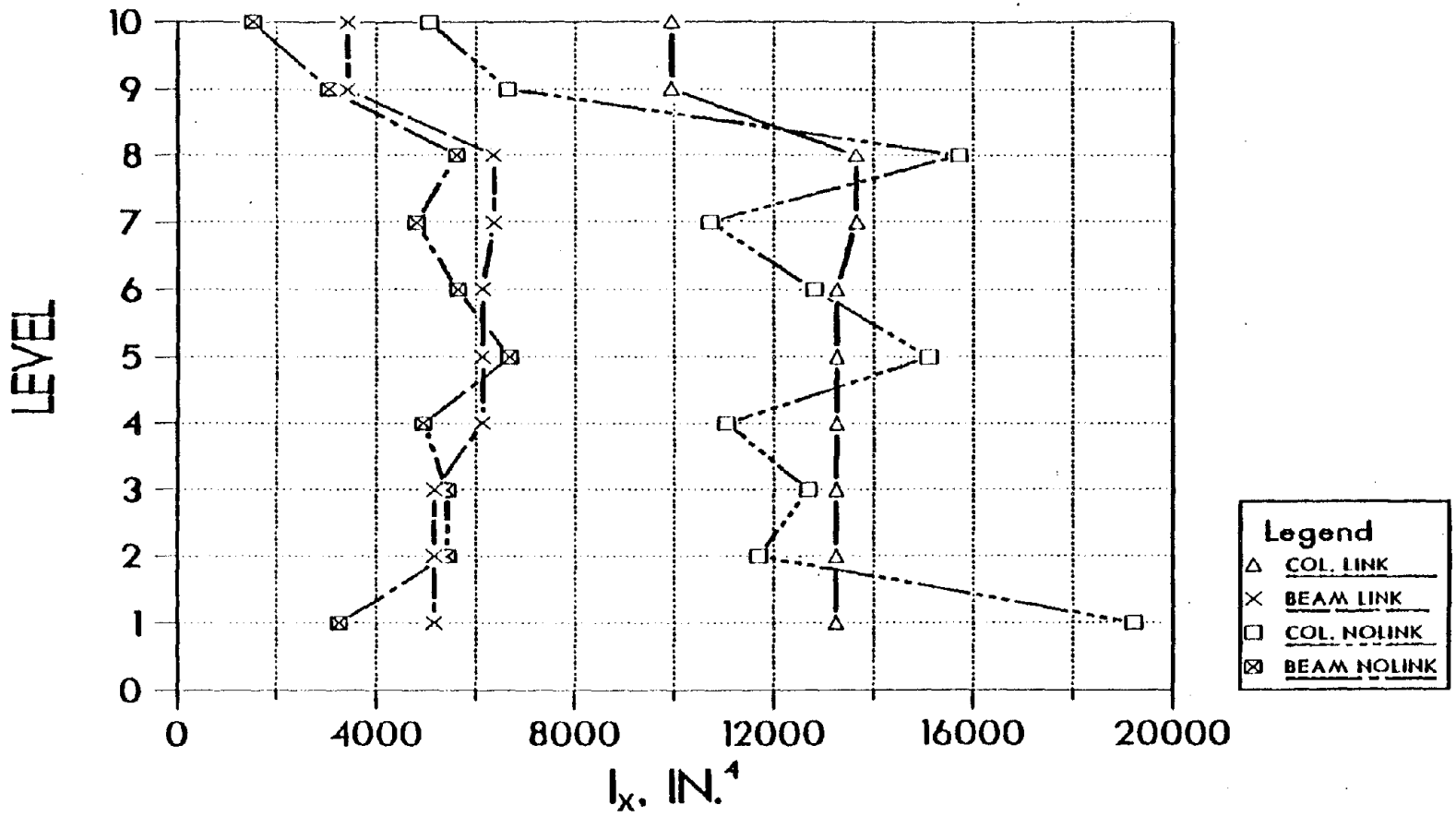

Figure 52. Column and Beam Stiffness Distributions for the Ten Story Setback Structure with and without Multiple Story Linking for ATC-03 Map Area Seven (1 in = 2.54 cm)

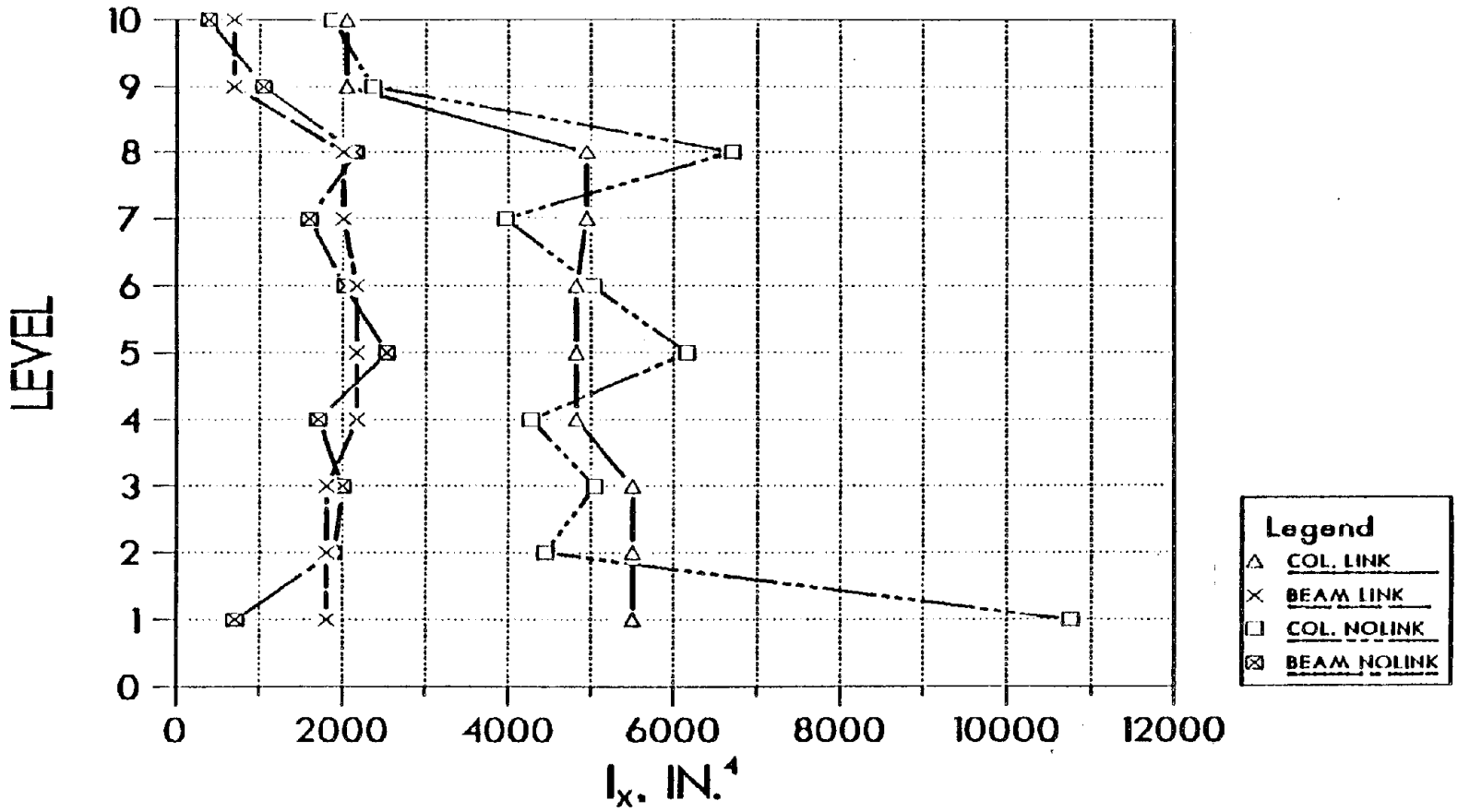

Figure 53. Column and Beam Stiffness Distributions for the Ten Story Setback Structure with and without Multiple Story Linking for ATC-03 Map Area Four (1 in = 2.54 cm)

in. (4.50 cm) and 1.47 in. (3.73 cm) for map areas 4 and 7, respectively, and the maximum drifts for the single story linked case are 1.79 in. (4.55 cm) and 1.69 in. (4.29 cm) for map areas 4 and 7, respectively. All values are well within the 2.16 in. (5.49 cm) allowable value. The maximum values decreased for each case when multiple story linking was used. This was not true for all levels. Map area 4 had some drifts smaller and some larger while map area 7 had nearly all drifts smaller for the multi-story linking case. The theta values (stability factors) for map area 4 tend to be similar but slightly larger for the multi-story linking, as seen in Figure 54. The maximum values are 0.058 and 0.049 for the multi-and single story cases, respectively. Most all of the theta values for map area 7 are smaller for the multi-story linking as seen in Figure 54. All theta values are well below the value of 0.1 specified by the ATC-03 provisions. Generally, this multi-story linking does not provide better response or enhance the resistance to drift or the stability factors, but it does provide a more realistic design. This type of optional design does not appear to cause any significant change in the optimal weight and generally leads to other design options. This might be a sequence used to develop a design. Use a single story linking or partial single story linking (only a few columns per floor instead of all columns) in order to find a preliminary design for the

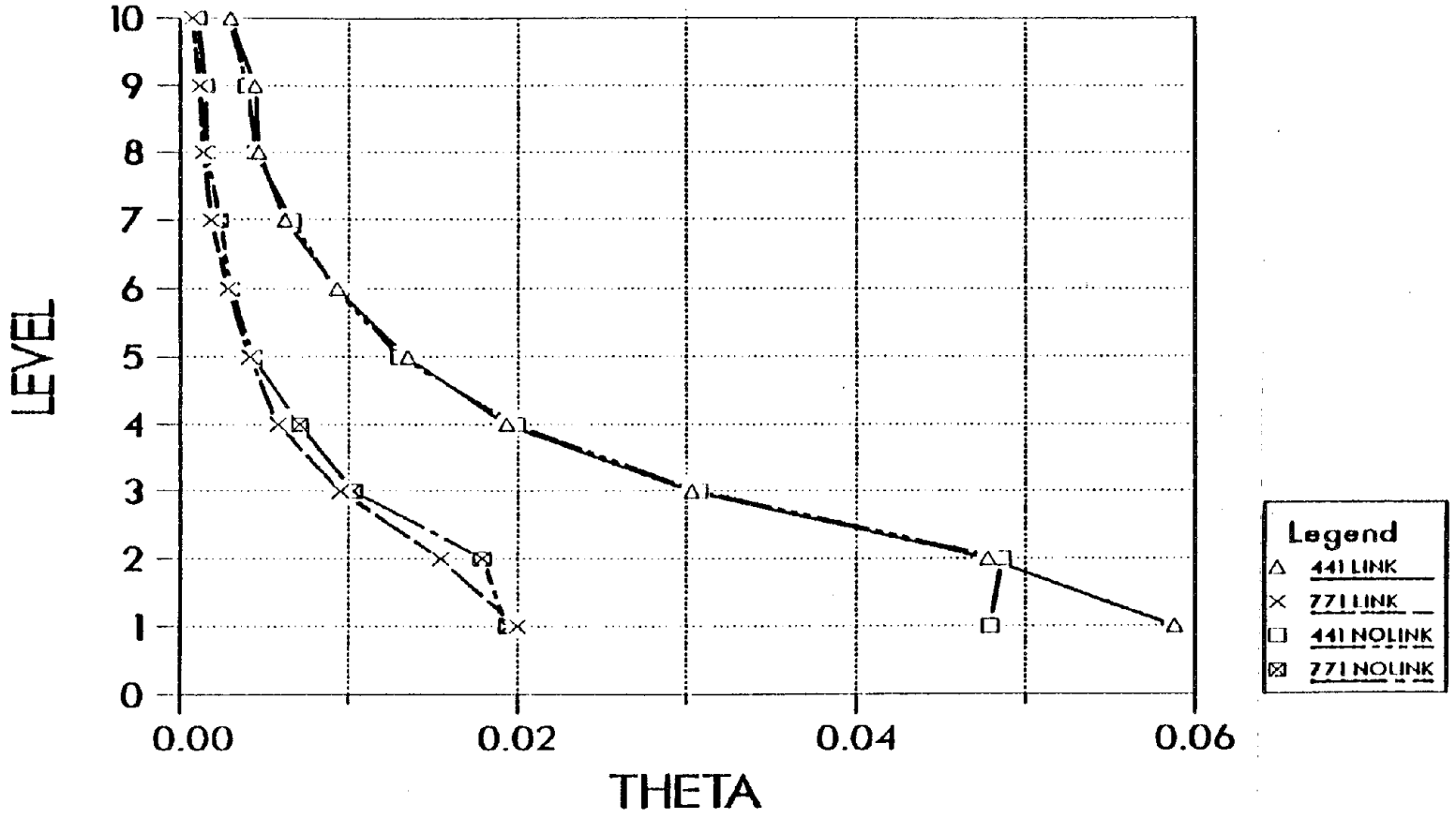

Figure 54. ATC-03 Stability Factors for the Ten Story Setback Structure with and without Multiple Story Linking

applied constraints and then to refine or try several linking combinations to provide a reasonable design.

Observations:

1. The effect of multi-story linking has little effect on the final optimal weight. The worst case produced a 6% increase over the single level linking case.
2. The multi-story linking case used less cycles in order to reach its optimal configuration. This is due to the reduction in design variables associated with the linking.
3. The multi-story linking produces an averaging effect with respect to the stiffness distributions as seen in Figures 51 and 52. It eliminates the large changes in stiffness associated with vertical irregularities.
4. Both cases have significant changes in stiffness at the two upper levels, but only moderate changes in the previous eight levels. This is due to the small amount of mass associated with the upper levels and the fact that the optimization is making these displacements active.
5. The multi-story linking also provides a much smaller column size at the base. This provides a more realistic base column size.
6. All drifts in both cases are well below the maximum value of 2.16 in. (5.49 cm). The multi-story linking

case provides smaller maximum drifts, but not necessarily smaller drifts at each level.

7. All stability factors are below 0.06 and the multi-story linking provides very similar stability factors to those produced by single story linking.

8. Multi-story linking does not create better solutions in terms of the objective, but it does provide a more realistic design in terms of stiffness distribution. The maximum increase of 6% due to multi-story linking could easily be absorbed into erection and fabrication cost reductions.

G. A COMPARISON OF ATC-03 ANALYSIS PROCEDURES FOR IRREGULAR STRUCTURES

1. Vertical Irregularities. A ten story regular plan structure, Figures 34 and 55, was used to test the effects of a stiffness irregularity with respect to the ATC-03 analysis procedures. As stated in Section IX.F, the ATC-03 prefers the use of the modal analysis procedure when the structure has plan or vertical irregularities. The vertical irregularities were introduced as taller stories within the structure in two story increments as shown in Figure 55. When discussing these different combinations and in the figure legends, the structures will be termed 12 modal or 12 ELF where (12 signifies the first and second levels) the numbers designate which

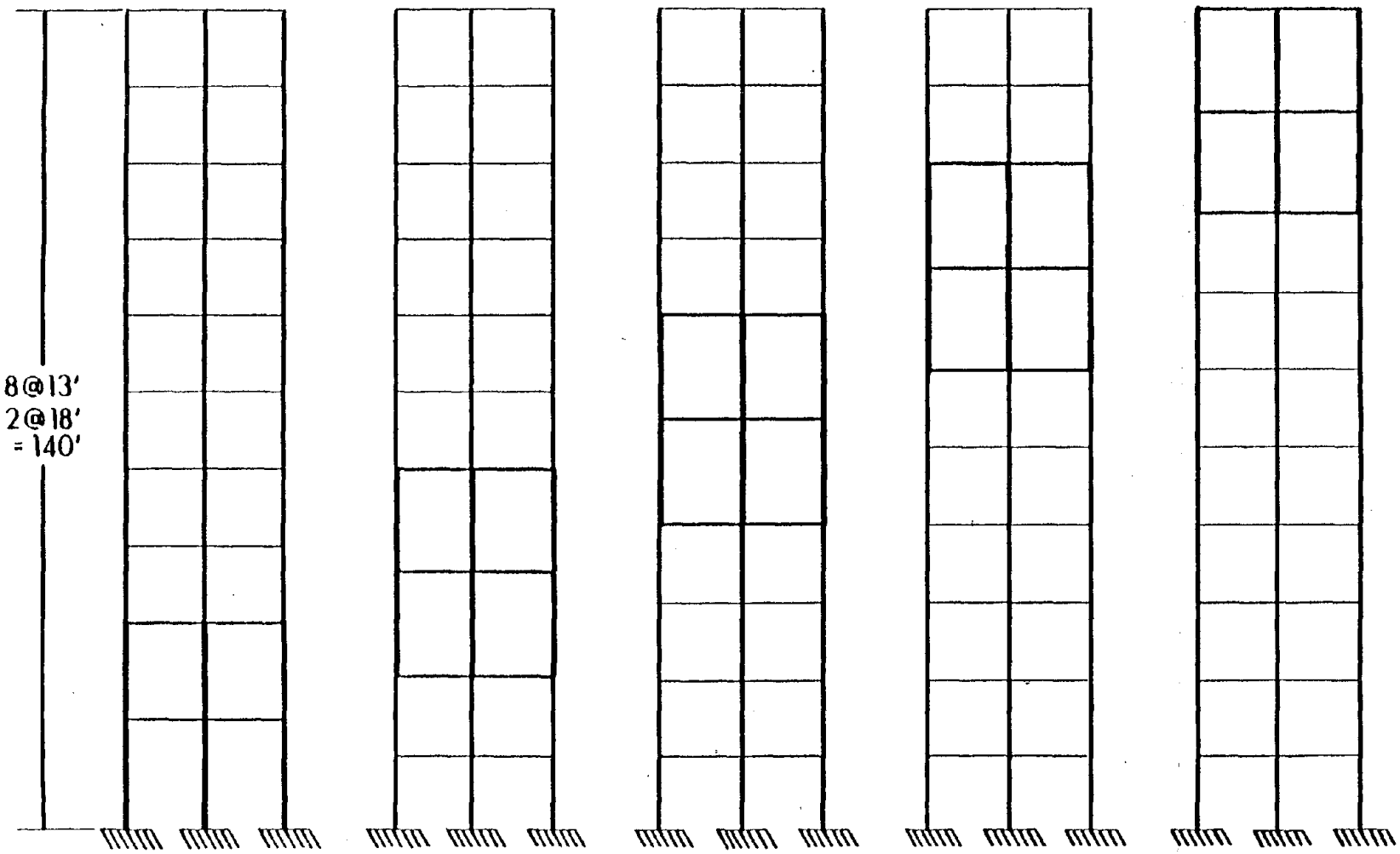

Figure 55. Elevations for the Ten Story Structure with Vertical Irregularities (1' = .305m)

levels, and modal or ELF represent the ATC-03 modal or equivalent lateral force approach, respectively. Normal story height consists of 13 feet (3.97 m), whereas, the tall story heights are 18 feet (5.49 m). Each level has a translational mass of 0.647 k-s^2/in. (113 Mg) and a rotational mass of 24,263 k-s^2-in. (2742 Mg-m^2). This mass was kept constant in order to eliminate any effects of an irregular mass distribution. Every element was considered to be a steel wide-flange section using Equations 3.15 to 3.29 representing the secondary to primary design variable relationships. Each level was linked such that all of the columns on a specific level were forced to have the same size and all of the beams on a specific level were forced to have the same size. The initial moment of inertia for all elements was 9500 in^4 (395,420 cm^4). Several of the structures required scaling during the initial optimization cycle which causes the structures to have different initial starting weights with respect to the optimization.

The optimization was performed using the two ATC-03 analysis provisions. Each structure was assumed to be within map area 6 for the effective peak acceleration and the effective peak velocity-related acceleration. They were also assumed to be within seismic performance category, C, with a response modification factor, R, of 4.50 and a deflection amplification factor, C_d, of 4.00. The soil condition was assumed to be stiff or soil

condition 1. The allowable drift for each level as determined from the ATC-03 provisions was 2.34 in. (5.94 cm) for the normal stories and 3.24 in. (8.23 cm) for the tall stories. Within the modal analysis procedure, four modes were used. The primary direction for the loads are in the x-direction with the required 30 percent of the total y-direction load applied in the y-direction. The ATC-03 requires two load cases, the first load case has a 5 percent eccentricity in the negative y-direction and the second has a 5 percent eccentricity in the positive y-direction. Only the lateral forces were considered. Since the building is forced to be plan symmetric these 5 percent eccentricities actually represent a symmetric loading with respect to the optimization and could have been represented with one loading case. This would save computer space and effort. This would not be true if the plan geometry was not symmetric and the linking scheme was not symmetric.

The optimization was controlled by a set of constant parameters. Termination of the optimization was to take place at the end of 25 optimization cycles, 30 analyses, or less than a 0.5 percent change in weight between optimization cycles. A convergence control parameter of 2 was used. Displacement constraints were 0.300 in. (0.762 cm) for the first level and 0.580 in. (1.47 cm) per floor above the first level with a lower range of ten

percent and an upper range of five percent for active constraint determination. This could be considered inconsistent with the drift requirements set by the ATC-03 which allowed the taller stories to have a larger relative displacement with respect to its upper and lower nodes. This linear relationship was used since a drift constraint was not a viable option. If these tall stories were allowed a larger displacement constraint the story above these would likely violate their ATC-03 drifts. It would be similar to the reasoning presented for decreasing the allowable first level displacement constraint. The story directly above the taller stories would stiffen in order to prevent a large rigid body deflection of the upper floors, and the next stories above that would become quite flexible with a good possibility of violating their ATC-03 drifts. Therefore, the linear displacement constraints (above the first level) were used, but were the same for all of the problems.

The results are presented in Table XVII and Figures 56 to 67. Figure 57 shows that for the equivalent lateral force method the solutions are converging to nearly identical weights. The weights are within a range of approximately 8.0 kips (3.6 Mg) or 3.5% difference from the lowest to highest weight. Even though the weights are nearly identical, the sets of active constraints are not. The table is somewhat of a misnomer in that the missing

TABLE XVII. Results for Vertical Irregularities within the Stiffness of a Ten Story Structure (1 in = 2.54 cm, 1 kip = 4.45 kN)

I.D.	Initial Weight (kips)	Final Weight (kips)	Active Constraints (in)
12E	406.0	220.2	$x_{10}-x_4$ *
34E	318.9	226.2	$x_{10}-x_3$
56E	291.2	226.6	$x_{10}-x_5$
78E	271.6	224.6	$x_{10}-x_5$
910E	275.7	218.3	$x_{10}-x_1$
12M	384.5	206.5	$x_{10}-x_1$
34M	295.3	209.6	$x_{10}-x_4$
56M	263.9	206.8	$x_{10}-x_5$
78M	254.2	205.4	$x_{10}-x_7$, x_5-x_4
910M	254.2	198.5	$x_{10}-x_1$

*$x_{10}-x_4$ indicates that the x-displacements on the 4th through the 10th floors are active.

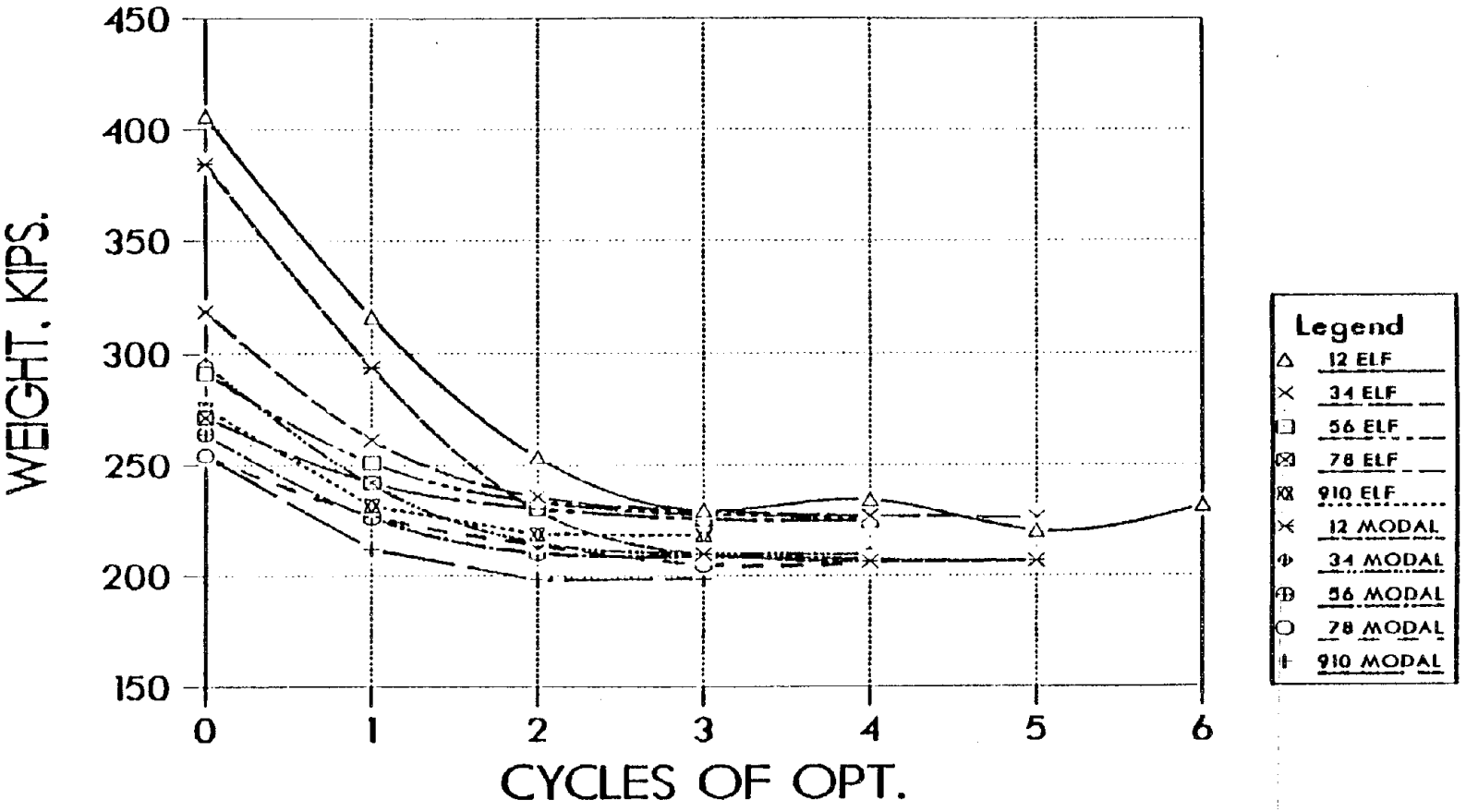

Figure 56. A Comparison of Weights for the Ten Story Structures with Vertical Irregularities (1 kip = 4.45 kN)

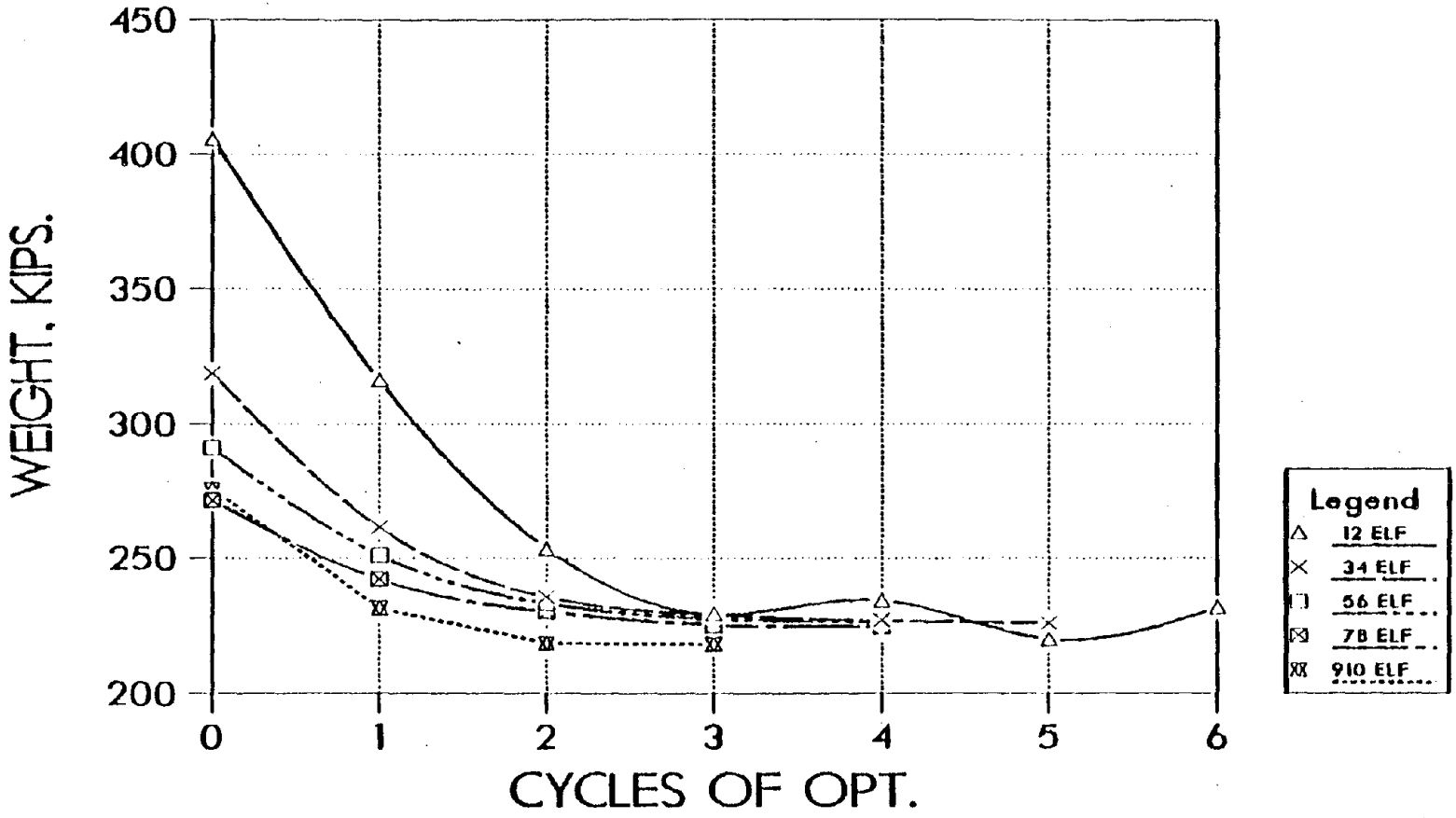

Figure 57. A Comparison of Weights for the Vertically Irregular Ten Story Structures Subjected to the ATC-03 Equivalent Lateral Force Loading (1 kip = 4.45 kN)

constraint possibilities are very close to the active values (Most are within fifteen percent of the constraint value). A similar trend for the modal analysis is seen in Figure 58. The final solutions have a range of approximately 11.0 kips (4.98 Mg) or approximately 5.0 percent of the largest weight. The lowest weight for both types of analysis occur when the taller stories are located at levels 9 and 10. The largest weights occur when the taller stories are located within the middle floors; levels 3 and 4 for the modal analysis and levels 5 and 6 for the equivalent lateral force approach. Note that the weight for the equivalent lateral force with the taller stories at 3 and 4 is only slightly lower than the largest weight for levels 5 and 6. This trend was expected due to the fixed base. The fixed base helps to provide rigidity to level 1 when the taller stories are at levels 1 and 2, therefore allowing the weight to decrease below that when the taller stories are within the middle levels. In theory, levels 3 and 4 should produce the largest weight, but numerically it is not so. In the same fashion, it was expected that when the taller stories were located at levels 9 and 10 the lowest weight would be found. This is due to the fact that the tall stories would not affect any displacements except those at levels 9 and 10, allowing the lower levels to use their shorter story heights to resist their displacements. If the two extreme cases were

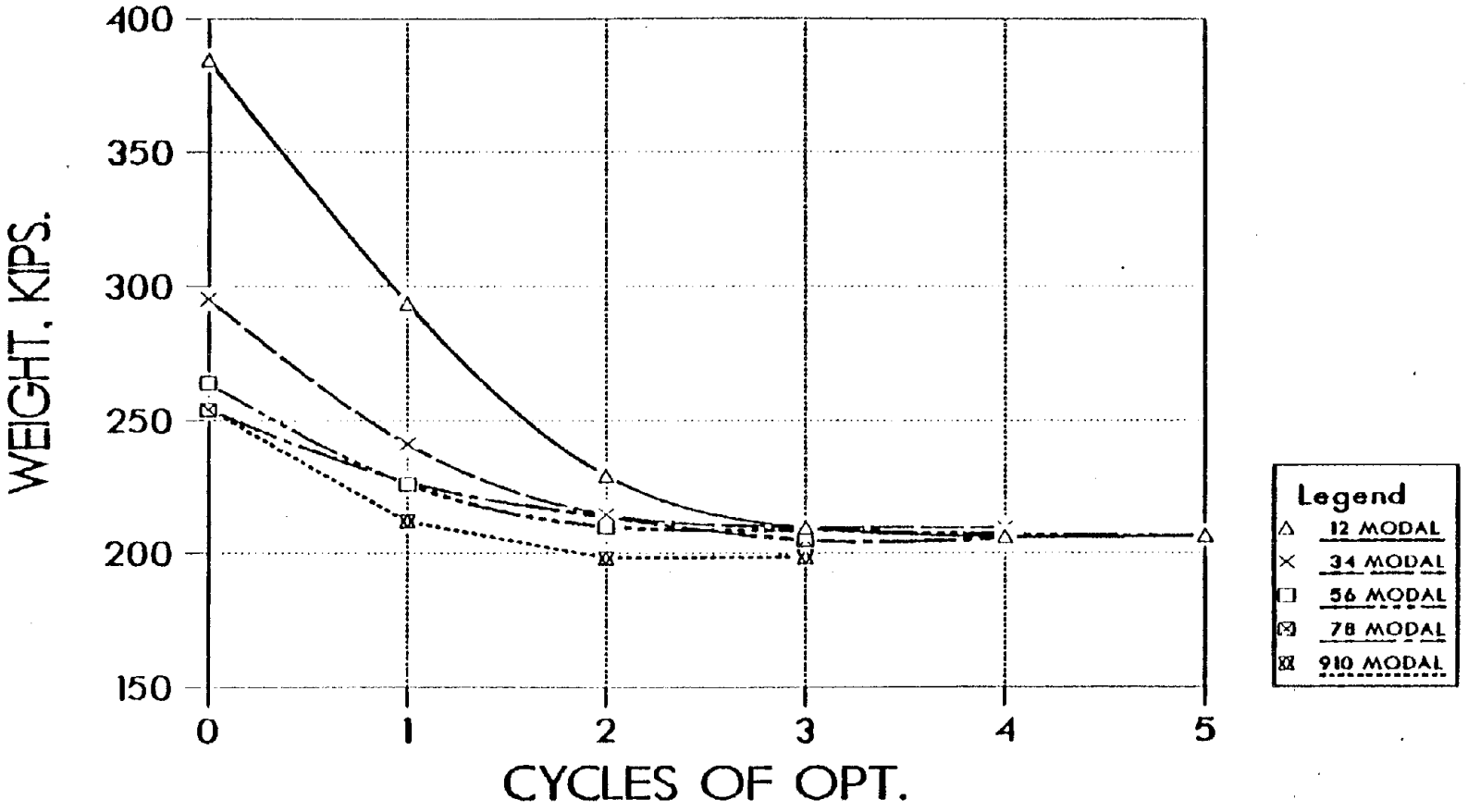

Figure 58. A Comparison of Weights for the Vertically Irregular Ten Story Structures Subjected to the ATC-03 Modal Analysis Procedures (1 kip = 4.45 kN)

excluded, the range of resulting weights would be 2.0 kips (0.91 Mg) for the equivalent lateral force analysis and 4.2 kips (1.90 Mg) for the modal analysis showing the trend to converge to a specific weight to be even stronger than originally expected. Figure 56 shows the weights for both types of analysis superimposed. Note the two distinct regions of convergence with modal analysis providing the smaller weights. These ideas can be seen with respect to the stiffness distributions.

The distribution of stiffness is not radically different as the ATC-03 provisions would lead one to believe. From Figures 59 to 64, the stiffness distributions for the columns and beams based on equivalent lateral force and modal analysis are nearly identical with the exception of the maximum values for the moments of inertia. Every case requires a large increase in column moments of inertia at the two levels where the taller stories are located, as shown in Figures 60 and 61, which was expected. The first being the reduction in stiffness due to the additional height, and secondly, the linear constraint distribution ignores the fact that the ATC-03 allows a slightly larger drift for these taller stories. Both cases tend to form an envelope of column sizes if the case where levels 1 and 2 have the taller columns is not considered. The levels above the irregularities all tend to follow similar paths along a lower boundary of column size from

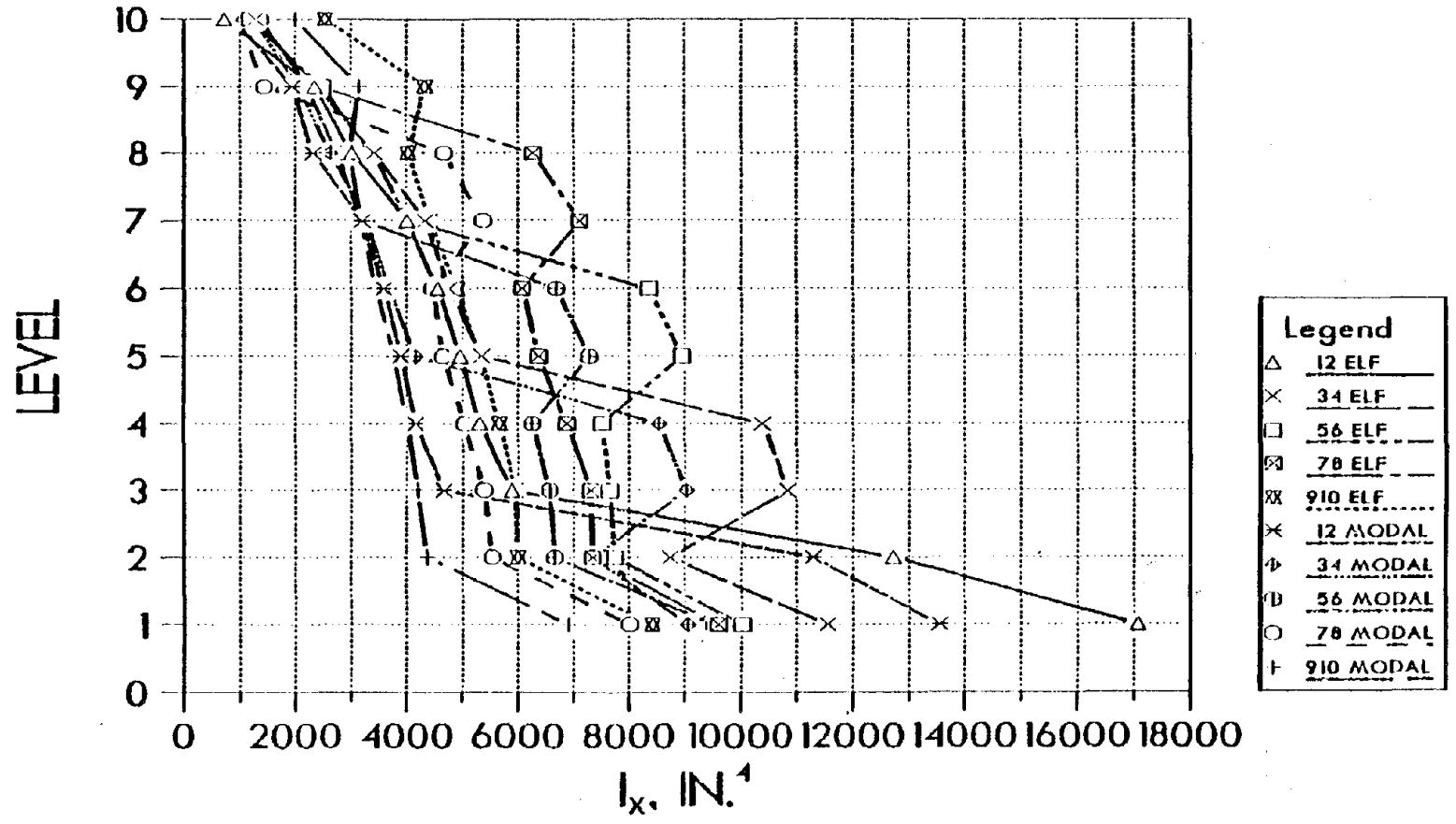

Figure 59. Column Stiffness Distributions for the Vertically Irregular Ten Story Structures (1 in = 2.54 cm)

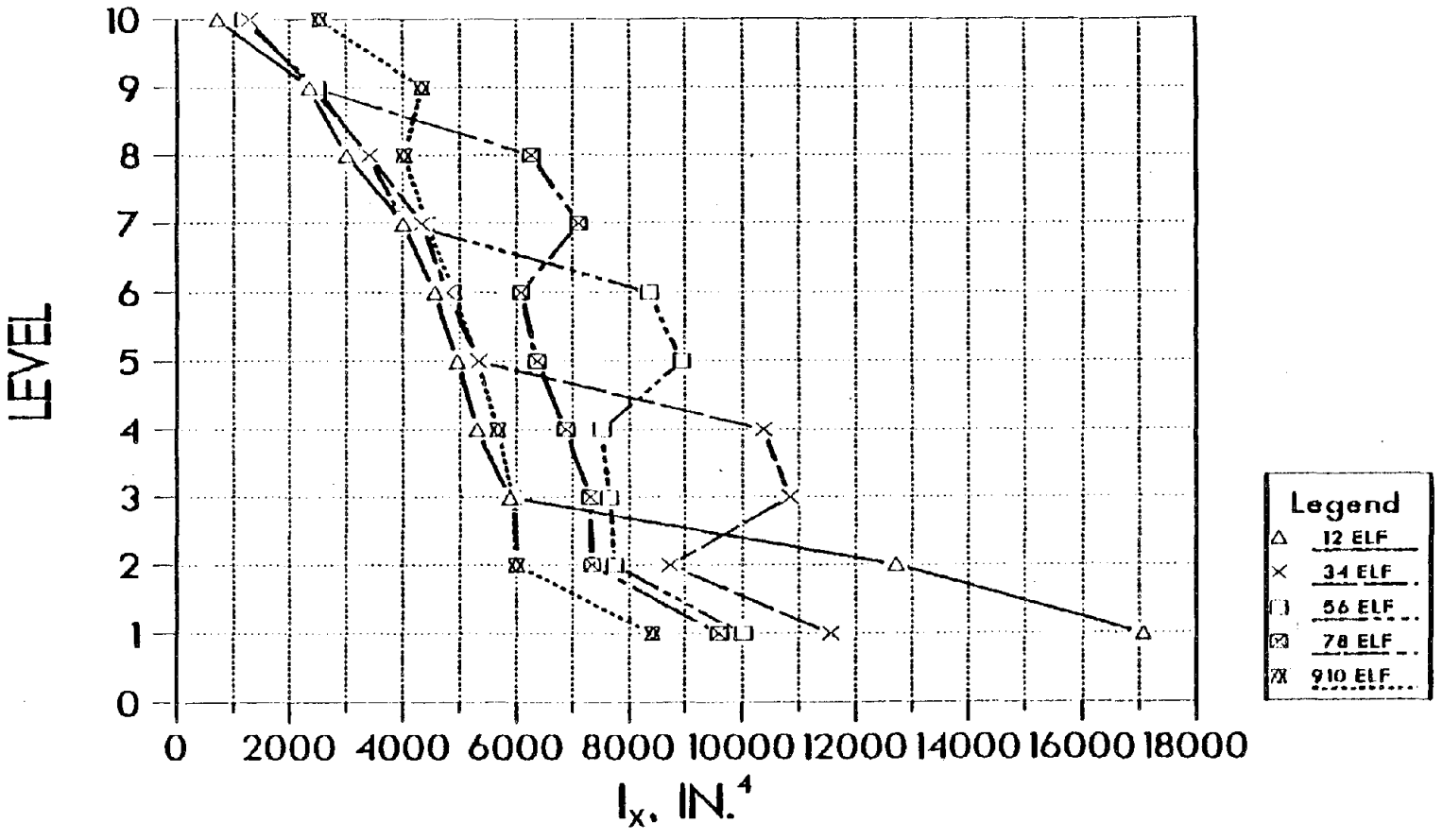

Figure 60. Column Stiffness Distributions for the Vertically Irregular Ten Story Structures Subjected to the ATC-03 Equivalent Lateral Force Loading (1 in = 2.54 cm)

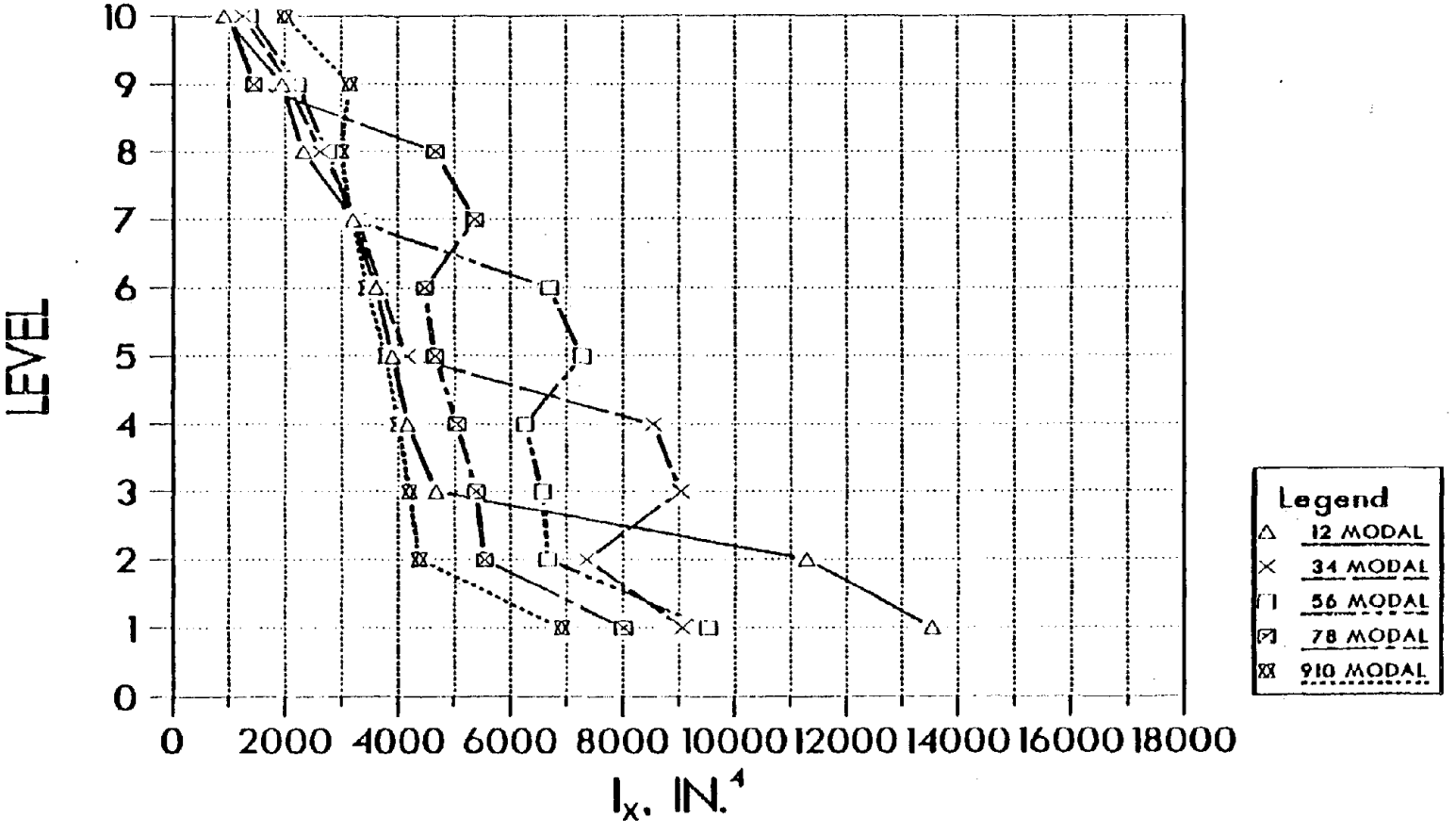

Figure 61. Column Stiffness Distributions for the Vertically Irregular Ten Story Structures Subjected to the ATC-03 Modal Analysis Procedure (1 in = 2.54 cm)

the top to the irregularity at which time a large increase in column size is required. This increase becomes larger as the irregularity moves down the structure. These moments of inertia at the stories appear to form an upper limit or envelope as long as the first level columns are not included. It is also interesting to note that below the vertical irregularity the column sizes seem to parallel the minimum size envelope. In fact, when the vertical irregularity is at levels 9 and 10, the lower level sizes lie along that lower limit. Figures 63 and 64 provide similar results for the beams in that two enveloping curves could be generated as an upper and lower limit for beam sizes. Above the irregularities the beam sizes lie along a relatively fixed curve, and below the irregularities they tend to have similar distributions. This trend is more regular for the equivalent lateral force approach than for the modal analysis. The change in beam size is nearly linear over the two irregularities, whereas the columns jumped to a large value for the upper level of the irregular stories and had only a slight change for the lower level of the irregularity. This shows the importance of the columns to the resistance of the prescribed displacements. As seen in most all of the examples, a strong column-weak beam design is found through the optimization, and the first level beam is smaller than the second level beam except for the case

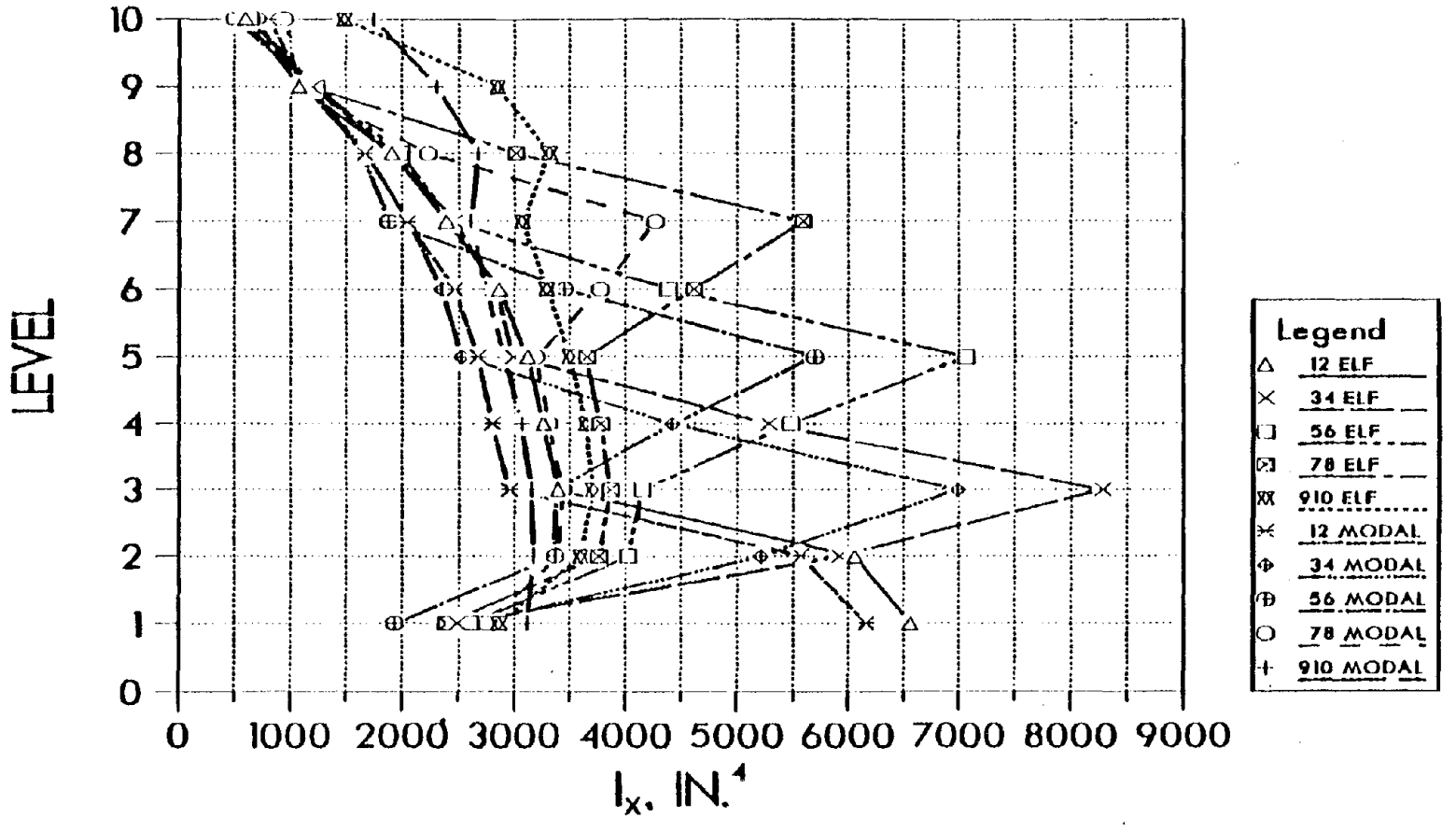

Figure 62. Beam Stiffness Distributions for the Vertically Irregular Ten Story Structure (1 in = 2.54 cm)

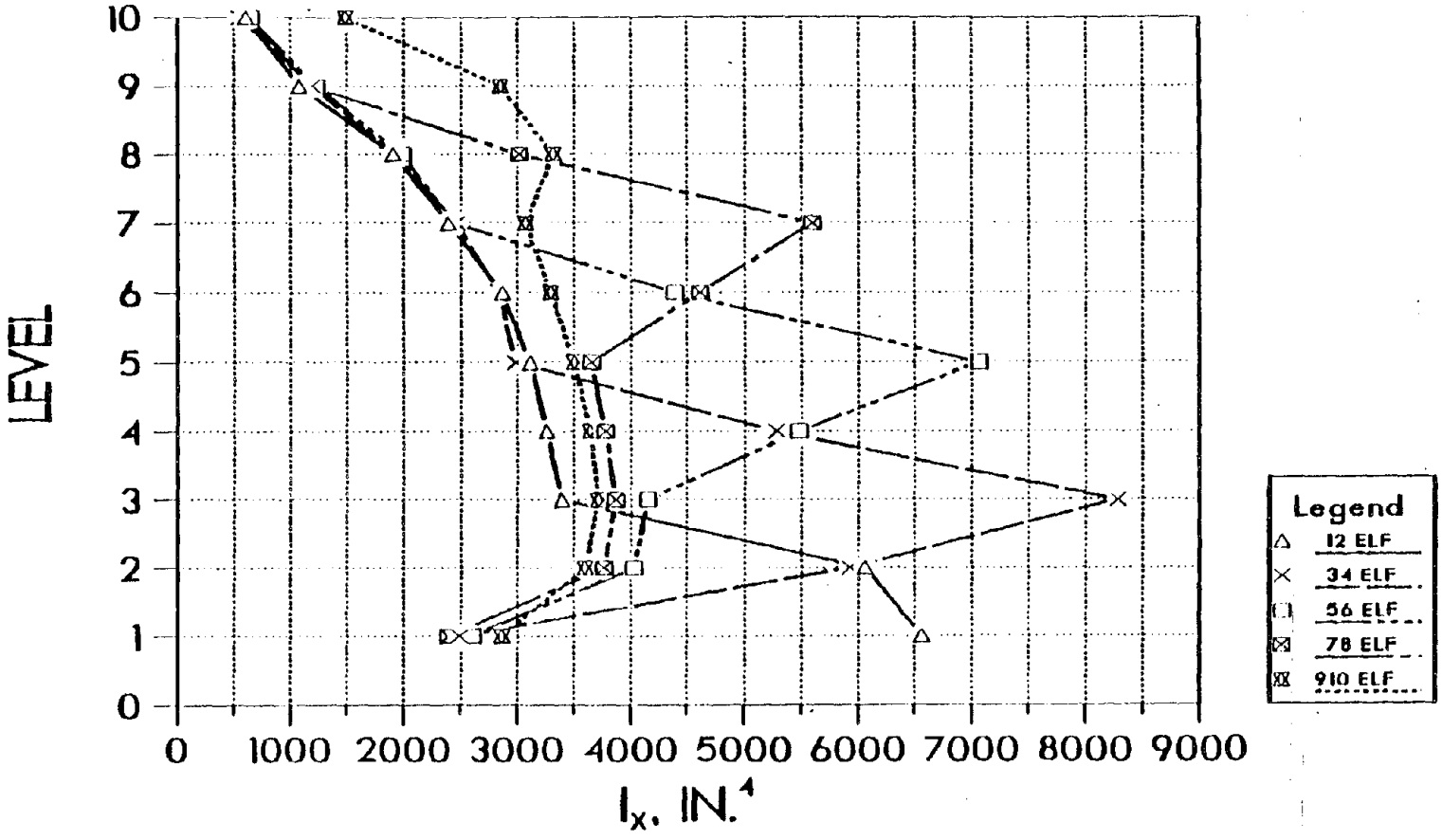

Figure 63. Beam Stiffness Distributions for the Vertically Irregular Ten Story Structures Subjected to the ATC-03 Equivalent Lateral Force Loading (1 in = 2.54 cm)

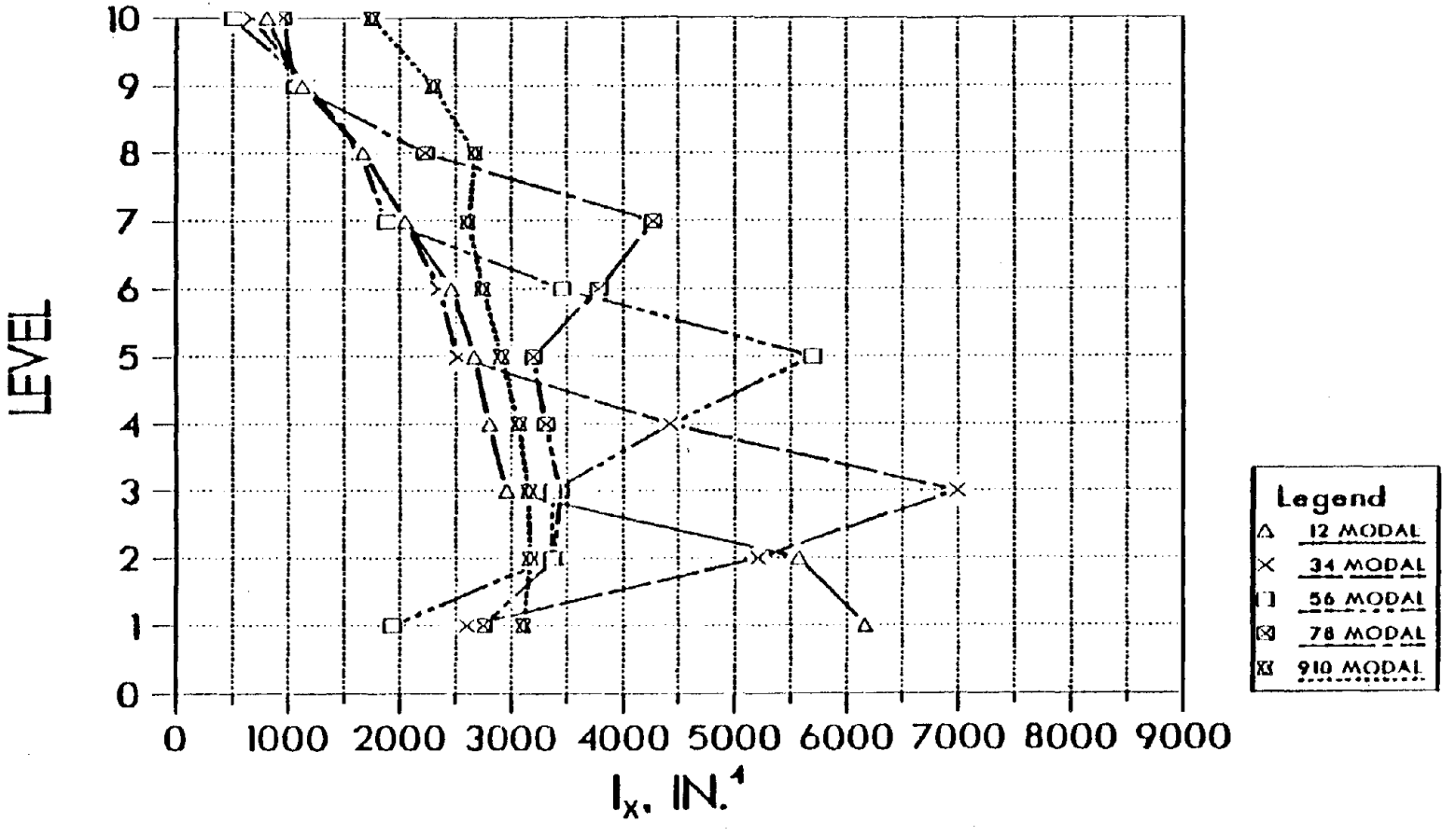

Figure 64. Beam Stiffness Distributions for the Vertically Irregular Ten Story Structures Subjected to the ATC-03 Modal Analysis Procedure (1 in = 2.54 cm)

where the taller stories are at the base. Due to the fixity, the beams for this case do not reach a value which would be along the envelope described previously. Figures 59 and 62 superimpose the equivalent lateral force and modal analysis results. By choosing the two curves representing the same irregularity with different analyses, these figures show that the results are nearly identical in distribution. The major differences occurs only in magnitude.

The last comparison to be made is shown in Figures 66 and 67 which represent the stability factors from the ATC-03 provisions. Both figures are very similar. The stability factors increase at the levels of irregularities and follow similar paths above the irregularities and have the same general shapes after the irregularities. This is a very general statement which must be considered most appropriate for those cases where the irregularities are in the middle levels. The major difference comes in numerical values again. The equivalent lateral force method produced stiffer, heavier structures which in effect caused a reduction in the P-delta effect, therefore, the stability factors are lower. Both sets of results provide theta values well below the 0.1 limit set by the ATC-03 provisions.

The curves presented all show similar trends for both sets of analyses. Above the irregularities the

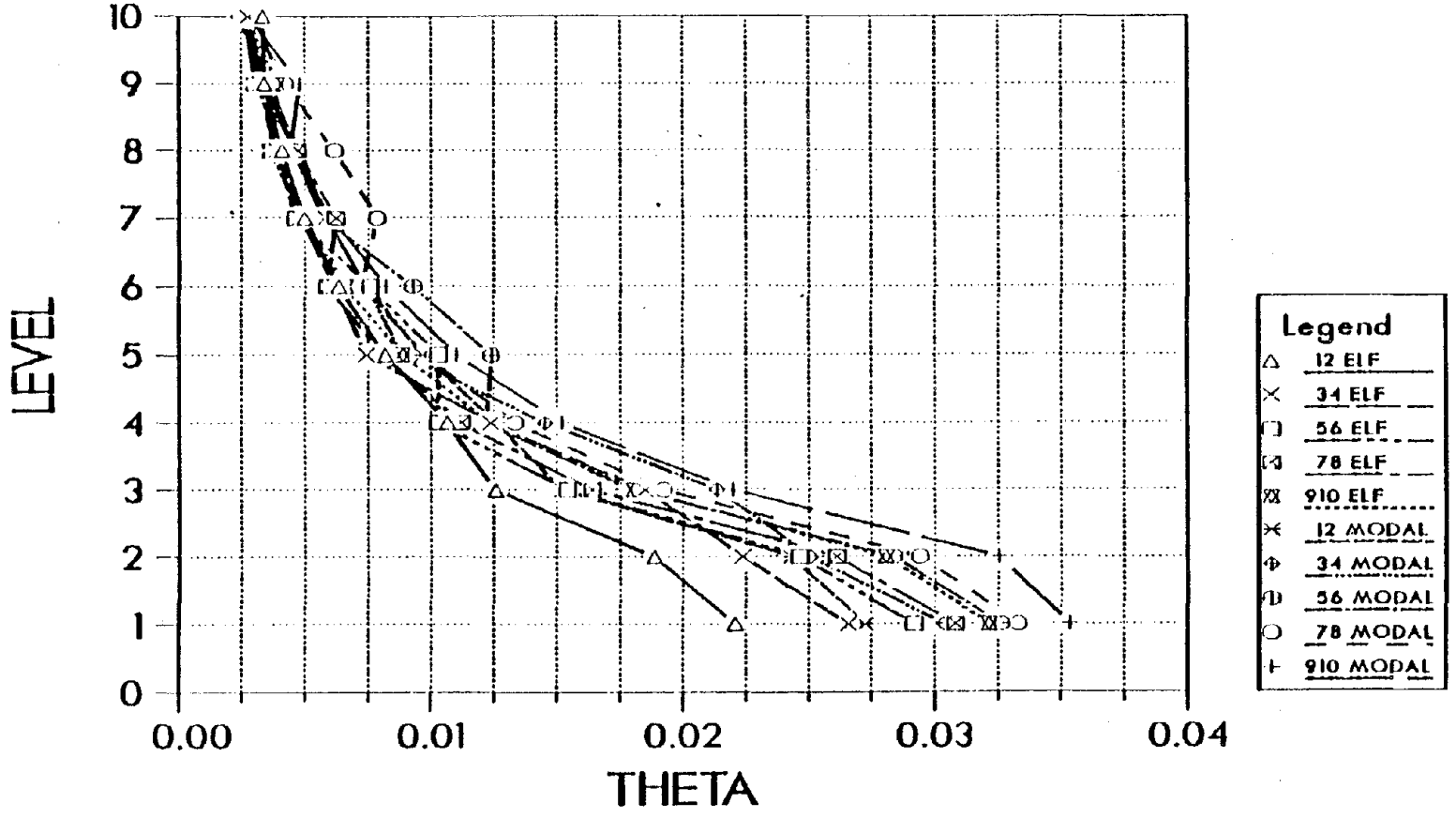

Figure 65. ATC-03 Stability Factors for the Vertically Irregular Ten Story Structures

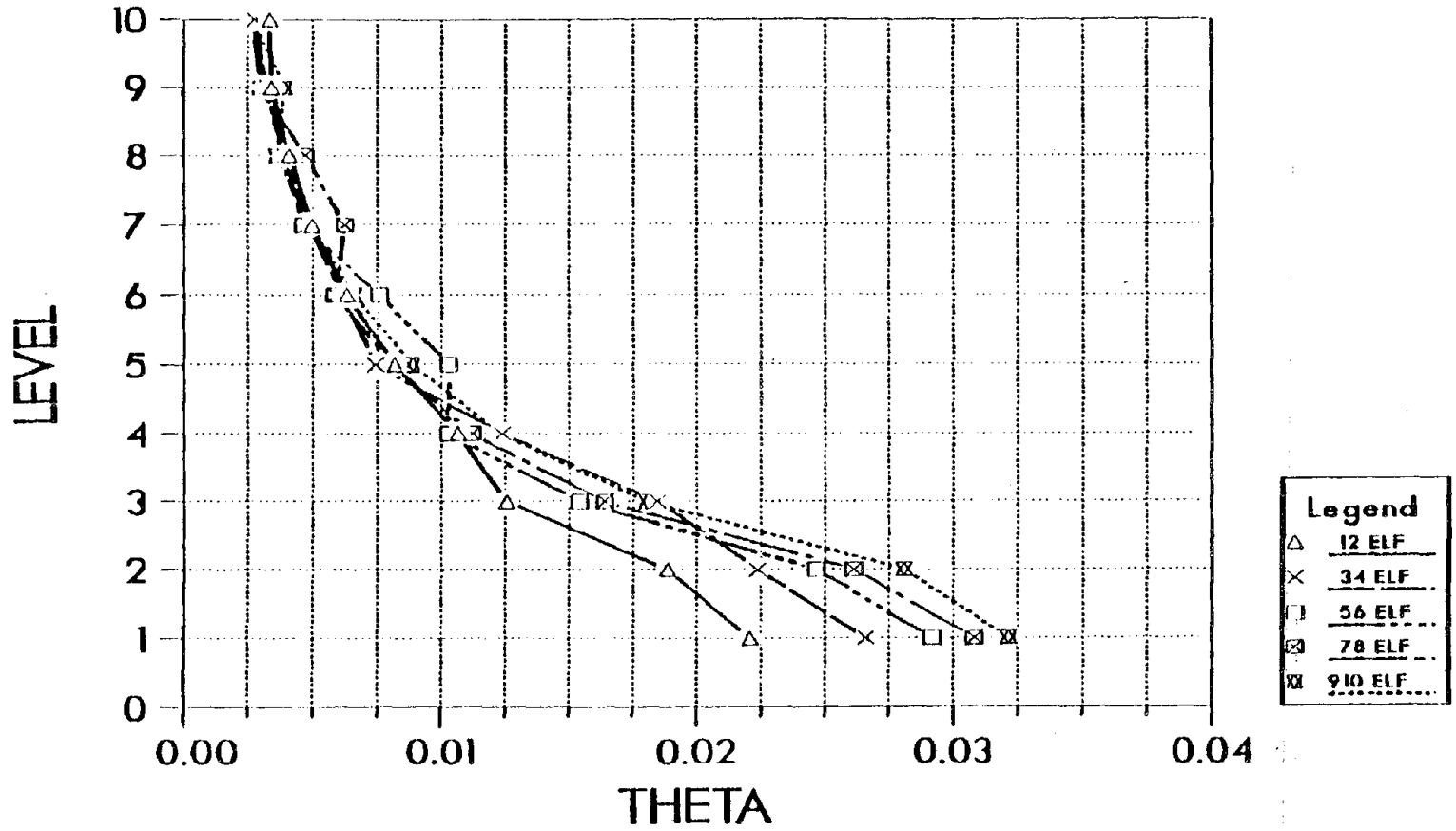

Figure 66. ATC-03 Stability Factors for the Vertically Irregular Ten Story Structures Subjected to the ATC-03 Equivalent Lateral Force Loading

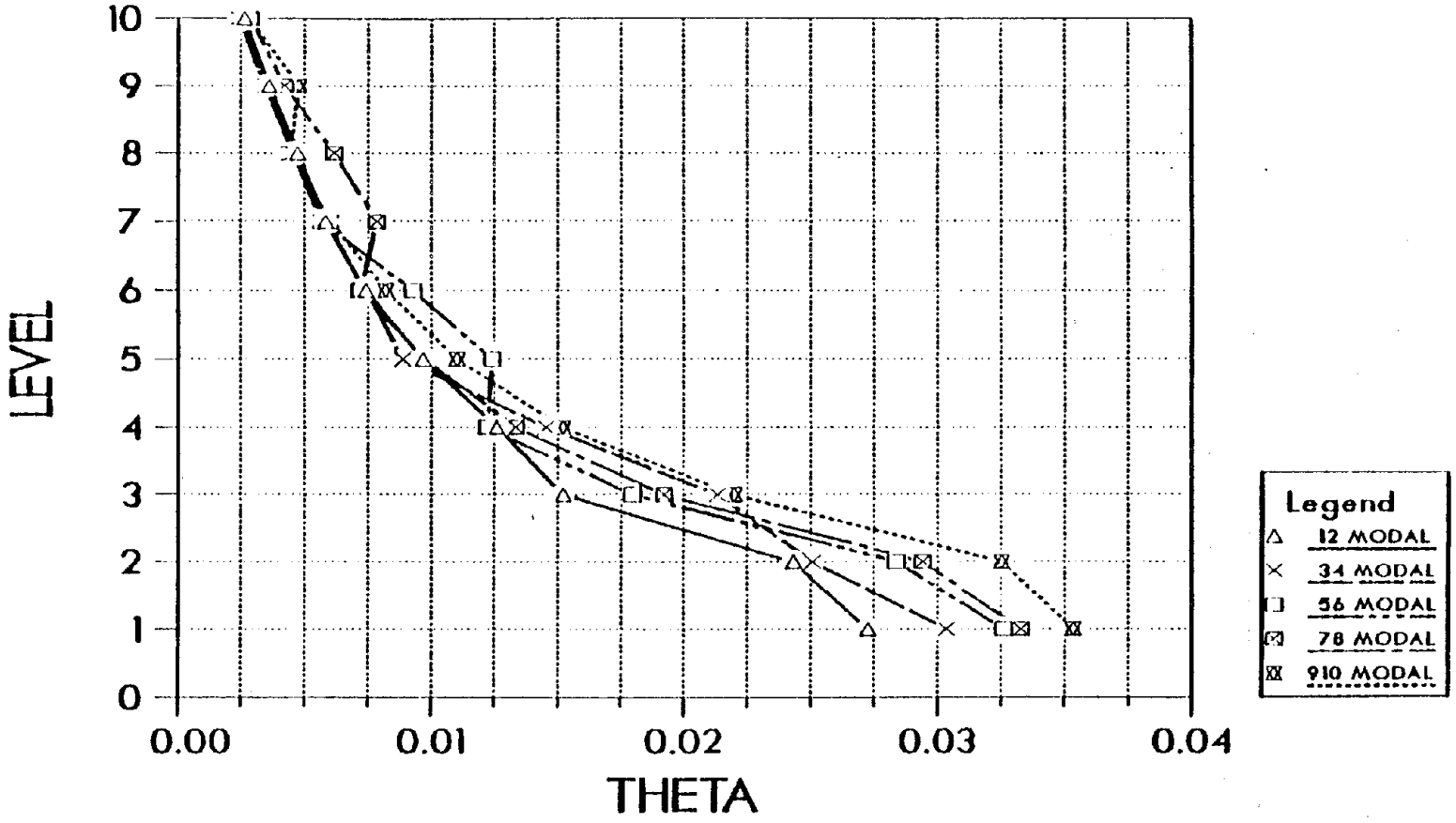

Figure 67. ATC-03 Stability Factors for the Vertically Irregular Ten Story Structures Subjected to the ATC-03 Modal Analysis Procedure

curves tend to lump together, at the irregularity an increase in sizes takes place, and below the irregularity parallel curves are generated. This points to the fact that the irregularity tends to affect only that local area of the optimal structure. The irregularity has very little effect on the distribution of the stiffness above it as long as those constraints are active. With these constraints active the optimization is essentially controlling the drift which is almost totally element (column) dependent. A similar statement could be made for the sizes below the irregularity as the increase or decrease in stiffness for a specific level is nearly identical for each case. Showing the need for only enough stiffness to stop its own drift with a small amount of stiffness added due to the additional height of the forces from the taller stories. These types of observations could possibly lead to the use of optimization in a piecewise fashion. In order to achieve this goal, it would require many additional cases to provide more conclusive evidence coupled with a more theoretical exploration. If this structure were taller or the two level irregularity were placed at the missed sequence of levels (i.e. six and seven, etc), it would be expected that the results would fill the gaps on the curves and form the maximum envelope of the stiffness as described.

Observations:

1. The stiffness distributions for the equivalent lateral force procedure are nearly identical to those of the modal analysis procedure. Although the magnitudes are different the trends are the same. As with the previous example, the equivalent lateral force produces heavier but similar structures with less computational effort. The similar stiffness distributions for the two analysis techniques contradicts the ATC-03 statement to use the modal analysis technique for this structure with vertical irregularities. This area could be studied in greater detail.
2. The beam and column stiffnesses are bounded by an envelope which consists of a lower bound determined by the stiffness distribution generated with the vertical irregularities at levels 1 and 2 and an upper limit which can be formed by connecting the stiffness of the taller stories as they progress through the building. This can be seen in Figures 58 to 63.
3. Each case requires a relatively large increase in stiffness within the taller stories. The beams tend to increase linearly to a large beam stiffness at the lowest story of the irregularities, whereas, the columns tend to have a large change in stiffness at both levels of discontinuity with relatively small change between these levels.

4. It is important to note that this type of vertical irregularity affects only that local area within the structure. Above and below the tall stories the stiffness distributions continue along nearly parallel paths.

5. Regardless of where the vertical irregularities are located the optimal solutions provide nearly identical optimal weights. The equivalent lateral force procedure has a range of 3.5 percent while the modal analysis procedure has a range of 5.0 percent.

6. The stability factors are all below 0.04 and have very similar distributions for the two analysis procedures. The stability factors are discontinuous at the levels which have the taller stories. This discontinuity is very mild.

7. The lightest structures are found when the vertical irregularities occur at levels 9 and 10 in both cases. Whereas, the heaviest structures are found when the irregular heights are located at levels 3 and 4 for the modal analysis and levels 5 and 6 for the equivalent lateral force procedure.

2. Plan Irregularities. A five story, irregular plan steel structure, as shown in Figure 68, was used to test the effects of a planar irregularity with respect to the ATC-03 analysis procedures. The ATC-03 provisions prefer the use of the modal procedure when the structure

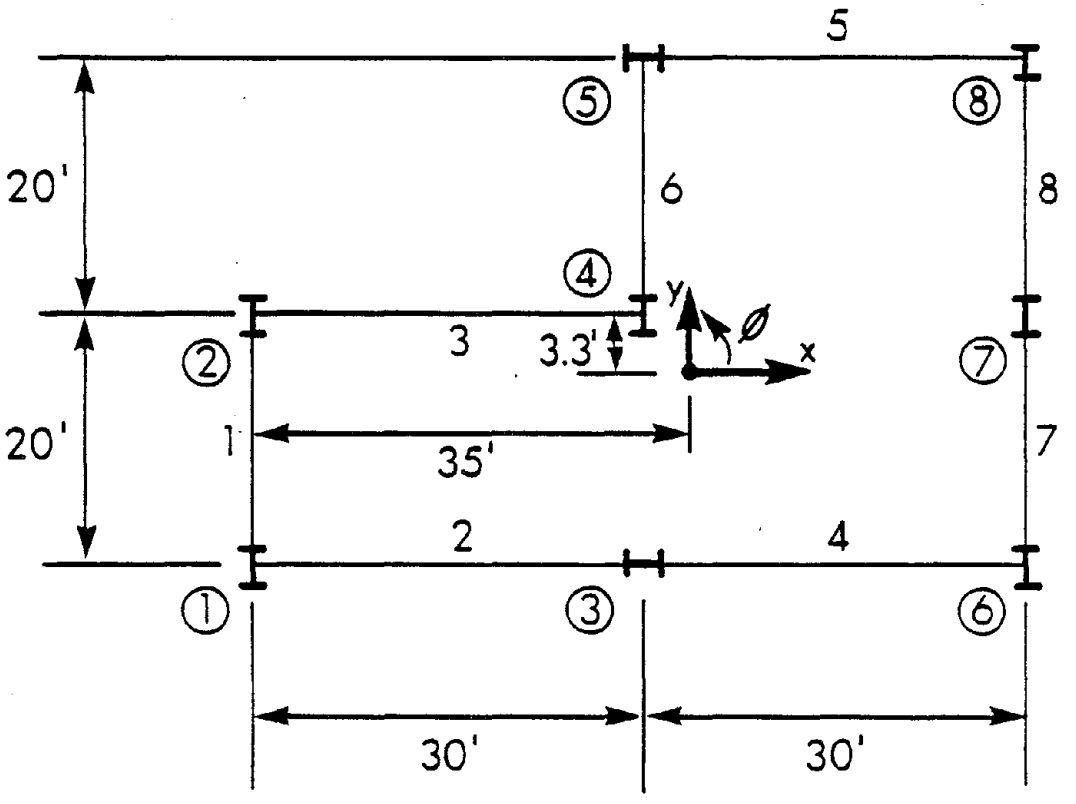

Figure 68. A Five Story Structure with an Irregular Plan (1' = .305m)

has plan or vertical irregularities. Each story is 12 feet (3.7 m) tall, and each level has a translational mass of 0.349 k-s^2/in (61.1 Mg) and a rotational mass of 19,985 k-s^2-in (2258 Mg-m^2). Every element was considered to be a steel wide-flange section represented by Equations 3.15 to 3.29. The initial major-axis moments of inertia for the columns were 9500 in^4 (395,420 cm^4) and for the beams were 9000 in^4 (374,600 cm^4). Each example required scaling during the initial optimization cycle causing the structures to have different initial starting weights.

The optimization was performed using the two ATC-03 analysis procedures. Each structure was assumed to be within map area 7 for the effective peak acceleration and the effective peak velocity-related acceleration. They were also assumed to be within seismic performance category, C, with a response modification factor of 4.50, and a deflection amplification factor of 4.00. The soil contition was assumed to be medium to soft or soil condition 2. The structure had no linking in effect, but it was required to have displacements below 0.45 in. (1.14 cm) per level. This is approximately 80 percent of the allowable elastic drift determined from the ATC-03 provisions. The modal anlaysis procedure used three modes, and both analysis techniques used the x-direction as the primary direction for the seismic loading along with the

required 30 percent of the total y-direction load. The 5 percent eccentricity was included within the two load cases.

The optimization algorithm was controlled by a set of constant parameters. Termination was to take place at the end of 30 optimization cycles, 30 analyses, or less than a 5 percent change in the weight between optimization cycles. A convergence control parameter of 2 was used. The active constraints had a lower bound of 10 percent and an upper bound of 5 percent.

The results are presented in Figures 69 to 71. Figure 69 shows the modal analysis procedure converging to a weight of 58.7 kips(26.6 Mg) in 8 cycles and the equivalent lateral force method converging to a weight of 62.6 kips(28.4 Mg) in 7 cycles. This is approximately a 6 percent difference in optimal weights. Both procedures terminate due to a smaller than a 5 percent change in weight between cycles. Both analyses produced a set of active constraints consisting of the x- and y-displacements on levels 3 through 5, as well as, the y-displacement on level 2.

The distribution of stiffness is not radically different as the ATC-03 provisions tend to infer. Since linking was not used, typical beams and columns were chosen in order to compare the analysis techniques in Figures 70 and 71. The columns can be grouped into three

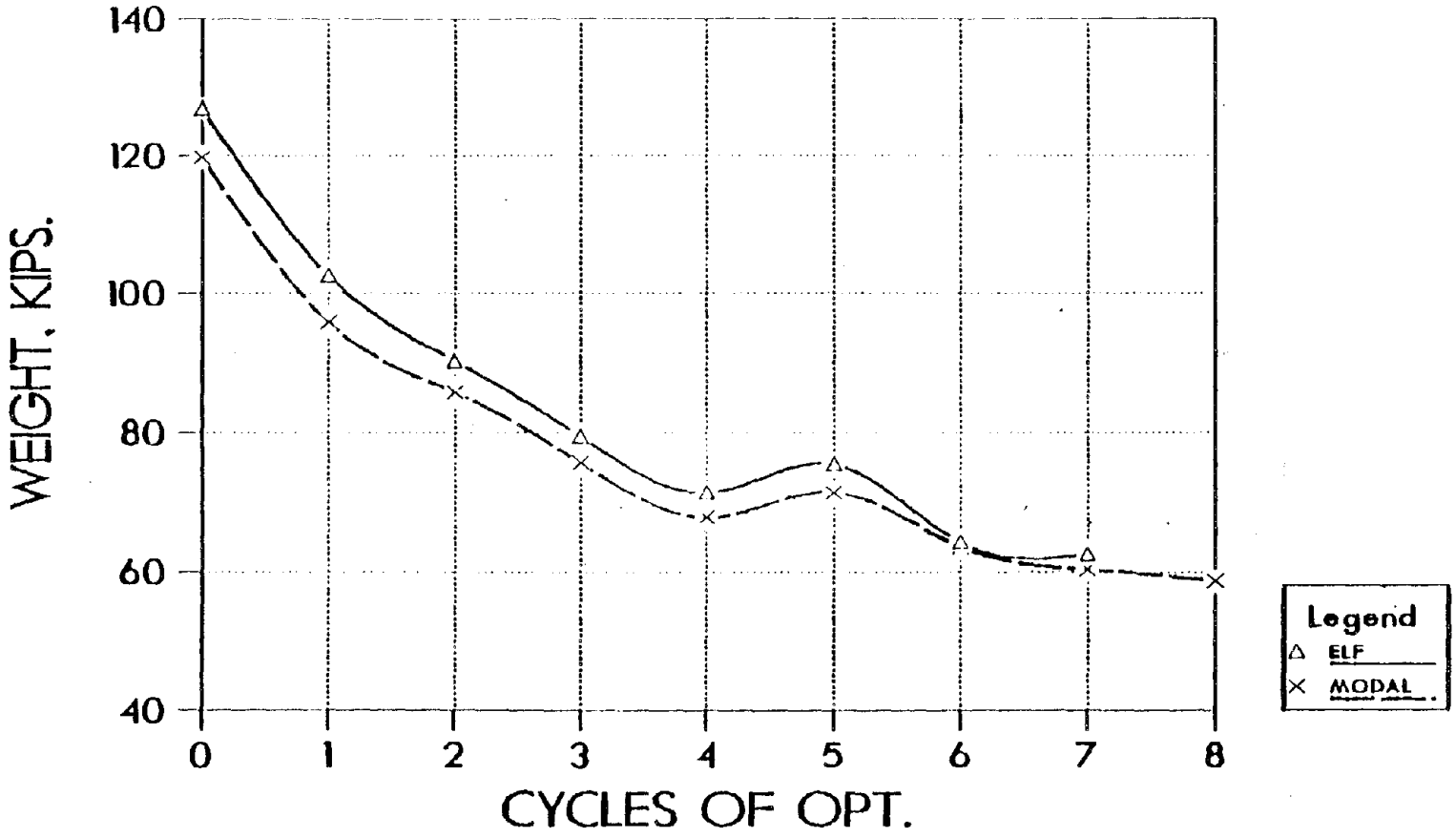

Figure 69. A Comparison of Weights for the Five Story Irregular Plan Structure Subjected to the ATC-03 Equivalent Lateral Forces and the Modal Analysis (1 kip = 4.45 kN)

categories. Columns 1, 6, and 8 provide the greatest amount of stiffness for levels 3 and 4 while providing little stiffness to levels 1 and 2. Columns 3 and 5 provide large stiffness for levels 1 and 2 while providing less stiffness for levels 3 and 4. Columns 2, 4, and 7 provide almost no stiffness for any level. These values are approximately 150 in^4 (6240 cm^4) for all levels. Therefore, the typical columns chosen to represent this structure were columns 3 and 8. The beams can be grouped into two categories. Beams 1, 3, 6, 7, and 8 provide very little stiffness to any level. Their maximum value is approximately 300 in^4 (12,480 cm^4), whereas, beams 2, 4, and 5 maximums range in values between 1800 in^4 (74,920 cm^4) and 3500 in^4 (145,700 cm^4). All of the beams are small at levels 1 and 5 with beams 2, 4, and 5 becoming stiffer in levels 2, 3 and 4. Therefore, two typical beams were chosen, beams 2 and 5. As seen from Figures 69 and 70, there is little difference in the stiffness distribution for each column or beam. The only major difference is in the magnitude, the general shape of the distribution for both techniques are similar.

The ATC-03 stability factors did not influence either analysis. Both approaches had maximum theta values of 0.01 or 10 percent of the maximum allowable value. This maximum occurred on level 4 for both analysis techniques.

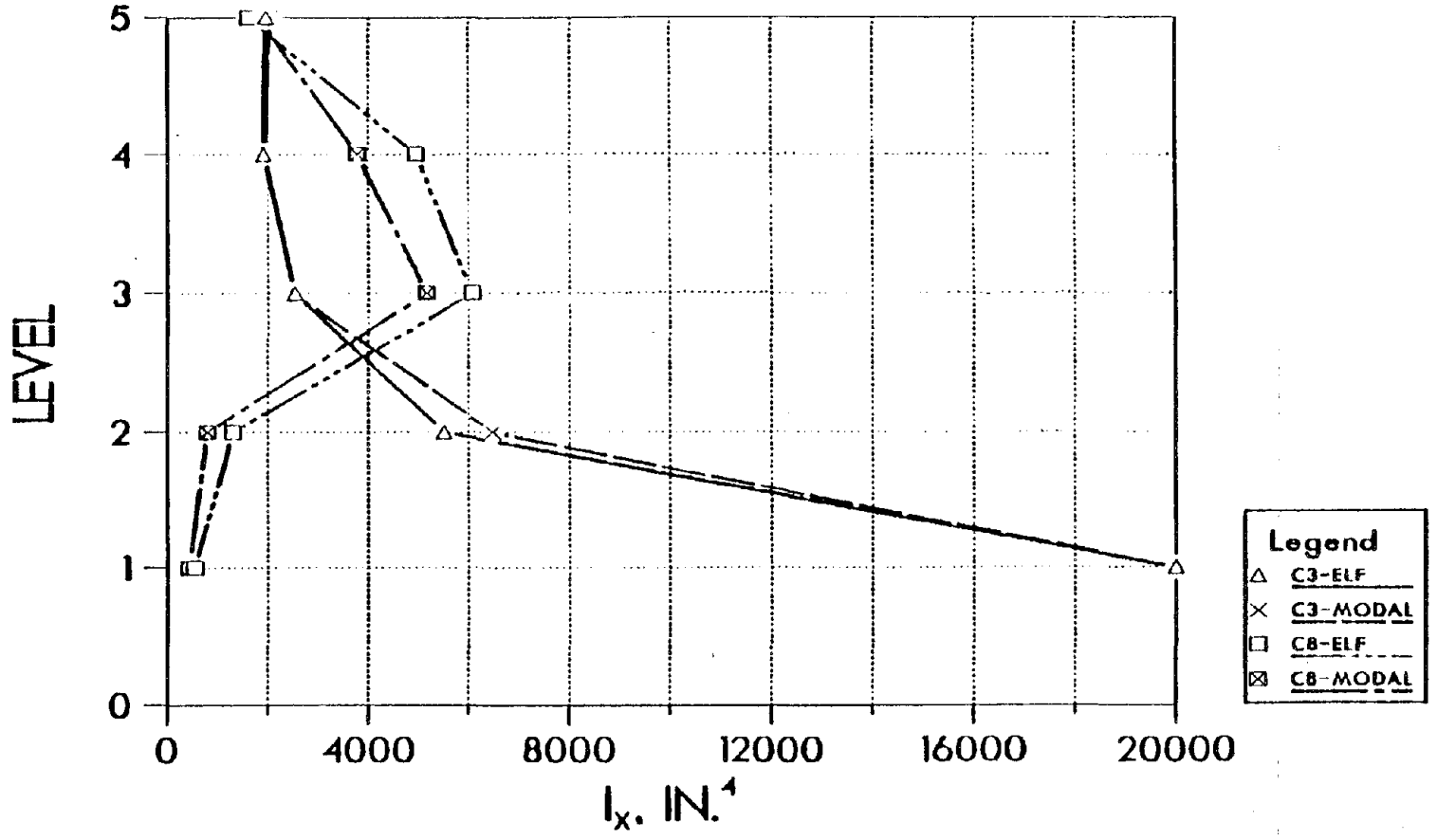

Figure 70. Column Stiffness Distributions for Columns 3 and 8 of the Five Story Irregular Plan Structure (1 in = 2.54 cm)

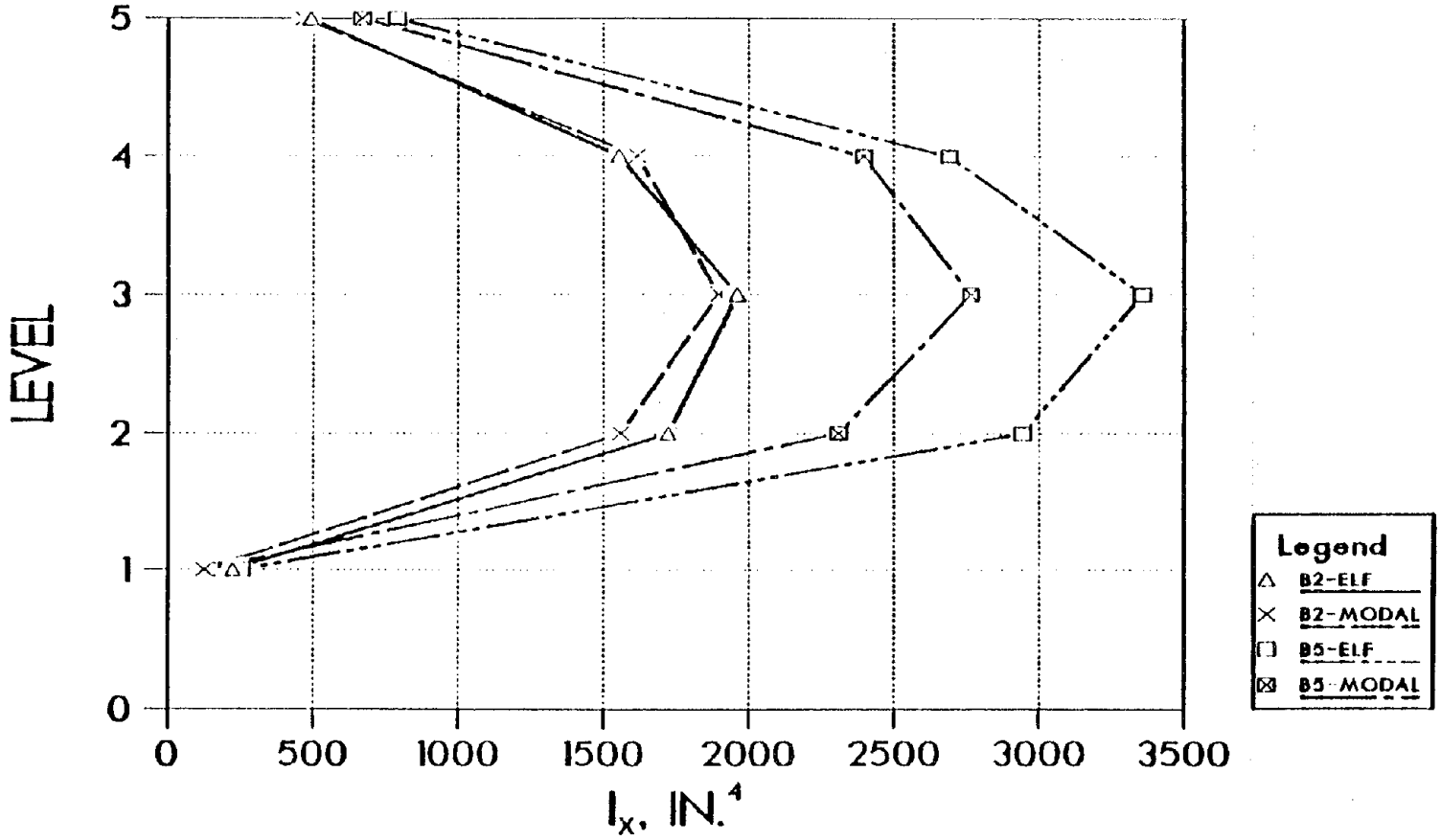

Figure 71. Beam Stiffness Distributions for Beams 2 and 5 of the Five Story Irregular Plan Structure (1 in = 2.54 cm)

As seen in the previous cases with vertical irregularities, the results for the equivalent lateral force method and the modal analysis approach provide similar results. The relative stiffness distributions are very similar. The largest dissimiliarity is the structural weight. In every case the modal analysis has provided a lighter structure. Although the modal analysis provides a lighter system, it requires an increase in computing effort over the equivalent lateral force technique. Therefore, these examples do not show a need for the extra computing since the final results generally are within 6 to 7 percent for the two analysis techniques.

Observations:

1. The plan irregularity (aspect ratio of 0.5) has little effect on the results produced by the equivalent lateral force procedure.
2. The relative distribution of stiffness of the two analysis methods is nearly identical, only the magnitudes are different.
3. The modal analysis procedure produces a lighter structure than the equivalent lateral force procedure.
4. Several columns and beams become important members while several become small with little effect on the total stiffness of the structure. Columns 1, 3, 5, 6, and 8 are important along with beams 2, 4, and 5.

5. The stability factors are all below 10 percent of the maximum value of 0.1.

H. STRUCTURAL OPTIMIZATION BASED ON RESIZING REINFORCED-CONCRETE MEMBERS

This example will be used to show one possible use of this algorithm and program with respect to design. The structure in Figure 72 will be designed to resist the lateral forces provided by the ATC-03 equivalent lateral force method. Only displacement constraints will be considered. Most likely the displacement constraints will control if the analysis is performed within a high risk seismic zone (map areas seven or six). The inclusion of stress constraints and additional load cases would require large amounts of both computer space and time. An initial design will be assumed which will be optimized and used to provide an initial design for the next design phase. In theory each design phase should provide better results than the previously optimized systems. Three phases will be presented, and they will be called "Design 1", "Design 2", and "Design 3" as they are produced.

Several element properties were held constant for each design phase. The eight perimeter columns are rectangular, concrete columns which are linked two stories at a time, i.e. all columns on levels 9 and 10, levels 7 and 8, etc., are forced to have the same cross section. The inner core, concrete shear walls, can be grouped into two sets, the

shear walls parallel to the x-direction and the shear walls parallel to the y-direction. Each of these sets are linked in the same manner as the columns. The steel beams are linked on a per floor basis. Keep in mind that the concrete elements have one fixed dimension with respect to the rectangular cross section while the other dimension is allowed to vary and represent the design parameter. All concrete elements were assumed to have a Young's modulus of 3,000 kips/in^2 (20.70 kN/m^2), a modular ratio of 10, a steel percentage of 0.015, and a shear modulus of 1150 kips/in^2 (7.935 kN/m^2). The steel beams have a Young's modulus of 30,000 kips/in^2 (207.0 kN/m^2).

The optimization was based on a set of fixed parameters. Termination of the algorithm was to take place if ten cycles of optimization were completed, fifteen analyses were completed, or less than a 5 percent weight change was achieved. A higher than normal weight change was used to decrease the redesign time. Since the previous optimization was to be used only as a guideline for the next phase an absolute optimal solution was not required. The convergence control parameter used was 2. The displacement constraints consisted of an allowable deflection of 0.45 in. (1.14 cm) per floor. Design 1 had a constraint range of 10 percent below and 5 percent above the constraint value, while Designs 2 and 3 had a range of 20 percent below and 5 percent above the constraint limits.

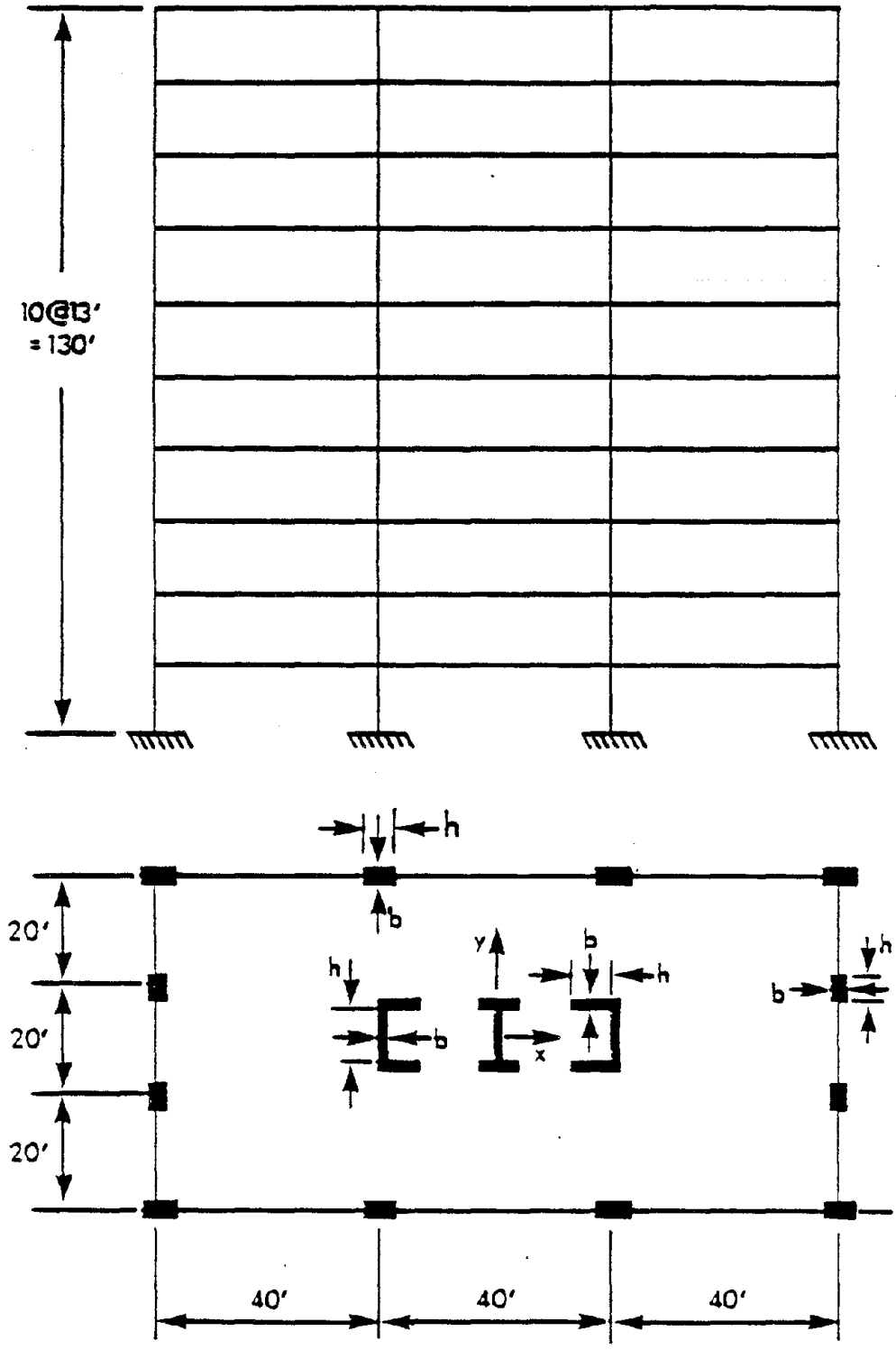

Figure 72. Ten Story Concrete Structure with Steel Beams (1' = .305m)

The ATC-03 equivalent lateral force analysis was based upon a constant set of ATC-03 and structural parameters. A non-structural translational mass of 3.26 kips-s^2/in. (570 Mg), and a non-structural rotational mass of 704,354 kip-s^2/in. (79592 Mg-m^2) were used for each level. Each level was assumed to be 13.0 feet (3.97m) tall. Each channel and I section in the core is composed of three elements. They are assumed as independent elements with respect to the x and y directions. Map area 7 was used for both the effective peak acceleration and the effective peak velocity-related acceleration. The structure was assumed to be in seismic hazard exposure group 2 with soil condition 3. The response modification factor was considered to be 5.5, and the deflection amplification factor was assumed to be 5.0. The two load cases consisted of ATC-03 x-direction loads with the plus and minus 5 percent eccentricity and 30 percent of the y-direction load. This structure was used to find the stiffness distribution that would best resist the lateral loads.

The results are presented in Tables XVIII to XXII along with the appropriate initial data which was not held constant for each design phase and in Figures 73 and 74. Obviously, the initial sizes for Design 1 are not within reason. These sizes were required in order to satisfy the constraints and were determined by scaling.

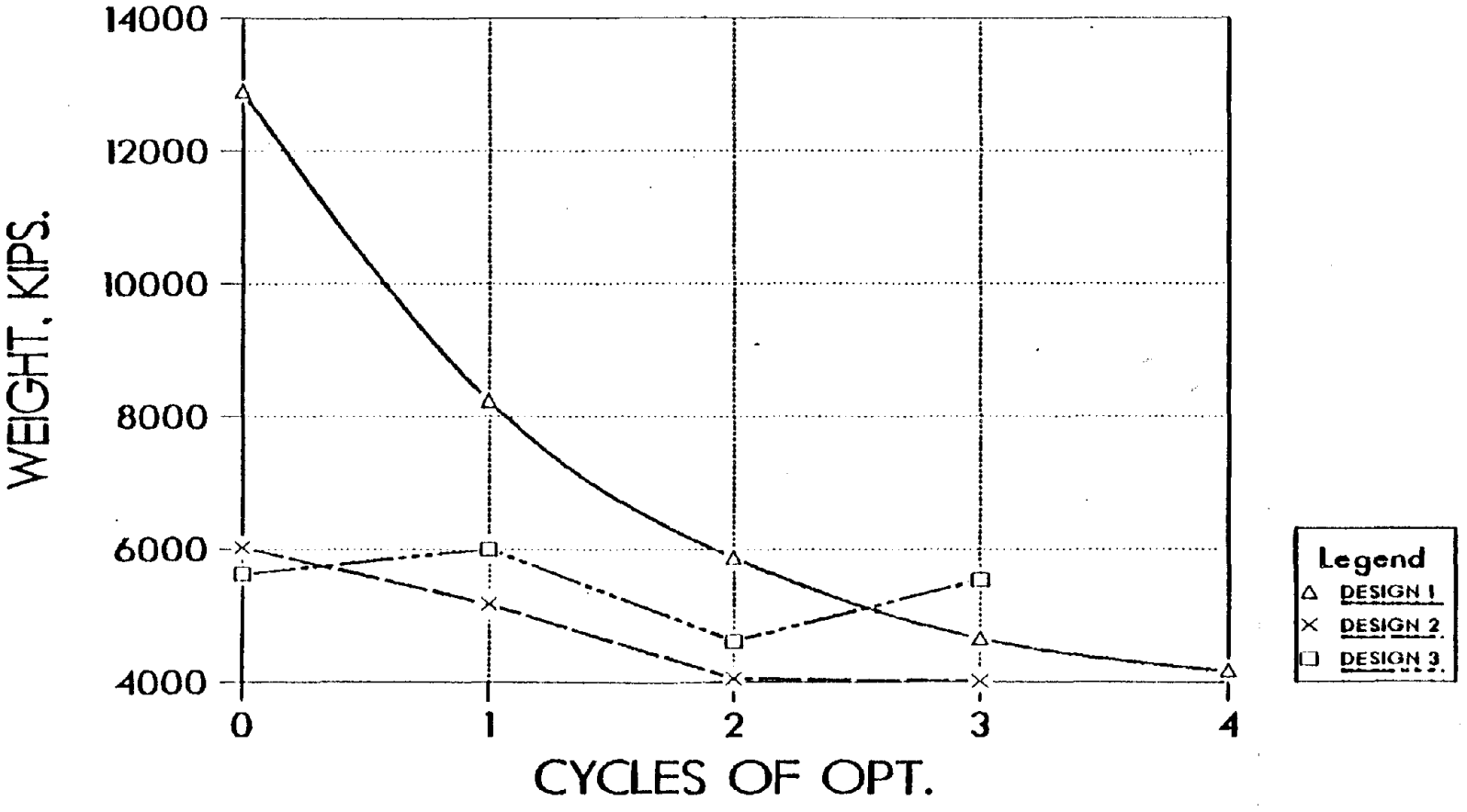

Figure 73. A Comparison of Weights for the Progressive Design of the Ten Story Concrete Structure with Steel Beams (1 kip = 4.45 kN)

The initial sizes for the second and third designs were progressively changed based upon the previous optimal results and are certainly more reasonable. Yet these parameters are set with the flexibility to optimize.

Design 1 was used to find a first set of reasonable relative sizes which would satisfy the constraints. These sizes were then modified slightly to form the initial set for Design 2. From the final sizes for Design 1, it was apparent that the shear wall results were unrealistic. Therefore, the primary design variable for shear walls parallel to the x-direction was changed for the second and third design phases. In Design 1, b, as shown in Figure 72 was used as the design variable which caused the shear walls parallel to the x-direction to be small while increasing the shear walls parallel to the y-direction to an excessively, unrealistically large size. In other words, the optimization was making use of the y-direction orientation which has a fixed width, h, and a variable depth, b, for the x-direction stiffness (moment of inertia). Between the second and third design phases, a new initial design is chosen along with new side constraints.

Design 1 produces a set of results which are unrealistic, as shown in Table XVIII. As discussed previously, the shear walls parallel to the y-direction are excessively large. In addition the columns have strange

Table XVIII. Initial and Final Design Sizes for the Vertical Members of Design 1
(1 in = 2.54 cm)

Columns

Levels	Initial (h×b) (in)	Final (h×b) (in)	b_{min} (in)	b_{max} (in)
9-10	12 × 65	12 × 42.1	5	240
7-8	14 × 75	14 × 26.9	5	240
5-6	16 × 90	16 × 16.6	5	240
3-4	18 × 100	18 × 12.1	5	240
1-2	20 × 110	20 × 12.7	5	240

Shear Walls (Parallel to y-direction)

Levels	Initial (h×b) (in)	Final (h×b) (in)	b_{min} (in)	b_{max} (in)
9-10	72 × 130	72 × 18.0	5	240
7-8	72 × 130	72 × 58.9	5	240
5-6	72 × 130	72 × 93.1	5	240
3-4	72 × 130	72 × 137.3	5	240
1-2	72 × 130	72 × 149.8	5	240

Shear Walls (Parallel to x-direction)

Levels	Initial (h×b) (in)	Final (h×b) (in)	b_{min} (in)	b_{max} (in)
9-10	60 × 130	60 × 8.8	5	240
7-8	60 × 130	60 × 10.4	5	240
5-6	60 × 130	60 × 12.7	5	240
3-4	60 × 130	60 × 13.7	5	240
1-2	60 × 130	60 × 12.9	5	240

cross-sectional sizes. The upper level columns are large while the lower level columns are small and they tend to have their major axes oriented in different directions. This is due to the shear walls. The optimization coupled with the dynamic analysis wants to eliminate the large structural mass at the upper levels and use the columns and beams to constrain the displacement, while at the lower level the shear walls are more efficient constraining the displacements. The shear walls parallel the x-direction are reasonably sized but provide little stiffness in comparison to the unreasonable y-direction shear walls.

The final results for Design 2 are shown in Table XIX. The columns were increased with respect to their, h, dimensions in an effort to reduce the aspect ratio of cross-sectional dimensions for the upper level columns. Since the primary design variable for the x-direction shear walls was changed from b to h, the side constraints were not changed in hopes that the lower level columns would achieve reasonable sizes (i.e. decrease the size of the lower level shear walls). The columns were assumed to have a width, b, of 28.5 in. (72.4 cm) which was based primarily on the average size of the upper three column widths from Design 1. The beams were chosen to be 8510 in^4 (354,210 cm^4) which is slightly larger than the average size of the top six levels. The new values for the shear

Table XIX. Initial and Final Design Sizes for the Vertical Members of Design 2 (1 in = 2.54 cm)

Columns

Levels	Initial (h×b) (in)	Final (h×b) (in)	b_{min} (in)	b_{max} (in)
9-10	16 × 28.5	16 × 19.9	5	36
7-8	18 × 28.5	18 × 20.1	5	36
5-6	20 × 28.5	20 × 12.4	5	36
3-4	22 × 28.5	22 × 8.5	5	36
1-2	24 × 28.5	24 × 7.5	5	36

Shear Walls (Parallel to y-direction)

Levels	Initial (h×b) (in)	Final (h×b) (in)	b_{min} (in)	b_{max} (in)
9-10	72 × 34.1	72 × 7.9	5	240
7-8	72 × 34.1	72 × 8.1	5	240
5-6	72 × 34.1	72 × 8.5	5	240
3-4	72 × 34.1	72 × 8.5	5	240
1-2	72 × 34.1	72 × 8.8	5	240

Shear Walls (Parallel to x-direction)

Levels	Initial (h×b) (in)	Final (h×b) (in)	h_{min}* (in)	h_{max}* (in)
9-10	123 × 36	28.8 × 36	5	240
7-8	123 × 36	45.1 × 36	5	240
5-6	123 × 36	91.4 × 36	5	240
3-4	123 × 36	134.3 × 36	5	240
1-2	123 × 36	191.1 × 36	5	240

*h is the primary design variable for these elements.

walls were determined to provide nearly equivalent stiffness, as Design 1, using 36 in. (91.4 cm) as the fixed width, b, for the shear walls parallel to the x-direction, and 72 in. (182.8 cm) as the fixed height, h, for the shear walls parallel to the y-direction. The results for Design 2 are considerably better than those for Design 1. The upper level column sizes are of reasonable sizes, but the lower columns still have unrealistic aspect ratios. Both sets of shear walls appear to have reasonable sizes with the shear walls parallel to the x-direction providing most of the lateral resistance. The upper levels x-direction shear walls are considerably smaller in size than the lower level due to the need to reduce the inertia effects. This reduction causes the upper and middle level displacements to be constrained primarily by the frame.

The initial sizes were of Design 3 determined from Design 2 in subjective manner with more emphasis placed on distribution and side constraints. In order to have a realistic distribution for the columns the maximum and minimum sizes for the columns and shear walls were adjusted in order to have more control over the final design. As seen in Equation 5.46, the side constraints are controlled through a discrete process. Generally, as the number of active side constraints increases, the potential for fluctuating Lagrange multipliers increases causing a nonmonotonic convergence.

The lower level column's fixed dimensions were reduced slightly and the variable dimension was forced to have a minimum value equivalent to the fixed value, see Table XX. The upper level column's fixed dimension was held constant for levels 9 and 10, but was slightly reduced for levels 7 and 8. These levels had a maximum value equivalent to the fixed dimension in order to control the cross-sectional dimensions. These side constraints were chosen based upon the two previous design histories. The shear walls parallel to the y-direction were given the same initial values as Design 2, but had the upper limit on the width reduced to a value which could be considered more realistic than the previous 240 in. (610 cm). The shear walls parallel to the x-direction were reduced in width with the intention of forcing the lower level columns to become more involved and to increase the depth of the shear wall cross section on the upper levels. Most of these objectives were realized as shown in Table XX. The columns all have reasonable aspect ratios and a reasonable distribution with the exception of levels 7 and 8 which might require a slightly larger width. Note that levels 9 and 10 have a column size which is approximately 25 percent larger than the allowable size. This occurs since the feasible design occured after a scaling which boosted the elements beyond their maximum values. The

Table XX. Initial and Final Design Sizes for the Vertical Members of Design 3 (1 in = 2.54 cm)

Columns:

Levels	Initial (h×b) (in)	Final (h×b) (in)	b_{min} (in)	b_{max} (in)
9-10	16 × 16	16 × 20	5	16
7-8	16 × 16	16 × 14	5	16
5-6	20 × 20	20 × 25	20	36
3-4	20 × 20	20 × 25	20	36
1-2	20 × 20	20 × 25	20	36

Shear Walls (Parallel to y-direction)

Levels	Initial (h×b) (in)	Final (h×b) (in)	b_{min} (in)	b_{max} (in)
9-10	72 × 34	72 × 10	8	24
7-8	72 × 34	72 × 10	8	24
5-6	72 × 34	72 × 10	8	24
3-4	72 × 34	72 × 10	8	24
1-2	72 × 34	72 × 10	8	24

Shear Walls (Parallel to x-direction)

Levels	Initial (h×b) (in)	Final (h×b) (in)	h_{min}* (in)	h_{max}* (in)
9-10	123 × 24	60 × 24	48	192
7-8	123 × 24	60 × 24	48	192
5-6	123 × 30	60 × 30	48	192
3-4	123 × 30	194 × 30	48	192
1-2	123 × 30	240 × 30	48	192

*h is the primary design variable for these elements.

shear walls all have reasonable sizes although the shear walls parallel to the x-direction violate the maximum allowable value due to the scaling. All of the beams except levels 1, 2, and 10 reach their passive value plus 25 percent for the scaling. The results are tabulated in Table XXI. If another redesign were performed, a reasonable limit should be applied to the beams. The large number of passive elements is the primary reason for the large scaling which caused the side constraint violation.

The global results for the optimization are given in Table XXII. Each design began with an initial weight which was smaller than the previous design showing the ability to use the optimal results with small adjustments to provide a reasonable structure for a final result. The final weights are all within 4,000 to 4,700 kips (1812 to 2129 Mg) which is a reduction in weight for all designs. The lightest design is achieved with the final results of Design 2, whereas, the heaviest design is for Design 3 which is in theory the best design. As more constraints are placed on the Design, the weights will generally increase. Termination of each optimization was different. Design 1 was terminated prematurely by the designer since it was a preliminary system. Within the last cycle it started to have oscillatory scalings. Design 2 was terminated as a result of the change in weight criteria between cycles. The large number of

TABLE XXI. Initial and Final Beam Sizes for Designs 1, 2, and 3

Level	Initial ($in.^4$)		Final ($in.^4$)		
	Design 1	Design 2&3	Design 1	Design 2	Design 3
10	5,500	8,510	5,285	5,163	15,475
9	5,500	8,510	11,198	11,266	25,056
8	5,500	8,510	11,324	13,792	25,056
7	5,500	8,510	12,158	14,614	25,056
6	5,500	8,510	9,180	12,037	25,056
5	5,500	8,510	7,137	9,231	25,056
4	5,500	8,510	4,077	6,380	25,056
3	5,500	8,510	1,958	4,455	25,056
2	5,500	8,510	848	3,052	15,692
1	5,500	8,510	474	2,281	9,058

TABLE XXII. Optimization Results for Designs 1, 2, and 3 (1 kip = 4.45 kN)

Design	Initial Wt. (kip)	Final Wt. (kip)	% Steel	% Concrete	No. Cycles	No. Analyses	Active Constraints
1	12,910	4,174	9.6	90.4	4	6	x_{10}, x_6
2	6,025	4,011	11.9	88.1	3	11	x_{10}, x_8
3	5,622	4,625	17.0	83.0	3	12	x_{10}, x_9

analyses is due to convergent, oscillatory scalings. Design 3 was terminated by default. All elements tried to become passive. This is a numerical problem which can occur when a large number of passive constraints with a relatively small range between upper and lower values are used.

The periods for the three final designs are 1.21 sec., 1.12 sec., and 1.17 sec. for Designs 1, 2, and 3, respectively. The values for T_a and 1.2 T_a are 0.96 sec. and 1.16 sec., respectively. According to the ATC-03, Designs 1 and 3 use 1.2 T_a as the design value while Design 2 which is less than 1.2 T_a was based upon the true period. As seen by the period values all three designs are very close to the value of 1.2 T_a.

The theta or stability factors are all well under the 0.1 maximum allowable value. As shown in Figure 74, Design 1 has the largest value of theta of 0.0032 with Design 2 and 3 having maximum thetas of 0.0024 and 0.0031, respectively. The shear walls are so rigid that the P-delta effect is negligible. The ATC-03 drifts on the other hand are exceeded for the upper floors of each design. The maximum drifts were between 3.53 and 3.99 in. (8.97 and 10.13 cm) for all three designs with the allowable value being 2.34 in. (5.94 cm).

The final sets of active constraints are very similar for all three designs. Each design has an active

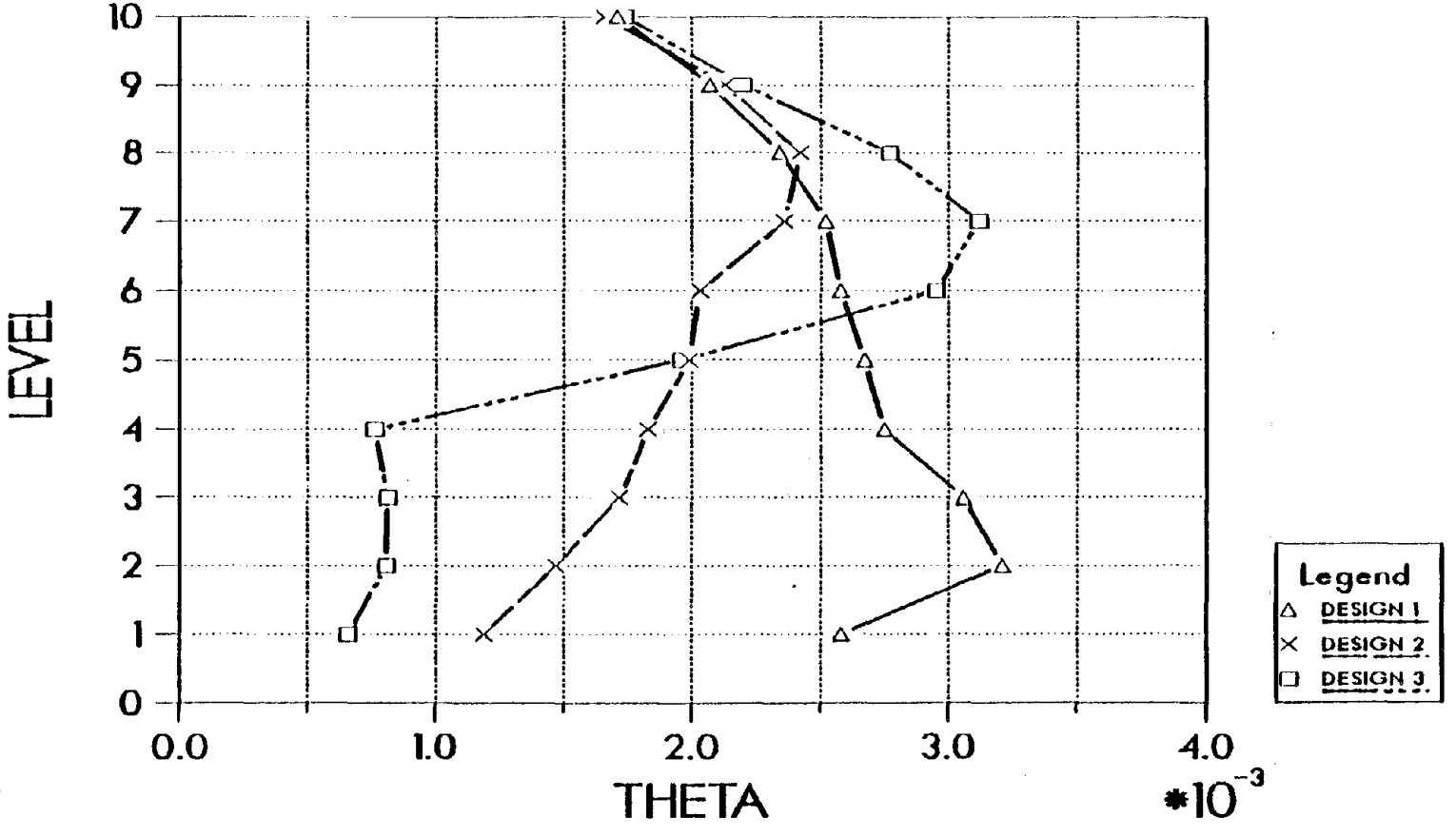

Figure 74. ATC-03 Stability Factors for the Final Designs of the Ten Story Concrete Structure with Steel Beams

x-displacement constraint at level 10 with one additional active constraints at either level 9 or level 8. All three designs have displacements in the top 4 levels which are close to the active values.

This is just one possible means of using this algorithm to reach a final design. It is best suited to provide a preliminary design such as Design 1, but is capable with the correct interpretation of results and application of its resources to proceed in the direction of a finalized design. In a similar manner the stress constraints and more involved loadings can be applied, but the interpretation of results become increasingly involved.

Observations:

1. This algorithm can be used to provide a series of optimal designs. Each previous solution can be adjusted and used as a "better" initial design for the next optimization.
2. This type of sequential design produces a series of feasible designs within each optimization solution, as well as, providing a series of feasible, optimal designs.
3. These types of results cannot be obtained by strictly analysis procedures. Each change in the design using intuition and reanalysis cannot guarantee a feasible

structure (one which will satisfy all of the constraints).

4. The algorithm presented guarantees that each design will be a feasible structure with respect to the constraints. Using this algorithm, successively better designs can be created by manipulation of the constraints and initial design's after each complete optimization.

5. Design 3 begins to fluctuate during the last cycle of optimization because of two reasons. First, the side constraints are very constrictive, and secondly, the discontinuity in the design period caused oscillatory scaling. The ATC-03 provisions allow the use of the calculated period as long as it is below 1.2 T_a, and the analysis provides a period which fluctuates above and below this value.

6. The ATC-03 stability factors were well below 0.1. The maximum value was 0.0032.

7. The maximum drifts were as high as 3.99 in. (10.13 cm) which is above the allowable value of 2.34 in. (5.94 cm). This maximum drift occurs at the level where the transition from non-active to active displacements occur. Although the ATC-03 drift is violated the set of displacement constraints are not. This shows the need to implement a drift constraint.

I. STRUCTURAL OPTIMIZATION USING COST AS AN OBJECTIVE FUNCTION

The objective function given in Equation 5.8 provides an optimal solution based upon a weighted minimum volume. This same objective function was used to minimize the cost of structures. This is a very simplified approach to representing the cost of a structure. Using Equation 5.8 as a cost gives an approximate cost and could not be the sole judgement of which design is most cost effective. The computer program accepts one cost per unit volume per material. It would be of great use if each element could have its own cost per unit volume. This would allow each element to be judged on an individual basis as to its cost which could include erection, forming, end connections, fireproofing, and any other incidental costs as well as material costs. Cheng and Juang (55) are using a more comprehensive cost function for the two-dimensional case, but it was considered too complex to extend to the three-dimensional case at this time.

The cost per unit weight for the steel and concrete elements were obtained from two sources. Dr. Arthur Monsey (retired vice-president from the consulting firm of Horner and Shifrin in St. Louis, Mo.) provided approximate figures of 750 dollars per kip (1655 dollars per Mg) for erected steel and 350 dollars per kip (773 dollars per Mg) for concrete columns (46). The second source was the Means

Construction Cost Data where the approximate average cost for steel buildings (apartments, offices, hospitals, etc.) was 600 dollars per kip (1,325 dollars per Mg) and for concrete buildings was 520 dollars per kip (1148 dollars per Mg) (47). The concrete costs were the average cost of columns, beams, and panels. Due to the more detailed nature of the Means Cost Data, its figures were chosen to be used and were converted to a cost per volume of 294 dollars per cubic foot (10,360 dollars per m^3) of steel and 78 dollars per cubic foot (2750 dollars per m^3) of concrete. This provides a ratio of steel to concrete cost factors of 3.77, whereas, the weights of 490 pounds per cubic foot (7323 kg/m^3) for steel and 150 pounds per cubic foot (2394 kg/m^3) of concrete provide a ratio of 3.27. These ratios are fairly close, therefore, little difference in the results would be expected between the results obtained using the cost over the weight objective functions. These costs are only rough estimates and at best could be used as a preliminary tool for selecting designs or structural layouts.

A five story, rectangular structure as shown in Figure 75, will be used to illustrate the effects of using the cost and weight factors in the objective function. This structure does not consider linking and has dynamic displacement constraints. The displacement constraints consist of 0.45 in (1.14 cm) per story and are for both

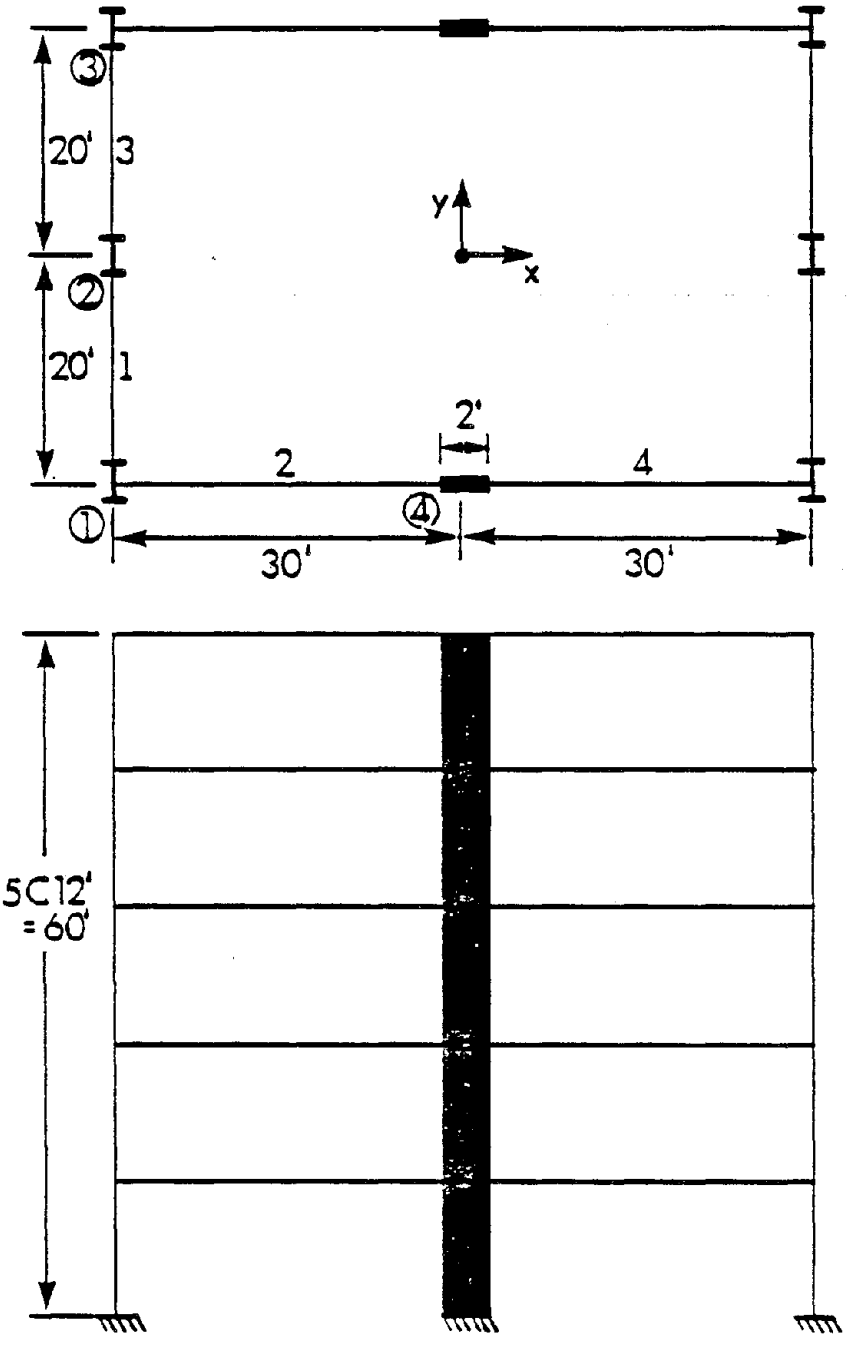

Figure 75. Five Story Steel and Concrete Structure (1' = .305m)

the x and y-directions. The active constraint range is between 10 percent for a lower-bound and 5 percent for an upper bound. The termination criteria was twenty cycles of optimization, twenty cycles of analysis, or a 1.0 percent change in weight, and the convergence control parameter was 2. The objective function used the factors of 294 dollars per cubic foot (10,360 dollars per m^3) of steel and 78 dollars per cubic foot (2750 dollars per m^3) of concrete for the cost objective and factors of 490 pounds per cubic foot (7823 kg/m^3) for steel and 150 pounds per cubic foot (2394 kg/m^3) for concrete for the weight objective.

The structure is composed of six steel columns, two concrete columns, and all steel beams. Each level has a translational mass of 0.47 $k\text{-}s^2/in$ (82.3 Mg) and a rotational mass of 29,068 $k\text{-}s^2\text{-}in$ (3284 $Mg\text{-}m^2$). Each steel column started with an initial size of 1000 in^4 (41,623 cm^4), each beam started with an initial size of 1100 in^4 (47,785 cm^4) and each concrete column had a gross section of 8 in. (20.3 cm) by 24 in. (61.0 cm) with a 0.02 percent steel ratio. The steel elements were constrained to be within 10.0 in^4 (416.2 cm^4) and 20,000 in^4 (832,460 cm^4) while the concrete column width was forced to be between 5.0 in. (12.7 cm) and 24.0 in. (61.0 cm). The analysis was performed using ATC-03 equivalent lateral forces. The structure was assumed to be

within map area 7 for both the effective peak acceleration and the effective peak-velocity related accelerations, the deflection amplification factor was chosen as 4.0, and the response modification factor was chosen as 4.5. (The ATC-03 does not provide the values for these mixed-material structures.) It was assumed to be in seismic group 2, and was located in soil condition 2. The ATC-03 primary direction of loading was in the x-direction with the required thirty percent in the y-direction. The two load cases consisted of the x and y loadings coupled with the plus and minus five percent eccentricity of the x-direction load. With both load cases and the geometric symmetry with respect to both elevation and plan, symmetric results were obtained which allows the results to be presented for the first four beams and three columns as shown in Figures 78 and 79.

The results are presented in Table XXIII and Figures 76 to 80. The initial design was scaled by a factor of 2.32 to give a cost of 89,402 dollars with six active constraints which were the x-displacements for load cases one and two at levels 2 through 4. This scaling was due to the small initial size of the concrete columns which are the primary x-direction load resisting elements. The final cost after six optimization cycles was 52,673 dollars with an optimization history as shown in Figure 77. In terms of weight the cost objective function problem had

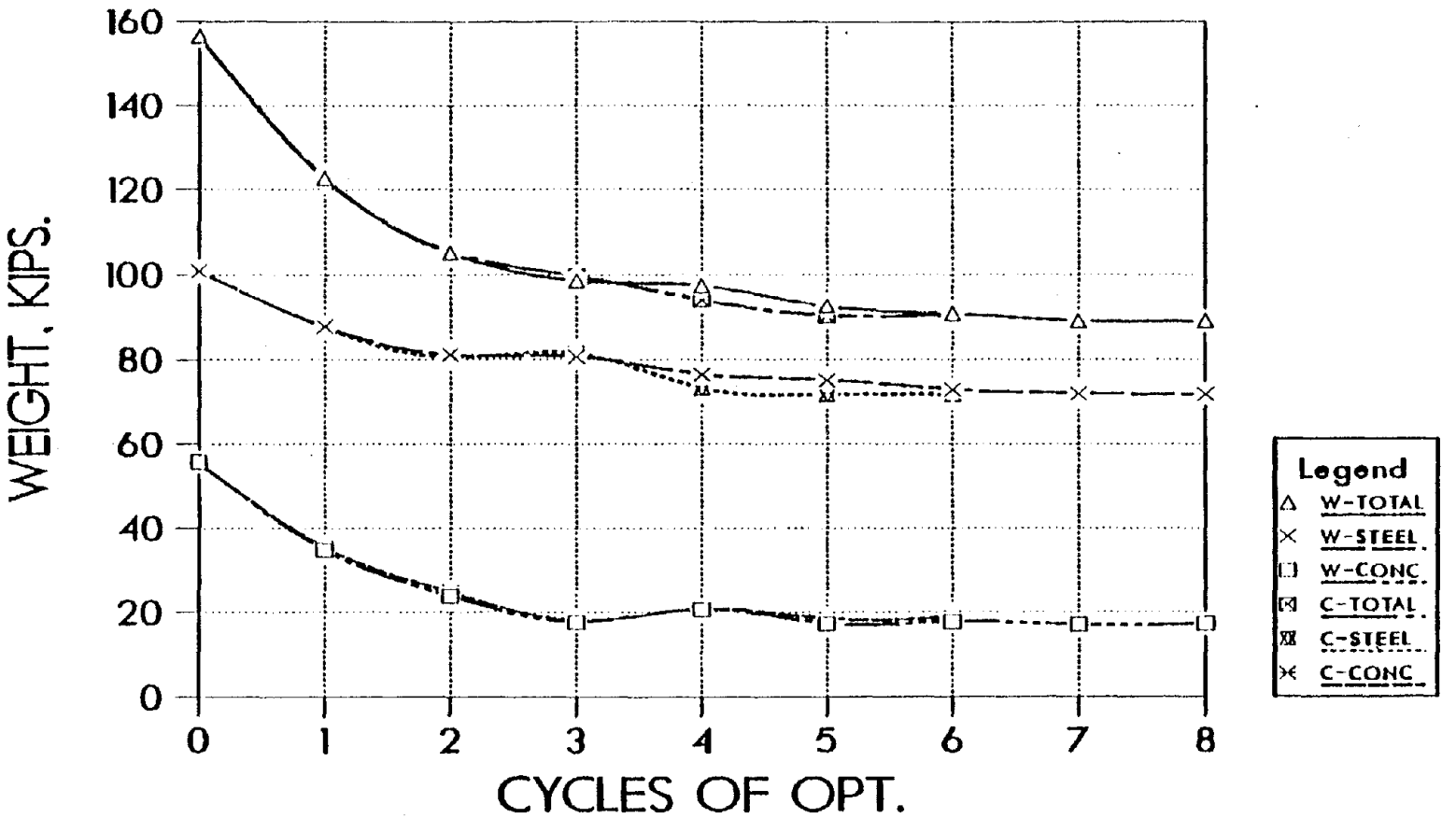

Figure 76. A Comparison of Weights for the Five Story Structure with Weight and Cost Objective Functions (1 kip = 4.45 kN)

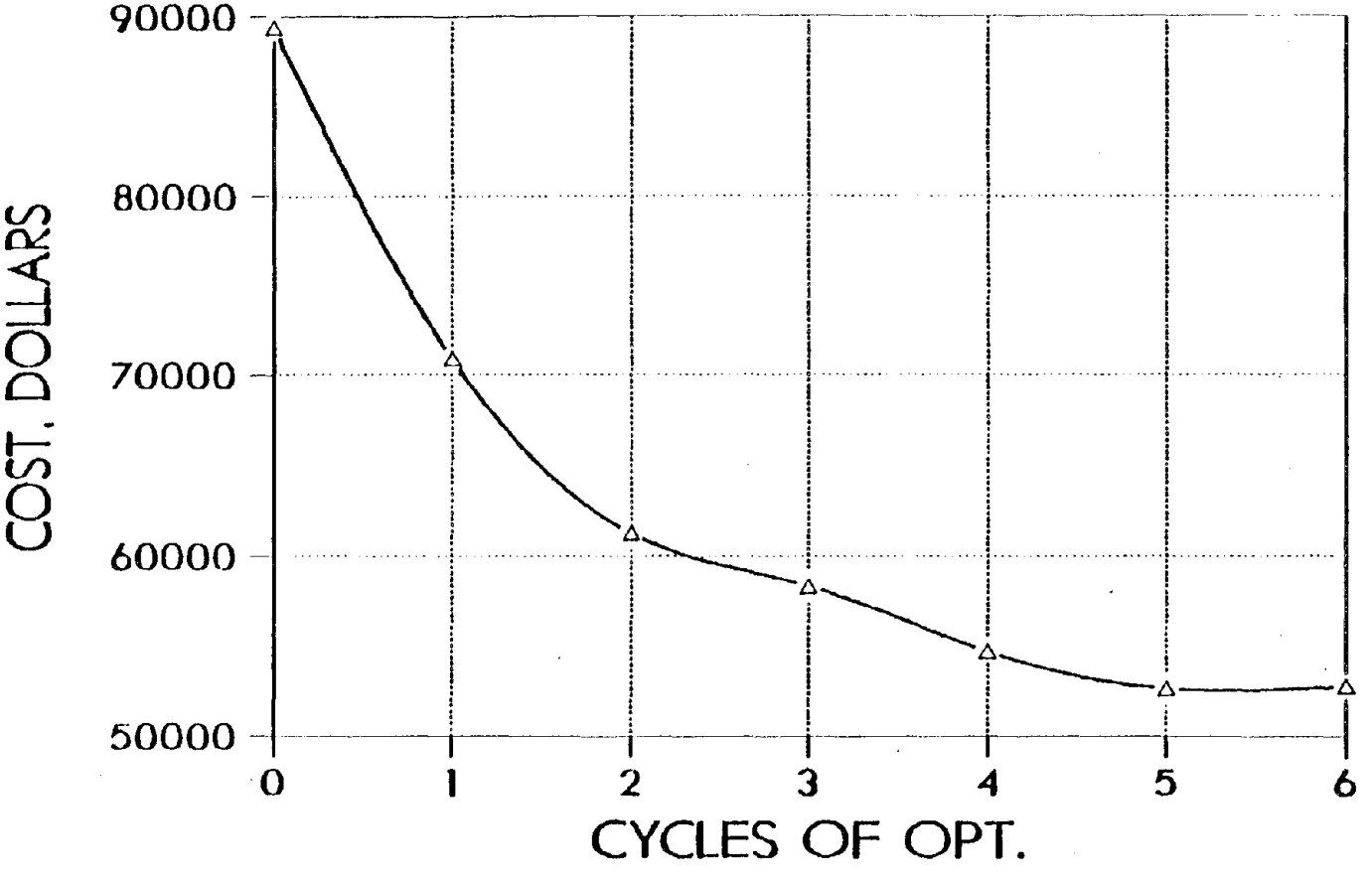

Figure 77. Cost versus Optimization Cycles for the Five Story Steel and Concrete Structure

an initial weight of 156.5 kip (70.89 Mg) and a final weight of 90.3 kip (40.9 Mg) with 71.8 kip (32.5 Mg) being steel and 18.5 kip (8.38 Mg) being concrete. These results are shown in Figure 76. The steel provides approximately eighty percent of the cost. The final set of active constraints consisted of sixteen displacements. Both the x and y-displacements for load cases one and two were active for levels 2 through 5. The weight objective function produced similar results with respect to the values given for the cost objective. The initial weight was the same since it is only analysis dependent. The final weight was 89.0 kips (40.3 Mg) or 1.3 kips (0.59 Mg) less than using the cost objective with 71.8 kips (32.5 Mg) of steel and 17.2 kips (7.79 Mg) of concrete. The entire amount of difference is within the concrete's weight. The final set of active constraints for this objective consisted of fourteen displacements. The x and y-displacements for both load cases were active on levels 3 through 5 while only the x-displacements for both load cases on level 2 were active. This minimum weight was found in 8 cycles. If the cost per kip values were applied to the minimum weight solution, it would provide a lower cost than when using the cost objective. This substantiates the fact that the path of optimization is important, and that there is no way to be certain that a global optimum has been obtained.

The major differences are in the stiffness distributions. The cost objective function requires larger beams and smaller steel columns than the weight objective function for the major elements, as shown in Figures 78 and 79 while the weight objective function requires smaller concrete columns. As seen in Table XXIII, the steel weights are the same even though the beams are much smaller in size, since they are considerably smaller than the columns. In both cases the concrete columns are at or near the minimum width for all but the first level. Their values are given in Table XXIII. This signifies that a redesign is in order since the minimum size 5.0 in. (12.7 cm) is small and provides a less than desirable aspect ratio of 4.8 for cross-sectional height to width. Once again both cases provide beams which are smaller than the columns by nearly a factor of 2, and both cases try to form rigid systems which are parallel to the x-direction. The beams and the intermediate column parallel to the y-direction are small. This is due to the added rigidity in y-direction provided by the concrete columns and the fact that only thirty percent of the y-load was applied in that direction. The concrete columns reacted in a typical fashion of trying to reduce themselves to a small size for the upper levels while providing large amounts of stiffness to the lower floors. This occurs for two reasons, the first is that the small width concrete columns with the

TABLE XXIII. Concrete Column Sizes for Different Objective Functions (1 in = 2.54 cm)

	Objective Function	
Level	Cost (in)	Weight (in)
5	5.0 × 24.0	5.0 × 24.0
4	5.0 × 24.0	5.0 × 24.0
3	5.0 × 24.0	5.4 × 24.0
2	5.2 × 24.0	5.1 × 24.0
1	8.5 × 24.0	10.4 × 24.0

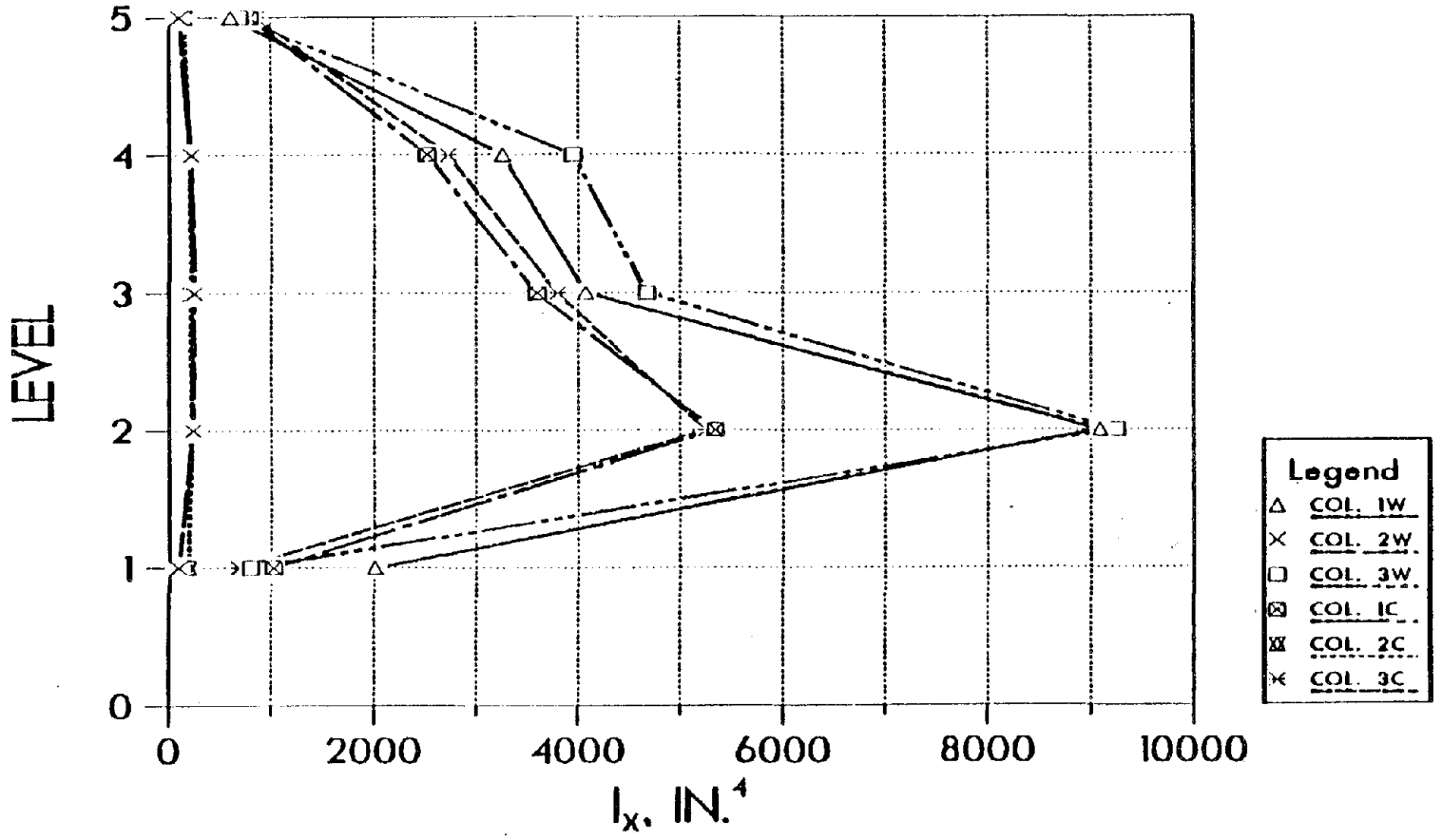

Figure 78. Steel Column Stiffness Distributions for the Five Story Structure with Weight and Cost Objective Functions (1 in = 2.54 cm)

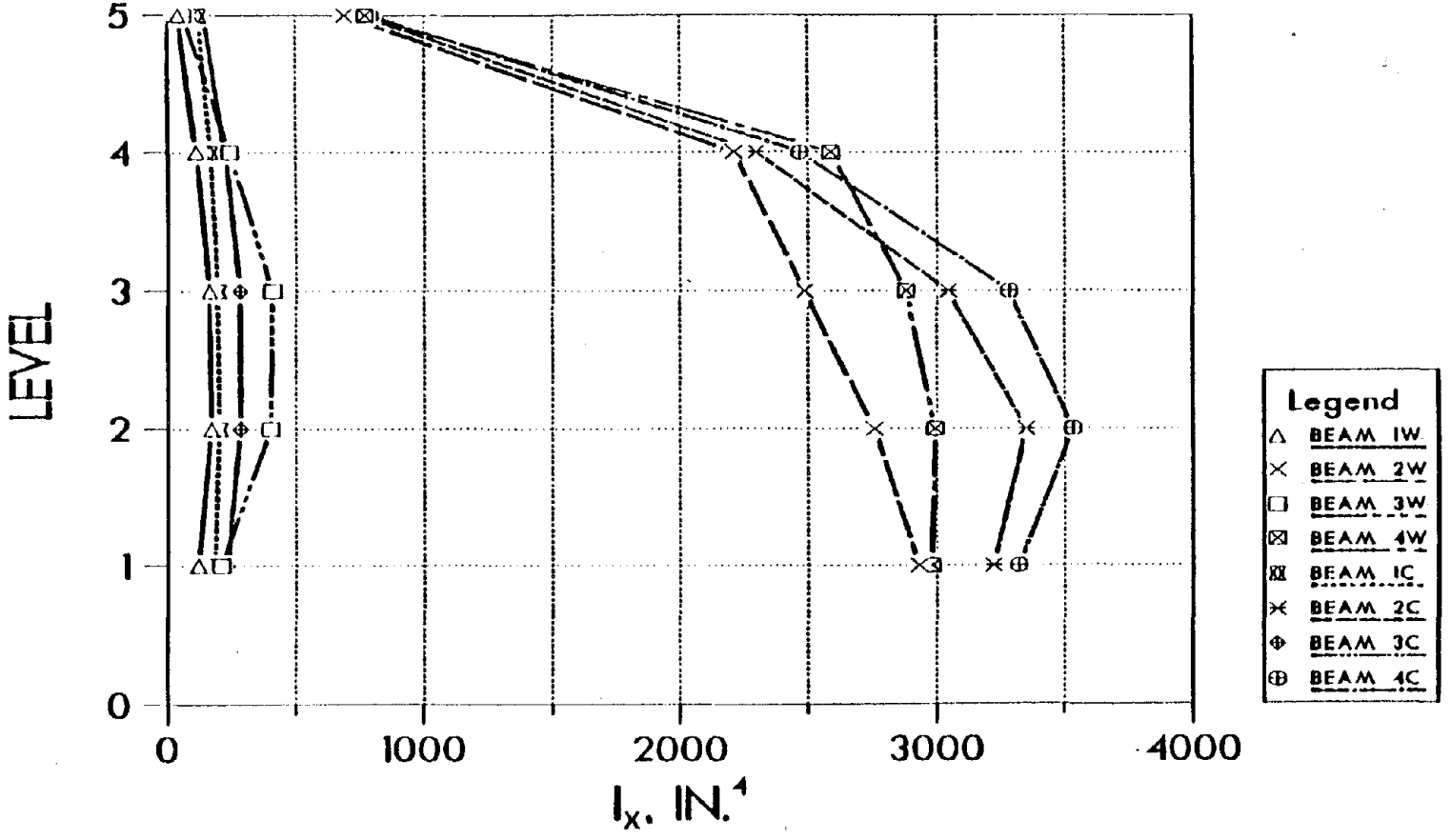

Figure 79. Beam Stiffness Distributions for the Five Story Structure with Weight and Cost Objective Functions (1 in = 2.54 cm)

prescribed percentage of steel still provide adequate stiffness, and secondly the reduction in column size considerably reduces the structural mass at those levels which in effect reduces the inertia loading from the ATC-03 code. From Figure 78, the steel columns are very large at the second level and this occurs because the concrete columns reduce significantly between the first and second levels as shown in Table XXIII, while the steel columns at level 1 are small using the converse reasoning. The beams, on the other hand, are less variable, but considerably smaller than the columns. The upper level has small beams and columns since they must only provide enough stiffness to stop excessive intrastory drift. These results suggest that a new model be developed for the concrete elements, in order to provide an aspect ratio which could be maintained during the optimization of the three-dimensional structure.

The ATC-03 stability factors for this structure and both objective functions are well below the maximum allowable value of 0.1. Both maximum factors are near 0.018 with very little difference for the two objective functions over all five stories, as seen in Figure 80.

This example provides several important results. The objective functions both provide nearly the same weight and cost which is due to the similarity in the ratios of the factors applied in the objective function. Although the

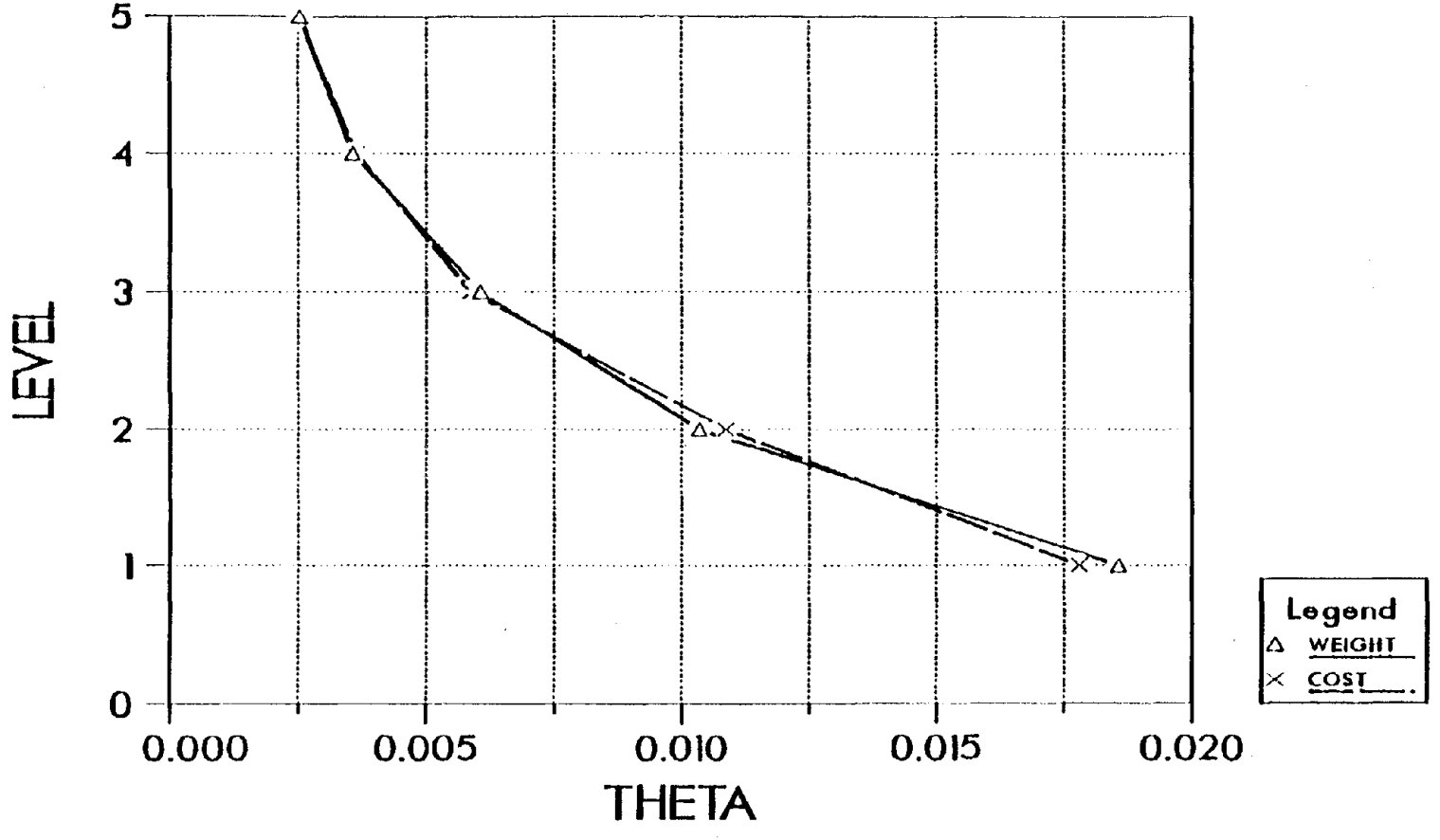

Figure 80. ATC-03 Stability Factors for the Five Story Structure with Weight and Cost Objective Functions

weights and cost are nearly identical they provide different sizes for the moments of inertia. These differences might be larger if the concrete column sizes were reduced to provide more nearly square columns which would change the objective value showing a larger difference. From this example, it is seen that different sizes can be found with a small change in the steel to concrete ratio of objective factors. Although these sizes are different the distribution of stiffness is similar for both cases. Therefore, the use of weight or cost is somewhat irrelevant. If the general distribution can be maintained this is reasonable for a preliminary design. A user must be cautious though, since the relative sizes of beams and columns do change. A slight change in the factors will generally produce similar distributions for the column and for the beams, but the relative size of beams and columns can be different. Since these distributions were similar and the final weights were nearly identical, the use of the cost function was limited to a few examples with the majority being handled with the weight objective.

Observations:

1. The cost and weight objective functions provide nearly identical optimal weights. The only difference being a 1.3 kips change in the total amount of concrete.

2. Although the final weights were close, the paths of optimization were different and they produced different magnitudes of beam and column stiffness. The cost function generated lighter steel columns and larger beams.
3. The stiffness distributions are similar for both cases even though the magnitudes are quite different.
4. The minimum weight solution provides a lesser cost than the cost function generated. This is due to the path dependent nature of optimization and the location of local minima.

J. STRUCTURAL SYSTEMS SUBJECTED TO MULTI-COMPONENT EXCITATION

1. Common Parameters. A five-story, L-shaped structure was used to study the effects of multi-component seismic excitation. The building system was considered as an all steel structure with seven column lines and seven beams. Each level was 12.0 ft. (3.66 m) tall. Each level has a non-structureal, translational mass of 0.311 $k\text{-}s^2/in$ (54.4 Mg) and a nonstructural, rotational mass of 16,400 $k\text{-}s^2\text{-}in$ (1,853 $Mg\text{-}m^2$). The modulus of elasticity is 30,000 k/in^2 (20,700 kN/cm^2), and the shear modulus is 11,500 k/in^2 (7935 kN/cm^2). Each load case used the response spectrum shown in Figure 16 and defined by Equations 3.56 and 4.57 with the modal analysis. This

structure was subjected to a variety of combinations of maximum ground accelerations coupled with a variety of external stiffness arrangements. The effects of linking were also considered.

2. Linked, Rectangular Element System. A five-story L-shaped structure, as shown in Figure 81, was optimally designed for various seismic inputs and external stiffness arrangements. Rectangular, steel cross-sections with a depth to width ratio of 1.5 was used for all elements. Therefore, Equations 3.13 and 3.14 are used to relate the secondary to the primary design variables. External stiffnesses were applied at the mass centers in order to prevent the structure from deflecting in that respective direction without preventing rotation.

This structure was subjected to six different load cases. The load cases consist of five cases with various applied lateral loading conditions and external stiffness arrangements and one case which has a different mass center than the previous five cases. Load cases 1 through 5 used a mass center located at point A, while load case 6 used a mass center located at point B which was 35 in. (88.9 cm) to the right and 15 in. (38.1 cm) above column 1 in Figure 81. The sixth load case was used to show the effect of the mass center location with respect to the rigidity center. Each modal analysis used three modes with direct modal superposition.

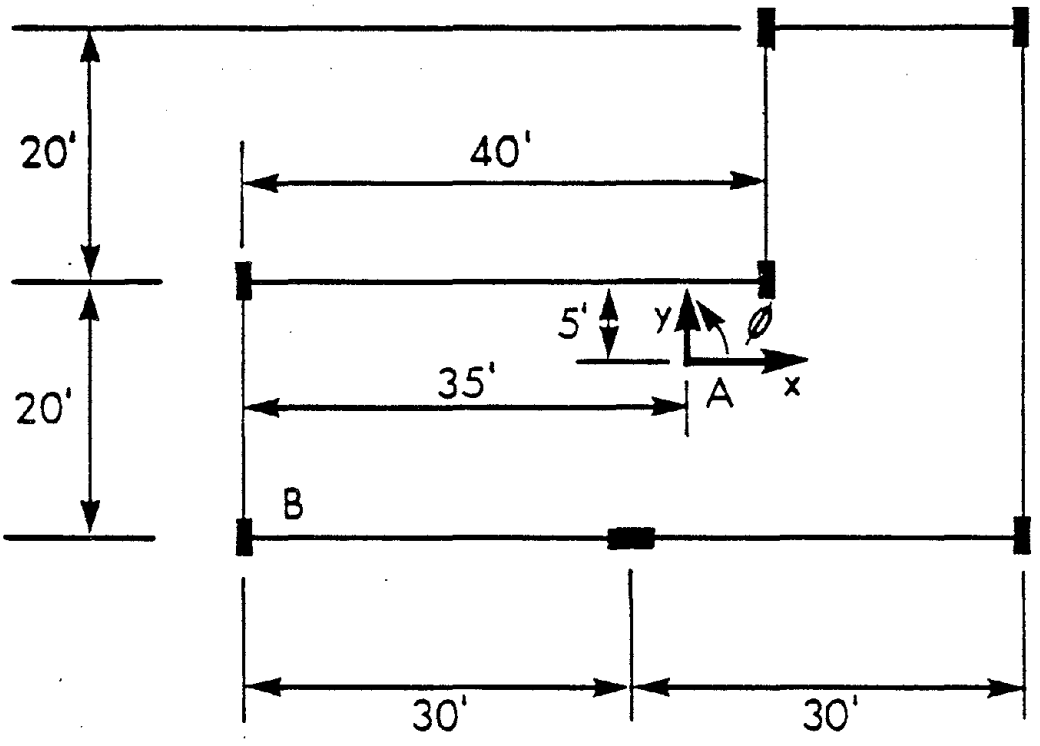

Figure 81. Five Story L-shaped Structure with Rectangular Columns - Plan
(1' = .305m)

The optimization was based upon a set of fixed parameters. The optimization process was to be terminated within 20 cycles of optimization, 25 analyses, or a weight change of less than 5 percent. The constraints were considered active if the response was within the 10 percent below or 5 percent above the limit for the response. Dynamic displacement constraints were chosen according to the ATC-03 recommendation as 0.00625h where h is the height of each level above the base. Linking of all columns per level and all beams per level was used.

The results of the optimization are given in Table XXIV and Figures 82 to 84. Figure 82 shows the rapid rate of convergence with all cases terminating within four cycles. Each termination was due to a small weight change. Table XXIV shows the final weights and active displacement constraints for each case. From Table XXIV and Figure 82, the load cases form two groups of optimal systems which are based upon the sets of active constraints. Load cases 1 and 2 have y-displacement active constraints, whereas, load cases 3 through 6 have x-displacement active constraints.

The results are heavily dependent upon the dominant components of loading. Load cases 1 and 2 were expected to produce lighter structural systems since the y-direction excitation was the dominate loading coupled with the

TABLE XXIV. Loads, External Stiffness, and Final Results for an L-shaped Structure Subjected to Multi-component Excitations (1 kip = 4.45 kN)

Case	Load (g) x	Load (g) y	Ext. Stiff	Final Wt. (kip)	Final Act. Const.
1	0	.225	-	251.5	y_5
2	.300	.225	x-dir	265.3	y_3
3	.300	.225	-	348.7	x_5, x_4
4	.300	0	-	349.3	x_5, x_4
5	.300	.225	y-dir	357.0	x_4, x_3
6	.300	.225	-	334.0	x_5, x_4

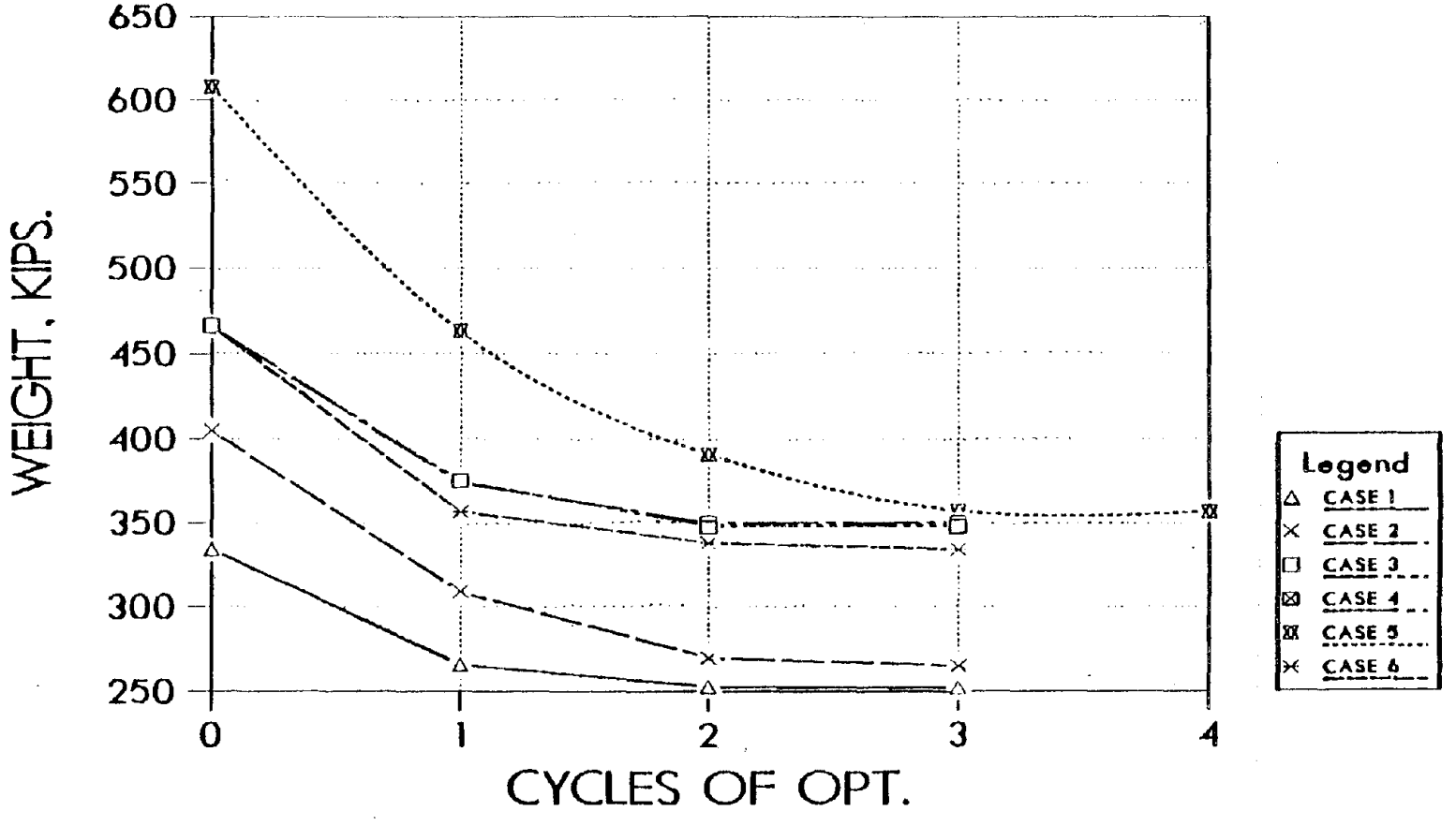

Figure 82. A Comparison of Weights for the Five Story L-shaped Structure Subjected to Single and Multi-component Excitations (1 kip = 4.45 kN)

fact that six of the columns are oriented with their major stiffness in that direction. Load cases 1 and 2 produce final solutions with similar weights. With an external stiffness applied in the x-direction load cases 1 and 2 were expected to produce similar results. Although the weights are similar the stiffness distributions are slightly different as seen in Figures 83 and 84. This is due to the fact that load cases 1 and 2 have different active constraints. By applying the x-direction external stiffness, it suppresses the x-modal components and adds additional y and ϕ dominant modes within the modal analysis. The difference in mode shapes produces a different set of responses between the two load cases. Due to the coupling of modes, it is not possible to state whether a mode is an x, y or ϕ mode. Note in Figures 83 and 84 that the stiffness distributions are similar above the third level where load case 2 has an active constraint. The increase in stiffness below the third level for load case 2 is used to control the third level displacement. Even though the external stiffness causes a change in the response, the final weights and stiffness distributions are similar.

Due to the rigid floor assumption the rotations can significantly affect the final solutions. Since the mass center and the center of rigidity do not coincide, the loads can cause significant rotations which can be helpful or detrimental in controlling the displacements at the

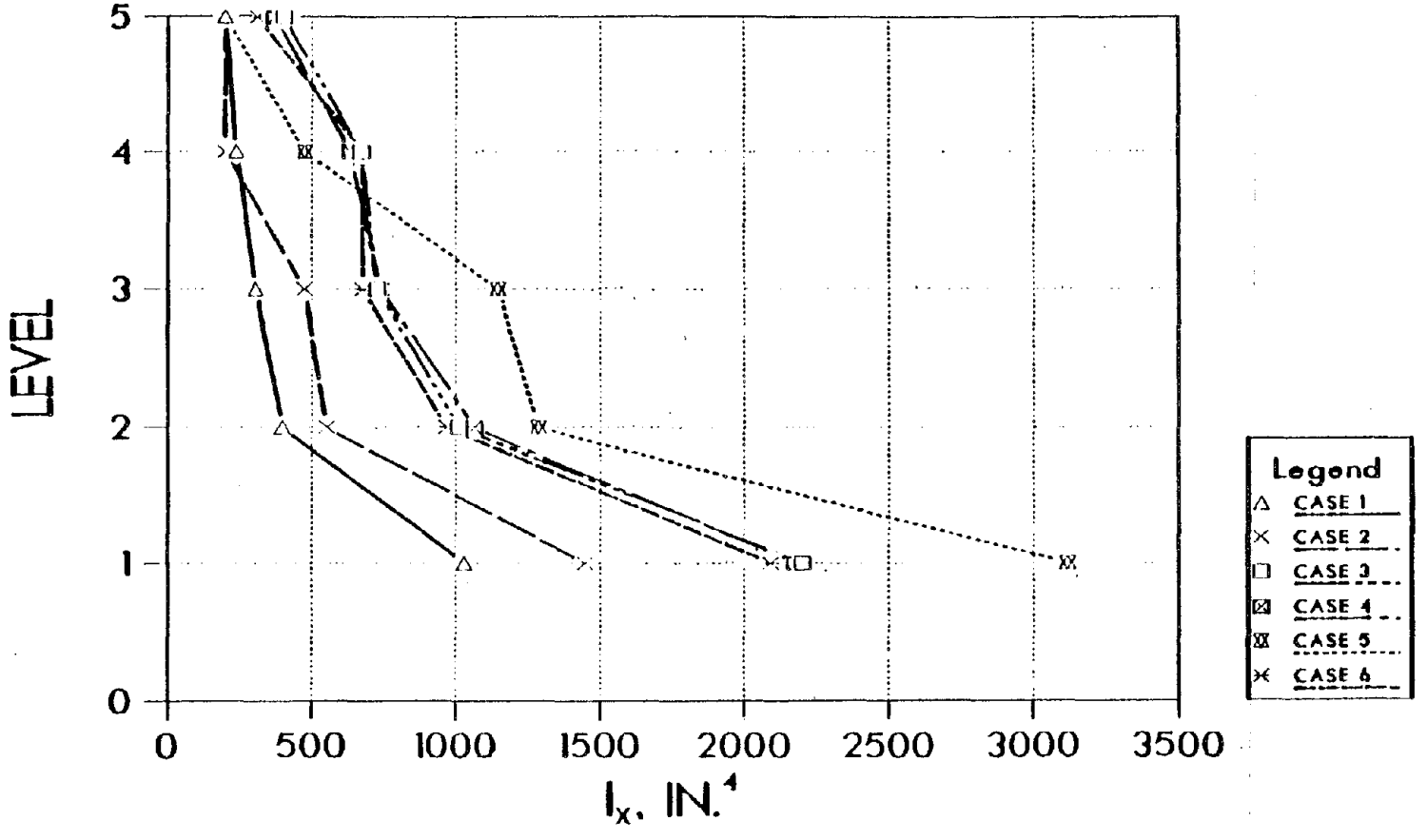

Figure 83. Column Stiffness Distributions for the Five Story L-shaped Structure Subjected to Single and Multi-component Excitations (1 in = 2.54 cm)

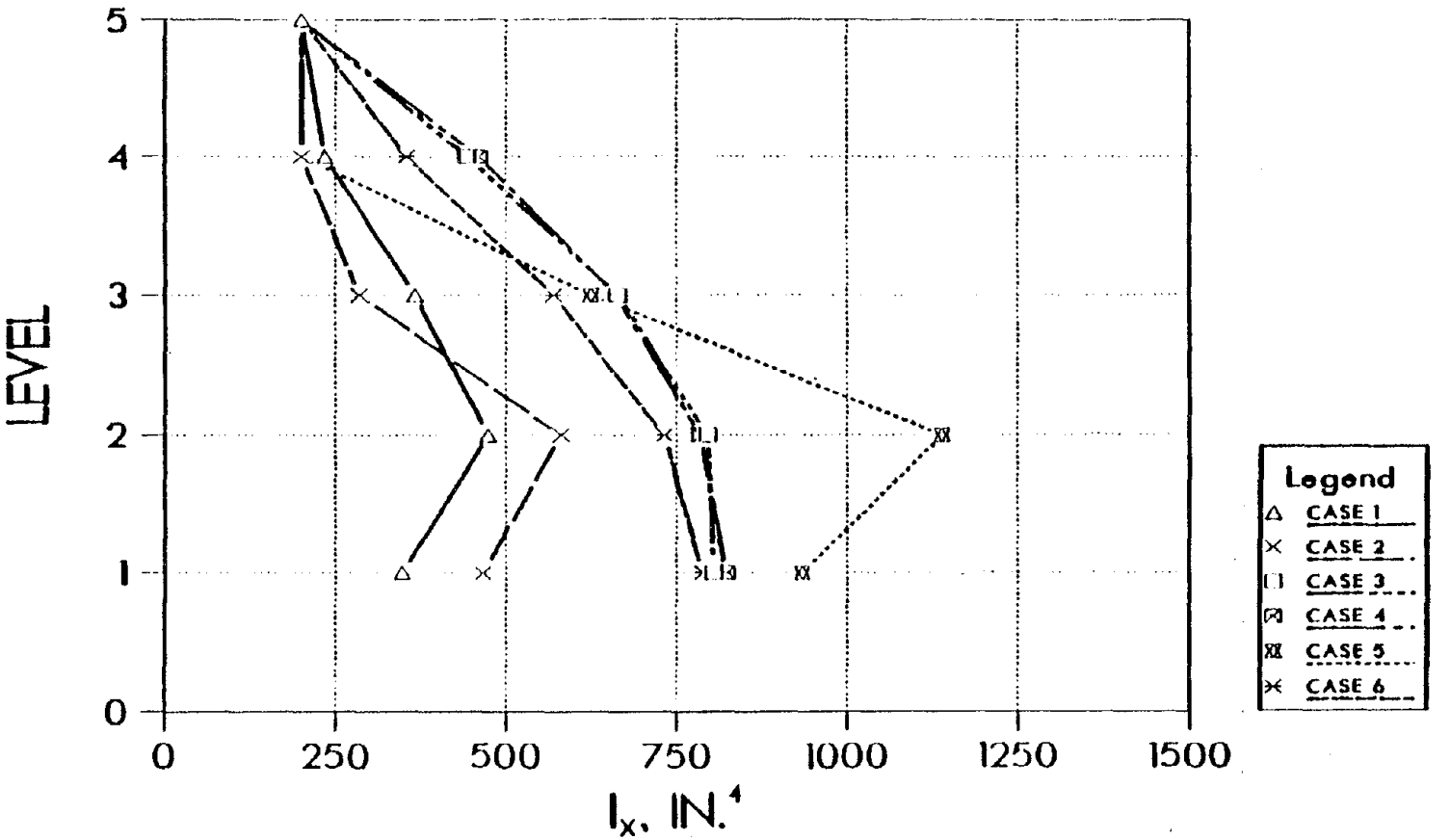

Figure 84. Beam Stiffness Distributions for the Five Story L-shaped Structure Subjected to Single and Multi-component Excitations (1 in = 2.54 cm)

mass center. (The center of rigidity is 33.1 feet (10.1 m) to the right and 14.5 feet (4.42 m) above column 1 in Figure 81.) This example has a rigidity center which is within the third quadrant of the reference system located at the mass center in Figure 81. Therefore, additional y-loading will help reduce the x-displacements. Since the x-displacements are active, a lighter structure is found for load case 3 compared to load case 4. The difference is very small since the rigidity center is close to the mass center, but in certain cases this can cause quite a large difference. As seen in Figures 83 and 84, the stiffness distributions are also nearly identical for load cases 3 and 4. If the y-component excitation were large enough to cause a y-displacement to become active the results of load case 3 and 4 would be different.

In order to explore this concept further, load case 6 was included where the center of rigidity is within the first quadrant of the mass center reference system. Loading 6 requires less weight than load case 3 because of the relative location of the mass center and center of rigidity. The y-component of load case 6 reduces the x-displacement without an increase in stiffness by creating a negative (clockwise) rotation about the center of rigidity. Load case 3 provides a small positive (clockwise) rotation about the center of rigidity which also helps to reduce the x-displacement as explained previously, but since its mass

center and stiffness center are close the effect is minimized. Since loading 6 had a different mass center its stiffness distribution was not included in Figures 82 and 83.

As in the case of loadings 1 and 2, load cases 4 and 5 can be compared. Load case 5 uses an external stiffness in the y-direction in order to simulate load case 4. From Figure 82 load cases 3, 4, and 5 produce nearly identical weights with the multi-component excitation (load case 3) providing a slightly smaller weight as explained previously. Load cases 4 and 5 have nearly identical final weights, but they optimized along different paths and have different active constraints. These results are similar to the comparison made with load cases 1 and 2. The difference comes from the effect of the external stiffness on the mode shapes used within the analysis. The y-components of the modes are suppressed providing load case 5 with three modes which are x and ϕ dependent. Figures 83 and 84 show a tremendous difference in the distribution of column and beam stiffness for the two cases even though the final weights are nearly identical. Load case 5 requires larger columns and beams below level 3 in order to control the displacement at that level while requiring less stiffness than load case 4 above level 3.

Figures 83 and 84 give the stiffness distributions for the first five loading cases. Each case requires large

first level columns with decreasing column sizes from bottom to top of each structure. Each optimization requires nearly identical column stiffnesses on the level of the active constraint and the level just below the active constraint. Also, it provides a large change in stiffness between levels of active constraints in order to allow the next level to displace to the active limit. These rigid first level columns reduce the need for large first level beams while the increased flexibility on the second level forces the beams to become large in order to stop excessive upper level displacements. All of the cases have passive beams on level 5, while, cases 1, 2, and 5 also have passive columns (200 in^4 = 8320 cm^4) on level 5. In addition, cases 2 and 5 have passive beams on level 4 and case 2, also, has passive columns on level 4. The trend is to stiffen the structures with large columns on the first level, and to stiffen the other levels with both the columns and beams.

Observations:

1. The relative location of the mass center and rigidity center can be helpful or detrimental to the optimal solution. The outcome is dependent upon their location as well as the type of constraints, number of seismic components, and the relative magnitudes of the seismic components.

2. The final results are heavily dependent upon the dominant components of loading. Cases 1 and 2 are dominated by the y component loads and provide active y-displacement constraints, where the other cases are dominated by the x-component loads and provide active x-displacement constraints.
3. Structures with external stiffnesses applied provided similar optimal weights, but different distributions of stiffness. They also produce different active constraints. This is due to the effect on the eigenmodes used in each analysis.
4. Each case requires large first level columns, and each case requires nearly identical column sizes on the level of and the level below an active constraint.
5. Each case also provides a large change in stiffness between levels of active constraints.
6. All six cases rapidly converged to an optimal solution. Each case terminated within four cycles due to less than a 5 percent change in weight.

3. Non-linked, Wide-flange System. This five-story, L-shaped structure was designed with respect to three separate loading cases. Wide-flange cross-sections were used with the major-axis orientation identical to that in Figure 85. The initial size of the columns and beams was 9500 in^4 (395,400 cm^4) for all levels. Each element was

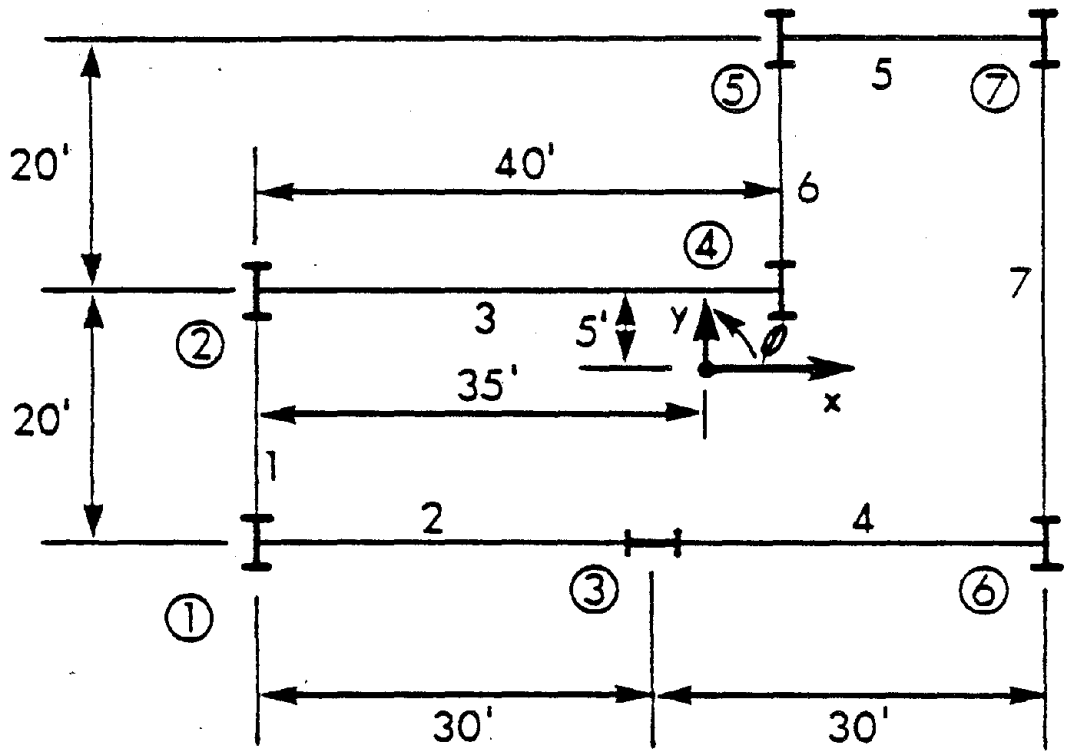

Figure 85. Five Story L-shaped Structure with Wide-flange Columns - Plan
(1' = .305m)

represented by Equations 3.15 to 3.29 and were forced to remain between 10 in^4 (416 cm^4) and 20,000 in^4 (832,000 cm^4). The constraints consisted of dynamic displacement constraints where the constraint value was determined as 0.45 in. (91.14 cm) per floor. All other values remain the same as those given in Section IX.J.1.

This structure was subjected to three separate load cases. The first case was to use 0.4g as the maximum ground acceleration in the x-direction, only. The second used maximum ground accelerations of 0.4g in the x-direction and 0.267g (2/3 of x) in the y-direction. The third used maximum ground accelerations of 0.4g in the x-direction and 0.267g for both the y- and z- (vertical) directions. A two-thirds factor was used based on a statement by Newmark and Hall in Reference 44. Essentially it states that the vertical motion response spectrum can be approximated by two-thirds times the horizontal motion response spectra. The modal analysis was performed with three modes and the same root of the sum of the squares method of modal superposition.

Initially each load case started with active x-displacement constraints on levels 2 through 4. The next cycle in each case added the fifth level x-displacement to the active set of constraints. Finally each loading produced active constraints in both the x- and y-directions as shown in Table XXV. The multi-component

TABLE XXV. Final Results for the Non-linked Five Story L-shaped Structure Subjected to Multi-component Seismic Loads (1 kip = 4.45 kN)

Excitation			Initial Wt.	Final Wt.	Active Constraints
x	y	z	(kips)	(kips)	
0.40g	-	-	274.1	108.2	x_4, x_5, y_4, y_5
0.40g	0.27g	-	261.7	135.6	x_4, x_5, y_2-y_5
0.40g	0.27g	0.27g	261.5	135.5	x_3-x_5, y_2-y_5

cases have additional y-displacement constraints, and the case with three components actually provides an additional x-displacement constraint. These solutions differ from the linked case given in Section IX.J.2. Due to the linking the y-displacements never became active even when three-fourths of the x-component load was applied in the y-direction. This will be discussed again in Section IX.J.3.

The final results are given in Figure 86 and Tables XXV to XXVIII. Table XXV provides a comparison of the weights and active constraints. Initially, the multi-component cases require a smaller initial weight. This is due to the fact that the rigidity center is located within the third quadrant of the global coordinate system. Therefore, the positive y-excitation causes a reduction in the x-displacements. Finally, the multi-component excited structures had nearly identical final weights which were approximately 25 percent larger than the single component excited structure. It is important to note that the center of rigidity for the non-linked structure is free to relocate on each level because of the redistribution of stiffness at each level for each cycle of optimization. The mass center on the other hand is assumed to remain fixed. As long as, the structural mass is small compared to the non-structural mass this assumption is valid. The convergence of each case is shown

TABLE XXVI. Final Stiffness Distribution for the Five Story L-shaped Structure Subjected to a Single Component Excitation (x=0.40g, y=0, z=0) (1 in^4 = 41.6 cm^4)

Columns (in^4)

Level \ ID	1	2	3	4	5	6	7
5	4039	1186	5778	1168	2339	4244	2455
4	7876	1228	6854	2188	4384	10864	3326
3	16631	1331	9106	1467	3489	4627	2979
2	17070	1389	8045	1966	6372	19220	6147
1	2621	984	20000	1043	2070	2380	1573

Beam (in^4)

Level \ ID	1	2	3	4	5	6	7
5	281	1564	217	1501	361	462	182
4	116	4367	401	4692	891	2164	199
3	10	7737	433	4827	928	2862	149
2	10	9715	478	6717	1174	400	96
1	50	9381	450	7300	914	154	141

TABLE XXVII. Final Stiffness Distribution for the Five Story L-shaped Structure Subjected to a Two Component Excitation (x=0.40g, y=0.27g, z=0) (1 in^4 = 41.6 cm^4)

Columns (in^4)

Level	ID 1	2	3	4	5	6	7
5	9235	2860	6736	3288	3556	6789	1898
4	10305	3913	8790	4068	4789	7697	2019
3	20000	4981	6472	4753	4929	14887	1612
2	20000	7503	12865	5487	5232	20000	2073
1	20000	20000	20000	6020	4547	4296	2417

Beam (in^4)

Level	ID 1	2	3	4	5	6	7
5	1833	2113	297	2395	314	2709	1095
4	5541	5760	543	7172	619	6895	894
3	8639	6697	541	7406	610	9612	879
2	12529	9065	621	9724	607	8184	664
1	9860	11601	790	7833	557	4323	727

TABLE XXVIII. Final Stiffness Distribution for the Five Story L-shaped Structure Subjected to a Three Component Excitation (x=0.40g, y=0.27g, z=0.27g) (1 in^4 = 41.6 cm^4)

Columns (in^4)

Level \ ID	1	2	3	4	5	6	7
5	9282	2866	6849	3227	3469	7320	1919
4	10247	3884	9195	3775	4100	7697	1840
3	20000	4836	6466	4750	4830	15916	1546
2	20000	6942	12846	5722	5023	20000	2243
1	20000	18544	20000	8807	5360	2254	1723

Beam (in^4)

Level \ ID	1	2	3	4	5	6	7
5	1856	2156	298	2448	313	2750	1172
4	5805	5953	531	7396	581	6000	835
3	8864	6749	524	7629	571	9046	847
2	12382	9008	584	9840	614	8247	680
1	9860	11692	776	7873	586	4586	739

in Figure 86. The increase in weight for the last cycle of the x-excitation case is due to a change in the active set of constraints. Each case was terminated due to less than a 5 percent change in weight.

The final distributions of stiffness are presented in Tables XXVI to XXVIII. These tables provide the necessary information to explore the affects of the multi-component excitation on the optimal structures. The x-only loading produces a structure which forms a strong frame using columns 1, 3, and 6 and beams 2 and 4. Note that beam 6 takes on substantial values at levels 3 and 4 in order to help resist the y-displacements. Keep in mind that column 3 is oriented such that its major-axis moment of inertia is used to resist the x-displacements, whereas the other columns are oriented such that their major-axis moments of inertia are primarily used to resist the y-deflections. Therefore, it was expected that column 3 would be an important element in resisting the x-displacements.

The multi-component systems produced nearly identical results to one another. The final results are slightly different as evidenced in Tables XXVII and XXVIII, but the trends are identical. Except for level 1, the dominant columns are again 1, 3, and 6 with beams 1, 2, 4 and 6. Columns 2, 4, and 5 also play an important role. Columns 1, 3, and 6 along with beams 2 and 4 are primarily used to

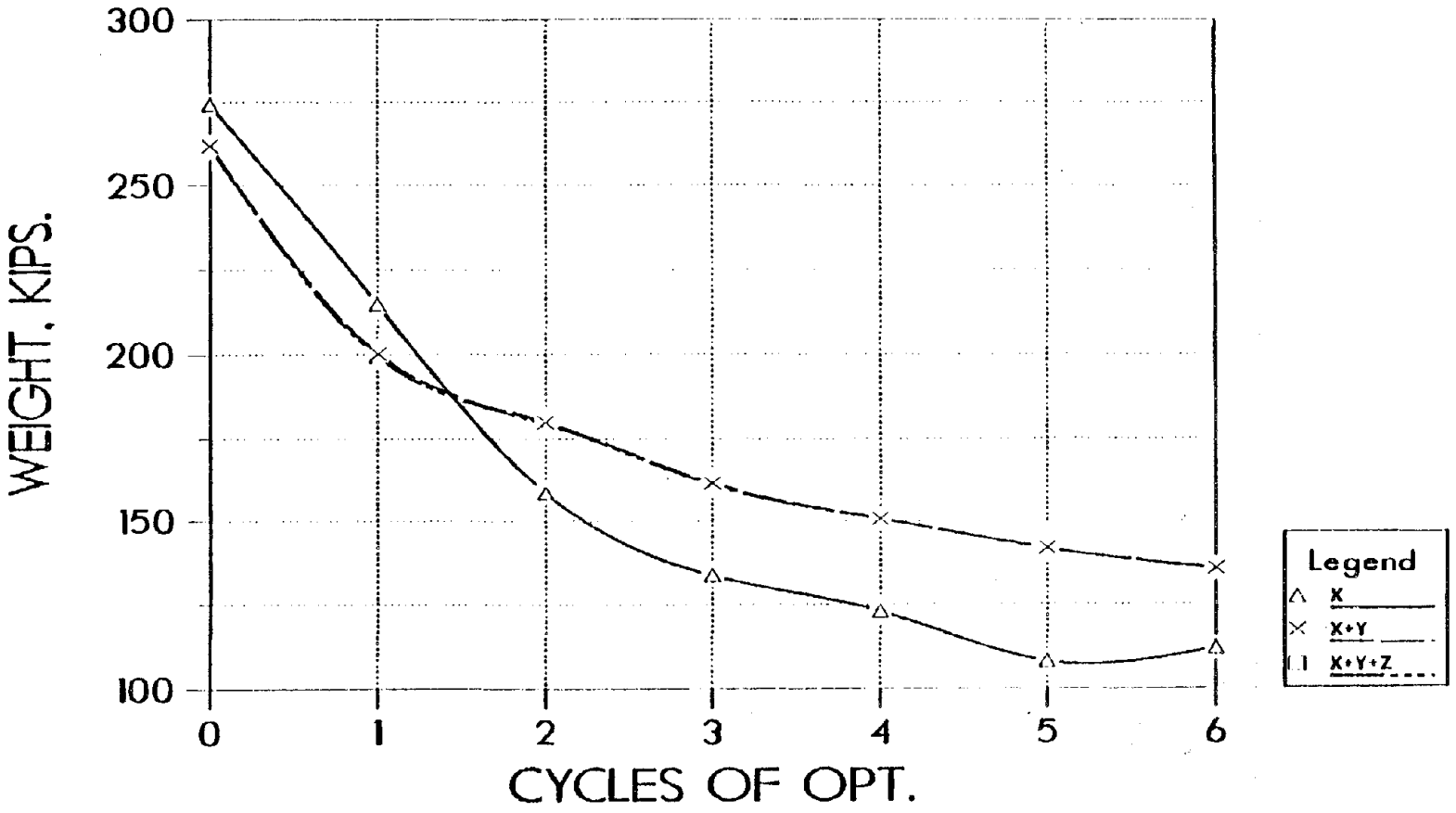

Figure 86. A Comparison of Weights for the Non-linked Five Story L-shaped Structure Subjected to Single and Multi-component Excitations (1 kip = 4.45 kN)

control the x-deflections, while columns 1, 2, 4, and 5 along with beams 1 and 6 are used to control the y-deflections. Due to the y-constraints becoming active at levels 2 through 5, beams 1 and 6 are of considerable size in order to help resist these deflections. Beam 7 was not a likely candidate for becoming a strong member due to its length which would require a larger moment of inertia in order to provide a similar resistance to that of beam 1 or 6, yet it doesn't become passive due to its location which help prevent the rotational effects from becoming large. Column 1 is critical for these loadings since it can be used effectively as part of the frame used to resist both sets of orthogonal deflection and at the same time force the rigidity center to be within the second quadrant. The effect of multi-component seismic excitation can be greatly attributed to the relative location of the mass center and the rigidity center.

The solutions try to provide resistances through the use of dominant bents. In addition to these strong frames, the optimization requires a lighter structural system by reducing the effects of the rotation about the center of rigidity. The center of rigidity is at a different location on each level. It is generally located within a quadrant of the mass center reference system which will provide the most active constraints for the given loading. The centers of rigidity are located in a fashion which

allows the y- and x-excitations to provide a reduction in the active constraint values allowing the structure to become lighter and to allow more constraints to become active. The square root of the sum of the squares does not allow the signs of the rotations to be determined, therefore it is difficult to predict exactly the effects of the location of the center of rigidity

These examples are very general and have several factors which may or may not affect the multi-component solutions. Equation 3.17 is used to provide the relationship of area with respect to the major-axis moment of inertia. This equation was developed as an upper bound for the wide-flange sections as given in the AISC Manual. Therefore, these areas could be overestimated and reducing the effects of the z-component load. Also, these examples used only three modes for the modal solution. These three modes although coupled do not include any modes directly associated with the vertical degrees of freedom. Possibly, the suppression of these modes also reduces the effect of the z-component loading. Most likely these modes will be within the higher modes with a very small period which would produce little effect. The period is effected by the mass and stiffness so possibly be increasing the mass and decreasing the area the vertical modes along with the vertical components could produce a larger difference between the x+y and x+y+z loading cases.

Observations:

1. The multi-component excitation provides larger optimal weights than the single component excitation when no linking is used.
2. Both multi-component loadings (x+y and x+y+z) provide nearly identical results. The effect of the vertical excitation on this structure are minimal. This is most likely due to the use of an elastic system.
3. Each system generated dominate bents to resist the deflections in the directions of active constraints. Certain elements definitely dominate the designs.
4. The continual relocation of the center of rigidity during the optimization allows the optimal systems to have many active constraints. Even the x-only loading produces active y-displacements at the upper two levels.
5. The dynamic response constrained problems converge rapidly and are terminated due to a small change in weight between cycles.

4. Linked, Wide-flange System. This structural system is identical to that used in the preceding section with the exception that linking is used. The initial data is exactly the same except that each level is required to have the same size columns throughout each level and the same size beams throughout each level. The

linking was used to stabilize the location of the rigidity center. Due to the orientation and linking of the columns, the rigidity center is located within the third quadrant of the mass center reference for each cycle and each level. Also, only the first two load cases of x-only and x+y were considered with the x-component being 0.40g and the y-component being 0.267g.

The final results for the linked, systems are given in Figure 87 and Table XXIX. The location of the center of rigidity allows the multi-component excited structure to continually produce results with less weight than the single component excitation as shown in Figure 87. The optimization of both systems have nearly parallel paths. This is a result of the column orientation. Most of the major axes are oriented to resist translation in the y-direction. This coupled with the linking of the columns produces active constraints only in the x-direction, therefore the only effect of the y-component loading is to reduce the deflection in the x-direction of the mass center due to the rotation about the rigidity center. (Since the minor axis of inertia needs to be fairly large in order to resist the x-deflections, the major axis moment of inertia must also be large according to Equation 3.15, therefore, none of the y-displacements become active.)

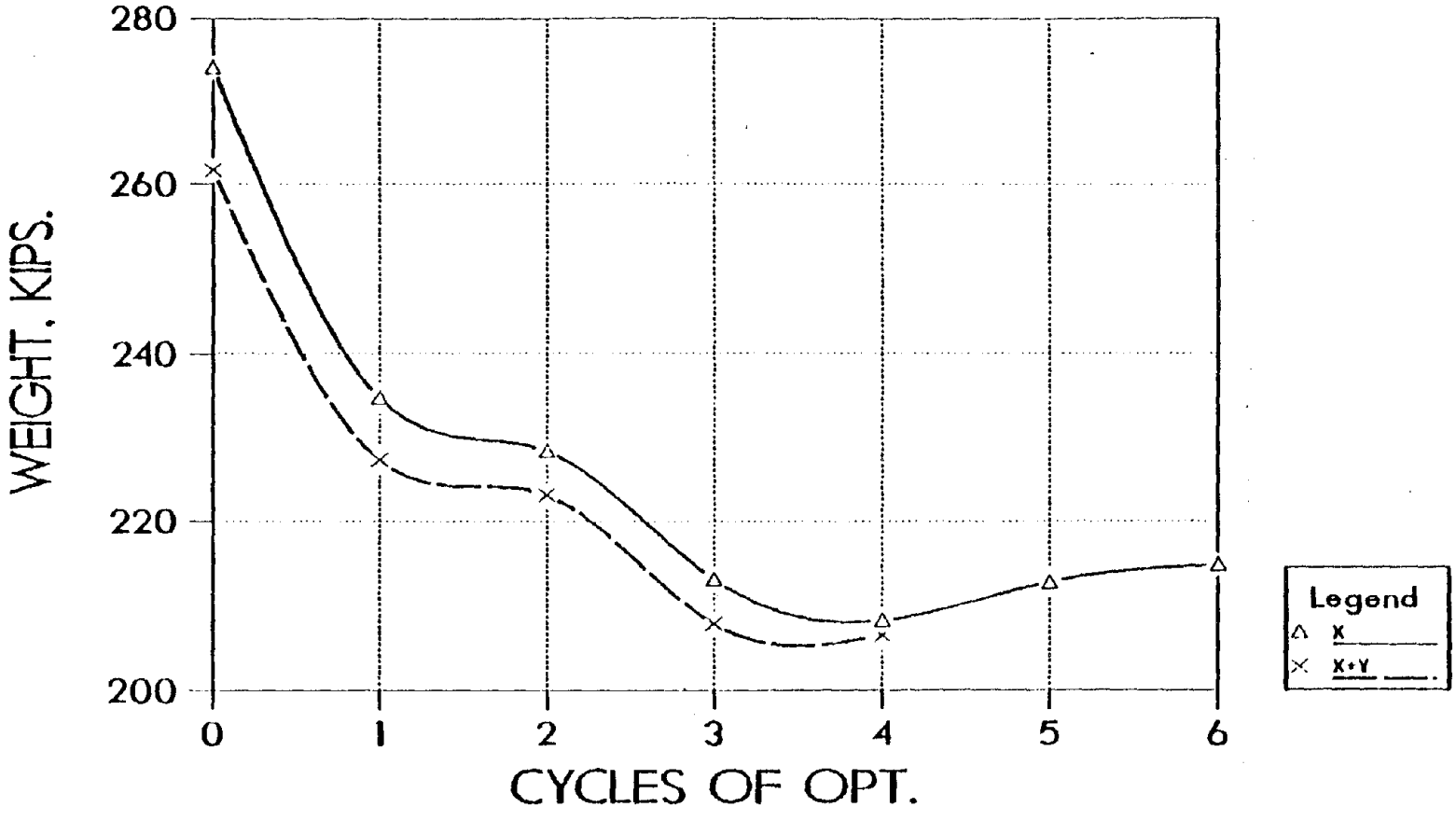

Figure 87. A Comparison of Weights for the Linked Five Story L-shaped Structure Subjected to Single and Multi-component Excitations
(1 kip = 4.45 kN)

TABLE XXIX. Comparison of Results for the Linked and Non-linked Five Story L-shaped Structure Subjected to Multi-component Seismic Loads (1 kip=4.45 kN)

Excitation		Linked	Initial Wt.	Final Wt.	Active Constraints
x	y		(kips)	(kips)	
0.40g	-	No	274.1	108.2	x_4, x_5, y_4, y_5
0.40g	-	Yes	274.1	208.2	x_2-x_5
0.40g	0.27g	No	261.7	135.6	x_4, x_5, y_2-y_5
0.40g	0.27g	Yes	261.7	206.5	x_2-x_5

The final results and comparison to the non-linked cases are given in Tables XXIX. The single component, linked case gives a final weight of 208.2 kips (94.3 Mg) which is a 92 percent increase over the non-linked case, while the multi-component, linked case provides a final weight of 206.5 kips (93.5 Mg) or a 52 percent increase over the non-linked case. Each linked system had a set of active constraints consisting of the x-displacements on levels 2 through 5. The y-displacements were approximately 7 to 10 percent of the limiting values for both of the linked cases. This is where the additional weight is accumulated. The non-linked cases allowed several of the elements to become quite small in order to allow the y-displacements to become active. The linking and orientation of the columns provide a distribution of stiffness which will not allow this to occur for the linked cases.

The stiffness distribution per level is shown in Figure 88. As seen in most linked cases the final results provide a strong column-weak beam syste. The beams for the two linked cases are nearly identical, but the columns are slightly different. Levels 3, 4, and 5 provide the most significant differences in stiffness. This is due to the accumulative effects of the positive rotations associated with the additional y-excitation. This effect helps reduce the upper level x-displacements and, therefore, requires less stiffness at these levels. Generally,

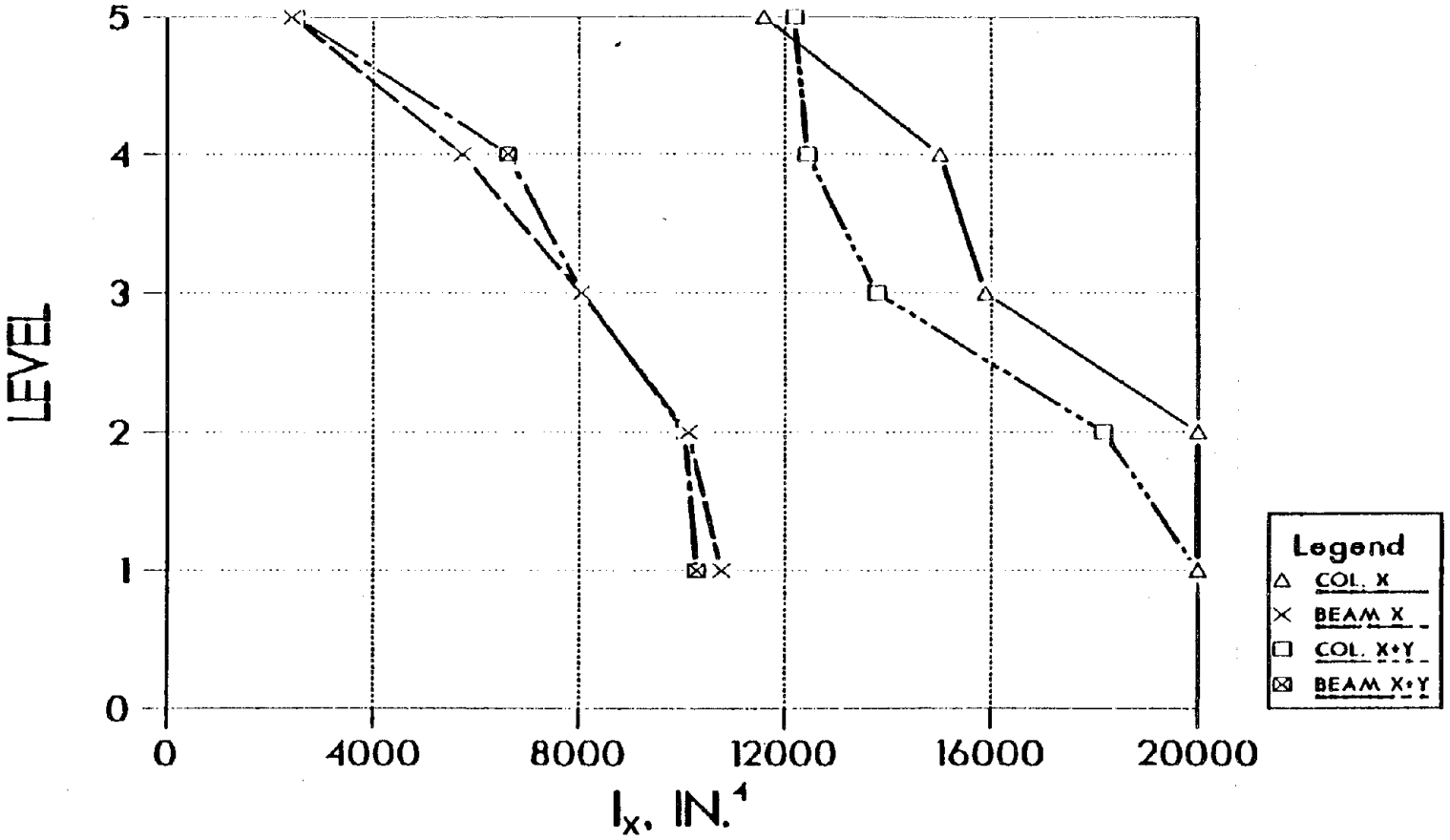

Figure 88. Stiffness Distributions for the Linked Five Story L-shaped Structure Subjected to Single and Multi-component Excitations
(1 in = 2.54 cm)

both cases provide the same design with no large changes in stiffness.

These results point out the fact that a new design is in order. A lighter structure could be obtained by reorienting several of the columns such that their major-axis moment of inertia would help to resist the x-deflections. This reorientation would most likely let several of the y-deflections become active providing a better balance in resistance.

Observations:

1. The multi-component linked system produces a lighter structure than the single-component linked system. This is due to the location of the rigidity center.
2. The orientation of the columns precludes any y-displacements from becoming active within the linked systems.
3. Both linked cases provide similar stiffness distributions with a slight reduction in the multi-component solution.
4. The linked cases provide solutions which are much heavier than the non-linked case. This is due to the fact that the linked cases cannot allow the y-displacements to become active without violating the x-displacement constraints.

5. These results suggest that a lighter structure could be obtained by reorienting several of the columns such that their major-axis moment of inertia would help resist the x-deflections.
6. The optimization of the structures occurs rapidly with each system terminating due to a small change in the weight between cycles.

X. OBSERVATIONS, REMARKS, AND RECOMMENDATIONS

The examples within Chapters VIII and IX were optimized and designed using an optimality criteria approach to structural optimization as presented in Chapters V and VI. Structural optimization provides a consistent means of studying and comparing the effects of structural-related parameters. In this vein, a three-dimensional structural optimization computer program ODRESB-3D, (Optimum Design of 3-Dimensional Reinforced-Concrete and Steel Buildings), was developed. The program has both static and dynamic capabilities. This was the tool used to study the effects of several structural and optimization parameters such as: types of constraints, combinations of constraints, types of objective functions, combinations of elements, irregularities in structures, effects of multi-component excitation, effect of ATC-03 parameters, and effects of analysis techniques. The results of Chapters VIII and IX will be consolidated and discussed within this chapter.

The primary objective was to develop an efficient means for the optimization of three-dimensional structural systems subjected to multiple types of constraints and different analysis techniques. As seen in the examples presented, the program is capable of optimizing a structure subjected to any combination of static displacement and stress, dynamic displacement and stress,

and frequency constraints. The use of frequency constraints with other types of constraints is more difficult than the combinations of stress and displacement constraints. In certain instances, a structure cannot be optimized when several restrictive frequency constraints are combined with other constraints. This situation implies that the structural geometry given cannot provide a system which would satisfy the frequency coupled with other constraints. Generally, the fewer and less restrictive the frequency constraints, the higher the probability of reaching an optimal solution. The use of frequency constraints is extremely helpful in keeping a structural system within a specific region of the response spectra used for a dynamic analysis. The use of strictly frequency constraints is very effective if the upper and lower limits on the frequencies do not represent an impossible situation. They are best used when the initial design provides natural frequencies which are reasonably close to the limits set for the optimization. The control of these natural frequency constraints and their combinations with other constraint types is an area where additional research is and should be pursued with respect to structural optimization.

The algorithm presented does provide an efficient means of optimizing three-dimensional structural systems. As seen within the examples presented, the algorithm

converges rapidly and monotonically for most systems. The rate of convergence of each problem must be examined independently since it is dependent upon the initial design, the convergence control parameter, the bandwidth for the active constraints, the type of constraints, the type of elements, the secondary to primary design variable relationships, and the type of analysis. Certain situations can cause a non-monotonic convergence. These situations are related to cases with a large number of highly restrictive constraints, a small convergence control parameter, or a numerical discontinuity. The highly restrictive set of constraints creates a "small" feasible design space which can cause optimality criteria algorithms to have a fluctuating set of active constraints. The nonconsistency of the constraints can cause some fluctuation within the convergence. Small convergence control parameters create a situation where the design variables change too rapidly which can cause constraint violation between cycles of optimization. A convergence control parameter of 2 has been acceptable for nearly all of the problems solved. Two types of numerical discontinuities can occur which will cause a non-monotonic convergence. The most common occurs when using the ATC-03 analysis procedures. When the fundamental period of a structural system fluctuates, during successive cycles of optimization, above and below the ATC-03 limit for the

fundamental period, a discontinuous situation arises where different periods are used in successive analyses. Therefore, the gradients based on the previous analysis cannot guarantee the control of the constraints within the next analysis using the new period. The second type of discontinuity occurs when stress constraints are used. If the element with the active stress constraint is near a discontinuity in the relationship between the secondary and primary design variables, a situation occurs where the stress constraint is not maintained during successive cycles of optimization. This second type of discontinuity rarely occurs. In most instances the algorithm will adjust and continue to optimize. The oscillatory convergence can be controlled by changing the appropriate parameters to avoid these situations. Most of the examples presented converge to a solution within eight to ten cycles with several converging as fast as two cycles. These examples provided initial to final weight changes of anywhere from 100 percent to 10 percent. Overall, the proposed algorithm is very efficient and quite capable of handling a variety of constraints.

A major asset of structural optimization is its ability to be used as a design tool. Each optimization of a structural system provides a series of designs (one for each cycle) which satisfy all of the design constraints. Every intermediate and final design of every

example was a feasible design solution which satisfied the constraints of that specific structural system. Theoretically, the final optimization cycle produces the "best" design for the given objective function subject to the applied constraints. In order to make the algorithm a useful design tool, side constraints and linking were provided. Realistic designs have certain limitations on the sizes for specific elements (side constraints), and they also use the same size elements for more than one element (linking). With these features included, the program becomes a useful tool for design. The structural optimization program is much more efficient and reliable than the current methods of intuitively readjusting and reanalyzing a given system. The current methods of design cannot guarantee that the constraints will be satisfied, whereas, the structural optimization resizes the elements based upon the effects of the critical constraints (gradients) and always produces a feasible design. Therefore, a single optimization provides a series of feasible design with each successive design being better than the previous. Another approach is to use a series of complete optimizations to produce increasingly better designs. After each optimization is completed changes can be made in the constraints, geometry, and optimal sizes in order to start a new optimization which will produce a better optimal design

than the previous optimization. For instance, if only the displacements in one direction are active after the first complete optimization, a better solution might result if certain columns are reoriented to produce a system where the displacements in two directions became active. After reorienting certain columns a new optimization is performed with a better solution. Due to the guaranteed feasible solution and the production of a series of designs, a structural optimization program such as ODRESB-3D can produce a series of reasonable designs with less time and effort than the current intuitive, reiteration techniques. This program in no way replaces structural designers, but is another tool at their disposal.

ODRESB-3D allows the flexibility of using any objective function which is based on the volume of structural steel and concrete used within the building system. Using cost information taken from the Means Cost Data For Building Construction, average costs per unit volume for steel and concrete elements were generated. A comparison of optimal results for the cost and weight objective functions was performed. It was found that the cost and weight objectives provide nearly identical stiffness distributions and nearly identical optimal weights. Since the results were so similar, the weight objective function was considered to be an adequate

representation for the cost objective function, and it was used for the majority of the examples. This would be acceptable as long as a preliminary design was the ultimate goal, but a final design could use more refined estimates of the cost per volume along with the cost function for a final design. Cheng and associates have been working on a variety of more complex objective functions for the two-dimensional systems. These objective functions have not been used with the three-dimensional systems to date.

Several examples were used to compare the results of using the ATC-03 analysis techniques. In all cases the ATC-03 modal analysis produced lighter optimal solutions than the equivalent lateral force procedure. The modal analysis also used the same or less number of cycles than equivalent lateral force methods to reach the optimal solution. Each type of analysis produced nearly identical stiffness distributions regardless of any plan or vertical discontinuities. This contradicts the statements within the ATC-03 provisions which suggest that the modal analysis procedure be used for any irregular structures. The equivalent lateral force procedure did show some irregularity in the stability coefficients, but these were still twenty percent of the ATC-03 maximum limit and of little consequence. All other parameters for both analysis techniques were

similar except the modal analysis provided less weight, lower drifts, and a smooth curve for the stability factors. These factors tend to support the use of the ATC-03 modal analysis but these factors have no connection to the fact that the structures are irregular. On the other hand, the equivalent lateral force method requires less computations and produces the same distribution of stiffness. The choice of which analysis to use seems to depend upon the importance of less weight or less computations not on the structural configuration.

A structure with vertical irregularities was used to explore the effects of their locations on the stiffness distribution. The irregularity was an increase in story height for two consecutive levels within the structure. As the location of these two tall stories was moved from top to bottom, it was found that the location had very little effect on the optimal structure weight. The lightest structure was found when the irregularity was at the upper two levels, and the heaviest structure was found when the irregularities were at the first levels above the base. Both ATC-03 analysis techniques provided similar stiffness distributions with the taller stories requiring large increases in stiffness at the locations with the tall stories. The beams tend to have a large increase in stiffness with a linear transition through the irregular portion of the

structure, whereas the columns tend to have a large increase with a nearly constant value through the irregular portion of the structure. The members above the irregularity have almost identical sizes for all cases, and parallel stiffness distributions below the irregularity. As the irregular stories are moved upwards in the structure the stiffness distributions are enclosed by an envelope with the lower bound being the curves of the distributions above the irregularities and by an upper bound formed by the large stiffness required by the irregularities. Therefore, the vertical irregularities tend to have a very localized affect on the stiffness which produces a series of results with similar weights.

A structure with two setback portions was used to explore the effects of vertical irregularities and the effects of linking columns above and below the first level of each setback portion. The first analysis was performed using linking of the columns on each level and linking the beams on each level (one column size per floor and one beam size per floor). The second analysis was performed where multiple level linking of the columns was used such that the same size column was used above and below the level where each setback began. The linking produced a slightly heavier system (six percent) but it used considerably less computations and produced a more realistic design. The vertical

irregularities created an irregular stiffness distribution along the height of the strucuture, whereas the linking created a system which was essentially an average of the irregular distribution. One significant contribution was a large decrease in the size of the first level column size. In general, the effect of the vertical irregularity was greatly minimized by using a continuous column size through at least the first level of the discontinuity.

Many of the examples were also used to explore the effects of various ATC-03 parameters on the optimal solutions of various building systems. All of these examples were based upon map areas which were larger than four for the effective peak acceleration and the effective peak velocity-related acceleration. Within the analyses performed the effective peak velocity-related acceleration and the soil conditions were the dominate factors. The effective peak acceleration had little or no effect on the solutions. These factors dominated due to the equations used for the base shear. All but one of the test structures had a calculated period above the ATC-03 limit. Note that as a structure is optimized, it generally becomes less stiff and the period increases or remains nearly constant. If the equivalent lateral force method is used it appears that a frequency analysis is not needed, but the algorithm should use the ATC-03 empirically determined

period directly. This creates a situation where the base shear formula which includes the effective peak velocity-related acceleration and the coefficient for the soil type was used in all instances. The optimal solutions for each structure with a variation in soil and/or effective peak velocity-related acceleration are nearly identical within an appropriate factor. The base shear equation includes the direct multiplication of the soil coefficient and the effective peak velocity-related acceleration which provides the approximate factors for comparison. It will not be an exact factor since the solution is dependent upon the optimization history. The ATC-03 drift is based upon an elastic representation of a psuedo-inelastic limit. It was found that this psuedo-inelastic drift could be controlled by using an elastic displacement constraint which was approximately 80 percent of the inelastic drift divided by the ATC-03 response modification factor. Most examples satisfy the ATC-03 drifts using these displacement constraints and generally the largest drift occurs at the level below the lowest level with an active displacement constraint. The ATC-03 stability factor was also checked for each optimal stiffness distribution. In all cases consider the stability factor never went above sixty percent of the maximum value, and in most cases it was below thirty percent of the maximum value. As the map area numbers decreased the optimal structures became

less stiff, therefore producing the larger stability factors. Possibly, if map areas below four were used these factors would become more significant.

In addition to the ATC-03 analysis procedures, a set of structures was subjected to a response spectra modal analysis. These examples were used to study the effects of multi-component excitations. It was found that the final results were heavily dependent upon the dominant component of the horizontal excitations with little effect from the vertical excitations. Also, the orientation of columns and the use of linking had significant effects on the solutions. The orientation of the columns affects the solutions by providing more or less total stiffness in a certain direction, as well as fixing a location of the center of rigidity if linking is used. If linking of columns on a per level basis is not used, the center of rigidity is free to relocate during each cycle of the optimization. The location of this rigidity center can be helpful or detrimental in constraining the displacements of the mass center depending upon their location relative to one another. In general, when linking is not used multi-component excitations provide larger optimal weights than the single components. When linking is used either of the cases multi-component or single component can produce a lighter system depending upon the location of the center of rigidity, the type of constraints, the magnitude of

component excitations, and the direction of the seismic components. The nonlinked systems are lighter than the linked systems since the center of rigidity is free to relocate on each level during the optimization. These nonlinked systems use the component of the excitation along with the location of the center of rigidity to have more active constraints and a more flexible system which is lighter than the linked systems. Within the multi-component excitations, the vertical component had little effect. This may be due to the structural systems designed were not tall and the longitudinal stiffnesses were not reduced when bending was considered. However the studies on inelastic models reported a greater effect with respect to vertical excitation. These modal analysis examples converge very rapidly and monotonically, but they require a large amount of computational effort. This optimization procedure requires the gradients of the eigenvector which requires the inversion of the $[[K]-\omega^2[M]]$ matrix for each eigenmode used in the analysis for each cycle of optimization. It is much more economical to use the ATC-03 procedures if possible.

A few general comments with respect to the linked and nonlinked solution are needed. The nonlinked systems produce unrealistic results in most cases. By trying to achieve the lightest structure they produce strong bents within the system while letting the other elements become as small as possible. This type of result does provide

some useful information as to which elements are most important in maintaining the active constraint for that combinations of loading. This information can be useful in determining major bents to be used to resist lateral loads. Linking is extremely useful for providing realistic designs. It generally reduces the number of cycles required for convergence in addition to producing realistic results.

Several of these areas could be researched in greater detail. The combination of frequency constraints with other constraints creates a difficult situation for finding solutions, therefore a series of guidelines or an adjustment to the algorithm might be studied. The use of only frequency constraints combined with modal analysis might be explored as a possible means of controlling dynamic response without additional constraints. Parametric studies of optimized regular systems might be considered in order to generate specific design aids. Optimization of irregular structures, both in plan and elevation, need to be studied with respect to ATC-03 analyses and modal analysis. Possibly these would generate some design aids and reinforce the idea that the ATC-03 modal analysis and equivalent lateral force methods produce similar results. It would be worthwhile to complete the required theory and implementation to constrain the center of rigidity rather than the mass

center. This theory would have to include the ability to let this center of rigidity move during each cycle of optimization. It would also be worthwhile to provide an efficient structural optimization algorithm for inelastic analysis.

Structural optimization, specifically the presented algorithm provides a consistent means for studying and comparing the effects of structural-related parameters. There are a multitude of topics that can be explored through structural optimization above and beyond the areas considered within this dissertation. The development of ODRESB-3D a three-dimensional structural optimization program with the ability to handle a variety of combinations of elements, analyses, materials and constraints should be a significant and worthwhile contribution to be used within the research and design of structural systems.

BIBLIOGRAPHY

1. Venkayya, V. B., "Design of Optimum Structures," J. Comp. Struct., 1971, pp. 265-324.
2. Venkayya, V. B., "Structural Optimization: A Review and Some Recommendations," Intl. J. Num. Methods Eng., 13, 1978.
3. Cheng, F. Y., V. B. Venkayya, N. Khachaturian, et al., Computer Methods of Optimum Structural Design, Short Course Notes, Vols. 1 and 2, University of Missouri-Rolla, Rolla, MO, 1976.
4. Feng, T. T., J. S. Arora, and J. E. Haug, "Optimum Structural Design Under Dynamic Loads," Intl. J. Num. Methods Eng., 11, 1977, pp. 39-52.
5. Pierson, B. L., "A Survey of Optimal Structural Design Under Dynamic Constraints," Intl. J. Num. Methods Eng., 4, 1972, pp. 491-499.
6. Khot, N. S., V. B. Venkayya, C. D. Johnson, and V. A. Tischler, "Application of Optimality Criterion to Fiber Reinforced Composites," AFFDL-TR-73-6, 1973.
7. Venkayya, V. B., N. S. Khot, and L. Berke, "Application of Optimality Criteria Approaches to Automated Design of Large Practical Structures," AGARD 2nd Symp. on Structural Optimization, No. 123, Milan, Italy, April 2-6, 1973.

8. Venkayya, V. B. and N. S. Khot, "Design of Optimum Structures to Impulse Type Loading," Am. Inst. Aeronaut. Astronautics J., 13 (8), 1975, pp. 989-994.

9. Venkayya, V. B. and F. Y. Cheng, "Resizing of Frames Subjected to Ground Motion," Proc. Intl. Symp. on Earthquake Structural Engineering, University of Missouri-Rolla, 1, August 1976, pp. 597-612.

10. Cheng, F. Y. and D. Srifuengfung, "Earthquake Structural Design Based on Optimality Criterion," in Vol. 5, Earthquake Resistant Design, Proc. 6th World Con. on Earthquake Engineering, New Delhi, India, January 1977.

11. Cheng, F. Y., D. Srifuengfung and L. H. Sheng, ODSEWS--Optimum Design of Static, Earthquake and Wind Steel Structures, Report prepared for the National Science Foundation, 1981. Available at the U.S. Department of Commerce, NTIS, Springfield, VA 22151, PB81-232738.

12. Cheng, F. Y., and D. Srifuengfung, "Optimum Structural Design for Simultaneous Multicomponent Static and Dynamic Inputs," Intl. J. for Num. Methods in Eng., Vol. 13, No. 2, 1978, pp. 353-372.

13. Cheng, F. Y., and D. Srifuengfung, "Discussion on Optimality Criteria for Seismic Tall Buildings with Specific Natural Frequencies", Proc. of 5th Japan Earthquake Engineering Symposium, 1978, pp. 1249-1256.

14. Kato, B., Y. Nakamura, and H. Anvoka, "Optimum Earthquake Design of Shear Buildings," J. Struct. Div., Am. Soc. Civil Engrs., 98, (EM4), August 1972, pp. 891-909.

15. Solnes, J. and O. L. Holst, "Optimization of Framed Structures Under Earthquake Loads," 5th World Conf. on Earthquake Engineering, Paper No. 376, Rome, Italy, 1973.

16. Cheng, F. Y. and M. E. Botkin, "Nonlinear Optimum Design of Dynamic Damped Frames," J. Struct. Div., Am. Soc. Civil Engrs., 102 (ST3), March 1976, pp. 609-628.

17. Cheng, F. Y. and M. E. Botkin, "P-Δ Effect of Optimum Design of Dynamic Tall Buildings," published by ASCE-IABSE Joint Committee for Regional Conference on Tall Buildings, January 23-25, 1974, pp. 621-632.

18. Ray, D., K. S. Pister, and E. Polak, "Sensitivity Analysis for Hysteretic Dynamic Systems: Theory and Applications," EERC Rept. 76-12, University of California, Berkeley, 1976.

19. Walker, N. D. and K. G. Pister, "Study of a Method of Feasible Directions for Optimal Elastic Design of Framed Structures Subjected to Earthquake Loading," Rept. EERC 75-39, University of California, Berkeley, 1975.

20. Bhatti, M. A. and K. S. Pister, "Application of Optimum Design to Structures Subjected to Earthquake Loading," in Optimization of Distributed Parameter Structural Systems, Vol. 1, Sijthhoff and Hoordhoff International, 1981.

21. Cheng, F. Y., "Optimum Design of Seismic Structures with Risk Consideration," paper #10, Proceeding of the U.S.-Japan Joint Seminar on Seismic Risk and its Use in Code Formulation, March, 1983.

22. Cheng, F. Y. and C. C. Chang, "Optimality Criteria for Safety-Based Design," Proc. the 5th ASCE-EMD Specialty Conference, 1984, Vol. 1, pp. 33-37.

23. Cheng, F. Y. and K. B. Oster, Dynamic Instability and Ultimate Capacity of Inelastic Systems Parametrically Excited by Earthquakes--Part II. Tech. Rept. National Science Foundation, Natl. Tech. Inf. Service, U.S. Dept. Commerce, PB261097/AS, 1976.

24. Cheng, F. Y. and K. Oster, "Ultimate Instability of Earthquake Structures," Journal of the Structural Division, American Society of Civil Engineers, Vol. 102, pp. 961-972.

25. Iyengar, R. N. and M. Shinozuka, "Effect of Self-Weight and Vertical Acceleration on the Behavior of Tall Structures During an Earthquake" in Earthquake Engineering and Structural Dynamics, July-September 1972.

26. Cheng, F. Y. and P. Kitipitayangkul, Investigation of the Effect of 3-D Parametric Earthquake Motions on Stability of Elastic and Inelastic Building Systems, Final Report prepared for the National Science Foundation. Available at the U.S. Department of Commerce, National Technical Information Service, Springfield, VA 22151, PB80, 176936, 1979.

27. Cheng, F. Y., "Inelastic Analysis of 3-D Mixed Steel and Reinforced Concrete Seismic Building Systems," J. Comp. Struct., 13, 1981, pp. 189-196.

28. Cheng, F. Y., "Inelastic Analysis of Dynamic Space Frames," Proc. 7th National Conference on Electronic Computations, American Society of Civil Engineers, 1979, pp. 537-552.

29. Proceedings of the 5th, 6th, and 7th World Conferences on Earthquake Engineering, 1972, 1976, 1980.

30. National Science Foundation RANN-Research Applications Directorate, "Earthquake Prediction and Hazard Mitigation Options for USGS and NSF Programs," September, 1976.

31. Universities Council for Earthquake Engineering Research, Proc. 4th Natl. Mtg., June 1976.

32. Kirsch, J., Optimum Structural Design: Concepts, Methods and Applications, New York, McGraw-Hill Book Company, 1981.

33. Haug, E. J. and J. S. Arora, Applied Optimal Design, New York, John Wiley and Sons, 1979.

34. Cheng, F. Y. and P. Kitipitayangkul, "INRESB-3D, A Computer Program for Inelastic Analysis of Reinforced-Concrete Steel Buildings Subjected to 3-Dimensional Ground Motions," Report No. 2, Civil Engineering Study Structural Series 79-11, University of Missouri-Rolla, Rolla, MO, August 1979.

35. ATC-03-06, Tentative Provisions for the Development of Seismic Regulations for Buildings, prepared by the Applied Technology Council, National Science Foundation and National Bureau of Standards, NBS Special Publication 510, NSF Publication 78-8, June 1978.

36. Wang, C. K., and C. G. Salmon, Reinforced Concrete Design, New York, Harper & Row Publishers, 1979.

37. Morris, A. J., Foundations of Structural Optimization: A Unified Approach, New York, John Wiley and Sons, 1982.

38. Cheng, F. Y., and L. H. Sheng, "Polynomial Curves for AISC Sections", Unpublished Report, 1981.

39. American Institute of Steel Construction Manual, Seventh and Eighth Editions, Chicago, American Institute of Steel Construction, 1973 and 1980.

40. Cheng, F. Y., "Computer Methods of Seismic Structural Analysis," Short Course, Lectures 10 and 11, University of Missouri-Rolla, Rolla, MO, May 7-11, 1979.

41. Bathe, K. J. and E. L. Wilson, Numerical Methods in Finite Element Analysis, Englewood Cliffs, New Jersey, Prentice-Hall, Inc., 1976.

42. Clough, Ray and J. Penzien, Dynamics of Structures, New York, McGraw-Hill Book Company, 1975.

43. Gould, P. L. and S. H. Abu-Sitta, Dynamic Response of Structures to Wind and Earthquake Loading, New York, John Wiley and Sons, 1980.

44. Newmark, N. M. and W. J. Hall, Earthquake Spectra and Design, Berkeley, Earthquake Engineering Research Institute, 1982.

45. Bazarra, Mokhtar and C. M. Shetty, Nonlinear Programming: Theory and Algorithms, New York, John Wiley and Sons, 1979.

46. Monsey, A., Interview at Washington University, St. Louis, MO, December, 1983.

47. Building Construction Cost Data 1984, Annual Edition, Duxbury, Mass., Robert Snow Means Company, Inc., 1984.

48. Khot, N. S., L. Berke, and V. B. Venkayya, "Comparison of Optimality Criteria Algorithms for Minimum Weight Design of Structures," AIAA Journal, Vol. 17, Feb. 1979, pp. 182-190.

49. Fox, R. L., and M. P. Kapoor, "Rates of Change of Eigenvalues and Eigenvectors," AIAA Journal, Vol. 6, No. 12, Dec. 1968, pp. 2426-2429.

50. Rogers, L. C., "Derivatives of Eigenvalues and Eigenvectors," AIAA Journal, Vol. 6, No. 5, May, 1970, pp. 943-944.

51. Plout, R. H. and K. Hussin, "Derivatives of Eigenvalues and Eigenvectors in Non-self Adjoint Systems," AIAA Journal, Vol. 11, No. 2, Feb. 1973, pp. 250-251.

52. Rudsill, C. S., "Derivatives of Eigenvalues and Eigenvectors for a General Matrix," AIAA Journal, Vol. 12, No. 5, May 1974, pp. 721-722.

53. Cheng, F. Y. and K. Truman, "ODRESB-3D, User's Manual of A Computer Program for Structural Optimization of Reinforced-Concrete and Steel Buildings for Static and Dynamic Loads," Structural Series 85-21, UMR, NSF Report 1985.

54. Seed, H.B., C. Ugas, and J. Lysmer, "Site Dependent Spectra for Earthquake-Resistant Design," Bulletin of the Seismological Society of America, Vol. 66, No. 1, February, 1976, pp. 221-244.

55. Cheng, F. Y. and Juang, D. S., "Assessment of ATC-03 for Steel Structures Based on Optimization Algorithm", Proceedings of the 8th World Conference, Vol. V, 1984, pp. 475-482.

56. Cheng, F. Y., "Evaluation of Frame Systems Based on Optimality Criteria with Multicomponent Seismic Inputs, Performance Constraints, and P-Δ Effect," published in Vol. I of the NSF-NATO Advanced Study Institute on Optimization of Distributed Parameter Structural Systems, Sijthoff & Noordhoff International, 1980, pp. 650-684.

57. Cheng, F. Y., and K. Z. Truman, "Optimization of 3-D Building Systems for Static and Seismic Loading", Modeling and Simulation in Engineering, Vol. III, New York, North-Holland Publishing Company, 1983, pp. 315-326.

58. Truman, K. Z., and F. Y. Cheng, "Optimum Design of Building Systems", Proceedings of the 4th ASCE-EMD Specialty Conference, Vol. I, 1983, pp. 98-101.

59. Truman, K. Z. and F. Y. Cheng, "Optimum Design of Steel and Reinforced Concrete 3-D Seismic Building Systems", Proceedings of the 8th World Conf. on Earthquake Engineering, Vol. V, 1984, pp. 475-482.

APPENDICES

APPENDIX A

MASS MOMENTS OF INERTIA OR ROTATORY MASS INERTIA AND THE TRANSFORMATION OF MASS MOMENTS OF INERTIA

In order to have a dynamic analysis it is imperative that the rotatory inertia be calculated. This appendix provides the means of determining the rotatory inertia using the techniques of classical statics. Assuming the mass to be represented by a volume of uniform thickness and homogeneous material the rotatory inertia about its own mass center which is the geometric centroid, G, as shown in Figure 89 is given as

$$M_R = \int r^2 dm \tag{A.1}$$

but $dm = \zeta' dV$ where ζ' is the mass per unit volume and dV is the differential volume giving

$$M_R = \zeta' \int_V r^2 dV \tag{A.2}$$

For regular shapes $dV = t\, dA = t\, dx\, dy$ where t is the constant thickness dA is the differential area, and dx and dy are the differential dimensions of dA which provides

$$M_R = \zeta' t \iint r^2 dx\, dy = \zeta' t \iint (x^2+y^2) dx\, dy \tag{A.3}$$

where x and y are the vector components of r.

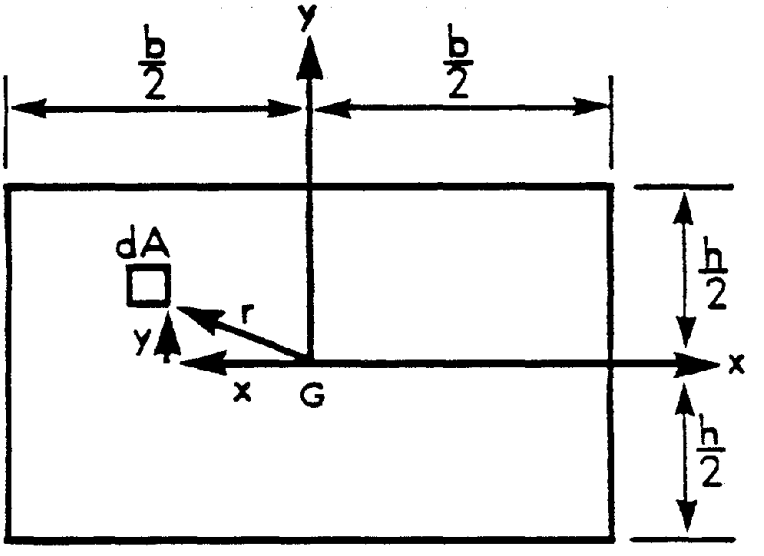

Figure 89. Typical Rectangular Element Used for the Derivation of the Rotatory Inertia

For a rectangular shape such as the one given in Figure 89, Equation A.3 can be easily solved

$$M_R = \zeta' t \int_{-b/2}^{b/2} \int_{-h/2}^{h/2} (x^2+y^2)\,dy\,dx \tag{A.4}$$

$$= \zeta' t \int_{-b/2}^{b/2} \frac{hx^2+h^3}{12}\,dx \tag{A.5}$$

$$= \zeta' t\left(h\,\frac{b^3}{12}\right) + \zeta t\left(b\,\frac{h^3}{12}\right) \tag{A.6}$$

$$= \zeta' tbh\left(\frac{b^2}{12} + \frac{h^2}{12}\right) = \frac{m}{12}\,(b^2+h^2) \tag{A.7}$$

where m is the total mass of the rectangular element.

In order to find the rotatory inertia about a point other than the mass center a transformation similar to the parallel-axis theorem can be used. Suppose the rotatory inertia about point z in Figure 90 is required the formula would be

$$M_z = \int (r')^2 dm = \int (d+r)^2 dm \tag{A.8}$$

$$= \int (d^2+2dr+r^2)\,dm \tag{A.9}$$

$$= \int r^2 dm + d^2 \int dm + 2d \int r dm \tag{A.10}$$

$$= M_R + d^2 m + 0 \tag{A.11}$$

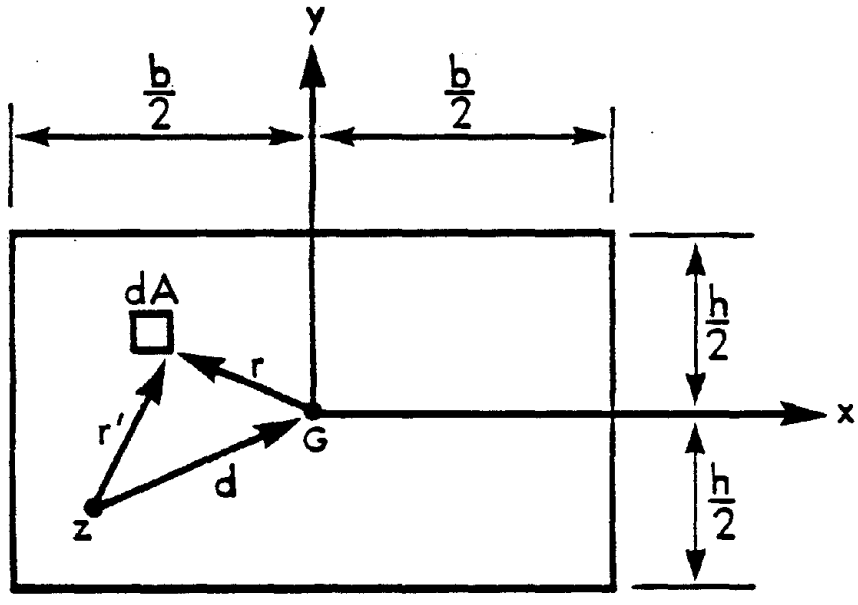

Figure 90. Transformation of the Rotatory Inertia

The last term of Equation A.10 is zero since the position vector r is with respect to the centroid of the geometric shape. Therefore the mass moment of inertia about some point, z, other than the mass center of the shape can be found by adding the mass moment of inertia about its own mass center to the product of the total mass of the shape and the square of the distance from the point z to the mass center of the shape itself.

APPENDIX B

GENERALIZED JACOBI ITERATION

The generalized Jacobi iteration technique is used to solve the generalized eigenvalue problem of the form

$$[K][\Phi] = [M][\Phi][\omega^2] \tag{B.1}$$

where [K], is the stiffness matrix,

[M], is the mass matrix,

[Φ], is the matrix of eigenvectors, and

[ω^2], is the diagonal matrix of eigenvalues.

Being a transformation technique, the approach is to find a series of orthogonal transformation matrices which will diagonalize the mass and stiffness matrices. This is an iterative technique where the transformation matrices are chosen in order to reduce the off-diagonal elements of [K] and [M] to zero. Writing the transformation matrices in this form

$$[T]_k = \begin{array}{c} \begin{matrix} & & \text{ith} & \text{jth} & \text{columns} \end{matrix} \\ \begin{bmatrix} 1 & & & & \\ & \ddots & & & \\ & & 1 & A & \\ & & B & 1 & \\ & & & & \ddots \\ & & & & & 1 \end{bmatrix} \begin{matrix} \\ \\ \text{ith} \\ \\ \text{jth} \\ \\ \end{matrix} \text{Rows} \end{array} \tag{B.2}$$

where k represents the iteration number, A and B are constants to be determined in a manner which will eliminate the off-diagonal elements. After pre and postmultiplying [K] and [M] by the transformation matrix, the $k_{ij}^{(k+1)}$ and $m_{ij}^{(k+1)}$ elements produce the two equations

$$Ak_{ii}^{k} + (1+AB)k_{ij}^{k} + Bk_{jj}^{k} = k_{ij}^{(k+1)} = 0 \qquad (B.3)$$

and

$$Am_{ii}^{k} + (1+AB)m_{ij}^{k} + Bm_{jj} = m_{ij}^{(k+1)} = 0 \qquad (B.4)$$

Multiplying Equation B.3 by m_{ij} and Equation B.4 by $-k_{ij}$ and adding the two new equations, a single equation can be found of the form

$$A(k_{ii}m_{ij}-k_{ij}m_{ii}) + B(k_{jj}m_{ij}-k_{ij}m_{jj}) = 0 \qquad (B.5)$$

which produces the solution (k, the iteration number has been omitted)

$$A = (k_{jj}m_{ij}-k_{ij}m_{jj}) \qquad (B.6)$$

and

$$B = -(k_{ii}m_{ij}-k_{ij}m_{ii}) \qquad (B.7)$$

Since Equations B.3 and B.4 are nonlinear this is not a solution to either equation, but Equations B.6 and B.7 do provide a means for a solution. Modifying Equations B.6 and B.7 to the form

$$A = \frac{(k_{jj}m_{ij}-k_{ij}m_{jj})}{C} \tag{B.8}$$

and

$$B = -\frac{(k_{ii}m_{ij}-k_{ij}m_{ii})}{C} \tag{B.9}$$

and substituting into Equation B.5 gives

$$\frac{1}{C}[k_{ij}k_{jj}m_{ii}-k_{ii}k_{ij}m_{jj}] - \frac{k_{ij}}{C^2}[k_{ii}k_{jj}m_{ij}^2-k_{ii}k_{ij}m_{ij}m_{jj}-$$

$$k_{jj}k_{ij}m_{ii}m_{ij}+k_{ij}^2m_{jj}m_{ii}] + k_{ij} = 0 \tag{B.10}$$

which is a quadratic equation. Dividing Equation B.10 by $(-k_{ij}/C^2)$ gives

$$-C^2 - C[k_{jj}m_{ii}-k_{ii}m_{jj}] + [k_{ii}k_{jj}m_{ij}^2-k_{ii}k_{ij}m_{ij}m_{jj}-$$

$$k_{jj}k_{ij}m_{ii}m_{ij}+k_{ij}^2m_{jj}m_{ii}] = 0 \tag{B.11}$$

or

$$C^2 + C[k_{jj}m_{ii}-k_{ii}m_{jj}] - [k_{ii}m_{ij}-m_{ii}k_{ij}][k_{jj}m_{ij}-m_{jj}k_{ij}] \tag{B.12}$$

and C can be written as

$$C = \frac{b}{2} \pm \left(\frac{b}{2}\right)^2 + c \tag{B.13}$$

where

$$b = [k_{ii}m_{jj} - k_{jj}m_{ii}] \tag{B.14}$$

$$c = [k_{ii}m_{ij} - m_{ii}k_{ij}][k_{jj}m_{ij} - m_{jj}k_{ij}] \tag{B.15}$$

Note that this transformation only zeros k_{ij}, k_{ji}, m_{ij} and m_{ji} for this iteration. The next transformation will force these elements to become nonzero again. Although the elements become nonzero, convergence can be guaranteed. The proof can be found in Reference 41. For a diagonal mass Equations B.8 and B.9 become

$$A = \frac{-k_{ij}m_{jj}}{C} \tag{B.16}$$

and

$$B = \frac{k_{ij}m_{ii}}{C} \tag{B.17}$$

and

$$C = \frac{b}{2} \pm \left(\frac{b}{2}\right)^2 + c \tag{B.18}$$

where

$$b = [k_{ii}m_{jj} - k_{jj}m_{ii}] \tag{B.19}$$

and

$$c = [-k_{ij}m_{ii}][-k_{ij}m_{jj}] = k_{ij}^2 m_{ii}m_{jj} \tag{B.20}$$

The sign in Equation B.18 is determined in accordance with the sign of b. The solution is considered acceptable when

$$\frac{|\omega_i^{2(k+1)} - \omega_i^{(k)}|}{\omega_i^{2(k+1)}} \leq 10^{-s} \qquad i = 1,\ldots,n \tag{B.21}$$

and

$$\left| \frac{(k_{ij}^{(k+1)})^2}{k_{ii}^{(k+1)} k_{jj}^{(k+1)}} \right|^{1/2} \leq 10^{-s} \qquad \begin{array}{l} i = 1,\ldots,n \text{ and} \\ j = 1,\ldots,n \end{array} \tag{B.22}$$

and

$$\left| \frac{(m_{ij}^{(k+1)})^2}{m_{ii}^{(k+1)} m_{jj}^{(k+1)}} \right|^{1/2} \leq 10^{-s} \qquad \begin{array}{l} i = 1,\ldots n \text{ and} \\ j = 1, \ldots,n \end{array} \tag{B.23}$$

where 10^{-s} is a convergence tolerance. Equations B.22 and B.23 are a means of testing whether the off-diagonal elements are sufficiently close to zero. The eigenvectors are determined as the multiplication of all the transformation

matrices used or

$$[\Phi] = [T]_1[T]_2 \cdots [T]_k \tag{B.24}$$

which is then normalized with respect to the mass. A computer program for the generalized Jacobi method is given in Reference 41.